


GLOBAL WARMING IMPACT ON TRANSITIONAL COASTAL ENVIRONMENTS: A METHODOLOGY FOR KNOWLEDGE-BASED MANAGEMENT AND DECISION MAKING

DOCTORAL THESIS

Juan del Rosal Salido

Supervisor: Miguel Ortega Sánchez

University of Granada

Doctoral Programme: Dynamics of Biogeochemical Flows and its Applications

September 2020

Editor: Universidad de Granada. Tesis Doctorales
Autor: Del Rosal Salido, Juan
ISBN: 978-84-1306-657-8
URI: http://hdl.handle.net/10481/63969

Agradecimientos

Este trabajo constituye para mí un proyecto muy especial que ha visto la luz gracias al esfuerzo de mucha gente también muy especial. Estoy profundamente agradecido a todos aquellos que con su conocimiento, sabiduría, paciencia, cariño, apoyo, ánimo, risas, entusiasmo y energía han hecho posible que esta Tesis sea una realidad. Me gustaría dedicar un agradecimiento especial a:

A *Miguel Á. Losada*, por enseñarnos el camino de la ciencia basada en el conocimiento y en el estudio. Gracias Miguel por ser una fuente de inspiración para todos y por tu capacidad inagotable de abrir camino donde otros no lo ven. A mi director de Tesis *Miguel Ortega Sánchez* por tu gran capacidad de guía y liderazgo. Migue quería agradecerte sobre todo la confianza que siempre depositaste en mí. Ha sido un placer tenerte siempre a mi lado para sacar este proyecto adelante.

A *Pedro Folgueras*, por tu gran corazón, paciencia y sentido crítico. Gracias Pedro por guiarme a través del maravilloso mundo de la estadística y por ser un pilar de apoyo fundamental en este proyecto. A *Pedro Magaña* por tu generosidad. Gracias Pedro por esas largas charlas y debates sobre como mejorar el mundo, pero sobre todo, GRACIAS por estar siempre ahí, disponible para los demás cuanto te hemos necesitado.

A *Asunción, Manolo, Antonio, María, Alex, Carmen, Tino y Javi y a mis compañeros de batalla Andrea, Pilar, María Jiménez, María Bermudez, Marian, Mariví y Cobos* porque esta Tesis tiene un pedacito de cada uno de vosotros en ella. Gracias de todo corazón. A mis amigos de siempre. Gracias *Enrique, Padilla, Héctor, Cobos, ...* se que pase lo que pase siempre estaréis ahí.

A *mi familia*, en especial a mi madre, a mi padre, mi hermana, mis tias, primos y a mi abuela quien cuidó de mi al principio de todo durante los años de carrera. Y por último quería dedicar unas palabras especiales de todo corazón a *Patri*, eres la luz que ilumina y guía cada uno de mis días. Gracias por todo tu apoyo incondicional y por recorrer este camino conmigo.

Este trabajo de investigación no habría sido posible sin el soporte económico proporcionado por (1) el "Programa Iberoamericano de Ciencia y Tecnología para el desarrollo" CYTED (proyecto PROTOCOL 917PTE0538) (2) el Ministerio de Economía y Competitividad de España (PCIN-2017-108) y (3) el Grupo de Dinámica de Flujos Ambientales de la Universidad de Granada (TEP-209). Gracias de corazón.

"*Sin método, orden, voluntad, esfuerzo y sacrificio no son posibles ni el genio ni el triunfo*"

Solón, uno de los siete sabios de la antigua Grecia.

"*An estuary is a semi-enclosed coastal body of water which has a free connection with the open sea and within which sea water is measurably diluted with fresh water derived from land drainage.*" (Cameron and Pritchard, 1963)

Abstract

Global warming is driving a progressive sea-level rise, which is expected to continue and accelerate in the next decades, leading to more frequent flooding events on the coast, damage to material assets, and increased risk of loss of human life. Since more than 60 % of the world's population lives in low-elevation coastal areas, and migration trends indicate that this number is expected to increase along the 21st-century, the general objective of this Thesis is: "to develop a comprehensive methodology with practical application tools for the characterization of the impact of global warming on flooding at a local scale in transitional coastal environments".

Among coastal areas, transitional environments (i.e., deltas and estuaries) exhibit high spatiotemporal variability in hydrodynamics caused by the superposition of multiple processes induced by concomitant (compatible and simultaneous) maritime, fluvial and atmospheric agents. Managing these environments requires a good understanding of both normal and extreme conditions. Due to the random nature of the agents, the multiple maritime-fluvial interactions of the simultaneous actions, and the progressive sea-level rise, the study of the extreme water level events in these systems implies analyzing the complex relationships between the statistics of the variable and how they are combined.

To address this challenge, most of the recent works have been focusing on studying the impact of global warming: (i) at global or regional scales, where the processes are simplified; (ii) at local scales in open coastal systems such as beaches, where the concomitance between agents is lower than in transitional systems; or (iii) by focusing only on certain characteristic storm events. Therefore, although progress has been made in this area, comprehensive methods focusing not only on the probabilistic study of flooding events at the local scale, but also on addressing the complex statistical relationships that provide insight into the formation mechanisms of such flood events, and even more so concerning the effects of sea-level rise, are currently lacking.

To meet this objective, this Thesis combines a set of very innovative techniques available separately in the field of Coastal Engineering while inheriting the advance in knowledge through the work of the Environmental Fluid Dynamics Group to address one of the main challenges that coastal managers and stakeholders will have to face along the next decades, especially in transitional coastal environments. This challenge consists of anticipating whether current flood defenses will be sufficient against global warming. Moreover, if they are not, this Thesis addresses the question of where and when flood defense will fail and by how much from a global, local, multivariate, and probabilistic approach.

The presented methodology in this Thesis is structured in three main blocks: the definition of the problem, the characterization and transfer of the natural forcing agents from the boundary to the transitional system, and the critical analysis of the results. In the first block (definition of the problem), the conceptual framework of the problem, together with the main hypothesis considered are defined. This block also defines the case study area used in this Thesis. After the theoretical development, continuos and progressive examples of application in each step of the presented methodology are shown. In this Thesis, the Guadalete estuary (Cádiz, SouthWestern Spain) is selected as a representative example of transitional areas of southern Europe, considered among the most complex areas for management due to the interactions between natural agents with different scales and periods, human interventions, and many stakeholders involved with different socioeconomic interests.

The second block characterizes and transfers the climatic agents' dynamics from the terrestrial and maritime boundaries to the transitional area. For the characterization, an open-access high-quality scientific software for climate analysis is developed using the software engineer skills as a primary and necessary step for sea-level rise impact assessment. Six modules have been implemented for reading, pre-processing, standardized, and analyzing climate data. The developed tool allows generating multiple products, from climate databases to automatic climate analysis reports, addressing different users from single source code. This information is used to simulate the forecasted series of climatic agents along the 21st-century, which, together with the sea-level rise scenarios, constitutes the inputs of the methodology presented in this Thesis. For this purpose, the lower limit of the IPCC-AR 5 (Church et al., 2013) RCP4.5 scenario and the upper limit for the RCP8.5 scenario have been considered as the SLR projections.

Systematic measurements of water levels along estuaries are rarely available and expensive, and even less information is available on the contribution of the different agents to these levels. Therefore, historical and forecasted climatic databases are transformed into a time series of historical (hindcasted) and future (forecasted) continuous water levels along transitional coastal environments through advanced hydrodynamic numerical models and downscaling techniques. The downscaling technique, initially used in the field of Coastal Engineering to downscale wavefields has been successfully adapted to being able to reconstruct not only large continuous time series of total water level series but also the water level components due to each individual forcing agents and the non-linear component due to the interaction between them along transitional coastal systems. The implementation of this methodology in the Guadalete estuary, has shown that these elevations present significant variabilities along the estuary. In particular, maximum elevations due to astronomical tide decrease upstream from the mouth (1.8 m)

to the inner part of the estuary (0.9 m) above LMSL. On the other hand, elevations due to the river discharge increase upstream from 0 (mouth) to 3 m (head). Weather surge elevations are found to be significantly lower than the rest of the components in the inner part of the estuary.

The third block of this Thesis (critical analysis of the results) uses all the water level information previously obtained along the system to address: (i) the number of flood failures, (ii) its magnitude in terms of the return period, and (iii) the mechanisms underlying that extreme events along the transitional coastal environment. In the first part of this block, the reconstructed historical and forecasted total water level series along the estuary is compared to the geometry of different transversal sections of the estuary to assess the number and duration of flood failures per year. In this Thesis, failure is defined as water levels higher than the flood defenses' crest height. This method, quite simple from a conceptual point of view, allows to quickly and inexpensively identify which areas will be the most sensitive to flooding in the coming years. In the case of the Guadalete estuary, an overflowing failure every 15 days during high tides coinciding with every spring tidal cycle per year are expected in the middle estuary in the most pessimistic SLR scenario considered in this Thesis if no mitigation actions are taken.

In the second part of the analysis block, the extra information provided by the water level components allows applying the well-known Joint Probability Methods to transitional coastal environments. The method is based on the sum of each component's probability density functions by considering all the possible combinations between them instead of only the ones that occurred in the past. This is especially interesting in highly regulated rivers, where river discharges usually coincide with neap tides due to the river regulation policy to reduce the risk of flooding. Joint extreme water level events (JETWL) obtained through the presented methodology are compared with the observed return levels. Similar values for both sides of the estuary are obtained. However, differences are observed in the middle part for long return periods where the observed return levels are 30% lower than the JETWL on average for the higher return periods due to the former interactions between the peaks and nonpeak of the astronomical tide and river discharge. As a result, the use of observed return levels instead of JETWL leads to lower probabilities than the obtained using the presented methodology, which may be risky in decision-making or urban planning. This method's application allows managers and coastal engineers to know the expected magnitude of flood events in probabilistic terms and the associated uncertainty, which constitutes the starting point for the design of protective measures. For example, if the estuary's central region is intended to be protected against events with a 50-year return period in 2100, a crest elevation between 2.5 m and 4 m will be necessary to prevent flooding with a 50 % and 95 % confidence,

respectively.

The disaggregated information of the water level components is used in the third part of the analysis block to address the mechanisms of the formation of extreme flood events. To this end, the statistical relationships that are established between the total water level that is a linear combination of a set of water level components that act simultaneously and the variables that are obtained from classifying each water level component in a set of mutually exclusive classes (extreme and non-extreme) are successfully adapted to transitional coastal environments building upon the work developed by Folgueras (2016). The development of a method that allows the identification of the agents responsible for the flooding processes and the combinations of extreme and non-extreme values that cause flooding is a significant advance in Coastal Engineering aimed at protecting coastal urban fronts against global warming. The obtained information allows the optimization of costs derived from protection measures since it is known on which agents and regime (extreme or normal) it is necessary to act for flooding risk mitigation.

The application of this analysis to the Guadalete estuary during the historical period shows that the extreme values of the total water level are explained only by the extremes of the astronomical tide in the outer estuary and only by the extremes of the river discharge in the inner estuary. However, a similar contribution between extreme values of the river discharge and extreme and mean values of the astronomical tide is found in the middle part of the estuary. Furthermore, these analyses indicate that in the Guadalete estuary case, the non-linear term's contribution to the magnitude and variability of the total water level's extreme events is nearly negligible. The analysis also shows that waves do not substantially impact the water levels along the Guadalete estuary due to the two breakwaters that protect the inlet avoiding wave breaking along the estuary.

This analysis is repeated for the different nodal cycles along the 21st-century period. Results show that the contribution of the non-extremes equals the contribution of the extremes in the formation of flood events by the end-century in the middle and upper estuary as a consequence of sea-level rise. It is also observed that the high interaction between astronomical tide and river discharge in the middle estuary is reduced. Therefore, fluvial discharge is limited only to the upper estuary, while the astronomical tide plus the sea-level rise dominated the formation of the flood events in the lower and middle estuary.

Despite the computational effort, all the presented methods along this Thesis have been fruitfully applied at multiple equidistant control points along the estuary and repeated for the eight nodal cycles between 1995 to 2100 for the two sea-level rise scenarios in the Guadalete estuary selected in this Thesis. As a result, the spatial

and temporal evolution of the results has been successfully addressed, providing much more valuable information about the impact of the sea-level rise in the flood events. This information is used to divide the estuary into homogeneous zones via three criteria: (i) the probability of extreme total water level events, (ii) the dominance of the agents, and (iii) the relationships between the components of the water level. These management maps constitute a valuable tool to support decision-making based on risk analysis, identify vulnerable areas, quantify the frequency of flooding, and identify the agents responsible for flooding at each area.

Assessed the impact of the sea-level rise on the flooding failure along transitional coastal environment, methods, and instruments to optimize the total cost of the protective maritime structures will be needed. To tackle this challenge, the final part of this Thesis provides a detailed method and an associated open-access numerical tool for the calculation of the probability distribution function of the total costs for any protective maritime structure at any location during its life-time cycle following the guidelines of the latest version of the ROM program (ROM-1.1, 2018) as a function of the forcing agents, the design and project factors and the work planning and strategies for construction and repair during the life-time of the structure. First, the definitions and formulations of the total costs are presented. A case example of the complete process of the total cost calculation for a rubble-mound breakwater is shown for two different strategies: "conservative" and "risky". After the calculations, the two strategies' results are compared in terms of the execution times, damages suffered during the life-time, and the total costs. Thus, demonstrating the usefulness of this type of tool when planning and designing coastal protection measures pursuing the highest level of efficiency.

As a final closure element, this Thesis can integrate all the developed methodologies into practical and comprehensive step-by-step guidelines to managers, coastal engineers, and decision-makers together with a set of tools to assess the impact that sea-level rise will have on coastal urban fronts at a local scale in transitional environments. These guidelines have been designed following the principles of preventive medicine, where the focus is not the finding of the solution, but the anticipation of the problem. Therefore, the so-called "preventive engineering" guidelines are based on three main blocks: symptoms, diagnosis, and treatment. In the symptoms stage, guidelines focus on identifying the problem that sea-level rise could originate shortly or during the next decades. During the diagnosis stage, users must be focused on three critical points: the gathering of all the available information and pay attention to monitoring and research if the available information is not sufficient; the in-depth definition of the problem; and the reproduction of the past in order to test and validate the models and methods. The treatment stage is divided into a set of three different development levels progressively increasing in

complexity and accuracy following the principles of the latest version of the ROM program: preliminary studies, the study of alternatives, and blueprint-investment project.

Resumen

El calentamiento global está provocando un aumento progresivo del nivel del mar, que se espera continúe y se acelere en los próximos años, lo que dará lugar a inundaciones más frecuentes en la costa, daños a los bienes materiales y un mayor riesgo de pérdida de vidas humanas. Dado que más del 60 % de la población mundial vive en zonas costeras de baja elevación, y que las tendencias de migración indican que se espera que esta cifra aumente a lo largo del siglo XXI, el objetivo general de esta Tesis es: "desarrollar una metodología integral con herramientas de aplicación práctica para la caracterización del impacto del calentamiento global en las inundaciones a escala local en sistemas costeros de transición".

Entre las zonas costeras, los sistemas de transición (i.e., los deltas, estuarios y desembocaduras) presentan una gran variabilidad espacio-temporal en la hidrodinámica causada por la superposición de múltiples procesos concomitantes (compatibles y simultáneos) inducidos por agentes marítimos, fluviales y atmosféricos. La gestión de esos entornos requiere una buena comprensión de las condiciones normales y extremas. Debido a la naturaleza aleatoria de los agentes naturales, a las múltiples interacciones marítimo-fluviales de las acciones simultáneas y a la elevación progresiva del nivel del mar, el estudio de los eventos extremos de nivel en estos sistemas implica el análisis de las complejas relaciones entre las estadísticas de las variables y la forma en que estas se combinan.

Para hacer frente a este desafío, la mayoría de los trabajos recientes se han centrado en el estudio del impacto del calentamiento global: i) a escala global o regional, donde los procesos se simplifican; ii) a escala local en sistemas costeros abiertos como las playas, donde la concomitancia entre los agentes es menor que en los sistemas de transición; o iii) centrándose sólo en ciertos eventos de tormentas características. Por lo tanto, aunque se han hecho progresos en esta área, actualmente faltan métodos integrales centrados no sólo en el estudio probabilístico de los eventos de inundación a escala local, sino también en el tratamiento de las complejas relaciones estadísticas que permiten comprender los mecanismos de formación de esos eventos de inundación, y más aún en lo que respecta a los efectos de la elevación del nivel del mar.

Para cumplir este objetivo, esta Tesis combina un conjunto de técnicas muy innovadoras disponibles por separado en el campo de la ingeniería costera, al tiempo que hereda el avance de los conocimientos gracias a la labor del Grupo de Dinámica de Fluidos Ambientales para abordar uno de los principales retos que los gestores y administradores de la costa tendrán que afrontar a lo largo de los próximos decenios, especialmente en los entornos costeros en transición. Dicho reto consiste en anticipar si las actuales defensas

costeras frente a la inundación serán suficientes contra el calentamiento global. Además, si no lo son, esta Tesis aborda la cuestión de dónde y cuándo fallarán las defensas contra las inundaciones y en qué medida desde un enfoque global, local, multivariado y probabilístico.

La metodología presentada en esta Tesis está estructurada en tres bloques principales: la definición del problema, la caracterización y transferencia de los agentes naturales forzadores desde los contornos o fronteras al sistema de transición, y el análisis crítico de los resultados. En el primer bloque (definición del problema) se define el marco conceptual del problema, junto con las principales hipótesis consideradas. En este bloque se define también el área de estudio que se utiliza en esta Tesis a modo de ejemplo de aplicación. Tras el desarrollo teórico, se muestran una serie de ejemplos progresivos de aplicación en cada uno de los pasos de la metodología presentada. En esta Tesis se ha seleccionado el estuario del Guadalete (Cádiz, Suroeste de España) como ejemplo representativo de los sistemas de transición costeros del sur de Europa, considerados entre las áreas más complejas para la gestión debido a las interacciones entre agentes naturales con diferentes escalas y períodos, las intervenciones humanas, y la participación de muchos actores involucrados con diferentes intereses socioeconómicos.

El segundo bloque (caracterización y transferencia) caracteriza y transfiere la dinámica de los agentes climáticos desde los límites terrestres y marítimos hasta la zona de transición. Para la caracterización se ha elaborado una herramienta informática-científica de alta calidad y acceso libre para el análisis del clima, utilizando los conocimientos y principios de la ingeniería informática como paso previo y necesario para la evaluación del impacto del aumento del nivel del mar. Se han puesto en marcha seis módulos para la lectura, el pre-procesamiento, la normalización y el análisis de los datos climáticos. La herramienta desarrollada permite generar múltiples productos, desde bases de datos climáticos hasta informes automáticos de análisis del clima marítimo, dirigidos a diferentes usuarios a partir de un único código fuente, lo cual facilita el mantenimiento y desarrollo de la herramienta considerablemente. Esta información es utilizada posteriormente para la simulación de las series temporales futuras de los descriptores de los agentes climáticos a lo largo del siglo XXI, lo que, junto con los escenarios de aumento del nivel del mar, constituye las entradas de la metodología presentada en esta Tesis. Para ello, el límite inferior del escenario RCP4.5 del IPCC-AR 5 (Church et al., 2013) y el límite superior del escenario RCP8.5 han sido considerados como las proyecciones para la subida del nivel del mar.

La información de mediciones sistemáticas de niveles totales a lo largo de los estuarios rara vez se encuentra disponible y son costosas. Pero, mucho menos disponibles se encuentra la información sobre la contribución de los diferentes agentes a esos niveles

totales. Por lo tanto, en esta segunda parte de la Tesis, las bases de datos climáticas históricos y futuras obtenidas anteriormente se transforman en series temporales continuas de niveles históricos (hindcast) y futuros (forecast) a lo largo de los sistemas costeros de transición mediante modelos numéricos hidrodinámicos avanzados y técnicas de downscaling. La técnica de downscaling o reducción de escala, utilizada inicialmente en el campo de la ingeniería costera para reducir la escala de los campos de olas, se ha adaptado con éxito en esta Tesis para poder reconstruir largas series temporales continuas de niveles de agua totales. Además, el método propuesto permite también reconstruir las componentes del nivel de agua debidos a cada uno de los agentes forzadores, así como la componente no lineal debido a las interacciones entre ellos. La aplicación de esta metodología en el estuario del Guadalete, ha demostrado que estas elevaciones presentan importantes variabilidades a lo largo del estuario. En particular, las elevaciones máximas debidas a la marea astronómica disminuyen desde la desembocadura, donde se obtienen valores de 1.8 m, hacia la parte interior del estuario, obteniéndose valores máximos de 0.9 m próximos a la cabecera. Por otro lado, las elevaciones debidas a la descarga fluvial aumentan aguas arriba desde los 0 m en desembocadura hasta los 3 m en cabecera. Las elevaciones debidas al oleaje y viento (surge) se han observado que son significativamente más bajas que el resto de los componentes en el interior del estuario.

El tercer bloque de esta Tesis (análisis crítico de los resultados) utiliza toda la información sobre los niveles obtenida en el segundo bloque para abordar: (i) el número de fallos por inundaciones, (ii) su magnitud en términos del período de retorno y (iii) los mecanismos de generación de dichos eventos extremos a lo largo del sistema de transición. En la primera parte de este bloque, la serie de niveles de agua totales reconstruidos, históricos y futuros se compara con la geometría de las diferentes secciones transversales del estuario para evaluar el número y la duración de los fallos por inundación al año. En esta Tesis, los fallos se definen como niveles de agua superiores a la altura de coronación de las defensas frente a inundaciones. Este método, en principio bastante sencillo desde el punto de vista conceptual, permite identificar de manera rápida y poco costosa qué zonas serán más sensibles a las inundaciones en los próximos años. En el caso del estuario del Guadalete, en caso de no adoptar medidas de mitigación, se prevé que, en la zona media del estuario para el escenario más pesimista de subida de nivel del mar de los dos considerados en esta Tesis, se produzca un fallo por desbordamiento del cauce cada 15 días durante todas y cada una de las pleamares dentro de los ciclos de mareas vivas.

En la segunda parte del bloque de análisis, la información adicional proporcionada por las distintas componentes del nivel total permite aplicar los conocidos métodos de probabilidad conjunta a los sistemas costeros de transición. El método se basa en la suma de las funciones de densidad de probabilidad de cada componente considerando así

todas las combinaciones posibles entre las componentes de nivel en lugar de sólo aquellas que se produjeron en el pasado. Esto es especialmente relevante en ríos altamente regulados, en los que las descargas fluviales suelen hacerse coincidir con las mareas vivas debido a la política de regulación de los ríos para reducir el riesgo de inundación. Los eventos extremos conjuntos de nivel de agua (JETWL por sus siglas en inglés) obtenidos mediante la metodología presentada se comparan con los niveles de retorno observados. Tras la aplicación al estuario del Guadalete, se obtienen valores similares para ambos lados del estuario. Sin embargo, se observan diferencias en la parte media para los períodos de retorno mayores, en los que los niveles de retorno observados durante el periodo histórico son un 30% inferiores a los JETWL en promedio para los períodos de retorno más altos, debido a las mencionadas interacciones entre los picos y los no picos de la marea astronómica y la descarga fluvial. Como resultado, el uso de los niveles de retorno observados históricos en lugar del JETWL da lugar a probabilidades más bajas que las obtenidas con la metodología presentada, lo que puede ser arriesgado a la hora de tomar decisiones o en la planificación de la respuesta al calentamiento global. La aplicación de este método permite a los administradores e ingenieros costeros conocer la magnitud prevista de los eventos extremos de nivel en términos probabilísticos junto con la incertidumbre asociada, lo que constituye el punto de partida para el diseño de medidas de protección. Por ejemplo, si se pretende proteger la región central del estuario, que se ha visto que es la mas vulnerable, contra eventos con un período de retorno de 50 años en 2100, será necesaria una elevación de las cotas de coronación de las defensas costeras de entre 2,5 m y 4 m para evitar la inundación con una confianza del 50 % y el 95 %, respectivamente.

La información desglosada de los componentes del nivel del agua se utiliza en la tercera parte del bloque de análisis para abordar los mecanismos de formación de los eventos extremos de inundación. Para ello, las relaciones estadísticas que se establecen entre el nivel total, el cual es una combinación lineal de un conjunto de componentes del nivel que actúan simultáneamente, y las variables que se obtienen de la clasificación de cada componente del nivel en un conjunto de clases mutuamente excluyentes (extremas y no extremas) se han adaptado con éxito en esta Tesis a los sistemas costeros de transición a partir del trabajo desarrollado por Folgueras (2016). El desarrollo de un método que permita identificar los agentes responsables de los procesos de inundación y las combinaciones de valores extremos y no extremos que causan las inundaciones es un avance significativo en la ingeniería costera destinada a proteger los frentes urbanos costeros contra el calentamiento global. La información obtenida en esta parte de la Tesis permite optimizar los costes derivados de las medidas de protección, ya que permite conocer sobre qué agentes y regímenes (extremal o normal) es necesario actuar para la mitigación del riesgo de inundación.

La aplicación de este análisis al estuario del Guadalete durante el período histórico muestra que los valores extremos del nivel total del agua se pueden explicar únicamente por los extremos de la marea astronómica en la zona de la desembocadura y sólo por los extremos de la descarga fluvial en cabecera. Sin embargo, en la parte media del estuario encontramos una contribución por igual entre los valores extremos de la descarga del río y los valores extremos y medios de la marea astronómica. Además, estos análisis indican que, en el caso del estuario del Guadalete, la contribución del término no lineal a la magnitud y variabilidad de los eventos extremos del nivel total del agua es casi insignificante. El análisis también muestra que el oleaje no afecta de manera significativa a los niveles extremos de agua a lo largo del estuario debido a que los dos diques que protegen la entrada del mismo evitan la rotura del oleaje y por consiguiente la sobreelevación del nivel asociada al mismo.

Dicho análisis se repite para los diferentes ciclos nodales existentes a lo largo del siglo XXI. Los resultados muestran que la contribución de los valores no extremos iguala a la contribución de los valores extremos en la formación de eventos de inundación para el final del siglo en el estuario medio y superior (cabecera) como consecuencia de la elevación del nivel del mar. Se observa también como se reduce la interacción entre la marea astronómica y la descarga fluvial en el estuario medio. Por lo tanto, la influencia de la descarga fluvial queda limitada únicamente a la zona de cabecera del estuario, mientras que la marea astronómica más la elevación del nivel del mar dominan la formación de los eventos de inundación en la zona de desembocadura y el estuario medio.

A pesar del esfuerzo de cálculo, todos los métodos presentados a lo largo de esta Tesis se han aplicado fructíferamente en múltiples puntos de control equidistantes a lo largo del estuario y se han repetido durante los ocho ciclos nodales entre 1995 y 2100 para los dos escenarios de subida del nivel del mar considerados en esta Tesis para el estuario del Guadalete. Como resultado, se ha abordado la evolución espacial y temporal de los resultados, lo que proporciona una información mucho más valiosa sobre el impacto de la elevación del nivel del mar en los eventos de inundación en frentes costeros urbanos situados en sistemas de transición. Esta información se utiliza para dividir el estuario en zonas homogéneas mediante tres criterios: i) la probabilidad de que se produzcan eventos extremos de nivel total del agua, ii) el predominio de los agentes y iii) las relaciones entre los componentes del nivel del agua. Estos mapas de gestión constituyen una valiosa herramienta de apoyo a la toma de decisiones basada en el análisis de riesgos ya que, identifican las zonas vulnerables, cuantifican la frecuencia de las inundaciones e identifican los agentes responsables de las inundaciones en cada zona.

Una vez evaluado el impacto de la elevación del nivel del mar en el fallo por inundación

a lo largo del sistema costero de transición, serán necesarios métodos e instrumentos para optimizar el coste total de las estructuras marítimas de protección. Para hacer frente a este desafío, la parte final de esta Tesis proporciona un método detallado y una herramienta numérica asociada de acceso abierto para el cálculo de la función de distribución de probabilidad de los costes totales de cualquier tipo de estructura marítima de protección en cualquier lugar durante su ciclo de vida útil, siguiendo las directrices de la última versión del programa ROM (ROM-1.1, 2018) en función de los agentes forzadores, los factores de diseño y de proyecto y la planificación del trabajo y las estrategias de construcción y reparación durante la vida útil de la estructura. En primer lugar, se presentan las definiciones y formulaciones de los costes totales. Y a continuación se proporciona un ejemplo práctico del proceso completo del cálculo de los costes totales de un dique en talud para dos estrategias diferentes: "conservadora" y "arriesgada". Tras los cálculos, se comparan los resultados de las dos estrategias en cuanto a los tiempos de ejecución, los daños sufridos durante la vida útil y los costes totales. De esta manera, se demuestra la utilidad de este tipo de herramienta en la planificación y diseño de medidas de protección costera en la búsqueda del más alto nivel de eficiencia.

Como elemento de cierre final, esta Tesis integra todas las metodologías desarrolladas a lo largo de la misma en una serie de directrices prácticas y paso a paso, junto con un conjunto de herramientas para que gestores, ingenieros costeros y responsables de la toma de decisiones puedan evaluar el impacto que la subida del nivel del mar en los frentes urbanos costeros a escala local en sistemas de transición. Estas directrices se han elaborado siguiendo los principios de la medicina preventiva, en la que el centro de atención no es la búsqueda de la solución, sino la anticipación del problema. Por lo tanto, las llamadas directrices de "ingeniería preventiva" se basan en tres bloques principales: síntomas, diagnóstico y tratamiento. En la etapa de los síntomas, las directrices se centran en la identificación del problema que el aumento del nivel del mar podría originar en breve o durante las próximas décadas. Durante la etapa de diagnóstico, los usuarios deben centrarse en tres puntos críticos: la recopilación de toda la información disponible y prestar atención a la monitorización y la investigación si la información disponible no es suficiente; la definición en profundidad del problema; y la reproducción del pasado para probar y validar los modelos y métodos. La etapa de tratamiento se divide a su vez en un conjunto de tres niveles de desarrollo diferentes que aumentan progresivamente en complejidad y precisión siguiendo los principios de la ROM-1.1 (2018): estudios preliminares, estudio de alternativas y proyecto de inversión.

CONTENTS

List of Figures

List of Tables

Part I

Introduction and definition of the problem

CHAPTER 1

INTRODUCTION

1.1 Motivation

Global warming (GW) is driving a progressive sea-level rise (SLR), which is expected to continue and accelerate in the next decades (DeConto and Pollard, 2016; Bars, Drijfhout, and Vries, 2017), leading to more frequent flooding events on the coast, damage to material assets and increased risk of loss of human life (Barredo, 2007; Diakakis and Deligiannakis, 2017; Gil-Guirado, Pérez-Morales, and Lopez-Martinez, 2019; Landau, Legro, and Vlašić, 2008; Schinko et al., 2020). These effects will be amplified in coastal cities due to the high concentration of activities, services, and population.

More than 60% of the world's population lives in low-elevation coastal zones (LECZs) (Vitousek et al., 1997), which are defined as contiguous and hydrologically connected coastal areas below 10 m of elevation with respect to the local mean sea level (LMSL) (McGranahan, Balk, and Anderson, 2007; Lichter et al., 2011). According to Merkens et al. (2016) global population in the coastal zone currently surpasses 600 million globally, and migration trends forecast an increase between 830 to 1.184 million by the end of the 21st-century, thus representing 30% to 85% growth compared with that in 2000.

The downside of this development is the exposure of these LECZs to natural hazards, such as storm surges, extreme waves, high river floods, dam breaks, tsunamis, tornados, and seismic and geotechnical risks. Furthermore, GW is producing a progressive SLR that represents a severe threat for the future (Hinkel et al., 2014; Hogarth, 2014; Vousdoukas

et al., 2017; Mentaschi et al., 2017; Marcos and Woodworth, 2017; Sayol and Marcos, 2018; Lincke and Hinkel, 2018). According to Vousdoukas et al. (2018), between the years 2000 and 2100, the global increase of extreme sea levels will vary between 34 and 76 cm under a moderate-emission-mitigation-policy scenario (RCP 4.5) and between 58 and 172 cm under a business-as-usual scenario (RCP 8.5). The joint impact of these hazard components, combined with long-term SLR, can increase the flood frequency and magnitude in the coming decades (Vitousek et al., 2017; Santamaria-Aguilar, Arns, and Vafeidis, 2017). If no mitigation actions are taken, and GW follows the RCP 8.5 scenario, this will result in annual flooding costs between US$ 14 and 27 trillion per year (Jevrejeva et al., 2018).

Among coastal areas, transitional coastal environments (TCE) such as estuaries, river mouths, deltas, and coastal lagoons, are considered the common geography between sea and land in man-occupied spaces. In many of these TCE, the failure return period of the flood defenses is currently being reassessed to include GW's effects. However, these environments are characterized by exhibit the highest spatial and temporal variabilities in hydrodynamics, which are caused by the superposition of multiple concomitants (compatible and simultaneous) climatic agents (ROM-0.0, 2001; ROM-1.0, 2009; ROM-1.1, 2018). Thus, a joint analysis of the concomitant agents is required in these areas. Furthermore, the management of extreme water levels in these environments requires a good understanding of both normal and extreme regimes, which are commonly driven by the non-stationarity conditions (Solari and Losada, 2016; Lira-Loarca et al., 2020) of different forcing agents that are often analyzed independently (Folgueras et al., 2016).

1.1.1 State of the art: present and future challenges

According to Toimil et al. (2020), some of the current challenges facing coastal engineers in assessing the risks of GW in coastal urban fronts include: (1) the need to transition from deterministic methods to more robust probabilistic approaches that account for the uncertainty, (2) the need for multi-hazard and global approaches to reproduce the real complexity of the underlying processes, including the system with its multiple variables, demography, economy, interdependencies and non-linear interactions among others, (3) the incorporation of GW into medium- and long-term planning decisions to design and maintain coastal protection structures in a changing climate scenario, and (4) flexible and adaptative methods that allow to progressively reduce the uncertainty, to anticipate the problems and to commit short-term actions while maintaining long-term options open for the less certain future.

In attempting to address these challenges, many authors have assessed the increased hazard of extreme total water level events as a result of GW on global and regional

scales (e.g., Vousdoukas et al. (2018), Anderson et al. (2019), and Vousdoukas et al. (2020)). These works are based on the calculation of each component of the water level independently and the propagation to the shore to obtain the Extreme Total Water Level events (ETWLe) by the linear addition of each component. Their work represents a step forward in the division of coastlines into segments depending on the dominance of the agents and the probability of extreme values on a global scale, including the effects of SLR. However, these works do not account for the interaction between simultaneous agents. Besides, the use of simplified bathymetries and formulations to propagate the offshore agents to the coast limits the applicability of these methodologies at local and detailed scales such as TCE.

On the other hand, works addressing the joint probability of extreme surge levels and waves in coastal areas at local scale has been widely studied by several authors (Tawn, 1992; Hawkes et al., 2002; Michele et al., 2007; Hawkes, 2008; Masina, Lamberti, and Archetti, 2015; Mazas et al., 2014; Mazas and Hamm, 2017) including the assessment of coastal flooding risks (Gouldby et al., 2014; Rueda et al., 2015; Sayol and Marcos, 2018). One of the shortcomings of these approaches is the lack of an analysis of the concomitance between simultaneous agents during the ETWLe and their relative contributions to the outcome. In TCE at a local scale, recent works have demonstrated that joint approaches are necessary for an accurate flooding risk assessment (Svensson and Jones, 2004). The work developed by Olbert et al. (2017) is pioneer in addressing the mechanism of flooding resulting from the interaction of storm surge, tide and, river discharge using a coupled ocean and hydrodynamic model. Their work demonstrates the potential of new flood modeling systems that combine multiple agents in complex areas to simulate flood inundation events in a very accurate way. However, the method is focused on the study of a single event. Although it provides valuable information, it needs to be combined with other studies to understand the mechanics and dynamics of coastal flooding. A second approach in the analysis of the compound flooding at a local scale consists of the disaggregation of the total water level into its components to analyze the impact of each agent separately and jointly using a three-dimensional hydrodynamic model (Chen and Liu, 2014; Kumbier et al., 2018). These works disaggregate the total water level into a storm-tide level and river discharge to analyze each one's contributions in terms of flood extent and depth and constitute a first approach in analyzing each agent's impact over the total water level. However, they are also focused on the study of particular flooding events, which are analyzed in detail. The high computational cost of these methods limits the statistical analysis of these combinations over time.

To overcome this issue, approaches based on hydrodynamic modeling and joint-probability methods have been used to investigate the flood severity resulting from the

combined effect of multiple agents (Lian, Xu, and Ma, 2013; Marcos and Woodworth, 2017; Yin, Xu, and Huang, 2018; Zellou and Rahali, 2019). These works also disaggregate the total water level into the marginal components to assess the probability of extreme total water level events. However, these techniques focus on calculating the joint impact of the simultaneous agents on the flooding risk rather than assessing the causes behind the flooding events.

As seen, progress has been made in combining multiple concomitant agents to assess the probability of ETWLe, both globally and locally, but mainly focused on the maritime forcing (Sayol and Marcos, 2018; Orejarena-Rondón et al., 2019; Marcos et al., 2019; Enríquez et al., 2019) without integrating rain-driven flooding. Hydrodynamic competition between marine and continental processes is indeed key to predicting extreme water levels along ocean-to-river gradients (Bermúdez, Cea, and Sopelana, 2019; Serafin et al., 2019). However, comprehensive methods focusing not only on the probabilistic study of flooding events at the local scale, but also on the analysis of the mechanisms underlying the formation of these extreme events, and even more so concerning the effects of GW, are currently lacking.

1.1.2 Previous works of the research group

In this context, the Environmental Fluid Dynamic Group (University of Granada) with the works developed by Payo, Baquerizo, and Losada (2004), Payo, Baquerizo, and Losada (2008), ROM-1.0 (2009) and the HUMOR project (Baquerizo and Losada, 2008) defined for the first time a dynamic modeling approach to estimate the uncertainty in medium and long term climate-driven and human-induced morphodynamic changes of the coast at the local scale. Then, Solari (2011), Solari and Losada (2011), and Solari and Losada (2012) described the non-stationary mixture probability distribution models for the maritime and atmospheric forcing agents. These works, combined with Solari and Gelder (2011), allowed the simulation of continuous time series of forcing agents maintaining the same statistical properties as the original series. Following this line, Folgueras et al. (2016) and Folgueras (2016) addressed an innovative procedure for decomposing a random variable into mutually exclusive classes to address the contribution of these classes to the statistics of their sum through the analysis of the relations of simultaneity and compatibility between the components and classes.

The motivation for this Thesis is closely related to the above difficulties and the way they are handled. Therefore, this Thesis combines a set of very innovative techniques available separately in the field of Coastal Engineering , while inheriting the advance in knowledge through the work of the Environmental Fluid Dynamics Group. As a result, it provides a functional method to solve a specific and challenging problem that coastal

managers and decision-makers will have to face throughout the 21st-century, particularly in TCE under a global and joint vision. This Thesis set up a probabilistic, multivariate, and comprehensive method to: (i) assess GW's impact on flooding in coastal urban fronts and (ii) to understand the mechanisms of the formation of extreme events at a local scale along the 21st-century in TCE. The proposed method allows both managers and stakeholders to anticipate problems derived from flooding related to GW by knowing in advance if current coastal defenses will be sufficient to protect coastal urban fronts throughout the 21st-century. Moreover, if they are not, to address the question of where and when flood defense will fail and how much to avoid material damage and even loss of human life. Subsequently, this Thesis helps to optimize costs for adaptation and risk mitigation of GW. It is therefore imperative that reliable methods to assess the probability of compound flooding from multiple concomitant agents be incorporated into the guidelines and recommendations for the cost-optimization of the construction and maintenance of protection structures against SLR (ROM-0.0, 2001; MEIPORT, 2016; ROM-1.1, 2018).

1.1.3 Framework of the Thesis

The development of this Thesis is framed within two projects: the PROTOCOL project (protection of coastal urban fronts against global warming) and the ROM-1.1 (2018) (Recommendations for Breakwater Construction Project). The PROTOCOL project (2017 - 2020) aims to develop a methodology and technical guidelines for the project, construction, and management of the protection of coastal urban fronts that present a high risk of flooding due to GW not be assumed by society or by infrastructures. Four countries of the Iberoamerican network constitute this project: Spain, Portugal, Mexico, and Uruguay being the Environmental Fluid Dynamic Group of the University of Granada (Spain), the group that leads the project. This project's principal characteristics are its strong commitment to the divulgation and transfer of results in addition to its research component. Therefore, this is the reason why from each chapter of this Thesis, different products of interest for managers and decision-makers are derived, such as climate analysis tools, reports, databases, methodologies for the characterization of extreme events, and guidelines with technical recommendations.

On the other hand, ROM-1.1 (2018) is the technical-economic instrument that facilitates and supports decision-making for breakwater investment projects. One of the specific objectives is to provide maritime engineering with an efficient method that can be used to design, construct, maintain, repair, and dismantle a breakwater, whose purpose is to protect a coastal area from climate agents. The final part of this Thesis, explicitly related to the calculation of the total cost distribution function of a protective maritime structure, is based on this ROM-1.1 (2018).

1.2 Objectives

The general objective of this Thesis is to develop a comprehensive methodology with practical application tools for the characterization of the impact of global warming on flooding at a local scale in transitional coastal environments. This methodology makes it possible to address the optimization of protection costs based on knowledge in areas facing an unacceptable risk of flooding. This general objective is addressed through the following specific objectives:

I. To develop an open-access numerical tool for the gathering, homogenization, characterization, and simulation of climate agents databases following software engineering guidelines.

II. To reconstruct the time series of historical (hindcasted) and future (forecasted) continuous water levels along transitional coastal environments through advanced hydrodynamic numerical models and downscaling techniques.

III. To quantify the number of flood defense failures to determine the sensitivity of transitional coastal environments to extreme flood events resulting from global warming.

IV. To assess the probability of extreme total water level events in terms of return period in transitional coastal environments considering the concomitance between the marine, river, and atmospheric forcing agents to characterize the magnitude of the flood events.

V. To analyze the simultaneity and compatibility relationships between the water level components to characterize the mechanisms underlying the occurrence of extreme total water level events leading to flooding.

VI. To determine the spatio-temporal variability of extreme water level events to characterize where and when flooding will occur.

VII. To develop a detailed method and an associated open-access numerical tool for calculating the probability distribution function of the total costs for any protective maritime structure at any location during its useful life cycle following the guidelines of ROM-1.1 (2018).

VIII. To integrate the methodology developed throughout this Thesis to present comprehensive guidelines for assessing the sea-level rise impact on coastal urban fronts at a local scale.

1.3 Thesis outline

This Thesis is structured into five parts, as shown in the diagram of Fig. 1.3.1. The first part (Chapters 1, and 2) comprises the introduction, the definition of the problem, and the theoretical framework for achieving the specific objectives. The second part (Chapters 3 and 4) develops the theoretical approach together with an example of practical application for the achievement of the first and second specific objectives, the characterization and transfer of the climatic forcing agents to the coast by reconstructing the continuous time series of the water levels. The third part (Chapters 5, 6, and 7) uses the former water level series for the characterization of the probability distribution function and the mechanisms of generation of the extreme total water level events and their impact on coastal urban fronts at a local scale, thus achieving the specific objectives from III to V. The developed methodology together with the results obtained in the second and third parts are collected, summarized and used in the fourth part (Chapters 8 and 9) for the development of practical step-by-step guidelines for the management of transitional coastal systems at risk of flooding from global warming and a practical application tool for the calculation of the total costs of a protective maritime structure following ROM-1.1 (2018) guidelines. Finally, in the fifth part (Chapter 10), the main conclusions of the work and future lines of research are presented. The content of each chapter is briefly described below.

Chapter 2

The conceptual framework of the problem to be solved is defined along with the main working hypotheses. The study area used as an example of the application of the methodology developed throughout this Thesis is described.

Chapter 3

The gathering, characterization, analysis, and simulations of the concomitant climatic agents' information constitutes the first step for assessing the impact of global warming in the transitional coastal environment at a local scale. Therefore, an open-access high-quality scientific software for climate analysis to collect and characterize the different historical atmospheric, maritime, and fluvial forcings is developed using software engineer skills. The simulation of continuous time series of the stochastic climatic agents' descriptors for the period 2020- 2100 is performed using the historical climatic databases together with the definition of the sea-level rise scenarios for the 21st-century.

Chapter 4

The reconstruction of the historical and future continuous time series of water levels along the transitional coastal environment is described. To this purpose, a downscaling technique (Camus, Mendez, and Medina, 2011), with specific modifications for the adaptation to transitional environments, is used. As a result, the individual water levels due to each forcing agent individually, as well as the total water level due to the simultaneous agents' concomitant effect, are obtained in this chapter along the transitional coastal environment.

Chapter 5

The total water level calculated in former chapter is compared with the transitional coastal environment's geometry to assess the evolution in the number and duration of failures per year due to the sea-level rise. The presented method allows assessing whether current flood defenses are sufficient to withstand the effects of global warming expected in this 21st-century.

Chapter 6

The disaggregated information of the water level components is used to evaluate the probability of flood events in terms of the return period. The application of this method allows managers and coastal engineers to know the expected magnitude of flood events in probabilistic terms together with the associated uncertainty, which constitutes the starting point for the design of protective measures.

Chapter 7

Once the magnitude of the flooding events has been characterized, the disaggregated information of the water level components is also used in this chapter to understand the mechanisms of the formation of such extreme events in order to know on which agents it is necessary to act to optimize the costs of the mitigation measurements. The statistical relations of simultaneity and compatibility between the water level components are obtained to address this objective.

Chapter 8

Preceding chapters focus on the characterization of the impact of the sea-level rise on the number, magnitude, and causes of flooding failures. Now, this chapter provides a detailed method and an associated open-access numerical tool for the calculation of the probability distribution function of the total costs for any type of protective maritime

structure at any location during its useful life cycle following the guidelines of ROM-1.1 (2018) as a function of the forcing agents, the design and project factors and the work planning and strategies for construction and repair during the life-time of the structure.

Chapter 9

This chapter integrates the methodology developed throughout this Thesis to present comprehensive guidelines for assessing the sea-level rise impact on coastal urban fronts at a local scale. These guidelines apply the principle of preventive medicine to Coastal Engineering in what we have called "preventive engineering," that is, not waiting until there is a problem to solve, but anticipating it. Therefore, these guidelines are structured in three main blocks: identification of the problem (symptoms), identification of the causes (diagnosis), and identification of the possible solutions (treatment).

Chapter 10

The conclusions derived from this research work are presented and the main future research lines are drown.

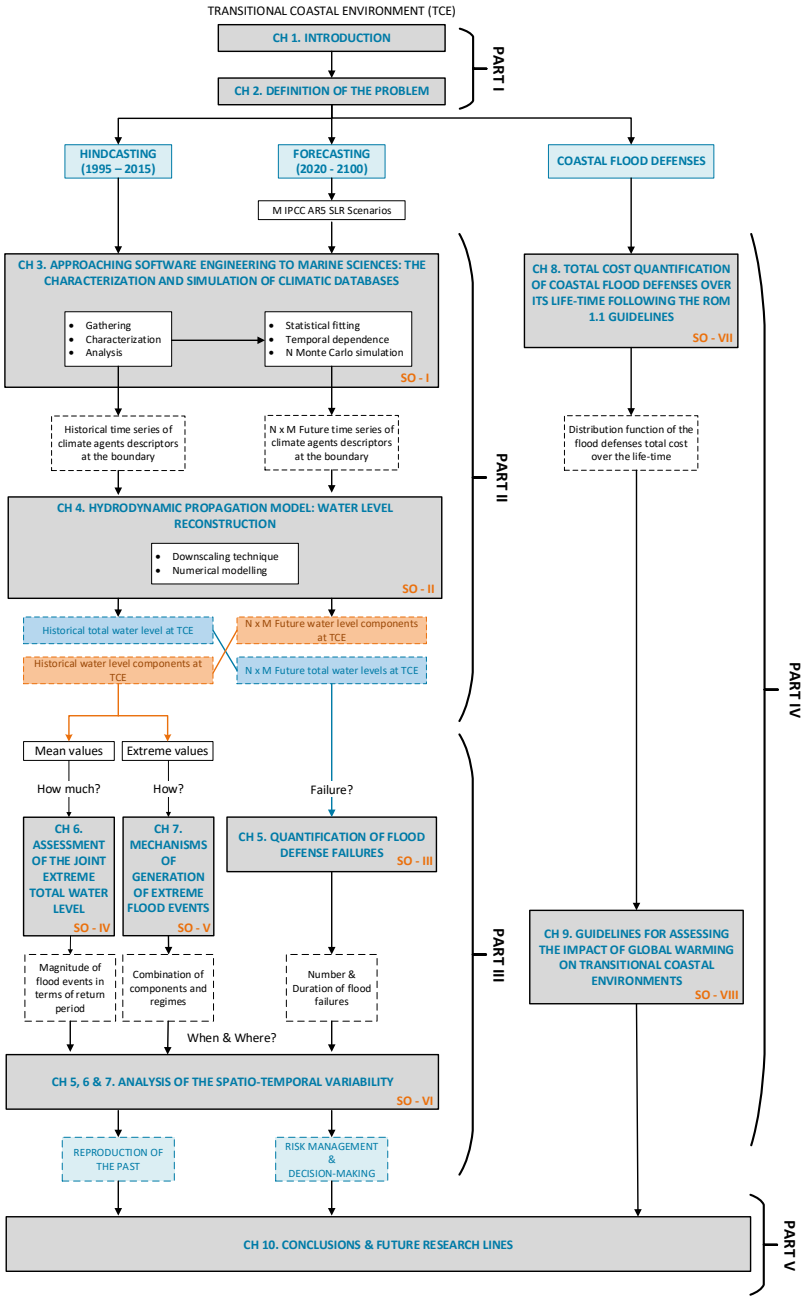

Figure 1.3.1: Thesis outline. Gray boxes indicate the different chapters of the Thesis with the specific objectives in orange. White boxes wth dashed lines indicated the inputs and outputs of the different chapters.

1.4 Publications derived from this Thesis

The work done throughout this Thesis has resulted in the following publications:

Journal Papers

- P. Magaña, R. J. Bergillos, J. D. Rosal-Salido, M. A. Reyes-Merlo, P. Díaz-Carrasco, and M. Ortega-Sánchez (2018a). "Integrating complex numerical approaches into a user-friendly application for the management of coastal environments". In: *Science of The Total Environment* 624, pp. 979 –990. ISSN: 0048-9697. URL: https://doi.org/10.1016/j.scitotenv.2017.12.154

- J. Del-Rosal-Salido, P. Folgueras, M. Ortega-Sánchez, and M. A. Losada (2019b). "Beyond flood probability assessment: An integrated approach for characterizing extreme water levels along transitional environments". In: *Coastal Engineering* 152, p. 103512. ISSN: 0378-3839. URL: https://doi.org/10.1016/j.coastaleng.2019.103512

- P. Magaña, J. Del-Rosal-Salido, M. Cobos, A. Lira-Loarca, and M. Ortega-Sánchez (2020). "Approaching Software Engineering for Marine Sciences: A Single Development Process for Multiple End-User Applications". In: *Journal of Marine Science and Engineering* 8.5. ISSN: 2077-1312. URL: https://doi.org/10.3390/jmse8050350

- J. Del-Rosal-Salido, P. Folgueras, M. Ortega-Sánchez, and M. A. Losada (2020). "Flood management challenges in transitional environments: assessing the effects of sea-level rise on compound flooding in the 21st century". In: *Coastal Engineering (Under review)*

International Conferences

- J. Del-Rosal-Salido, C. Zarzuelo-Romero, M. Díez-Minguito, M. Ortega-Sánchez, and M. A. Losada (2015b). "Residual circulation in the Bay of Cádiz (SW Spain): field analysis and numerical modeling". In: *Proceedings of 2015 Aquatic Sciences Meeting*. Granada, Spain

- C. Zarzuelo, M. Díez-Minguito, A. D. D'Alpaos, L. Carniello, J. Del-Rosal-Salido, and M. Ortega-Sánchez (2016). "Morphodynamic response to human activities in the Bay of Cádiz (2012-2015)". In: *35th International Conference on Coastal Engineering (ICCE)*. Istanbul , Turkey

- J. Del-Rosal-Salido, P. Folgueras, M. Ortega-Sánchez, and M. A. Losada (2017b). "Probabilities of extreme water levels on estuarine urban fronts". In: *Proceedings of International Short Course and Conference on Applied Coastal Research (SCACR 2017)*. Santander, Spain

- J. Del-Rosal-Salido, P. Magaña, P. Bergillos RJ. Díaz-Carrasco, and M. Ortega-Sánchez (2018b). "Easing entry barriers into coastal flooding risk analysis for both end users and researchers: the development of a climatic open-access tool". In: *Proceedings of EGU General Assembly 2018*. Vienna, Austria

- J. Del-Rosal-Salido, P. Díaz-Carrasco, P. Magaña, R. J. Bergillos, M. Clavero, A. López-Ruíz, M. A. Losada, A. Moñino, M. G. Neves, R. Silva, E. Mendoza, S. Solari, and M. Ortega-Sánchez (2018a). "Protection of coastal urban fronts against global warming". In: *Proceedings of EGU General Assembly 2018*. Vienna, Austria

- J. Del-Rosal-Salido, P. Díaz-Carrasco, P. Magaña, R. J. Bergillos, M. Clavero, A. López-Ruíz, M. A. Losada, A. Moñino, M. G. Neves, R. Silva, E. Mendoza, S. Solari, and M. Ortega-Sánchez (2019a). "Addressing the challenge of flooding risk induced by global warming: PROTOCOL Project". In: *Proceedings of 38th IAHR World Congress (IAHR 2019)*. Panamá city, Panamá

- J. Del-Rosal-Salido, P. Magaña, and M. Ortega-Sánchez (2019). "Bridging the gap between software and hydraulic engineering: the development of a climatic open-access tool". In: *Proceedings of 38th IAHR World Congress (IAHR 2019)*. Panamá city, Panamá

- P. Folgueras, J. Del-Rosal-Salido, M. V. Moragues, J. D. Lopez, and M. A. Losada (2018). "Accumulated damage evolution and investment costs of breakwaters". In: *Proceedings of 36th International Conference on Coastal Engineering (ICCE)*. Baltimore, Maryland, USA

Spanish Conferences

- J. Del-Rosal-Salido, C. Zarzuelo-Romero, M. Díez-Minguito, M. Ortega-Sánchez, and M. A. Losada (2015a). " Circulación residual en la Bahía de Cádiz: análisis de datos de campo y modelado numérico". In: *Proceedings of XIII Jornadas Españolas de Ingeniería de Costas y Puertos*. Avilés, Spain

- J. Del-Rosal-Salido, P. Folgueras, M. Ortega-Sánchez, and M. A. Losada (2017a). "Metodología para la tramificación de zonas de transición basada en la interacción entre agentes". In: *Proceedings of XIV Jornadas Españolas de Ingeniería de Costas y Puertos*. Alicante, Spain

- P. Magaña, J. Del-Rosal-Salido, M. Cobos, A. Lira-Loarca, M. Ortega-Sánchez, and M. A. Losada (2019). "Desarrollo de software científico en el ámbito de la ingeniería de costas". In: *Proceedings of XV Jornadas Españolas de Ingeniería de Costas y Puertos*. Torremolinos, Spain

- J. Del-Rosal-Salido, P. Folgueras, M. Ortega-Sánchez, and M. A. Losada (2019c). "Método integrado para la gestión del efecto combinado de agentes climáticos en sistemas costeros de transición". In: *Proceedings of XV Jornadas Españolas de Ingeniería de Costas y Puertos*. Torremolinos, Spain

CHAPTER 2

DEFINITION OF THE PROBLEM

2.1 Introduction

This chapter defines the conceptual framework of the problem to be solved to achieve the general objective of this Thesis, together with the main hypotheses considered. The sections of this chapter are organized as follows: in §2.2, the problem to be solved and the principal hypotheses are stated and defined, whereas the study area used as an example of the application of the defined methodology is described in §2.3.

2.2 Statement of the problem

The primary variable of this work is the total water level, $\eta_T(x,y,t)$, defined as the vertical distance between the water surface and a fixed reference (Local Mean Sea Level, LMSL). This random variable is driven in transitional coastal environments (TCE) by the concomitant effects of mean sea-level rise (SLR), astronomical tide (AT), river discharge (RD), wind waves (WV), and wind effects (WD). The joint effect of these components and their temporal and spatial variabilities are key to analyzing the state of the estuary and its hydrodynamical processes and managing the decision-making process for flood risk analysis.

The temporal framework for the analysis is the state, which is a time interval that ensures the stationarity of the statistical and spectral descriptors of each component.

These descriptors are the amplitudes ($A_i(x,y,t)$) and phases ($\Phi_i(x,y,t)$) of the main dominant tidal harmonic for AT (Serrano et al., 2020); the river flow ($Q(x,y,t)$) for RD; the significant wave height ($H_{m0}(x,y,t)$), the wave period ($T_p(x,y,t)$) and the wave direction ($w_\Theta(x,y,t)$) for WV; and the wind velocity at 10 m height ($u_{10}(x,y,t)$), the wind direction ($u_\Theta(x,y,t)$) and the atmospheric pressure at the mean sea level ($slp(x,y,t)$) for WD. Some of these descriptors (mainly those related to WV and WD) are controlled by the same physical processes, leading to strong relations of dependence between them.

A hydrodynamic model is used to propagate and transform the agents into water levels. To assure weaker dependencies between the variables, the total water level is decomposed (see Eq. 2.1) on the sum of the levels caused by the sea-level rise ($\eta_{SLR}(x,y,t)$) and the astronomical tide, $\eta_{AT}(x,y,t)$ which constitutes the deterministic components; the river discharge, $\eta_{RD}(x,y,t)$, and the weather surges, $\eta_{WS}(x,y,t)$, defined as the water levels related to the agents whose occurrence is associated with the occurrence of a storm (ROM-0.0, 2001; ROM-1.1, 2018) such as the wave set-up, run-up, and storm surge. Finally, the nonlinear component ($\eta_{NL}(x,y,t)$) due to the interaction between the former concomitant variables (Eq.2.1) is also considered.

$$\eta_T(x,y,t) = \eta_{AT} + \eta_{RD} + \eta_{WS} + \eta_{NL} \begin{cases} \eta_{AT}(x,y,t) = f(A_i, \Phi_i) \\ \eta_{RD}(x,y,t) = f(Q) \\ \eta_{WS}(x,y,t) = f(u_{10}, u_\Theta, slp, H_{m0}, T_p, w_\Theta) \\ \eta_{SLR}(x,y,t) \\ \eta_{NL}(x,y,t) = f(\eta_{AT}, \eta_{RD}, \eta_{WS}, \eta_{SLR}) \end{cases} \tag{2.1}$$

This Thesis focused on the stochastic characterization of extreme total water level events (η_T^e) in a specific location (x,y) and instant (t), as the responsible variable of the flood events. In this regard, any given extreme value of the total water level (η_T^e) can be explained as the sum of a number D_s of simultaneous extremes of the η_i^e components plus the contribution of the remaining $D - D_s$ non-extreme elevations η_i^{ne} (Eq. 2.2), where η_i^e, η_i^{ne} and D_s are random variables and D is the number of the water level components. While the normal conditions of the total water level are often a consequence of the combination of mean values of the components ($D_s = 0$), identifying the combination of components (mean or extreme) that leads to extremes is a key factor for the flood risk analysis.

$$\eta_T^e = \sum_{i=1}^{D_s} \eta_i^e + \sum_{i=1}^{D-D_s} \eta_i^{ne} \tag{2.2}$$

2.2.1 Hypothesis

The hypotheses on which the method is based are:

I. The bottom morphology is assumed as fixed. Although it is an important limitation, this hypothesis can be assumed, especially in channelized transitional coastal environments such as river mouths or estuaries where the lateral walls of the channel are fixed, and the bottom changes are smaller than on beaches.

II. This work does not consider the changes due to GW effects in either the forcing agents' distribution function or the main tidal harmonics' components due to the weak and unclear future trends (Woodworth, Menéndez, and Roland Gehrels, 2011; Marcos and Woodworth, 2017; Toimil et al., 2020), which would lead to an increase in the uncertainty of the presented results. Therefore, GW effects are considered through deterministic SLR scenarios. However, it is important to notice that, once the future trend of forced agents is clear, the consideration of these variable agents does not imply any added difficulty to the presented methodology.

III. The transitional coastal environments are considered well-mixed, what allows the use of 2DH hydrodynamic models.

IV. The temporal framework for the analysis is the state, which is a time interval that ensures the stationarity of the statistical and spectral descriptors of each component.

2.3 Description of the study site

The steps of the methodology for the characterization of GW's impact on flooding in coastal urban fronts presented in this Thesis are accompanied by a real case study in the Guadalete estuary. The Guadalete estuary is located in the southwestern part of the Iberian Peninsula ($36°39'N - 36°23'N$, $6°32'W - 6°5'W$). The estuary extends 17 km inland from its mouth in the outer part of the Bay of Cádiz (Atlantic Ocean) to the El Portal dam, as seen in Fig. 2.3.1. The tidal range at the mouth is mesotidal (3.5 m in spring tides (Zarzuelo et al., 2015)), and the main tidal constituent is the semidiurnal M2. The 18.61-year nodal cycle's amplitude at the outer, medium and inner estuary are 1.8, 1.45, and 0.88 m, respectively. Widths are quite variable along the channel of the estuary. Artificial walls channelize the first 4 km (CP 1 - CP 3) on both sides. Widths in this part range from 530 m (CP 1) to 90 m (CP3) and, floodwall height varies from 4 m (CP 1) to 2 m (CP 3) with respect to LMSL. The width in the second part of the estuary (CP 3 - CP 7) varies with high and low tides from 170 to 90 m, while the width in the final part (CP 7 -

El Portal dam) is 65 m. In this region, flood defenses are levees at both sides, whose crest height is between 1.5 and 2.5 m. The channel mean depth oscillates between 5 to 6 m.

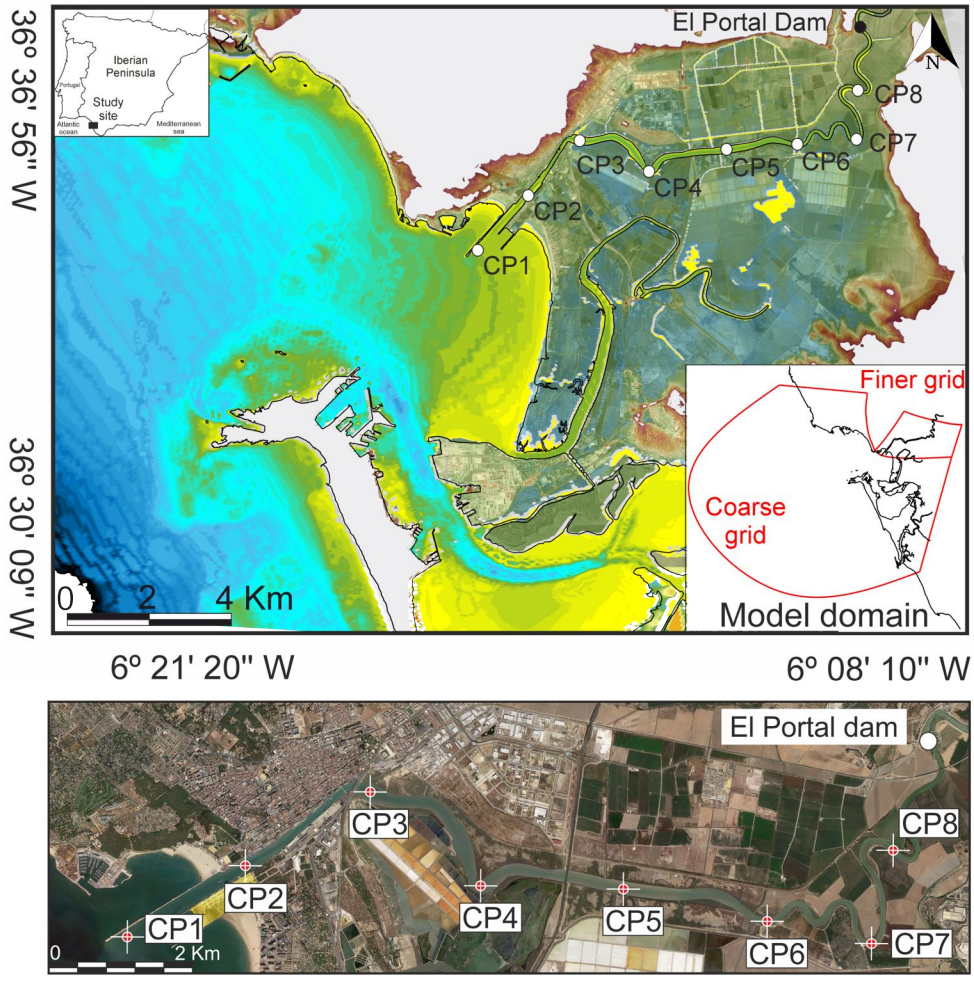

Figure 2.3.1: Study site: Guadalete estuary (Cádiz, southwestern Spain). Red lines show the boundaries of the model grid. The white areas in the color maps of the bathymetry and the topography indicate elevation values above 10 m. Black dots represent the location of the ADCPs and AWAC used in the model calibration. The lower panel shows the control points, where results are obtained, located along the main channel of the estuary.

The Guadalete estuary is a representative example of transitional areas of southern Europe. Its complexity lies in the high number of elements that interact with each other,

giving rise to a hydrodynamically very active and complex area to manage. Fig. 2.3.2 shows the different elements and human alterations that constitute the estuary.

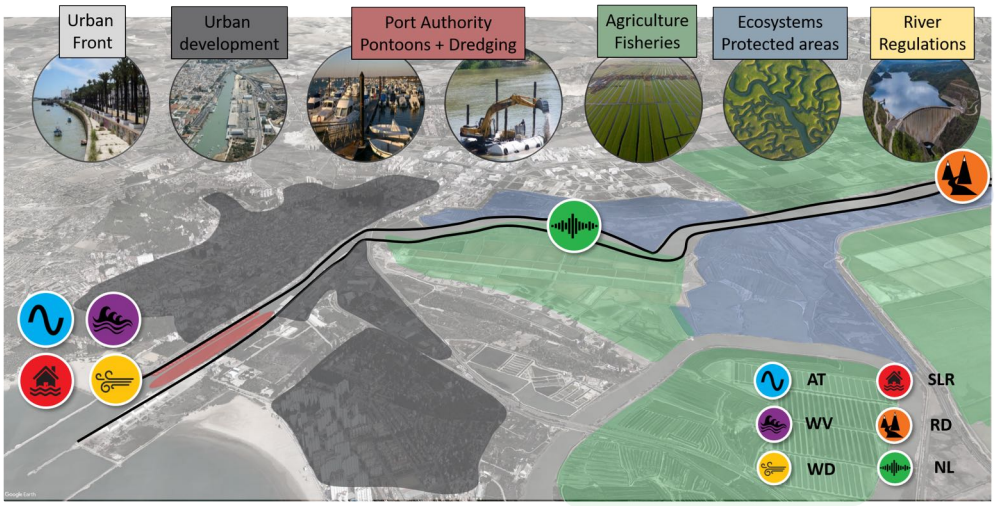

Figure 2.3.2: The elements of the estuary. AT: astronomical tide; WV: waves; WD: wind and sea-level pressure; SLR: sea-level rise; RD: river discharge; and NL: non-linear interactions.

The length of the Guadalete river is 160 km from the Grazalema region to the mouth. Its basin covers an area of 3677 km^2, including the rainiest area in Spain, with an average annual precipitation of 1150 mm in the wet cycles (Tánago et al., 2015; Egüen et al., 2016). The river presents numerous alterations due to human interventions from the mouth to the headwaters. Within the last 3 km, the right margin of the Guadalete estuary is occupied by a recreational marina that reduces the free section of the river. The estuary is channeled by artificial walls on both sides to protect the highly urbanized area from flood events.

The Majaceite River is the main tributary that joins the main stem at Las Juntas (Figure 2.3.3). The upper part of the Majaceite and Guadalete rivers are regulated by five large dams (Table 2.3.1) along their courses (Figure 2.3.3).

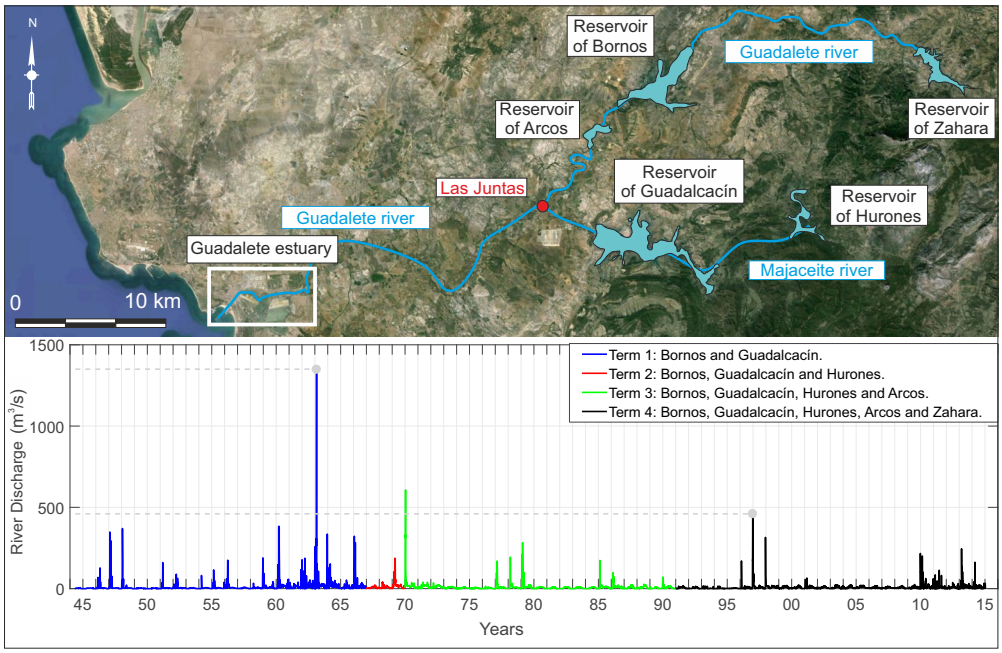

Figure 2.3.3: Upper panel: location of the different reservoirs that regulate the Guadalete and Majaceite rivers. Red points and rectangles indicate the junction of the former two rivers and the case study area, respectively. Lower panel: the sum of the river discharge spilled by the last two dams of the Majaceite and Guadalete rivers from 1945 to 2015. The data are divided into four periods of time (1944-1967; 1967-1970; 1970-1991; 1991-2015) with different colors representing the start of a new dam. Black represents the last period when all river dams were active (1991 - 2015). Gray dots represent the difference of peak discharge between the 1960s (1400 $m^3 s^{-1}$) and 1990s (400 $m^3 s^{-1}$).

Reservoir	River	Storage capacity (hm^3)	Spillway capacity ($m^3 s^{-1}$)	Starting year
Guadalcacín	Majaceite	800	450	1944 (1995)
Hurones	Majaceite	135	917	1967
Arcos	Guadalete	15	1728	1970
Bornos	Guadalete	200	1400	1959
Zahara	Guadalete	223	515	1991

Table 2.3.1: Characteristics of the dams that regulate the Guadalete and Majaceite rivers.

Since 1945, the river discharge into the estuary has been affected several times by constructing five dams along the Guadalete and Majaceite rivers (Tab. 2.3.1.). Therefore, discharges observed in the estuary are seasonal and regulated. The interannual variability of the discharges is conditioned by the wet-dry cycles. In contrast, the intraannual variability reflects the effects of the regulation of the hydrographic basin upstream from the El Portal dam, which increases the river flow during the driest months (Egüen, 2016;

Solari et al., 2017). As observed in the historical record, extreme discharge events only occur during wet cycles due to the need to reduce the volume of the water stored at the dams in case of high precipitation. Despite the river regulation, flooding events have been frequent in the estuary due to the interaction between marine and river oscillations, being especially well-remembered the extraordinary peak flows occurred in the wet period of 1996 - 1997 (450 $m^3 s^{-1}$) and 2009-2010 (250 $m^3 s^{-1}$) when all the dams were already in operation.

Therefore, the Guadalete estuary constitutes a valuable example of transitional areas, and it is also a representative for the southern Europe coasts, considered among the most complex areas for management. This includes the interaction between natural agents with different scales and periods, human interventions, and many stakeholders with different socioeconomic interests.

Part II

Transfer of the dynamics of the climatic agents to the coast

CHAPTER 3

APPROACHING SOFTWARE ENGINEERING TO MARINE SCIENCES: THE CHARATERIZATION AND SIMULATION OF CLIMATIC DATABASES

3.1 Introduction

One of the key and necessary elements to achieve the objectives of this Thesis, to address the impact of SLR on flooding in TCE, is the adequate study and modeling of climate data. Due to the numerous current data sources, formats, as well as diverse methods of analysis, it was proposed to design a necessary tool that allows: (i) gathering the concomitant climate agents from multiple sources; (ii) homogenizing the data from multiple different formats; and (iii) characterizing and analyzing these data. However, software design within the scientific community has certain drawbacks.

Researchers solve problems that are highly specific to their field of expertise. The straightforward application of off-the-shelf software cannot solve these problems, so researchers need to develop tools bound to their exact needs (Brett et al., 2017). Some decades ago, most of the computing work done by scientists was relatively straightforward. However, as computers and programming tools have grown more complex, scientists have hit a steep learning curve.

In Hannay et al. (2009), a survey of almost 2000 scientists was presented. Some of the main conclusions indicated that 91 percent of respondents said using scientific software is important for their research, 84 percent said developing scientific software

is important for their research, and 38 percent spend at least one-fifth of their time developing software. Nevertheless, the most notable finding was that the knowledge required to develop and use scientific software was primarily acquired from peers and through self-study, rather than from formal education and training, which may lead to problems in the future.

As an illustration, researchers do not test or document their programs rigorously as a general rule. They rarely release their codes, making it almost impossible to reproduce and verify published results generated by scientific software. At best, poorly written programs cause researchers to waste valuable time and energy. However, the coding problems can sometimes cause substantial harm and have forced some scientists to retract papers (Miller, 2006; Merali, 2010).

When a researcher publishes an article with code in a scientific journal, other colleagues may adopt this code and build their research upon this software. Many of these scientists rely on the fact that the software has appeared in a peer-reviewed article. This is scientifically misplaced, as the software code used to conduct the science is not formally peer-reviewed. This is especially important when a disconnection occurs between the equations and algorithms published in peer-reviewed literature and how those are implemented in the reportedly used software (Ince, Hatton, and Graham-Cumming, 2012).

Although these warnings have been sent before by some researchers (Peng, 2011; Goble, 2014; Baker, 2017), they are not having a visible effect. Software is pervasive in research, but its vital role is often overlooked by funders, universities, assessment committees, and even the research community itself. It needs to be made clear that if the scientific software is incorrect, so will be science (Miller, 2006).

A possible solution to deal with these problems is hiring software engineers to perform the development of scientific software. While this approach will solve many issues related to the poor quality of scientific software, it usually lacks the physical interpretation or the correct validation of results. Pure software engineers suffer from a lack of expert knowledge in the scientific discipline of the software they are developing. Furthermore, the availability of massive datasets and the application of cutting-edge technologies, such as data mining or deep learning, does not mean that reliable scientific software is being built.

To overcome these issues, a more appropriate proposal is to create a new academic, professional designation, the Research Software Engineer (RSE), which is dedicated to complementing the existing postdoctoral career structure (Robert et al., 2012). RSEs

are both a part of the scholarly community and are professional software developers, who understand the scientific literature and research questions and have a professional attitude towards software development. Their work should be evaluated by both software and academic metrics. Developers of scientific software should have both strong scientific and software engineer background.

Since this Thesis is part of the PROTOCOL project, which has important dissemination and transfer component, in this chapter, an open-access high-quality scientific software for climate data analysis is developed using the software engineer skills mentioned before. Due to its general nature, this tool and methodology are intended to be applied by multiple administrations and coastal managers at any location on Earth. The latest version of the developed tool is available in the following public repository: `https://github.com/gdfa-ugr/protocol`.

In addition to the climate database characterization, to study the impact of the SLR on the flooding along TCE, as well as the analysis of the associated uncertainty, it is necessary to obtain multiple continuous time series of the climatic forcing agents' descriptors along the 21st-century through the simulation technique. Among the different simulation models for climatic variables, it is important to distinguish between those mainly focused on the extreme behavior of the variables. The most common approach is to simulate the time series of storms without simulating the average values of the variables (Callaghan et al., 2008; Lira-Loarca et al., 2020). On the contrary, if the interest is on all the range of values of the variable, various authors proposed methods to simulate the complete series (Guedes-Soares and Ferreira, 1996; Y. Cai and Hawkes, 2007). However, the latter tend to focus on the autocorrelation of the series, and not perform a rigorous check of the time dependence between the series and the extreme behavior. Once the historical climatic databases are characterized, this chapter applied the method proposed by Solari and Losada (2011) and Solari (2011) and Solari and Losada (2012) to simulate the continuous time series of the stochastic climatic agents' descriptors for the period 2020- 2100. This technique constitutes an essential tool for probabilistic design in Coastal Engineering.

The chapter is organized as follows. In §3.2.1 the development of the climate characterization tool is presented. The methodology for the simulation of the climatic forcing agents for the period 2020-2100 is then presented in §3.2.2. Finally in §3.3.1 the deliverables obtained through the application of the tool as well as the results of the characterization (§3.3.2) and simulation (§3.3.3) of the maritime, atmospheric and fluvial agents in the Guadalete estuary are presented.

3.2 Methodology

3.2.1 The development of a climate analysis tool

In the last few years, relevant advances have been made in the field of climate analysis as a primary step for the assessment of flood risk (Rueda et al., 2015; Vousdoukas et al., 2018; Sayol and Marcos, 2018; Del-Rosal-Salido et al., 2019b). However, tools and results are often excessively complicated and time-consuming for stakeholders and end-users; consequently, there is a need for developing simpler tools. The work developed in this chapter fills this gap by developing a simple, modular, and expandable climate tool comprising six modules that simplify the labor of analyzing the joint behavior of the concomitant climatic drivers.

The tool consists of two main blocks, the first centered on data entry and pre-processing, and the second on data analysis. In turn, each of them is divided into three different modules, as shown in Fig. 3.2.1. The first module of the pre-processing block allows the reading of data from various sources, from major European databases such as Copernicus (Hans et al., 2019) to numerical model outputs such as WAVEWATCH III (WW3DG, 2019). The tool then performs a quality analysis of the data. It uses processing functions that have been specifically designed and incorporated for gap-filling or null value detection, among others. Since the tool reads data from multiple sources with different formats, it is necessary to homogenize these formats into a standard one so that the rest of the modules can work independently from the original data source. The developed format, named MetOcean DataFrame, is composed of a Pandas DataFrame plus a series of attributes such as the location or depth (section 3.2.1.1).

The analysis block is, in turn, composed of three other modules. The first module summarizes the fundamental climate analysis, including histograms, wind and wave roses, density functions of the main variables and their correlations, as well as a complete summary of the data, among other options. The tool allows both the automatic graphic representation of the results and the saving of this information with different output formats. The second module performs an analysis of the different variables' normal regime, adjusting different theoretical distribution functions to the data. The tool gives the user flexibility to select different functions and to analyze the fit according to goodness-of-fit tests. Finally, the third module performs an extreme analysis of the variables using the "Peak Over Threshold" (POT) method and fitting the extreme distributions to a Generalized Pareto Distribution (GPD) (Coles, 2001) to be able to extrapolate the data.

Although the functionalities of the developed tool may seem limited, the following considerations should be made. The first one is that the tool is assembled in a modular

way, allowing users, developers, and scientists to add new functionalities according to their needs. Thus, it is possible to quickly and directly incorporate new analysis functions, different graphic representations, or output formats of the results, among others. The second one is related to its versatility; it is essential to highlight that the developed tool automatically reads climate data from any point of the globe and generates a climate analysis report with a low computational cost and for free. This can have a significant impact on developing countries that do not have their instruments or means to analyze their data, but that requires this information to develop their port infrastructures and the protection and improvement of coastal management. The following subsections highlight the main features used during the tool programming.

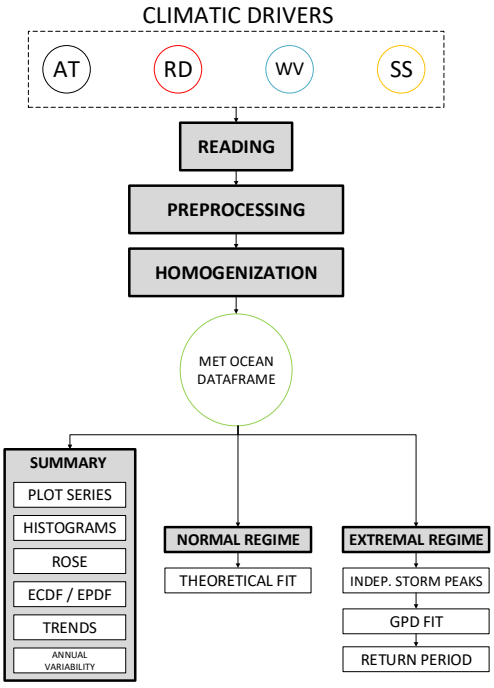

Figure 3.2.1: Scheme of the different modules of the tool. AT, RD, WV and SS stand for Astronomical Tide, River Discharge, Wave and Storm Surge, respectively.

3.2.1.1 The use of open-source tools

While most of the team members had experience with Matlab's scientific platforms, one of the major decisions was the use of the programming language Python. The choice of programming language has many scientific and practical consequences. Python is an increasingly popular and free recommendation of programming language for scientists

(Perkel, 2015). It combines simple syntax and abundant online resources. As a general-purpose programming language, it has no specific support for scientific data structures or algorithms, unlike scientific platforms like Matlab or R. However, it provides a rich ecosystem of science-focused toolkits with strong community support.

One of the significant downsides in the past for Python was its installation. This is currently solved by scientific distributions of Python, such as Anaconda, which have greatly facilitated the adoption of this language. Anaconda includes the SciPy ecosystem, and several code editors so that the scientist can start working with Python without installing anything else. Anaconda includes, among others, packages to perform data cleaning, aggregations and exploratory analysis (Pandas); numerical computation (NumPy); visualizing data (Matplotlib and Seaborn); domain-specific toolboxes (SciPy); machine learning (scikit-learn); organizing large amounts of data (netCDF4, h5py, pygrib); interactive data apps (Flask, Bokeh) or scientific dissemination and divulgation (Jupyter, PyLaTeX).

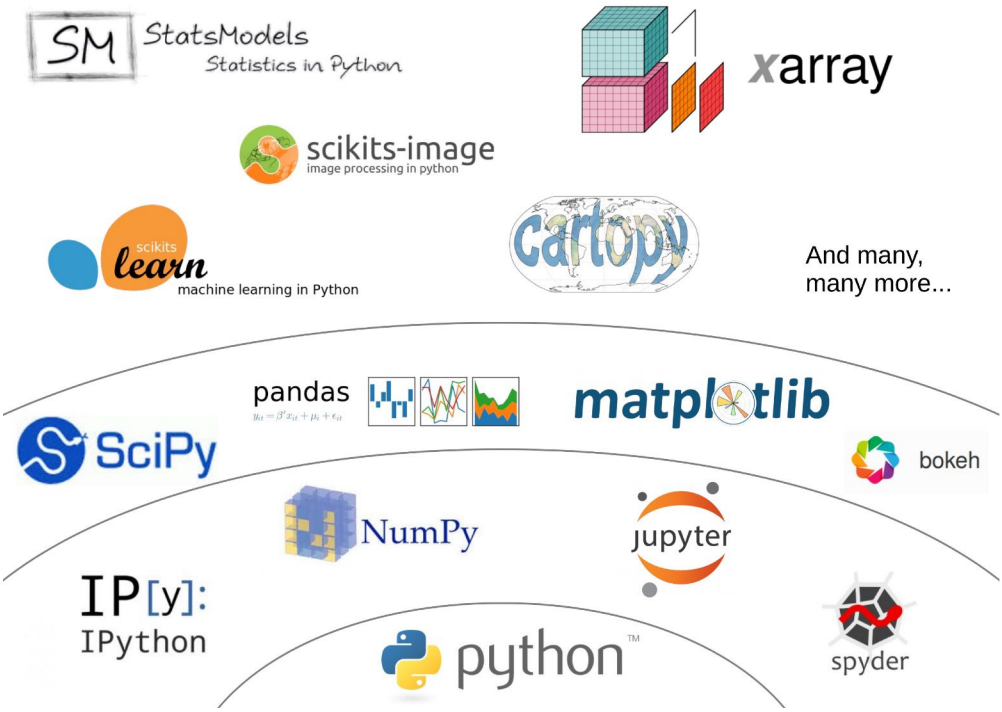

Figure 3.2.2: Scientific Python Ecosystem.

3.2.1.2 Inline code documentation

In the same way that a well-documented experimental protocol makes research methods easier to reproduce, proper documentation helps people understand code. This makes the code more reusable and lowers maintenance costs. The best way to create and maintain reference documentation is to embed the documentation for a piece of software in that software. Python makes this task more comfortable by using documentation strings, also known as docstrings.

Docstrings allow generating documentation into a wide range of output formats, including HTML, LaTeX (for printable PDF versions), manual pages, or plain text. This user-friendly documentation allows other researchers to understand the code, find errors, or even adapt it to their own needs.

3.2.1.3 Modular programming

Modular programming consists of organizing the source code of a program into different modules. Dividing the source code into modules (Python files) and packages (collections of modules) makes it possible to logically organize the program and minimize the number of problems.

As the program grows and changes, it is often necessary to rewrite parts of the source code. Modular programming helps make these changes by isolating where they should occur and minimizing side effects, keeping the code under control, and making it scalable.

The goal of source code separation should be to have modules without any or few dependencies on other modules. When a modular system is created, several modules are built separately and independently. The final application will be created by putting them together. Furthermore, many of these modules and packages could also be reused to build other applications, facilitating the code's reusability.

3.2.1.4 Quality control process

Programs should be thoroughly tested according to the test plans developed in the design phase. We can define unit tests to subject each piece to a series of tests because of our software's modularity nature. Well-designed unit tests may be used to address whether a particular module of code is working correctly and allows testing to proceed piecemeal and iteratively throughout the development process. Robustness is significantly increased because it is easier to test and debug separate components before integrated into a more extensive software system.

Once the unit tests have been successfully passed, the integration tests verify the

correct assemblage between the different components. The integration tests should focus on the interfaces and data flows between the different source code modules. When completed, integration tests verify the data input, flow, and output storage through a string of code modules.

3.2.1.5 Distributed control version

One of the most significant challenges scientists face when coding is the need to track the changes and reverting them if something fails. When the software is built collaboratively, this is even more challenging. It is difficult to determine which changes are in which versions or to exactly how particular results were computed at a later date.

The standard solution in both industry and the open-source world is to use a distributed version control system. Programmers can modify their working copy of the project at will, then commit changes to the repository when they are satisfied with the results to share them with colleagues.

The fact that each developer has its copy of the repository increases the robustness of the version control system since integration is always done on the developers' computers and never on the shared copy of the server. If a problem occurs, it must be solved before changes can be uploaded to the server. This is a noticeable difference to the more common centralized version control systems of the past.

3.2.1.6 Code performance analysis

Although efficiency is a crucial concern in science, it is one of the most ignored facets of scientific software development. As a consequence of the fact that this task is carried out in advanced stages of software development, and usually due to lack of time and other resources, not all the necessary attention is devoted to it.

In scientific software development where computational efficiency is one of the main goals, running-time profiling is necessary. The key to speeding up applications is often understanding where the elapsed time is spent, and why. Profiling helps to extract this information and aid program optimization.

3.2.2 Simulation of climatic agents

3.2.2.1 Maritime and atmospheric forcing agents

Characterized the climatic agents for the historical period, the continuous time series of the stochastic maritime and atmospheric agents' descriptors were simulated for the period 2020-2100 using the approach proposed by Solari (2011) and Solari and Losada

(2011) and Solari and Losada (2012). The simulation of climate time series is a key tool not only for the medium to long-term forecasting but also for its uncertainty assessment, particularly when Monte Carlo techniques for probabilistic designs are applied. According to the mixture distribution models proposed by Solari and Losada (2011) and Solari and Losada (2012), climatic variables can be classified into the lower tail, central regime (the bulk of the data), and upper tail (extremes). While the first two parts of the distributions correspond to the more frequent values, the former is used to define the variable's extremal distribution. This approach is based on fitting a non-stationary simple or mixture model for the lower tail, central regime, and upper tail of the data distribution. A vector autoregressive model (VAR) proposed by Solari and Gelder (2011) was then used to analyze the evolution of the temporal dependence of a variable with itself and with the other variables. This model allows the description of each studied variable's evolution from its own values and the values of the other variables in previous instants of time. These models guarantee that simulated continuous time series have the following same properties as the original (historical) series: marginal probability distribution; seasonal and yearly variations of the statistical descriptors; temporal dependence, autocorrelation, and persistence; storm and peak over threshold (POT) regimes; and rate of annual maximums. As mentioned in the initial hypotheses of this thesis, this method does not consider the GW changes in either the forcing agents' distribution function or the components of the main tidal harmonics.

3.2.2.2 Fluvial forcing agents

However, the former approach was not suitable for the river discharge simulation because of the different behavior observed between dry and wet periods. This behavior is characteristic of highly regulated rivers of southern Europe where the discharges are conditioned not only by the rainfall but also by the river's regulatory regime. Therefore, a POT analysis was performed on the discharge time series to separate the discharge events from the low-flow periods. The selection of a proper threshold is necessary for a confident fitting of the extreme domain. Here, we propose using the automatic methodology from Solari et al. (2017) because it quantifies the uncertainty of the threshold estimation. A different theoretical distribution function was fitted to each regime. A VAR model was then applied to model the temporal dependence.

Once discharge events and low-flow periods are simulated, it is necessary to evaluate the temporal distribution to obtain a complete time series of the river discharge. The standardized precipitation evapotranspiration index (SPEI) (Vicente-Serrano, Beguería, and López-Moreno, 2010), a meteorological drought index, was used to identify the wet and dry seasons. A sample of the following variables was then extracted: (i) number of extreme events during wet seasons, (ii) time interval between extreme events during the

wet seasons, and (iii) time interval between wet seasons. Extreme events during wet seasons were modeled by a Poisson distribution, while the time interval between them followed an exponential distribution due to being rare events (Egüen, 2016). The Normal distribution was then used to model the time interval between the wet seasons. Finally, the continuous hourly time series of river discharge were obtained throughout a Monte Carlo simulation of the variables involved. First, the time interval until the next wet season was simulated. The number of extreme discharge events and the time interval between them was simulated to model the wet cycle. This process was repeated until the end of the simulated period, adding the simulation of the low-flow periods between the extreme discharge events.

The time series of the astronomical tide, of a deterministic nature, were predicted for the 21st-century at the boundary of the study area. The amplitudes and phases of the twelve tidal harmonics along the boundary domain were calculated using the Oregon State Tidal Prediction Software (Egbert and Erofeeva, 2002).

3.3 Results

The developed tool for maritime, atmospheric, and fluvial climate analysis allows having a single source code to generate multiple products addressing different users, as shown in Fig. 3.3.1. Moreover, a new addition to the source code is immediately available to all the products, and thus to every user. Deliverables currently available are tutorials in Jupyter notebooks, users-friendly automated reports, or relational databases. Some potential users include public and private managers, specialized technicians, engineering students, stakeholders, or other scientists.

The tool has been widely tested by the application to different locations along the coast worldwide from open beaches in the Atlantic Ocean to Mediterranean estuaries (Fig. 3.3.2). In particular, it has been applied to obtain the climate analysis at the different study areas of the countries involved in the PROTOCOL project: Caribbean sea (Cancun, Mexico), the Pacific ocean (Valparaiso, Chile), the South Atlantic Ocean (Juan Lacaze, Uruguay), the North Atlantic (Figueira da Foz, Portugal, and El Puerto de Santa María, Spain), and the Mediterranean (Granada Spain) as seen in Fig. 3.3.2. The following are the results obtained for the case study area of Guadalete River estuary located in El Puerto de Santa María, Spain.

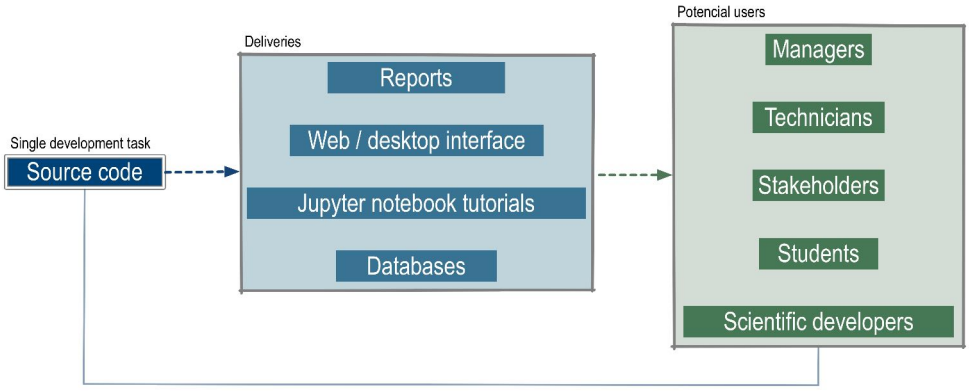

Figure 3.3.1: Diagram with the deliveries and potencial users derived from the single development source code.

Figure 3.3.2: Location of the case studies for the testing and application of the climate analysis tool.

3.3.1 Deliveries of the climate analysis tool

3.3.1.1 Reports

In Coastal Engineering , as in other engineering fields, it is frequent to have to carry out previous and specific studies whose methodology is similar, and in which the input data and the analysis of the results obtained vary. Notably, the maritime climate analysis is essential in any project or study to be carried out on the coast.

The developed tool allows the automatic creation of elaborate LaTeX reports (Fig. 3.3.3) that can be customized according to the specific needs of the user (Code 3.1). Thus, the end-user can choose the output language, the sections to be included, or the types of analysis to be carried out. Empty blocks are also included, in which the user can write (e.g., to discuss the results) that are respected each time the program is run. For example, if a new analysis is included or the length of the data time series is increased, when the code is recompiled, and a new version of the report is obtained, the writing is not deleted.

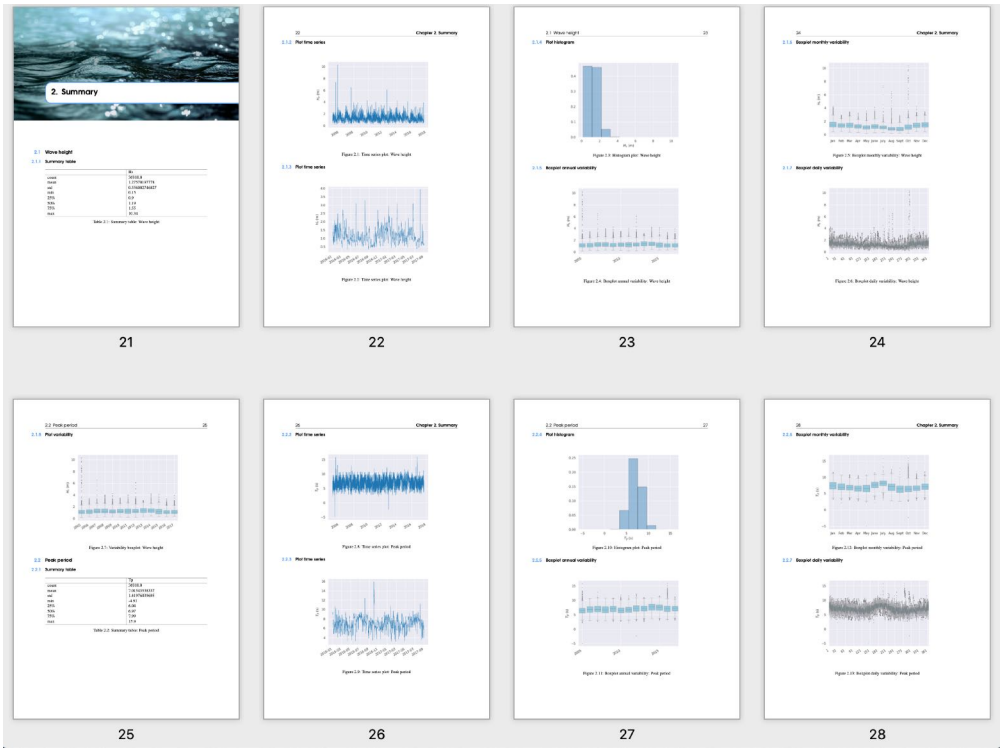

Figure 3.3.3: User-friendly report generated automatically from the tool.

Listing 3.1: Extract of a report template

```
[LANGUAGE]
lang = 'english'

[VARIABLES]
title = 'Cancun (Mexico)'
subtitle = 'Astronomical tide'
author = 'Environmental Fluid Dynamics'

[METOCEAN]
location = 'cancun'

[DRIVERS]

[[TIDE]]
title = 'Tide'

[[[Eta]]]
title = 'Astronomical tide level'
var_name = '$\eta$'
unit = 'm'
ignore_sections = PLOT_GPD_FIT_PEAKS_OVER_THRESHOLD

[[[TABLE_SUMMARY]]]

[[[PLOT_SERIES]]]

[[[PLOT_SERIES_PERIOD_TIME]]]
initial_date = '2016-01-01'
final_date = '2018-01-01'

[[[PLOT_HISTOGRAM]]]
bins = 10
kernel = False
```

3.3.1.2 Jupyter notebook tutorials

One of the most exciting packages for scientists that is currently drawing much attention is the Jupyter notebook (Perkel, 2018). Jupyter is an interactive web tool that researchers can use to combine software code, computational output, explanatory text, and multimedia resources in a single document. Although the use of Jupyter notebooks does not replace conventional development, it does simplify the accomplishment of specific interactive tasks. Its use is especially indicated for data exploration, communication of results, and interactive tutorials. Besides, this tool facilitates reproducibility research.

The technological development that has taken place in recent years has challenged traditional teaching methods. While the theoretical foundations and concepts of the Coastal Engineering field should not be abandoned, the advanced tools currently available need to be integrated into the current teaching systems. To this respect, Ortega-Sánchez et al. (2018) showed (1) the importance of implementing the use of the latest state-of-the-

art technologies and (2) how these methods also help trigger student awareness towards a multidisciplinary, integrated and sustainable way of addressing real engineering problems. Although many advanced numerical models exist today (both commercial and free), technicians working in the field of Coastal Engineering still need to be able not only to analyze advanced data or interpret results but also increasingly, to perform their codes affordably.

For this reason, several tutorial notebooks have been developed interactively explaining the tool's functionalities. Fig. 3.3.4 shows an example that corresponds to the exploratory analysis of a circular variable.

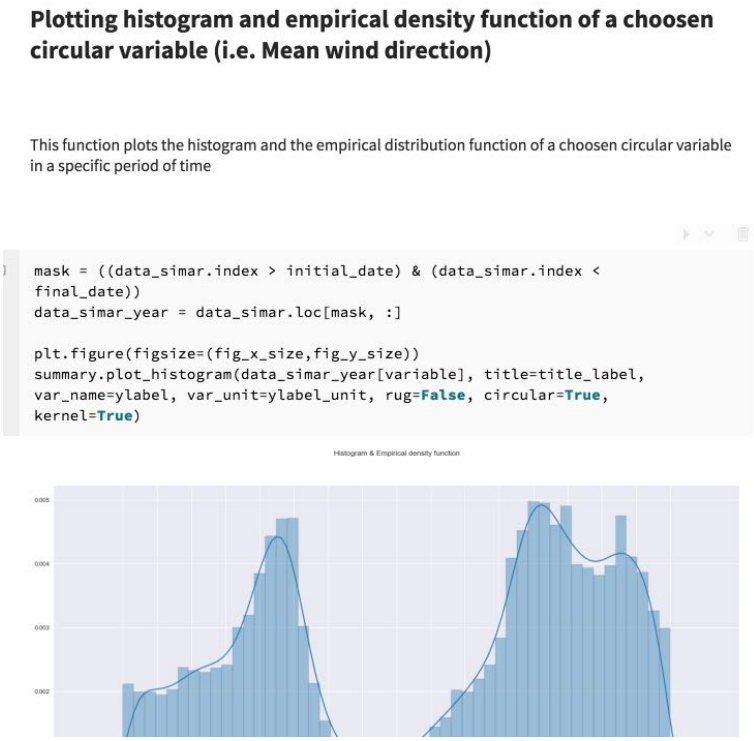

Figure 3.3.4: Histogram and empirical density function of a circular variable in the form of a Jupyter Notebook.

3.3.1.3 Web/desktop interface

The transfer of results and tools to users, administrations, and stakeholders is one of the ultimate goals that applied research should have. Therefore, the development of

methodologies, new calculation methods, or advanced tools must guarantee their smooth transfer and use by end-users.

The disparity of the operating systems used, the different prior training of end-users or even the difficulty of providing physical support has highlighted the importance of promoting applications via the web. This is what is known today as cloud computing, and applications developed within this framework have numerous advantages.

One of the most interesting features of scientific software is prompt support and deployment. The installation and maintenance of scientific software are complicated, involving many packages that may suffer at given time incompatibilities between versions. Cloud computing allows this maintenance to be conducted on the server transparently.

Furthermore, no user requirements are necessary except for a web browser and an internet connection. The processing is done on the server, so it does not matter how powerful the end-users' computers are. They can access it from their different devices (desktop computers, laptop computers, smartphones, or tablets) without any additional effort.

However, if it is necessary for different needs (privacy, or computing capacity) that the calculation is done locally, it is also possible to generate a desktop application without much additional technological effort. The development with web frameworks allows this type of local applications with minimum adjustments.

3.3.1.4 Databases

During the last decades, there has been a vast development of the technology related to the measurement, storage, and analysis of massive data (Bryant, 2011). Thus, today, cloud computing methods and analysis tools, such as data mining (Magaña et al., 2014), machine learning, and artificial intelligence, in general, are being applied in practically all areas of society.

In the field of Coastal Engineering and earth sciences, there has also been a substantial development due to a higher computing capacity, which allows large datasets infrastructures (Hans et al., 2019) to be obtained at a global and regional level. At the local level, the measurement techniques and the implementation of detailed numerical models are also allowing to have significant sources of data not only climatic but also, for example, hydrodynamic or bathymetric. One of the critical elements of all these data sources is their standardization and implementation in Geographic Information Systems for easy use by different users.

This tool has allowed the automatic creation of a database (Fig. 3.3.5). By implementing a relational database, the applications can interact and integrate the information it stores to be reused.

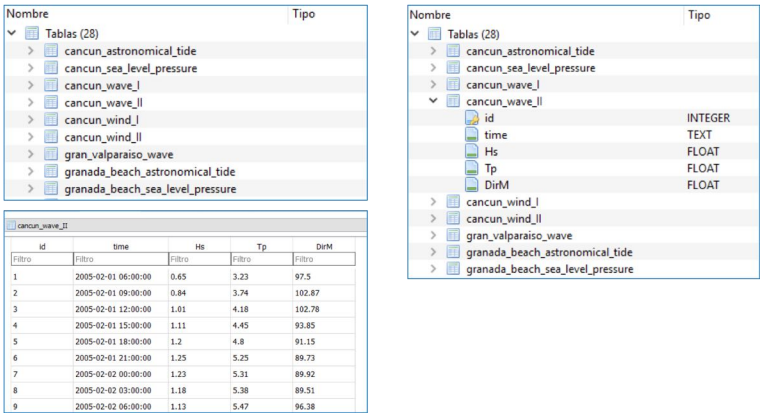

Figure 3.3.5: Automatic generated databased.

3.3.2 Characterization of climatic agents

3.3.2.1 Maritime and atmospheric forcing agents

In the case study analyzed in this Thesis, hourly waves and wind parameters are recorded at the Buoy of Cádiz (data provided by Puertos del Estado, Spain) from 1995 to 2015 (Fig. 4.3.1). This period comprises the only historical complete nodal cycle in which all the dams in the Guadalete estuary were in operation (Tab. 2.3.1). The wave climate analysis in the Bay of Cádiz indicates that the prevailing incoming wave directions are West-Southwest (Atlantic storms). The 50th, 90th, and 99th percentile of the significant wave height distribution are 1 m, 2.5 m, and 4 m. Values above 5 m have been registered during extreme storm events. The central body (25 - 75th percentiles) of the wind direction takes values between 100 and 300 degrees with no annual seasonality (Fig. 3.3.6). Thus, predominant wind direction is southwest with peaks of extreme wind events over 15 $\mathrm{m\,s^{-1}}$. Mean sea level pressure series have been obtained from the ERA-Interim, a global atmospheric reanalysis model updated in real-time since 1979 (Dee et al., 2011).

The amplitudes and phases of the twelve dominant tidal harmonics along the boundary domain are determined using Oregon State Tidal Prediction Software (Egbert and Erofeeva, 2002). The maximum amplitudes of the AT in this estuary are approximately ±2 m respect LMSL. Fig. 3.3.7 represents the time series of the forcing maritime agents from 1995 to 2015.

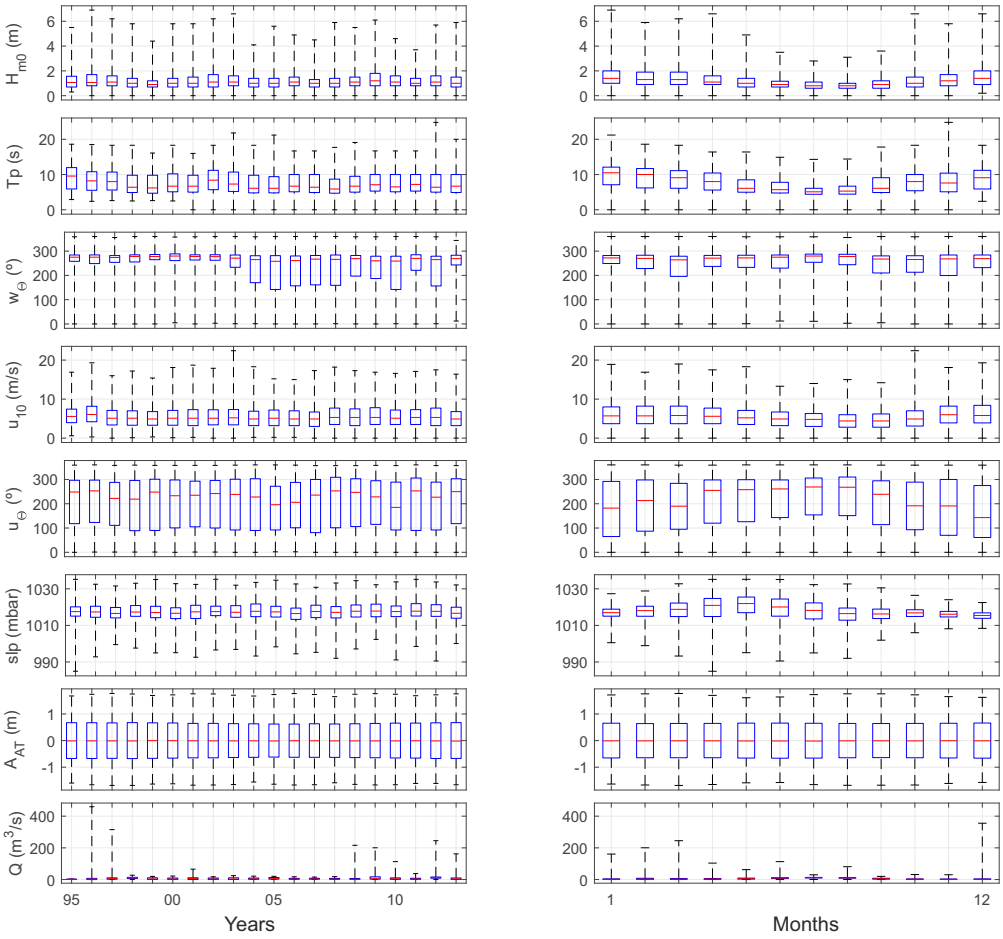

Figure 3.3.6: Boxplots with the annual (left) and monthly (right) variability of the descriptors of the agents: significant wave height (H_{m0}), wave period (T_p), wave direction (w_Θ), wind velocity at 10 m height (u_{10}), wind direction (u_Θ), atmospheric pressure at the mean sea level (slp), amplitudes of tidal wave (A_{AT}) and river flow (Q).

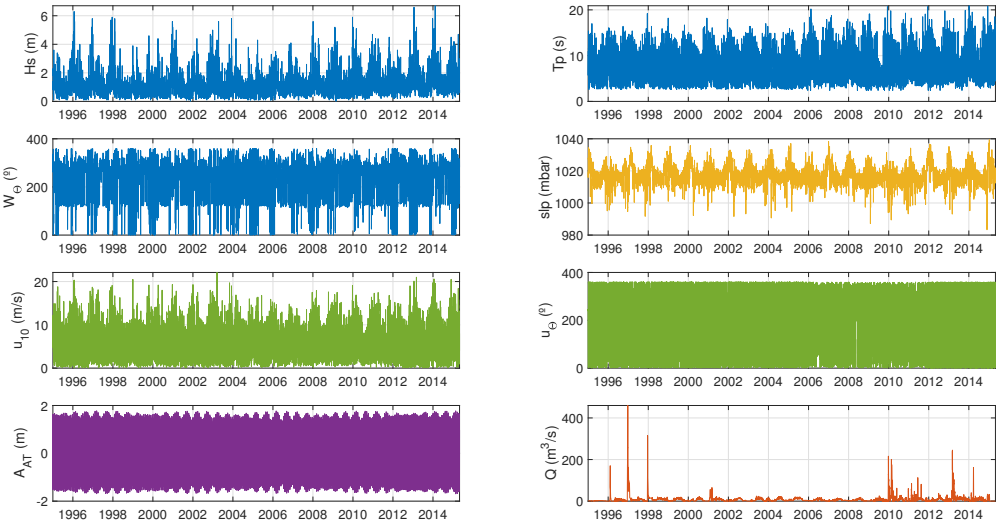

Figure 3.3.7: Historical time series of climatic forcing agents' descriptors.

Fig. 3.3.8 shows a sample of the outputs of the summary module of the developed climate analysis tools applied to the Bay of Cádiz. The first row illustrates the wave (left) and wind (right) roses, the second row shows the scatter diagram between significant wave height and wave direction (left) and wind velocity and direction (right). The third row shows the empirical cumulative distribution function for the significant wave height and wind velocity. Fig. 3.3.9 illustrates the empirical (orange dots) and theoretical (blue line) extreme values of the significant wave height (left), wind velocity (middle), and river discharge (right) for the different return values with the 95 % confidence bands.

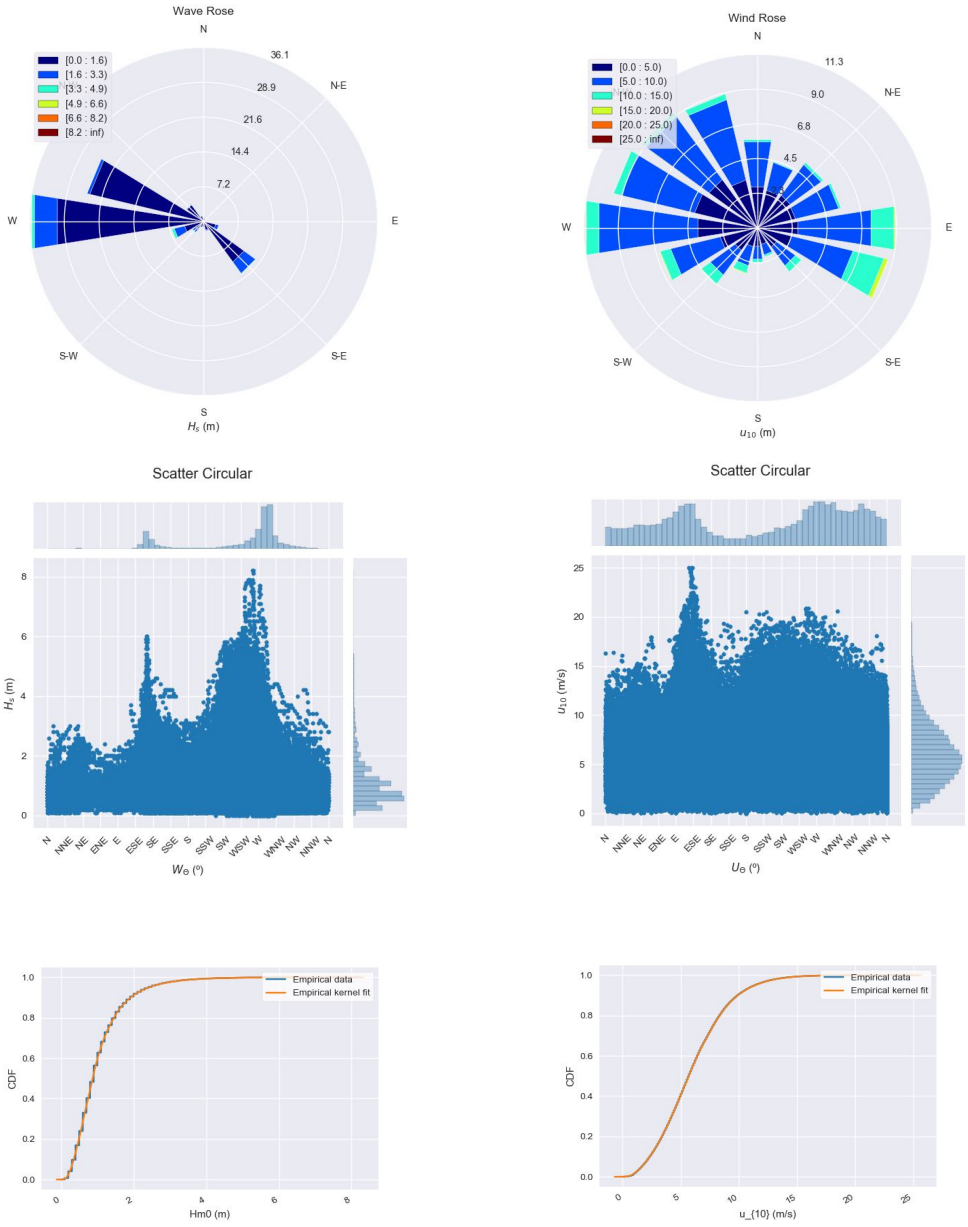

Figure 3.3.8: Outputs of the summary module of the climatic analysis tool.

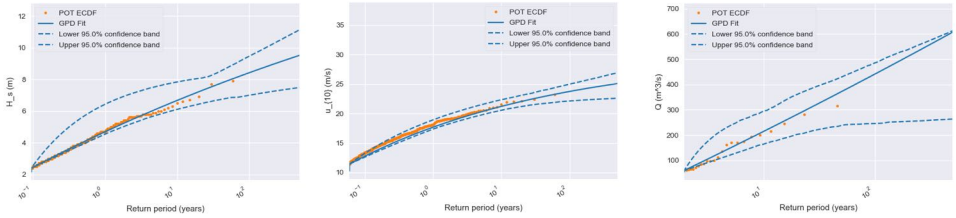

Figure 3.3.9: Outputs of the extremal module of the climatic analysis tool. Orange dots correspond with the empirical extreme values, the blue curve represents the theoretical extreme value curve for the different return periods and the doted blue lines represent the 95 % confidence bands

3.3.2.2 Fluvial forcing agent

The fluvial agents are considered through the sum of the water spilled by the last two dams of the Majaceite (Guadalcacín) and Guadalete (Arcos) rivers since all the dams were active (1995) measured by the SAIH, Andalusian Regional Government (see Fig. 2.3.3). The fluvial regime has a pronounced seasonal variability between the wet season (i.e., from December to March) and the driest months of July and August, when the river discharge may be nearly zero (Fig. 3.3.6). The 50th (median), 90th and 99th percentiles of the river discharge distribution measured at Las Juntas in the period 1995 - 2015 are 4 $m^3 s^{-1}$, 15 $m^3 s^{-1}$ and 85 $m^3 s^{-1}$, respectively.

As seen in the time series of Fig. 2.3.3, the river regulation has reduced the river peak flow by 70%, from 1400 $m^3 s^{-1}$ in the 1960s to over 400 $m^3 s^{-1}$ in 1990s. In both decades, the registered annual precipitation was approximately 3000 mm in the Grazalema region. However, river discharges exceeding 1400 $m^3 s^{-1}$ can be expected if the reservoirs are approaching full capacity (Table 2.3.1).

3.3.3 Simulation of climatic agents

3.3.3.1 Maritime and atmospheric forcing agents

Following the methodology described in section 3.2.2, continuous time series of the stochastic maritime and atmospheric agents' descriptors (Hm_0, T_p, w_Θ, u_{10}, u_Θ, slp) are simulated for the period 2020-2100 (80 years) using historical data. A log-normal distribution for the central region and a Generalized Pareto distribution for the tails were used to describe the significant wave height (Hm_0). Two log-normal distributions and two truncated normal distributions were used to describe the spectral peak period (T_p) and the incoming offshore wave direction (w_Θ) to reproduce the bimodal wave climate

observed in this case. For the atmospheric variables, a Weibull and normal distribution functions were used to model the wind velocity (u_{10}) and sea level pressure (slp). Two truncated normal distributions were also used for the wind directions (u_Θ) to capture the wind's two main directions. The former distribution models have been widely used in Coastal Engineering (e.g., Magaña et al. (2018b) and López-Ruiz et al. (2018)). A fourth-order non-stationary distribution function was selected in these cases, to capture from annual variabilities up to one month and a half. Fig. 3.3.10 shows a range of percentiles of the non-stationary empirical (orange) and fitted (blue) cumulative distribution function (CDF) for the six maritime and atmospheric agents' descriptors. As seen, the selected theoretical distributions adequately reproduce the behavior of the hindcasted data.

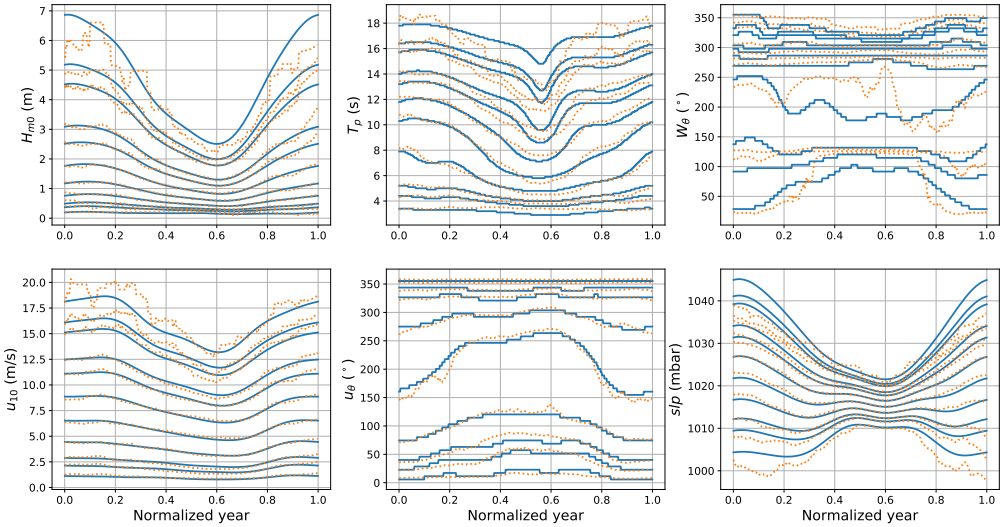

Figure 3.3.10: Non-stationary empirical (orange) and fitted (blue) CDFs for 0.01, 0.05, 0.1, 0.25, 0.5, 0.75, 0.9, 0.95, 0.99, 0.995 and 0.999 percentiles along a normalized year for the stochastic maritime and atmospheric agents' descriptors.

3.3.3.2 Fluvial forcing agents

Regarding the river discharge, a different behavior was observed between dry and wet periods due to the high river flow regulation of the five dams along the hydrological basin. Dry periods present a low-flow regime with an intraannual variability from zero discharge to 30 $m^3 s^{-1}$ to maintain the ecological river flow. On the contrary, in wet seasons, an extreme discharge event per year is observed during winter months on average. These extreme events are similar to pulses where the discharge increases from 30 to 450 $m^3 s^{-1}$ in several days (Egüen, 2016). Therefore, a POT analysis (Solari et al., 2017) was performed over the discharge time series to separate the discharge events

from the rest of the series. A stationary Weibull distribution function was used to model the discharge events. In contrast, a non-stationary second-order normal distribution was used to describe the river flow's low-flow periods.

To assess the continuous 21st-century time series of the river discharge, the SPEI (Vicente-Serrano, Beguería, and López-Moreno, 2010) was then used to identify the wet and dry seasons. Fig. 3.3.11 illustrates the normalized historical time series of the SPEI (data obtained from https://spei.csic.es/index.html) and river discharge into the Guadalete estuary. Red and yellow areas correspond to wet and dry seasons, respectively. The blue line represents the river discharge time series from 1960 to 2015. As seen, extreme discharge events correspond with wet seasons, and no more than one event is observed per year during winter months. Therefore, the extreme events during wet seasons and the time interval between them were modeled by a Poisson distribution and an exponential distribution. Normal distribution was then used to model the time interval between the wet seasons. Due to the continuous problems of filtration in the Guadalcacín dam, this dam is capable of containing a high volume of water. However, as soon as the water volume in this reservoir exceeds a certain threshold, the dam discharges 100 % of the water that enters the reservoir due to the risk of breaking it. This explains the extreme river discharge peaks in a short period of time observed in Fig. 3.3.11 during floods (Egüen, 2016).

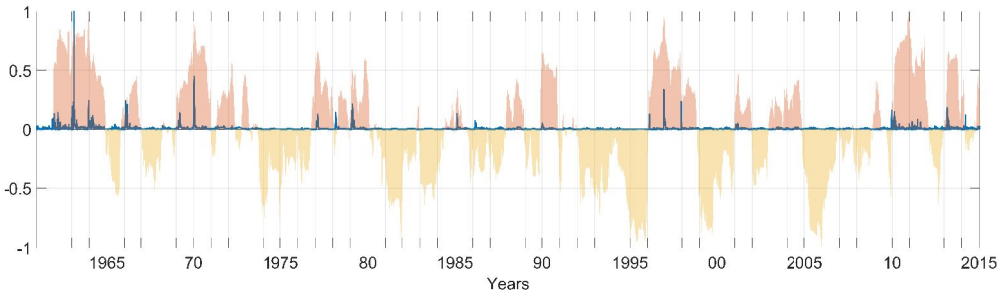

Figure 3.3.11: Normalized historical SPEI index and river discharge time series from 1960 to 2015. Red and yellow areas correspond with wet and dry seasons respectively. Blue line represent the river discharge time series from 1960 to 2015.

Fig. 3.3.12 shows the comparison between the empirical cumulative distribution functions of the hindcasted data (blue) and the forecasted simulations (orange) for the eight forcing agents' descriptors. A deviation of the simulations from the hindcasted data is observed for cumulative probability values above 99.9 % for some agents' descriptors, especially for the river discharge. These deviations are since both the number of wet cycles and the number and magnitude of discharge events within each wet cycle show

considerable variability between the different simulations. Thus, we can find simulations with low intensity and frequency of river discharge events called from now on “low-frequency discharge simulations”, and simulations with frequent and intense river discharge events, denominated as “high-frequency discharge simulations”. A different number of simulations have been tested to assess the uncertainty related to the variation of the stochastic climatic agents, particularly the river discharge. No changes are observed in the results when increasing the number of simulations above 100.

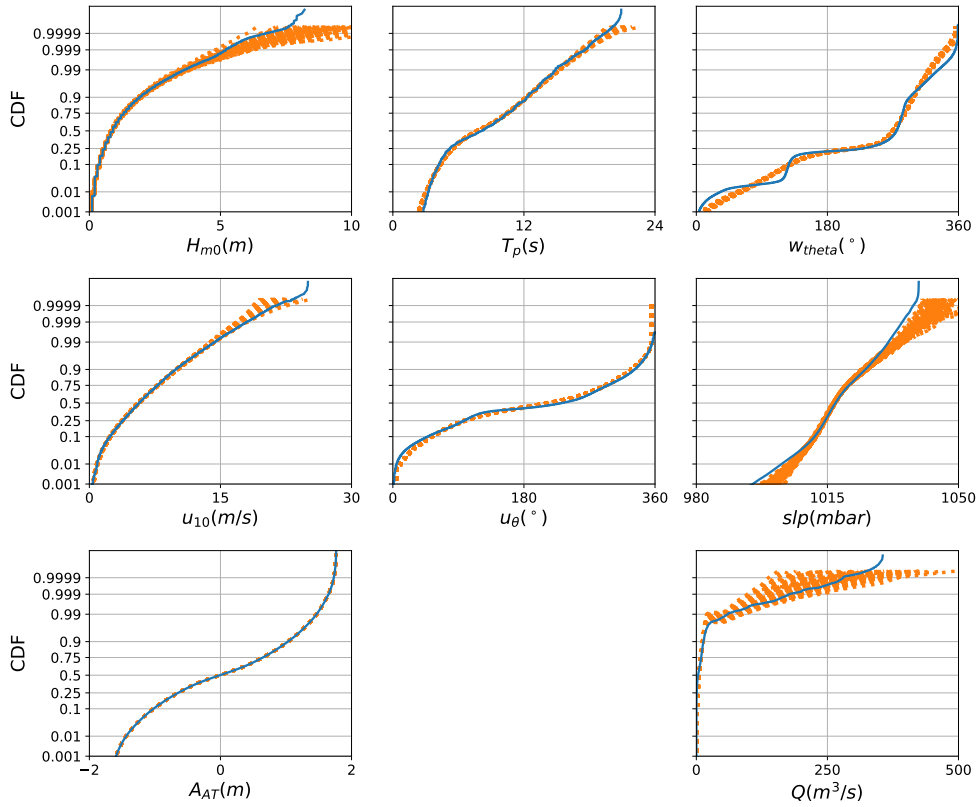

Figure 3.3.12: Empirical (blue) and simulated (orange) cumulative distribution function for the Hm_0, T_p, w_Θ, u_{10}, u_Θ, slp, A_{AT} and Q .

3.3.4 Sea-level rise scenarios

Yearly global mean SLR projections up to 2100 for the Southwestern part of the Iberian Peninsula, obtained from the Fifth Assessment Report of the Intergovernmental Panel on Climate Change (IPCC-AR5) (Church et al., 2013) and available through the Integrated

Climate Data Center website hosted at the University of Hamburg (https://icdc.cen.uni-hamburg.de/en/ar5-slr.html), have been used. These projections consist of 1° × 1° gridded sea surface height fields relative to the average for the period 1985-2005 that include dynamic ocean changes, global ocean thermal expansion, inverted barometer effect, melting land ice from Greenland, Antarctica and glaciers, changes in land water storage and glacial isostatic adjustment. Although more updated SLR projections exist (Jevrejeva et al., 2019), the IPCC provides the most widely accepted scientific information about climate change. The projections included in the latest published version of the Assessment Report (IPCC AR5) were the most up-to-date datasets available for central range projections (probability of at least 66 % of the distribution). Therefore, to consider the set of projections that span the aforementioned central range, in this Thesis the lower limit of the central range of the IPCC-AR 5 RCP4.5 (from now on denominated in this Thesis as RCP4.5_05) scenario and the upper limit for the RCP8.5 (RCP8.5_95) scenario have been considered as the SLR projections in this Thesis (Fig. 3.3.13).

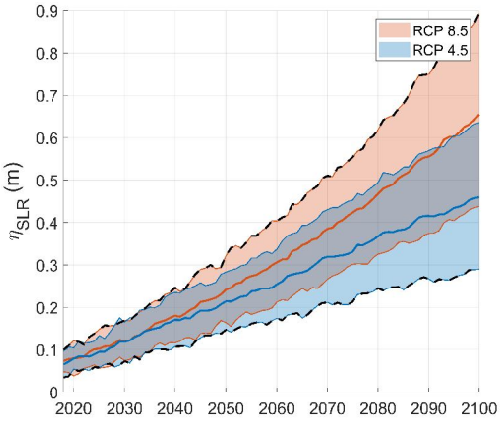

Figure 3.3.13: Total ensemble mean SLR curves with the confidence bands for the RCP 4.5 (blue) and RCP8.5 (orange) IPCC AR 5 datasets (Church et al., 2013) for the Southwestern coast of the Iberian Peninsula. Dashed lines represent the RCP4.5_05 and RCP8.5_95 SLR scenarios used in this work.

3.4 Summary and conclusions

The use of scientific software is an indispensable tool for the research community today. However, researchers need to develop their own software to adapt it to their needs. The use of commercial software is not valid, and this presents significant disadvantages for science. First of all, most researchers do not know about software development, which makes the developed codes of poor quality and difficult to use by the rest of the scientific

community. Secondly, when a researcher publishes an article with code in a scientific journal, other colleagues may adopt it and build their research upon it. However, the software code used to conduct the science is not formally peer-reviewed on most occasions.

In this chapter, an open-access high-quality scientific software for climate analysis to characterize the different atmospheric, maritime, and fluvial forcings is developed using the software engineer skills. The latest version of the developed tool is available in the following public repository: https://github.com/gdfa-ugr/protocol. The characterization of the climate database is the first necessary step in characterizing the impact that sea-level rise will have on flooding in coastal urban fronts. This chapter is structured in two parts, methodology and results, which are subdivided into two other parts. The first part develops the tool for the analysis of the offshore climate database. In contrast, the second part focuses on the future simulation of the historical database to have climate series throughout the 21st-century. The following conclusions can be drawn from the analysis presented in the previous sections:

- A software tool has been built following some software engineering design guidelines to bridge the gap between Coastal Engineering and software development. This framework provides the tool with great robustness, versatility, and the possibility of scalability and improvement in the future.
- Once the framework has been developed, some modules have been implemented for reading, pre-processing, standardized, and analyzing the climate data. This analysis includes histograms and density functions of the main variables and their correlations, a complete summary of the data, and a complete analysis of the extreme regime.
- With a single development, the designed tool allows the creation of different products oriented to different users: from managers to students, including also profiles such as researchers or developers. Some of the products already available from the tool include Jupyter notebooks and the automatic generation of elaborate reports and relational databases.
- The analysis of the maritime and atmospheric agents indicates that the prevailing incoming wave directions are West-Southwest (Atlantic storms) with extreme wave height up to 5 m. Regarding the river discharge, a completely different behavior was observed between dry and wet periods due to the high river flow regulation with maximum peaks of river discharge around 450 $m^3 s^{-1}$ since all the dams in the river basin were active. The maximum amplitudes of the AT in this estuary are approximately ± 2 m respect LMSL.

- The simulation of climate time series is a key tool not only for the medium to long-term forecasting, but also for its uncertainty assessment, particularly when Monte Carlo techniques for probabilistic designs are applied. These simulations account for the wave, wind, sea-level pressure, and river discharge descriptors. In this Thesis, we follow the approach of Solari and Losada (2011) and Solari and Losada (2012) for the simulation of 100 continuous time series of the forcing agents along the 21st-century.
- Two deterministic SLR scenarios are considered to assess the uncertainty related to the SLR variability: the lower confidence band of the RCP 4.5 (defined as RCP4.5_05) and the upper band of the RCP 8.5 (defined as RCP8.5_95).

CHAPTER 4

HYDRODYNAMIC PROPAGATION MODEL: WATER LEVEL RECONSTRUCTION

4.1 Introduction

Systematic measurements of water levels along estuaries are rarely available (Díez-Minguito et al., 2013; Losada, Díez-Minguito, and Reyes-Merlo, 2017) and expensive, and even less information is available on the contribution of the different agents to these levels. This chapter presents the methodology for propagating and transforming the historical and future continuous time series of the climatic agents' statistical descriptors, located in the boundaries of the study area, into continuous time series of water levels along the estuary.

Because of the complexity of this transformation, the use of an advanced numerical model is proposed. In terms of computational cost, using a long time series of simultaneous climatic variables to reconstruct total water levels is challenging. The number of variables involved and the span of the dataset implies a vast number of numerical calculations with advanced numerical models. According to Camus, Mendez, and Medina (2011) three general approaches have been developed to downscale the large-scale information: (i) a dynamical approach consisting on nesting higher resolution models that account for the hydrodynamic and wave propagation processes; (ii) a statistical approach, in which an empirical relationship between offshore and nearshore variables is used to obtain reliable small-scale information; and (iii) a hybrid approach which combines dynamical

(numerical models) and statistical downscaling in order to reduce the computational effort.

This chapter is organized as follows. First, the description of the two complementary approaches for the reconstruction of the total water level and its components are defined in §4.2.1. Each approach is then described in-depth in §4.2.2. Regarding the results section, where the methodology is applied to the case study area, the implementation and calibration of the numerical hydrodynamic model are shown in §4.3.1, whereas the reconstruction of the water level for the historical and future periods are shown in §4.3.2 and §4.3.3 respectively.

4.2 Methodology

4.2.1 Model description

This section presents the methodology for the reconstruction of historical and future continuous time series of water levels along a transitional coastal system. Therefore, the use of the hybrid downscaling technique (Camus, Mendez, and Medina, 2011), with the specific modification described below to adapt this methodology to water levels in transitional coastal areas, is proposed in this Thesis to reduce this computational cost.

To isolate each component's contribution to the total water level, two different approaches, dependent and independent, have been defined (Fig. 4.2.1). The independent approach calculates the time series corresponding to each water level component by propagating each agent individually and setting the remaining agents to zero. In the dependent approach, the time series of the total water level is calculated considering the simultaneous effects of the concomitant agents, including the non-linear interactions between them. Hence, the non-linear term can be easily calculated through Eq. 4.1. This approach is first applied to the historical climatic database to reconstruct the historical time series of water levels. The approach is then repeated for each simulation of the climatic forcing agents throughout the 21st-century to reconstruct the future water levels.

$$\eta_{NL}(x,y,t) = \eta_{T}(x,y,t) - \left[\eta_{AT}(x,y,t) + \eta_{RD}(x,y,t) + \eta_{WS}(x,y,t)\right] \tag{4.1}$$

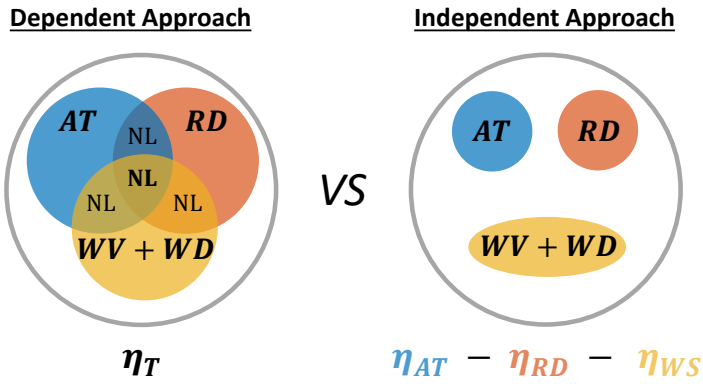

Figure 4.2.1: Dependent (left) versus independent (right) approaches defined in this work.

4.2.2 Water level reconstruction

First, from the whole set of climatic agents' descriptors (dependent approach), a reduced number of "M selected cases" is extracted using the Maximum Dissimilarity Algorithm (MDA), which finds the most dissimilar data in the database and properly represents the outer limits of the input boundary space (Camus et al., 2011; Gouldby et al., 2014; Rueda et al., 2015). On the one hand, vector components (X_i) must be normalized to be equally weighted in a similar criterion, defined by the Euclidean distance (Eq. 4.2)

$$
\begin{aligned}
||X_i - D_j|| = \Bigg[& (H_{m0_i} - H^D_{m0_j})^2 + (T_{p_i} - T^D_{p_j})^2 + \left(min\left(|W_{\theta_i} - W^D_{\theta_j}|, 2 - |W_{\theta_i} - W^D_{\theta_j}| \right) \right)^2 \\
& (slp_i - slp^D_j)^2 + (u_{10_i} - u^D_{10_j})^2 + \left(min\left(|u_{\theta_i} - u^D_{\theta_j}|, 2 - |u_{\theta_i} - u^D_{\theta_j}| \right) \right)^2 \\
& + (A_{AT_i} - A^D_{AT_j})^2 + (Q_i - Q^D_j)^2 \Bigg]^{1/2}
\end{aligned}
\tag{4.2}
$$

The MDA subset is therefore defined by: $D^*_j = H^D_{m0_j}, T^D_{p_j}, W^D_{\theta_j}, slp^D_j, u^D_{10_j}, u^D_{\theta_j}, A^D_{AT_j}, Q^D_j; j = 1, ...M$.. Second, the hydrodynamical and wave propagation models are used to transform these outer M cases into water level values at different locations along the estuary. To guarantee the stationarity of the resulting water levels, the numerical hydrodynamic model is forced with the selected constant values between 24 and 48 hours. The water level value associated with the forcing agents is extracted, taking into account the time-lag at each point due to the agents' propagation. Finally, the reconstruction of the total water level time series is performed via the radial basis functions (RBF) (Franke, 1982; Hardy, 1990), which represents a very convenient interpolation technique for

scattered and multivariate data (Camus, Mendez, and Medina, 2011; Guanche et al., 2013; Gouldby et al., 2014). The RBF interpolation method consists of a weighted sum of radially symmetric basic function located at the data points. The interpolation function is calculated by means of this expression:

$$RBF(x) = p(x) + \sum_{j=1}^{M} a_j \Phi(||x - x_j||) \tag{4.3}$$

where Φ, is a Gaussian function with a shape parameter c:

$$\Phi(||X_i - D_j||) = exp\left(-\frac{||X_i - D_j||^2}{2c^2}\right) \tag{4.4}$$

$||||$ the Euclidean norm; $p(x)$ is a monomial basis $[p_0, p_1, ..., p_n]$, formed of a number of monomials of degree 1 equal to the data dimensions (n) and a monomial degree 0, being $b = [b_0, b_1, ..., b_n]$ the coefficients of these monomials. The RBF coefficients a_j and the monomial coefficients b are obtained by enforcing the interpolation constraints $RBF(x_i) = f_i$. Where, $f_i = f(x_j); j = 1, ..., M.$ are the real-values that we want to approximate obtained through the numerical model. The algorithm proposed by Rippa (1999) is used to select the optimal value of the shape parameter of the radial basis functions. For further details about the MDA and RBF functions, readers are referred to Camus et al. (2011) where algorithms are described in detail.

At this point, a sensitivity analysis is needed to optimize the number of "selected cases" that minimizes the error of the reconstructed elevations. The individual water level components are obtained via the repetition of previous steps for each agent separately (independent approach).

Once the historical water levels are reconstructed, a similar process is followed to reconstruct the future water levels along the 21st-century. The significant difference lies in the multiple time series for each forcing agent at the boundary associated with the different simulations. For each SLR scenario, the same method is used to reconstruct the future hourly time series of total and individual water levels corresponding to the forcing agents' first simulation. A subset of representative cases is extracted from the whole dataset using a clustering approach MDA algorithm. Then, the hydrodynamic model is used to transform the selected cases to the total water level. In this process, the parameters that relate the boundary agents with the total water level in the estuary are calculated. With these transformation parameters, the continuous time series of the total water level is reconstructed for the first simulation throughout RBF. For the

remaining simulations, the transformation parameters obtained in the first simulation were used to directly calculate the corresponding total water level series (dependent approach), minimizing the computational cost. The same technique is applied to each agent individually to obtain the future water level time series associated with each component (in the so-called independent approach).

4.3 Results

4.3.1 Delft3D implementation and calibration

Delft3D WAVE and FLOW modules (Lesser et al., 2004; Lesser, 2009) have been used to propagate and transform the agents into the associated water levels along the estuary. Wind-generated waves are computed by Delft3D-WAVE using SWAN (Booij, Ris, and Holthuijsen, 1999) to accurately reproduce the wave propagation processes in coastal areas such as refraction, diffraction, wave-wave interactions, and dissipation processes. In contrast, the Delft3D-FLOW solves the Navier-Stokes equations for an incompressible fluid under the shallow water and the Boussinesq assumptions to calculate the nonsteady flow that results from tidal, meteorological and river forcing on a curvilinear, boundary fitted grid. The model configuration used in this work is 2DH (depth-averaged), which is a convenient configuration for tides, waves, storm surges, and river discharge modeling in vertically well-mixed flow regimes. FLOW module is coupled online with Delft3D WAVE. In this regard, the WAVE module has a dynamic interaction with the FLOW module (i.e., two-way wave-current interaction). Through this coupling, both the effects of waves on currents and the effects of flow on waves are accounted for, which is the most appropriate configuration for a hydrodynamic complex area such as river mouth and estuaries (Olabarrieta, Warner, and Kumar, 2011; Elias, Gelfenbaum, and Westhuysen, 2012; Elias and Hansen, 2013; Fortunato et al., 2017)). Then, the FLOW and WAVE modules are run in quasi-nonstationary mode. This involves a two-way coupling of a nonstationary hydrodynamic calculation in combination with stationary wave model simulation.

According to Elias, Gelfenbaum, and Westhuysen (2012), grid schematization for any numerical model is always a tradeoff between computational time and processes to be modeled. Although recent improvements in numerical modeling now allow simulating compound flooding from watershed to the ocean without any nesting Ye et al. (2020), the latest version of D-FLOW and D-WAVE with Flexible Mesh technique is not open-source yet. Therefore, to accurately capture the processes and interactions along the estuary, two nested grids are defined for the WAVE module Delft (2020). A coarse (oceanic) grid of O(170 m) is defined for the oceanic area, and a finer grid O(25 m) is used for the estuarine area. In the FLOW module, a domain decomposition technique (DD-Boundary) is used,

consisting of dividing the model grid into several smaller model domains. The domain decomposition approach is a double-way coupling (Townend and Pethick, 2002) based on a subdivision of the domain into non-overlapping domains, with the possibility for grid refinement. The outer coarse grid (Fig. 4.3.1) covers the whole bay with 244 × 181 cells of 170 x 170 m. The open boundary covers the whole range of directions between SSE (150º) and NNW (300º) with a length of approximately 100 km. This grid is used for the wave, astronomical tide and storm surge (due to the wind and sea-level pressure) propagation to the study zone. The inner and finer grid covers the river from the mouth up to El Portal Dam (Fig. 4.3.1) with 721 × 721 cells of 10 x 10 m. This grid is used to propagate the river discharge, model the interactions between the marine-induced and river oscillation, and calculate the water levels along the estuary. The cell size allows at least ten cells in the narrowest parts of the river to guarantee the accuracy of both the longitudinal and transversal circulations in the modeling.

High-resolution multibeam bathymetric surveys were carried out in 2015 in the first 4 km of the estuary and 2008 along the Bay of Cádiz by the Andalusian Institute for Earth System Research and the Spanish Ministry of Environmental and Rural Marine, respectively. The data were acquired using the Differential Global Positioning System (DGPS) navigation referring to the WGS-84 ellipsoid. Data from the digital terrain model supplied by the National Geographical Institute of Spain with 5 m of cell resolution were used for the topography. The accuracy of the topography of the first 4 km of river banks was increased using different topographic surveys supplied by the Local Government and the Port Authority. Topography, bathymetry, and the water levels are referred to as the Local Mean Sea Level (LMSL) datum.

The FLOW module was previously calibrated and validated for the Bay of Cádiz by Zarzuelo et al. (2015) at the ADCPs located at I1 and I2 (black squares in Fig. 4.3.1) for water levels (η), longitudinal and transversal instant and residual currents (u, v, $|U_{res}|$, and $|V_{res}|$). Using these parameters, excellent agreement was achieved between observations and simulated water level (correlation coefficient R = 0.99). Tab. 4.3.1 shows the validation indexes RMSE, Normalized RMSE, R and Skill for the I_1 and I_2 locations. As seen, normalized RMSE for water levels, currents, residual currents are around 5 %, 15 %, and 25 %, which according to the classification proposed by Rijn et al. (2003), indicate that the agreement is good. In this Thesis, the WAVE module is calibrated using field data collected from 25 December 2012 to 15 March 2013 at I1 (black square in Fig. 4.3.1). The model was forced with the Buoy of Cádiz data considering the following physical processes: wind effects, refraction, white-capping (Van der Westhuysen formulation), depth-induced breaking ($\alpha = 1, \gamma = 1.2$), bottom friction (Type $Collins$, coefficient = 0.01), nonlinear triad interaction ($\alpha = 0.1, \beta = 9$) and diffraction (smoothing coefficient = 0.9, smoothing

steps = 900). A comparison of the observations and modeled significant wave heights generated a correlation coefficient R and skill value S (Olabarrieta, Warner, and Kumar, 2011) of 0.90 and 0.84 respectively. Furthermore, a RMSE of 0.074 m is obtained for H_{m0}. Although there are no consistent means of normalization in the literature, common choices are the mean or the range (defined as the maximum value minus the minimum value) of the measured data. The obtained NRMSE using the mean and the range values are 19 % and 8 %, respectively, which is similar to the results obtained in other works in the Atlantic, thus providing confidence in the results of the model (e.g., (Dodet, Bertin, and Taborda, 2010), (Fernandez-Fernandez et al., 2019)). Fig. 4.3.2 shows the time series of both measured (blue) and modeled (orange) significant wave heights and wave directions. The gaps in the modeled time series correspond to periods with local north-east wind-waves that cannot be reproduced with the established open boundary of the grid (Fig. 4.3.2). Besides, two scatter plots between normalized measured and modeled significant wave heights and wave directions are shown in Fig. 4.3.3. As seen, no significant bias is observed.

The calibrated parameters for the FLOW and WAVE modules of Delft3D used in this Thesis are collected in Table 4.3.1. Regarding the horizontal eddy viscosity, a sensitivity test was performed by Zarzuelo et al. (2015) at the Bay of Cadiz. Although no significant variability was observed in the hydrodynamics, a value of 1 $m^2 s^{-1}$ was selected as the best fit. However, this value was unable to reproduce the hydrodynamics of the extreme flooding events along the estuary with high river discharges that have been reported in the past. Hence, different values of this parameter ranging from 1 to 30 $m^2 s^{-1}$ were tested at different estuary points. Although no differences in the hydrodynamics were observed at the mouth, the value of 25 $m^2 s^{-1}$ was the best to reproduce the extreme flooding events. This value agrees with other authors' horizontal eddy viscosity in similar areas, such as bays, tidal channels, and estuaries along the Atlantic coast of the Iberian Peninsula (Dias and Lopes, 2006; Iglesias and Carballo, 2010; Iglesias et al., 2012). Furthermore, a theoretical study of the residual flow generated by the eddy viscosity-shear covariance was performed by Chen and Swart (2018) in a narrow estuary with the Delft3D model driven by the astronomical tide and high river flows; in this work, they used a horizontal eddy viscosity of 50 $m^2 s^{-1}$.

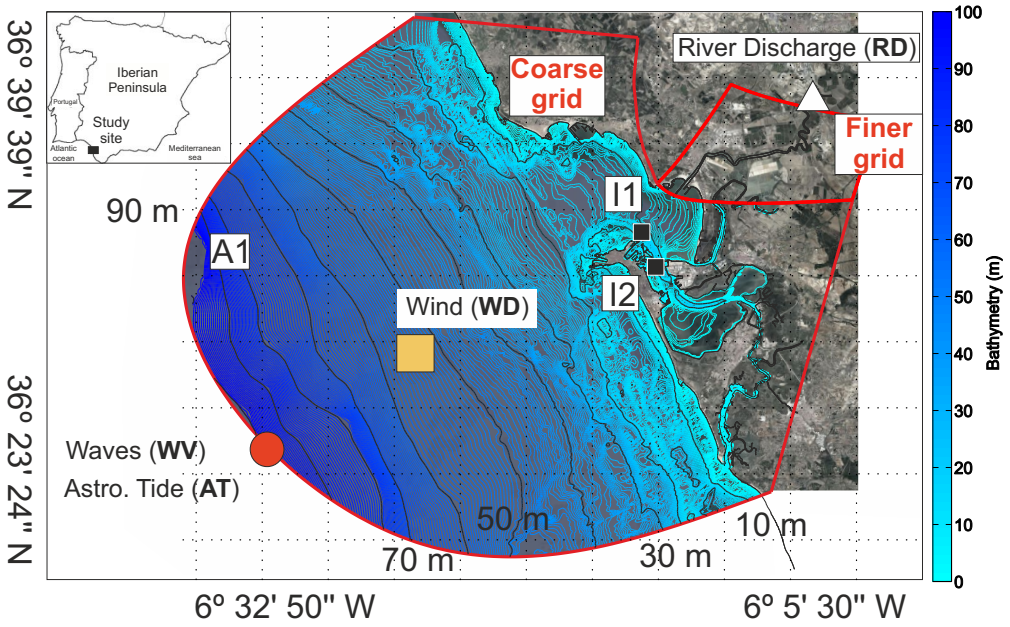

Figure 4.3.1: Guadalete estuary (Cádiz, southwestern Spain). Red point, yellow square and white triangle indicate the boundary entrance for the marine-induced oscillation, the wind and sea level pressure field and the boundary entrance for the river-induced oscillation, respectively. Black squares (I_1 and I_2) represent the location of the ADCPs and AWAC used in the model calibration, respectively. Red lines show the boundaries of the coarse and finer grids defined for the numerical models.

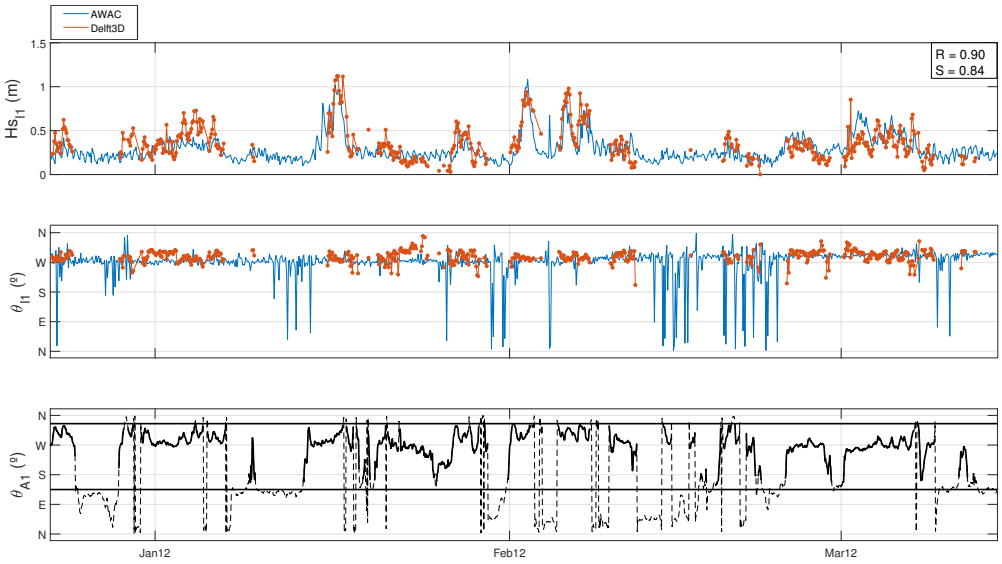

Figure 4.3.2: Upper panel: Comparison of the time series of measured (blue) and modeled (orange) wave heights at location I1 (Fig. 4.3.1). Middle panel: Comparison of the time series of measured (blue) and modeled (orange) wave directions at location I1. Lower panel: measured wave directions at the boundary A1 (Fig. 4.3.1) between 145º (SSE) and 355º (NNW).

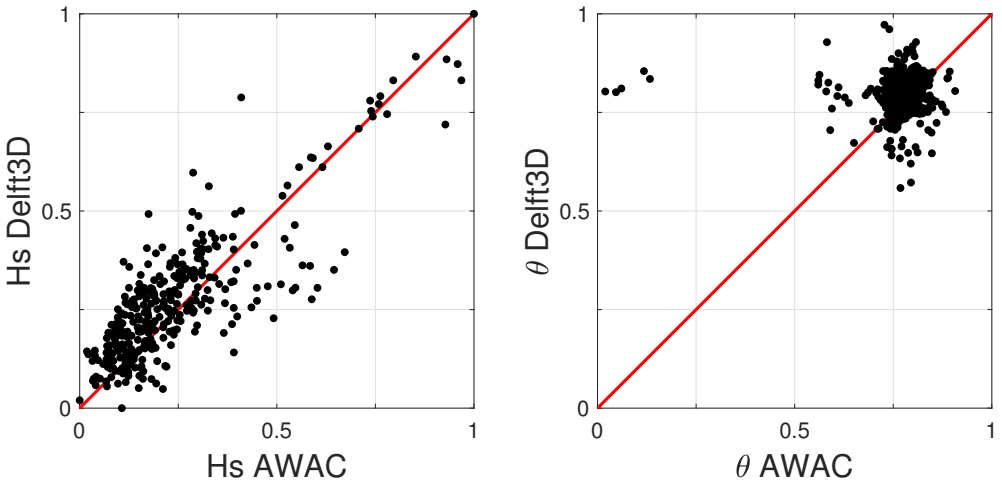

Figure 4.3.3: Scatter plots between normalized measured (AWAC) and modeled (Delft3D) significant wave heights (left) and wave directions (right). Red diagonal line indicates perfect match.

FLOW module parameters	
Wind drag coefficient	0.005
Roughness	Chezy (80, 60) $m^{1/2}s^{-1}$
Horizontal eddy viscosity	25 m^2s^{-1}
Max. Courant number	10
WAVE module parameters	
Wind effects	Yes
Refraction	Yes
White-capping	Van der Westhuysen formulation
Depth-induced breaking	$\alpha = 1, \gamma = 1.2$
Non-linear triad interaction	$\alpha = 0.1, \beta = 9$
Bottom friction	Collins formulation (0.01)
Difraction	Yes

Table 4.3.1: Calibration parameters settings of WAVE and FLOW module of Delft3D used in the case study. Source: Zarzuelo et al. (2015) and Del-Rosal-Salido et al. (2019b)
.

Tab. 4.3.2 shows the validation indexes RMSE, Normalized RMSE, R and Skill for the I_1 and I_2 locations (Fig. 4.3.1) using field data for water levels (η), longitudinal and transversal instant and residual currents (u, v, $|U_{res}|$, and $|V_{res}|$), and significant wave height (H_{m0}).

	η_{I1}	η_{I2}	u_{I1}	u_{I2}	v_{I1}	v_{I2}	$\|U_{res_{I1}}\|$	$\|U_{res_{I2}}\|$	H_{m0}
RMSE	0.14 m	0.15 m	0.15 m/s	0.13 m/s	0.16 m/s	0.19 m/s	0.04 /s	0.05 m/s	0.074 m
NRMSE	4.3 %	4.7 %	15 %	13 %	15 %	17 %	23 %	29 %	8 - 19 %
R	0.99	0.99	0.93	0.88	0.93	0.90	0.79	0.78	0.90
S	0.99	0.99	0.73	0.73	0.89	0.83	0.79	0.77	0.84

Table 4.3.2: Calibration indexes for WAVE and FLOW modules of Delft3D

The model was also tested to check the ability to reproduce flooding events in the past that occurred in 1996 and 2010. The upper panels of Fig. 4.3.4 shows the total water level for the 1996 (left) and 2010 (right) events. However, this trial is not considered as a validation nor calibration of the model, but rather as a test because of the lack of available data in the study area to compare. The lower panel shows the water column above the terrain only at the emerged points, which is defined as the vertical distance between the terrain and the water surface.

According to historical information, during the event of 2010, the combination of the tide and the large river flow ($> 250 m^3 s^{-1}$) caused the overflowing of the river in the middle part of the estuary (right panels in Fig. 4.3.4). In particular, agricultural fields were flooded (area C in Fig. 4.3.4), although the flooding did not reach the village (area B) at this time. The other hot spot of flooding damage occurred in an Industrial

Polygon (area A), which remained flooded during days. In the flooding event of 1996 (left panels), 400 m3/s of river flow caused the partial evacuation of the village (area B) and the inundation of area D, causing the temporary closure of the railway. According to the photographic evidence, the elevation of the water during the flooding events reached 0.5 m.

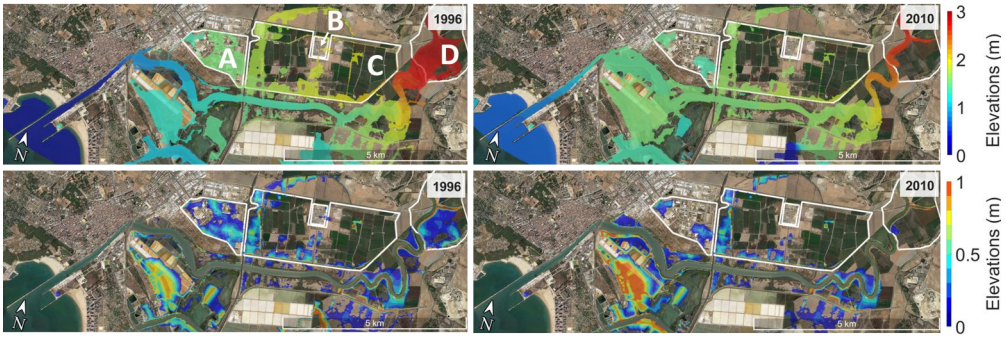

Figure 4.3.4: Upper panels represent the total water levels with respect to the LMSL for the 1996 (left) and 2010 (right) flooding events. Lower panel shows the vertical distance between the terrain and the water surface at emerged points, thus representing the water column above the terrain only at the emerged points.

4.3.2 Historical water level reconstruction

Following the steps described in section 4.2, in the dependent approach, a subset of 600 elements have been extracted from the data sample by applying the MDA algorithm. Fig. 4.3.5 shows the 28-bidimensional combinations of the eight considered variables and the extracted subsets for different sizes.

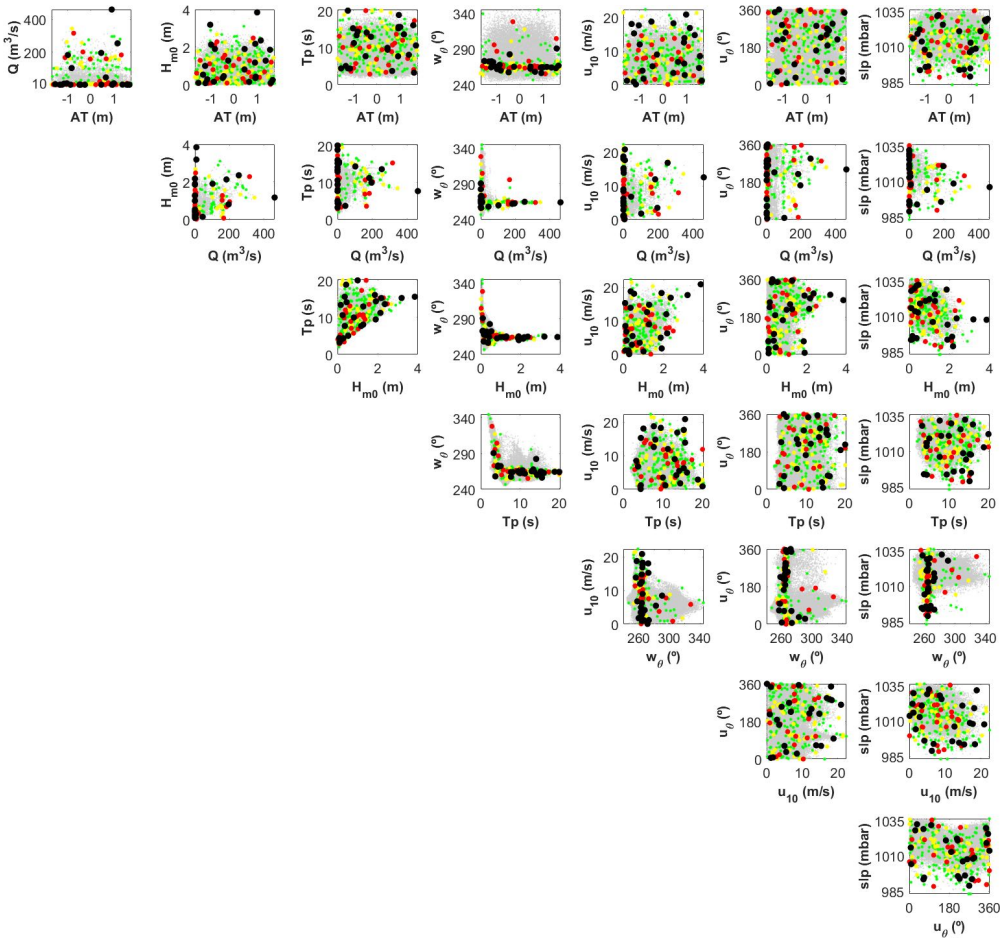

Figure 4.3.5: Distribution of the selected cases by the MDA algorithm ($M = 1-25$ black points, $M = 26-50$ red points, $M = 51-100$ yellow points and $M = 101-600$ green points).

For each simulation with the Delft3D model, the numerical model is forced over 48 h with constant values of each agent to guarantee the stationarity of the resulting water levels. As a result, a database of 600 stationary total water level values is obtained for different control points. Finally, a historical 20-year (from 1995 to 2015) hourly series of the total water level is reconstructed by applying the RBF to the input boundary agents and the propagated database of total elevations along the estuary.

The accuracy of the reconstruction of the time series is highly dependent on the number of selected cases. Therefore, a sensitivity analysis has been performed to optimize the number of cases that minimize the error in the reconstruction. This procedure is

repeated every 10 cases from 10 to 600. The results, shown in Fig. 4.3.6, indicate that the difference in the reconstructed elevations between 300 and 600 cases are less than 2.5% of the total water at the considered control points along the estuary. Finally, to validate the reconstructed elevations by the dependent approach, the total water level time series are simulated with the model at four different periods of one week. The error between the modeled and the reconstructed elevations is quantified and shown in the first row of Fig. 4.3.7. Correlation coefficients (R) of 1 (mouth) and 0.95 (head) are obtained.

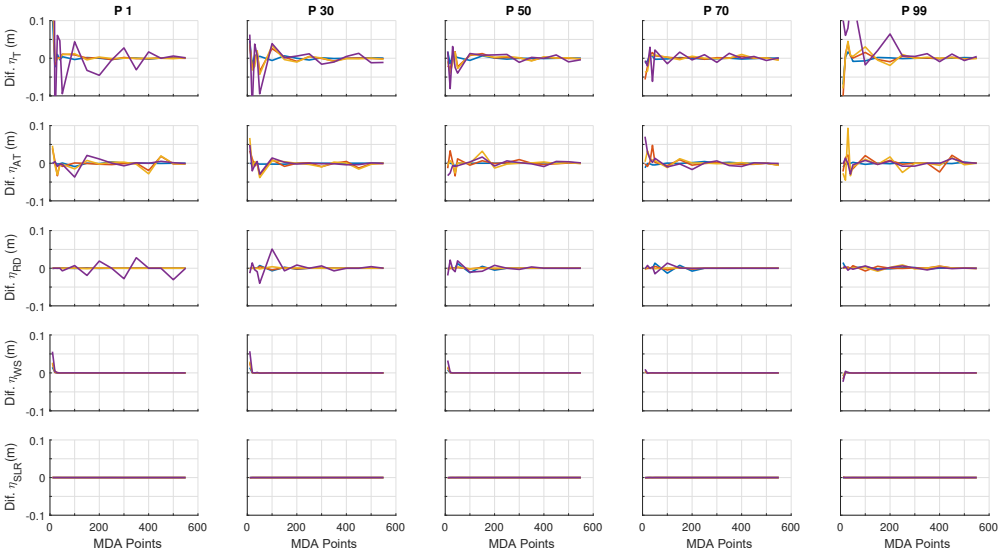

Figure 4.3.6: Differences in the reconstructed water levels according to the number of points used during the selection of representative cases with the MDA algorithm. The columns indicate the differences in the different percentiles of the empirical distribution function. Blue, orange, yellow and purple colors correspond to water levels at CP 1, CP 3, CP 5 and CP 7.

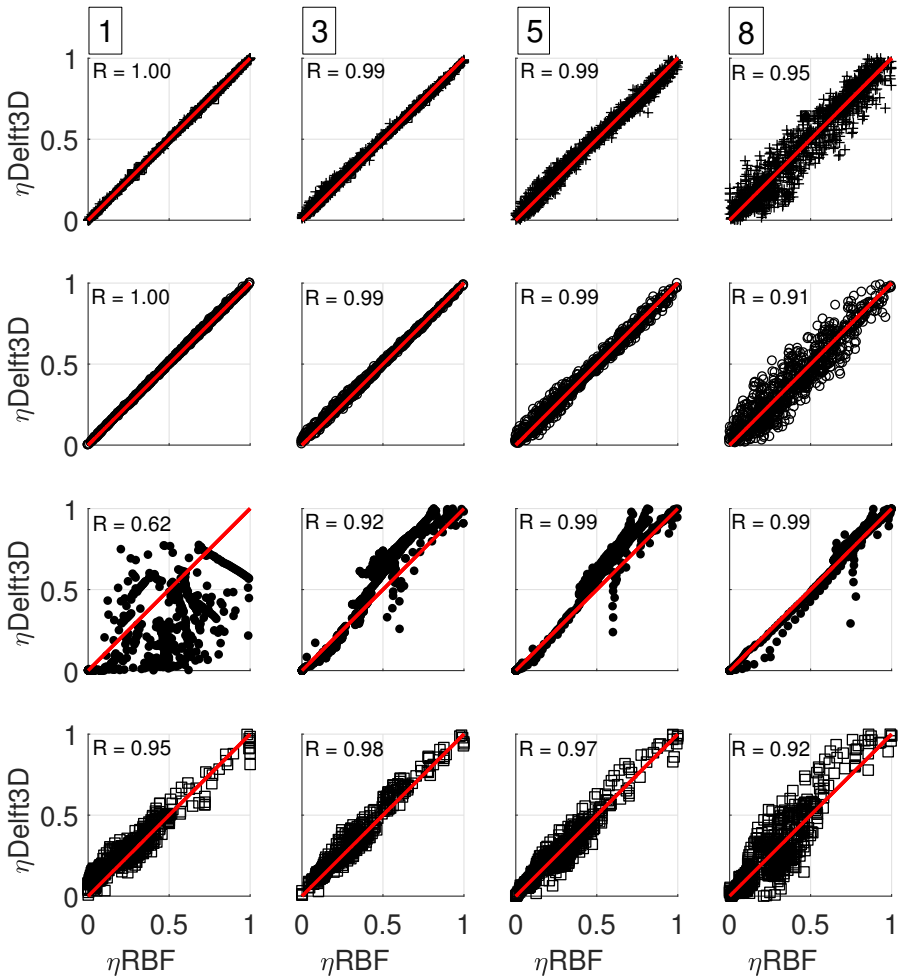

Figure 4.3.7: Comparison between the non-dimensional simulated water level with Delft3D ($\eta_{Delft3D}$) and reconstructed water level via hybrid downscaling (η_{RBF}) at different points along the estuary (CP 1, CP 3, CP 5 and CP 8) for the total water level (first row); water level due to astronomical tide (second row); water level due to river discharge (third row); and water level due to weather surge (fourth row). The red line indicates an agreement of R = 1 between elevations.

The isolated components of the elevation (independent approach) are also obtained by repeating the previous (hybrid downscaling) steps for each agent separately. Finally, the non-linear term (η_{NL}) is extracted from the total elevation via Eq. 4.1. The same method used in the dependent approach is applied to validate each component of the

water level along the estuary. As seen in Fig. 4.3.7, a correlation coefficient beyond 0.9 is obtained between non-dimensional modeled and reconstructed elevations except for the river discharge elevation at the mouth (control point CP1). At CP1, the water level due to river discharge is around 5-10 centimeters above mean sea level (reference level), leading to a time series of water level near zero. When the elevations are too small, Delft3D tends to smooth the time series, whereas RBF results in a much more chaotic time series, increasing the scatter at this point.

Fig. 4.3.7 also shows that the scatter between the modeled and reconstructed total water levels (first row) and water level due to astronomical tide (second row) increases along the estuary from the mouth to the head. At the mouth, water levels are quite similar to the astronomical tide. However, as we move upstream, they are modified due to the propagation effects and the influence of the river discharge. For a fixed number of selected cases, the reconstruction is more straightforward when the time series of the agents' descriptors and the water levels are similar. The scatter increases when these time series differ due to the propagation effects and the affection of another agent unless the number of selected cases increases in the downscaling process. It is also shown that the scatter in the weather surge component (fourth row) is higher than the rest. The surge elevations are mainly driven by the wind's magnitude and direction, which presents a higher variability than the astronomical tide or the river discharge. This variability hampers the reconstruction by the radial basis functions compared to the astronomical tide and river discharge, where the trend of the elevations is more evident.

The total and isolated reconstructed elevations are shown in Fig. 4.3.8 at the outer (CP1), middle (CP5) and inner (CP8) part of the estuary. As seen, the tidal range at the mouth during the historical nodal cycle is approximately 3.5 m, while the elevation because of the remaining agents is nearly negligible. However, at the upper part of the estuary, the tidal range reduces to 1 m, and the river discharge peaks reach 3 m above the LMSL. The magnitude of peaks of the weather surge elevation increases upstream from 0.05 to 0.25 m. Transitional behavior is observed in CP5. The time series of the non-linear term is shown at the bottom of Fig. 4.3.8 in green. The magnitudes of the non-linear term peaks vary along the estuary between 0.15 (mouth) and 0.5 (headwaters).

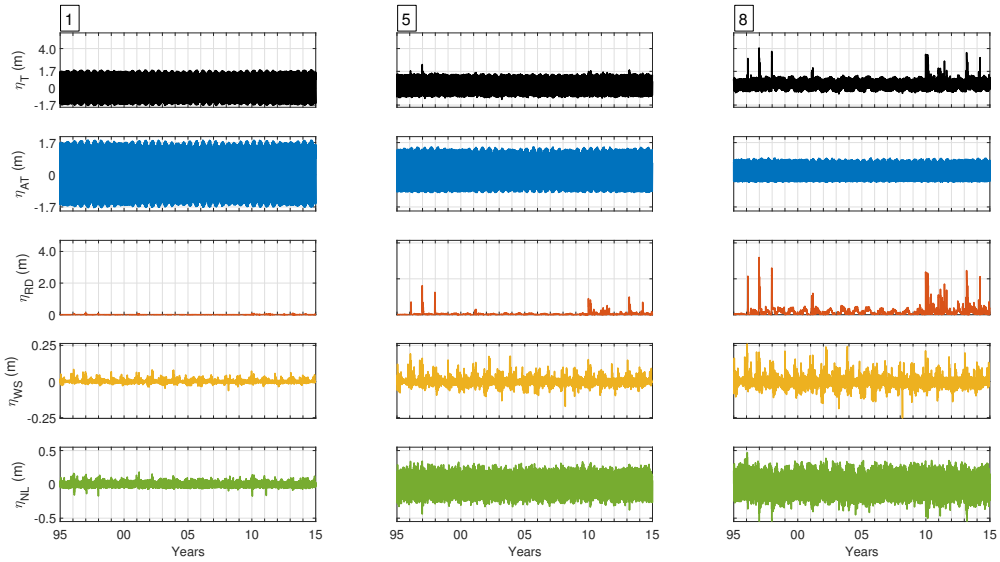

Figure 4.3.8: Reconstruction of historical 20-year total water levels (black) and elevations due to the astronomical tide (blue), river discharge (orange), weather surge (yellow) and nonlinear interactions (green) at the mouth (CP 1), middle (CP 5) and head (CP 8) of the estuary.

4.3.3 Future water level reconstruction along the 21st-century

The set of 100 simulations of the climatic forcing agents at the boundary are propagated and transformed into hourly 80-years time series of total water level. The procedure explained in the previous sections is used to downscale the first simulation. A subset of 300 representative cases is extracted from the whole dataset using a clustering approach. Then, the Delft3D model is used to transform the selected cases to the total water level. In this process, the parameters that relate the boundary agents with the total water level in the estuary are calculated. With these transformation parameters, the total water level's continuous time series is reconstructed for the first simulation throughout the radial basis functions (RBF) (Fig. 4.3.9). To validate these RBF-reconstructed elevations, a 48-hour water level time series have also been simulated using Delft3D around the dates of each of the selected representative cases. Delft3D elevations are then compared with the RBF-reconstructed ones in Fig. 4.3.11 at different points of the estuary. As seen, a correlation and Skill coefficients between 0.97 and 0.99 are obtained for the different points along the estuary. Validation indexes are shown in Tab. 4.3.3.

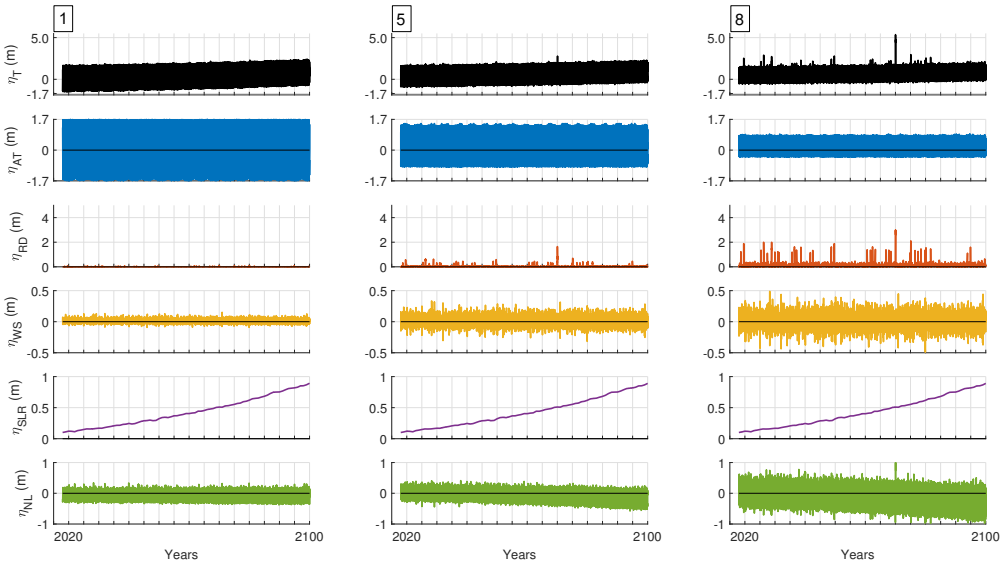

Figure 4.3.9: Reconstruction of forecasted 80-year total water levels (black) and elevations due to the astronomical tide (blue), river discharge (orange), weather surge (yellow) and nonlinear interactions (green) at the mouth (CP 1), middle (CP 5) and head (CP 8) of the estuary.

For the remaining 99 simulations, the obtained transformation parameters in the first simulation were used to directly calculate the corresponding total water level series to minimize the computational cost. Therefore, a total of 100 hourly time series from 2020 to 2100 of the total water level have been obtained at the eight different control points of the estuary (Fig. 4.3.10). The same technique is applied to each agent individually to obtain the water level time series associated with each component (independent approach). As a result, another 100 time series of water level due to: astronomical tide (η_{AT}), river discharge (η_{RD}), weather surge (η_{WS}) and sea-level rise (η_{SLR}) are also obtained. Finally, the non-linear term ($\eta_N L$) is obtained through Eq. 4.1 for each simulation. Validation indexes are summarized in Tab. 4.3.3.

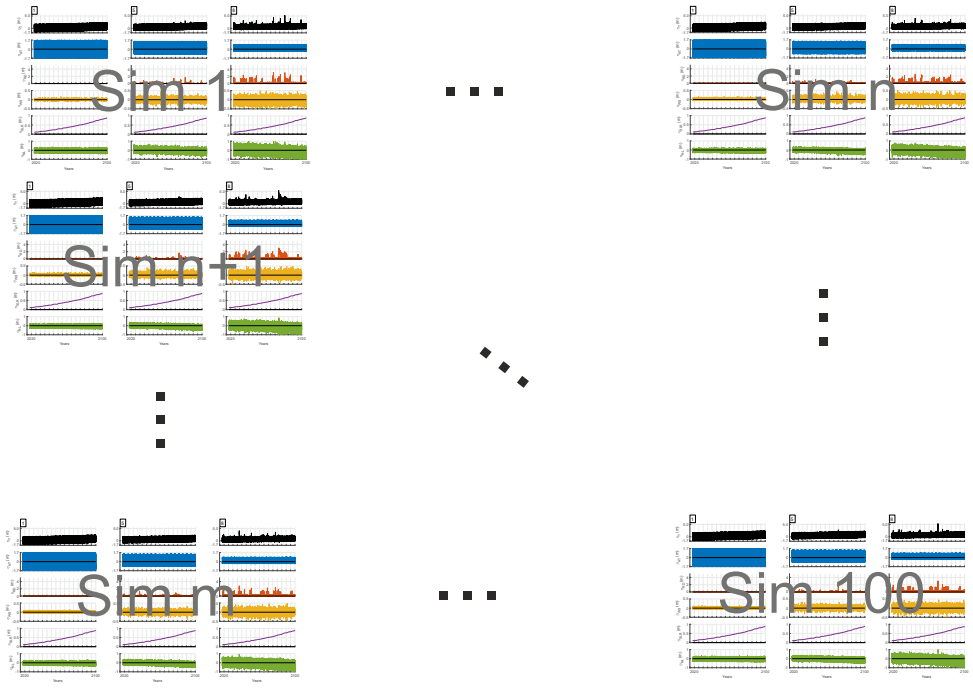

Figure 4.3.10: Rerepresentation of the 100 simulations of forecasted 80-year total water levels (black) and elevations due to the astronomical tide (blue), river discharge (orange), weather surge (yellow) and nonlinear interactions (green) at the mouth (CP 1), middle (CP 5) and head (CP 8) of the estuary.

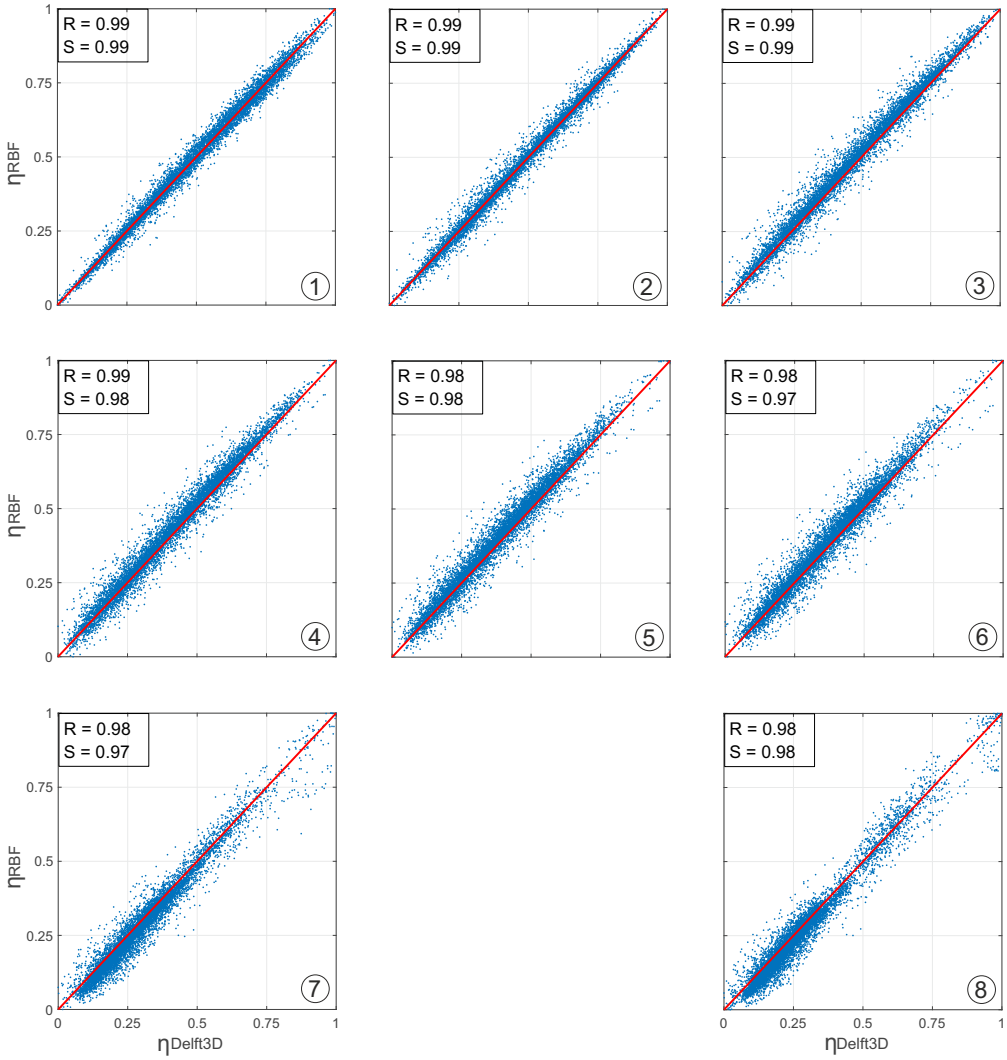

Figure 4.3.11: Comparison between the non-dimensional modeled total water level with Delft3D ($\eta_{Delft3D}$) and reconstructed total water level via hybrid downscaling (η_{RBF}) at the different control points along the estuary for the total water level. Red line indicates an agreement of R = 1 between elevations.

4.4 Summary and conclusions

This chapter develops a working method for the reconstruction of both the historical and future continuous time series of the water levels along a transitional coastal environment,

η_T	**CP 1**	**CP 3**	**CP 5**	**CP 8**
Historical	R = 0.99	0.99	0.99	0.95
	S = 0.99	0.99	0.98	0.96
	RMSE = 3.66 cm	3.66 cm	7.02 cm	12.67 cm
	NMSE = 0.91 %	0.91 %	1.75 %	3.17 %
RCP_4.5_05	0.99	0.99	0.98	0.98
	0.99	0.99	0.97	0.97
	6.80 cm	7.01 cm	8.07 cm	9.66 cm
	1.70 %	1.75 %	2.2 %	2.41 %
RCP_8.5_95	0.99	0.99	0.98	0.98
	0.99	0.99	0.98	0.98
	7.94 cm	7.33 cm	8.25 cm	9.97 cm
	1.98 %	1.88 %	2.06 %	2.49 %

Table 4.3.3: Calibration indexes of the water level reconstruction.

where systematic measurements are rarely available and expensive. The method is based on the hybrid downscaling technique adapted to the reconstruction of water levels in transitional systems. This technique starts with a clustering technique (MDA algorithm) for the selection of representative cases. A hydrodynamic and wave propagation model is then used to transfer the forcing agents dynamic to the coast and transform them into water levels. Finally, Radial Basis Functions are used to reconstruct the continuous time series of water levels. Therefore, two different approaches are defined, dependent, and independent. The independent approach is responsible for calculating each of the water level components by propagating each agent separately. In contrast, the dependent approach calculates the total water level considering the simultaneous effects of the concomitant agents, including the non-linear interactions between them. The following conclusions can be drawn from the analysis presented in the previous sections:

- Delft3D model proves to be a fully adequate model for hydrodynamic propagation in complex coastal systems such as a mesotidal estuary in the interior of a Bay. In order to model all processes and interactions between the different agents, cells up to 10 m wide have been used in the narrowest parts of the Guadalete estuary. FLOW model has been widely used in this area for hydrodynamic studies within the Bay of Cádiz. However, it is in this work when the WAVE and FLOW modules are first used in this Bay for the joint propagation of wave, wind, tide, and river discharge, as well as for the reconstruction of hydrodynamic variables along the estuary including sea-level rise.

- The hybrid downscaling technique results in an efficient method of reducing the computational costs associated with reconstructing the total and isolated components of the water level in transitional systems. Furthermore, the presented method allows reconstruction of the non-linear water level component due to the forcing agents' interactions. These elevations present a large variability along the

estuary. In particular, elevations due to astronomical tide decrease upstream from the mouth (±1.8) m to the inner part of the estuary (±0.9) m above LMSL, whereas river discharge increases upstream from 0 to 3 m. Weather surge elevations are found to be significantly lower than the rest of the components.

- Although in this work only the water level variable is reconstructed, this methodology allows being used for the reconstruction of other hydrodynamic variables such as wave height, currents, temperature, salinity, among others.

Part III

Flood impact assessment

CHAPTER 5

QUANTIFICATION OF FLOOD DEFENSE FAILURES

5.1 Introduction

This chapter quantifies the number of flood defense failures to determine the sensitivity of the TCE to the spatial and temporal evolution of flood events resulting from GW along the 21st-century. To this end, the total water level obtained using the "dependent approach" calculated in section 4.2 of this Thesis is analyzed and compared with the geometry of the TCE to assess the number and duration of failures per year. The sections of this chapter organize as follows. In §5.2.1, the definition and methodology for the flood defense failure are described. The results after applying the methodology to the Guadalete estuary regarding the impact of the SLR in the number and duration of failures during the historical and future periods are presented in §5.3.1 and §5.3.2 respectively.

5.2 Methodology

5.2.1 Flood defense failure

The concept and conceptual framework of coastal protection structures failures are detailed in-depth in ROM-0.0 (2001), ROM-1.0 (2009), and ROM-1.1 (2018). Although there are several failure modes related to flood events (e.g., Plomaritis, Ferreira, and Costas (2018)), in this Thesis, failure is defined as water levels higher than the crest height of the flood defenses (e.g., floodwalls and levees) for a period exceeding 3 hours

to consider the water level oscillations due to the astronomical tide. To consider two failures as independent, a minimum 14-hour gap is considered between the water levels that equal the flood defense's crest height. In this way, the method takes into account the astronomical tide-induced oscillations during a spring tidal cycle. Therefore, as seen in Fig. 5.2.1 two failure durations are obtained from the analysis: (1) the total failure duration (t_{total}), that considers the time between the first and the last overflowing (including periods with water levels lower than the flood defenses due to tidal oscillations); (2) the effective failure duration ($t_{effective}$), defined as the time during which water levels are strictly above the crest height of the flood defenses. This analysis is first performed for the forcing agents' historical time series and then repeated for each future simulation of the forcing agents.

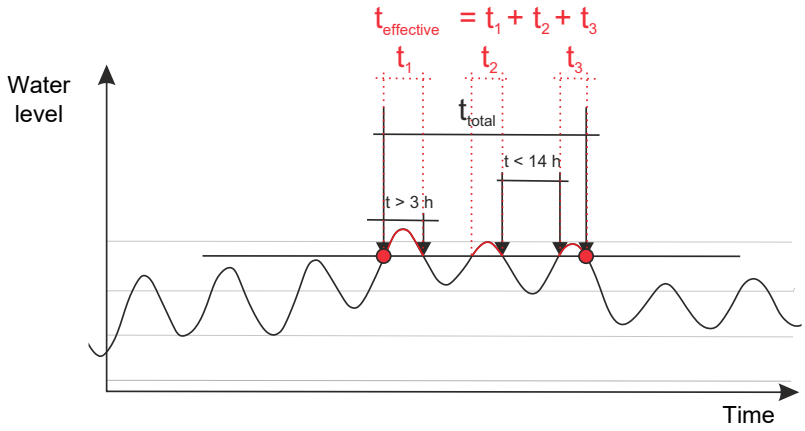

Figure 5.2.1: Theoretical scheme of flooding failure considered in this thesis.

To count the number of failures, it is necessary to define the topography of the estuary precisely. For this purpose, a digital elevation model around the study area has been constructed with a cell size of 5 m. Once the terrain surface has been modeled, eight different cross-sections have been defined, coinciding with each of the control points along the TCE. In Fig. 5.2.3 each of the cross-sections (blue) obtained are represented together with the crest height of the flood defenses (orange) obtained for each section.

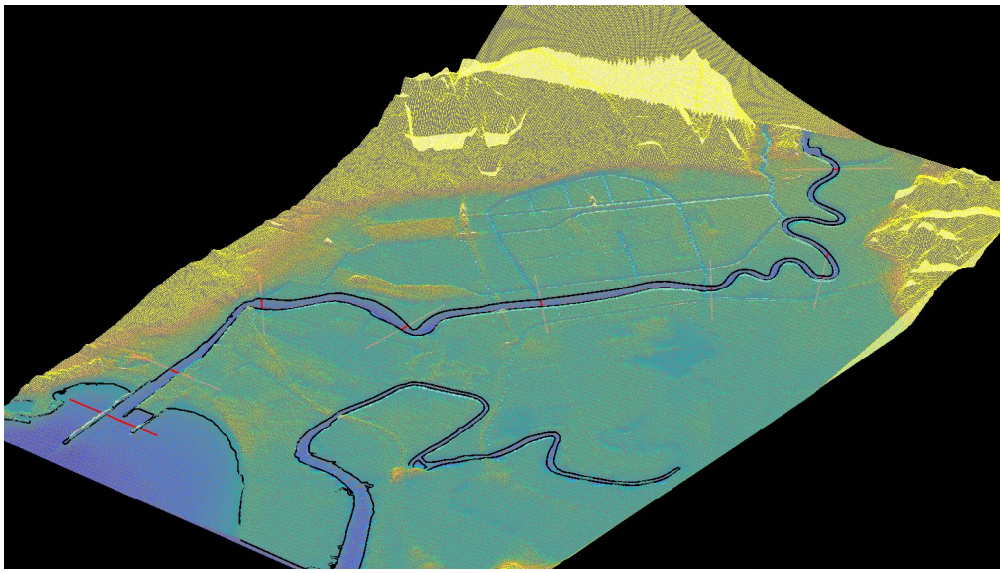

Figure 5.2.2: Digital elevation model for the Guadalete estuary. The red lines in the main channel represent the selected cross sections.

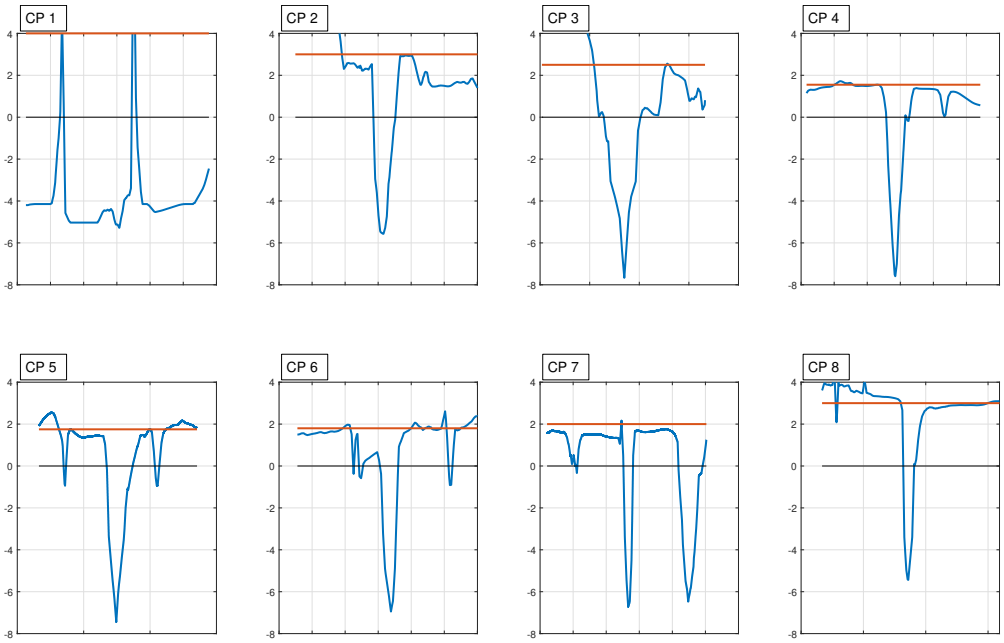

Figure 5.2.3: Cross sections of the Guadalete estuary channel for each of the chosen control points. The black line represents the mean sea level while the orange line indicates the height of the coastal defences at each point.

5.3 Results

5.3.1 Historical flood defense failure

The methodology described in section 5.2.1 was used to assess the historical number and duration of the flood defense failures. The results are presented in Fig. 5.3.1. Boxplots in the left column represent the mode and quartiles of the number of failures per year grouped in 5-year periods from 1995 to 2015. In the right column, the duration of these failures is shown in two ways: total and effective failure duration. The total duration of the failures is depicted in boxplot graphics, while the mean of the effective duration is represented with purple dots. Lack of boxplots indicates no flooding failure in that period.

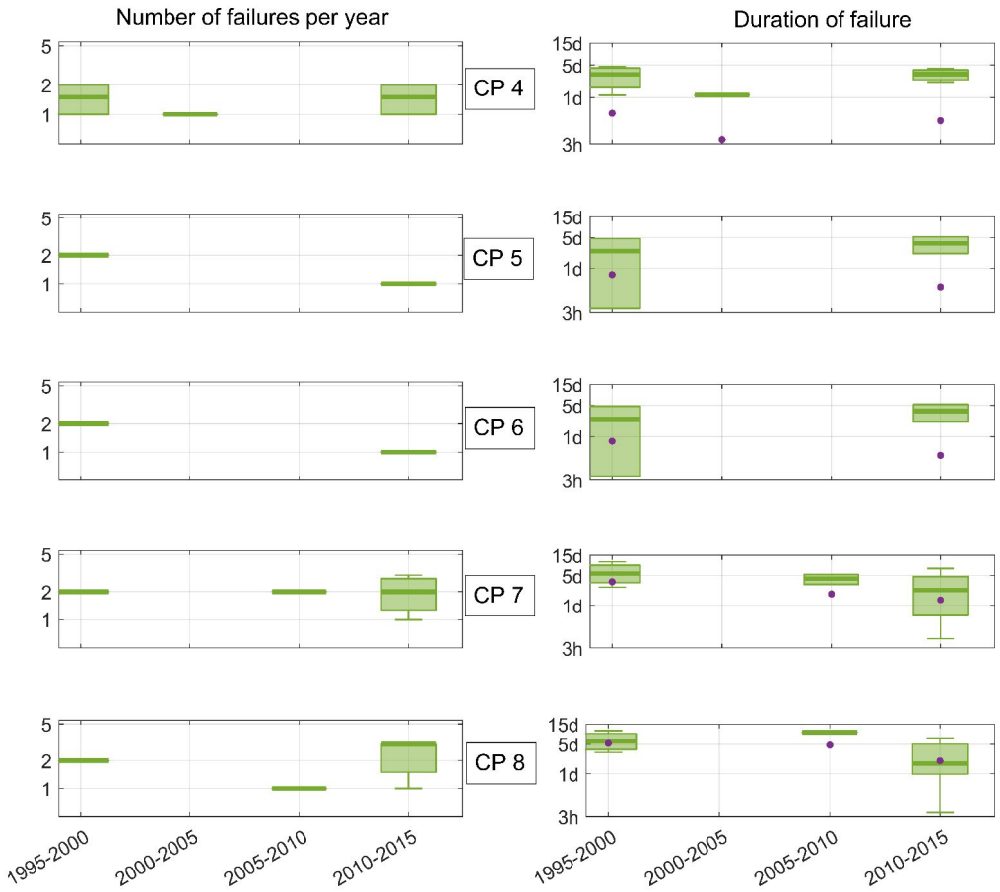

Figure 5.3.1: Spatiotemporal evolution of the historical number and duration of failures between 1995 and 2015. Purple dots indicates the mean value of the effective duration of failure. If no boxplots are shown, then no failures occur.

As shown in Fig. 5.3.1, the sensitive part of the estuary to flooding during the historical period is from the PC4 onwards, i.e., from the km 6 onwards from the mouth. It can be seen that the flood defense failures coincide with the significant river discharge events that occurred in 1996, 2010, and more recently in 2013 and 2014. It is also observed that the average number of failures is between one and two per year, coinciding with these river discharge events mentioned above.

Concerning the duration of the failure, the following is observed. The average value of the total duration is between 1 and 3 days in the first half of the estuary (CP4 - CP5), while at the points closest to the headwaters (CP7 - CP8), this average duration rises to

5 days. However, high variability is observed in the data, ranging in some cases from overflowing with total durations of between 3 hours and five days.

Another interesting observation is related to the effective duration of the failure. As shown in Fig. 5.3.1, as we move upwards in the estuary towards the headwaters, the average values of the effective duration (purple dots) coincide with the average values of the total duration (boxplot). The reason for this is found in the mechanisms of the formation of the extreme events of the total level that lead to the failure. As it will be seen in Chapter 7, in the middle region of the estuary, extreme water level events are produced by the combination of astronomical tides and river discharge. High and low tide oscillations caused by the astronomical tide together with an increase of the mean water level caused by the river discharge result in the total level fluctuating above and below the crest height of flood defenses within the definition of failure described in section 5.2.1. However, in the region near the headwaters (CP 7 and CP 8), the failures are mainly caused by the river discharge with a much less marked tidal oscillation. For this reason, the total and effective durations almost coincide in the upper region.

5.3.2 Forecast flood defense failure

This section now characterizes the spatial variability and temporal evolution of the number and duration of the flood defense failures as a consequence of the SLR along the 21st-century using the methodology described in section 5.2.1. The results are presented in Fig. 5.3.2. As in the historical section, boxplots in the left column represent the mode and quartiles of the number of failures per year grouped in 5-year periods from 2020 to 2100, while the continuous line represents the mean number of failures per year. In the right column, the duration of these failures is shown in two ways, as total and effective failure duration. The total duration of the failures is depicted in boxplot graphics, while the mean of the effective duration is represented with a continuous line. Warm colors represent the RCP8.5_95 scenario, while cold colors represent the RCP4.5_05. Lack of boxplots is due to insufficient or no number of failures.

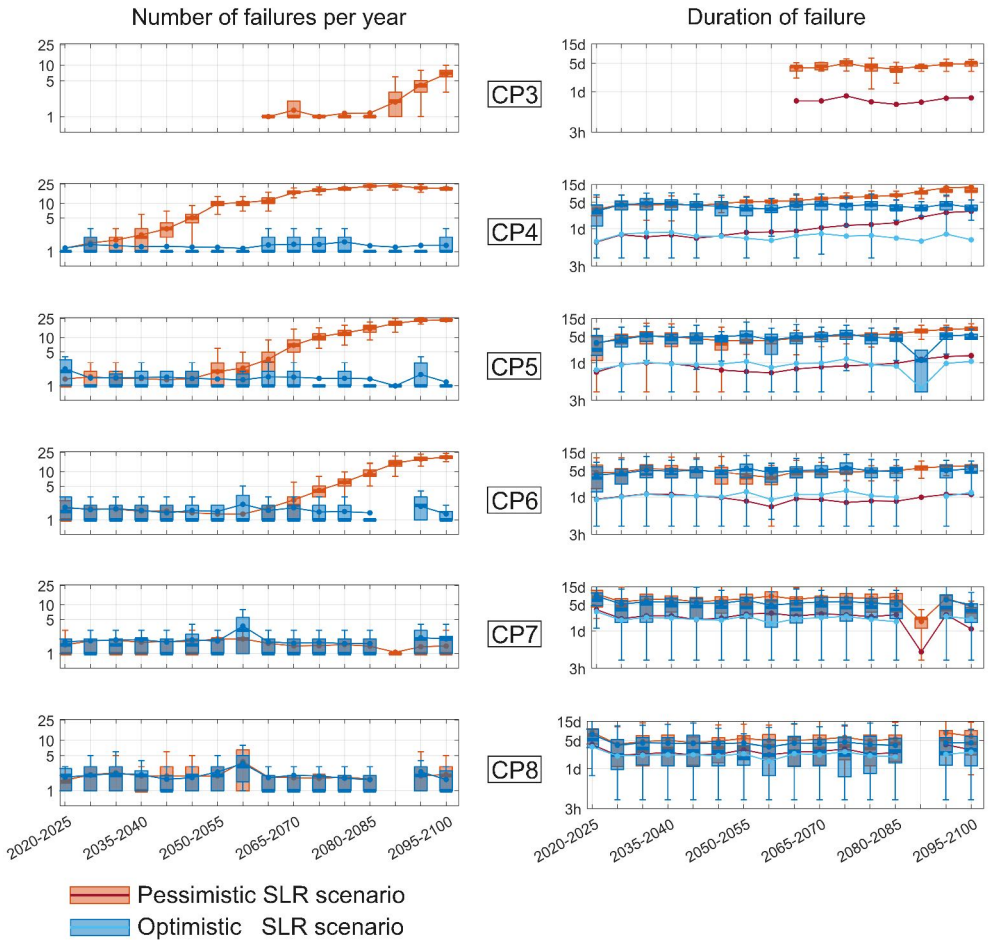

Figure 5.3.2: Spatiotemporal evolution of the number and duration of failures throughout the 21st-century. Orange and dark red colors represent the RCP8.5_95 SLR scenario, while dark and light blue represent the RCP4.5_05 one. If no boxplots are shown, then no failures occur.

In the historical period analyzed, the sensitive area to flooding in the estuary was from CP 4 onwards. As seen, the first effects of the SLR on the failures are observed in CP 3 from 2060 onwards for the RCP8.5_95 SLR scenario. At this control point, the mean number of failures per year increases from 1 in 2060 to 5-10 in 2100. The next 8 km of the estuary (CP 3 - CP 6) represents a hotspot of vulnerability, where the number of failures per year is maximum for the RCP8.5_95 SLR scenario. These failures per year vary from 1 in 2020 to 24 in 2100. However, the growth trend is different. In CP 4, the number of

failures increases from 2030 onwards, in CP 5 from 2050 and in CP 6 from 2060. The stabilization of the number of failures per year in 24 is found in the combination of the astronomical tide and SLR. A spring tidal cycle occurs every 15 days. Therefore a set of 24 spring cycles is observed per year. Under current conditions, the water level during the spring tidal cycle does not reach the levee's height in these area. However, by the end of the 21st-century in the RCP8.5_95 SLR scenario, a natural high tide during the spring tidal cycle will lead to a failure in the middle estuary. On the contrary, there is no difference in the number of failures for the RCP4.5_05 scenario with respect to the current situation in this part of the estuary.

In the upper part of the estuary (CP 7 and CP 8), completely different behavior is found. At these points, the combination of astronomical tide and SLR is not enough to overtop the levee system; on the contrary, the number of failures is determined by the intensity and frequency of river discharge events. Consequently, the number of failures is the same for both SLR scenarios, and the failure rate remains constant, as shown in the two bottom-left Panels of Fig. 5.3.2. However, higher variability in the number of failures per year is observed in this region. This is due to the variability in the intensity and frequency of the river discharge events between the different simulations.

Regarding the duration of the failures, differences are observed between total and effective durations and between the SLR scenarios in the first part of the estuary. Such differences are reduced as we move upstream. In CP 3, the mean total duration of failure is constant and equal to the spring cycle duration, five days for the RCP8.5_95 scenario. However, the effective duration is limited to 20 hours (four hours a day during the 5-days high tides of the spring tidal cycle). Similar behavior is found in CP 5 and CP 6. The worst flooding conditions are observed in CP 4, where the levee height is minimum, and the combined effect of SLR and the astronomical tide is the highest. Therefore, the total duration of the failures grows to 12 days by the end-century, and the effective duration, up to 2 days (again, four hours a day during the 12 days of spring tidal cycle).

In CP 7 and CP 8, neither differences between SLR scenarios nor between the averaged effective and total duration of flooding are observed. As in the historical period, the reason is found in the fluvial dominance in this area. On the other hand, the duration of the failures varies from hours to days, depending on the river discharge events' intensity and frequency.

As shown, the presented results allow the direct identification of the SLR effect on the estuary's flood failures. These results identify the severity of the failure, by quantifying the number of failures per year and their duration, and the areas and periods most susceptible to flooding. Besides, the results include not only the mean value but

also the quartiles of the statistical distribution, which allows evaluating the associated uncertainty.

5.4 Summary and conclusion

The total water level obtained in Chapter 4 through the dependent approach is used here to quantify the number and duration of flood defense failures along the 21st-century. Failures are defined in this Thesis as water levels higher than the crest height of the flood defenses, floodwalls, and levees for a period exceeding 3 hours. A digital elevation model with a cell size of 5 m is used to model the estuary's topography. Although a 2D approach could have been used to model the flooding in the estuary with the Delft3D, the use of such a long time series makes the computational cost unfeasible. Therefore, in this chapter, instead of only modeling some extreme events, the complete time series reconstructed during the 21st-century are compared with the estuary geometry at eight equidistant control points to account for flooding failures. Although, in later chapters, we will go deeper into the calculation of the probability of extreme water level events, as well as the mechanisms that cause them, the method presented in this chapter allows us to quickly and easily quantify the impact that sea-level rise has on the flooding of the estuary. It also allows us to assess whether current flood defenses are sufficient to withstand the effects of global warming expected in this 21st-century. The following conclusions can be drawn from the analysis presented in the previous sections:

- During the historical period (1995 - 2015), the first 6 km of the estuary are not sensitive to flooding. However, by 2050, the insensitive area is reduced only to the first 4 km.
- It is observed that flood defense failures during the historical period coincide with the major river discharges that occurred in the past during the historical period. Therefore, the average number of failures along the estuary is between one and two per year, coinciding with former river discharges.
- However, according to the obtained results, the number of failures is dramatically increased from the mid-century to the end-century as a consequence of global warming. Twenty-four failures per year are expected in the middle estuary in the RCP8.5_95 SLR scenario if no mitigation actions are taken. The former means, an overflowing failure every 15 days coinciding with every spring tidal cycle.
- Regarding the duration of the failures, the worst conditions are observed in the middle estuary (from CP3 to CP 6), where the mean of the total duration of failure is

around 5 to 12 days by the end-century for the RCP8.5_95 SLR scenario. However, the effective durations are limited to four hours per day during the high tides.

CHAPTER 6

ASSESSMENT OF THE JOINT EXTREME TOTAL WATER LEVEL EVENTS

6.1 Introduction

This chapter evaluates the probability of flood events in terms of the return period. For this purpose, all the disaggregated information of the water level components obtained through the "independent approach" (section 4.2) is used. The application of this method allows managers and coastal engineers to know the expected magnitude of flood events in probabilistic terms and the associated uncertainty, which constitutes the starting point for the design of protective measures. The sections of this chapter organize as follows. The methodology for the assessment of the Joint Extreme Total Water Level (JETWL) is presented in §6.2.1 and §6.2.2 for the historical and the future period, respectively. The results of applying the developed methodology to the Guadalete estuary are then presented in §6.3.

6.2 Methodology

The methodology of this chapter is developed based on the well-known Joint Probability Method (JPM) (Tawn, Vassie, and Gumbel, 1989; Tawn, 1992), with the variations proposed in Mazas et al. (2014) for this purpose. Nevertheless, additional modifications have been included in this Thesis to adapt this method, mainly used in open coasts such as beaches, to TCE. Particularly, (i) a double convolution has been added to consider the additional river discharge variable, (ii) an automatic piecewise function fitting method

have been used to model the duration of the extreme water levels events $d_z(z)$ (see below), (iii) a bootstrapping technique has been added to model the confidence bands in order to assess the uncertainty related to the results, and (iv) the temporal evolution has been introduced in order to consider the impact of the SLR in the probability of the extreme total water level events. The method is first developed to obtain the historical probability of extreme events of total water level during the nodal cycle 1995 - 2015. The method has then been readjusted to evaluate the spatial and temporal variations in the magnitude of extreme water level events in terms of return period across the TCE for the 21st-century.

6.2.1 Historical period: 1995 - 2015

In this section, the JPM is applied to the historical water level components to characterize the probability of the extreme total water level events during the historical period between 1995 to 2015. Fig. 6.2.1 shows the conceptual framework of the overall process.

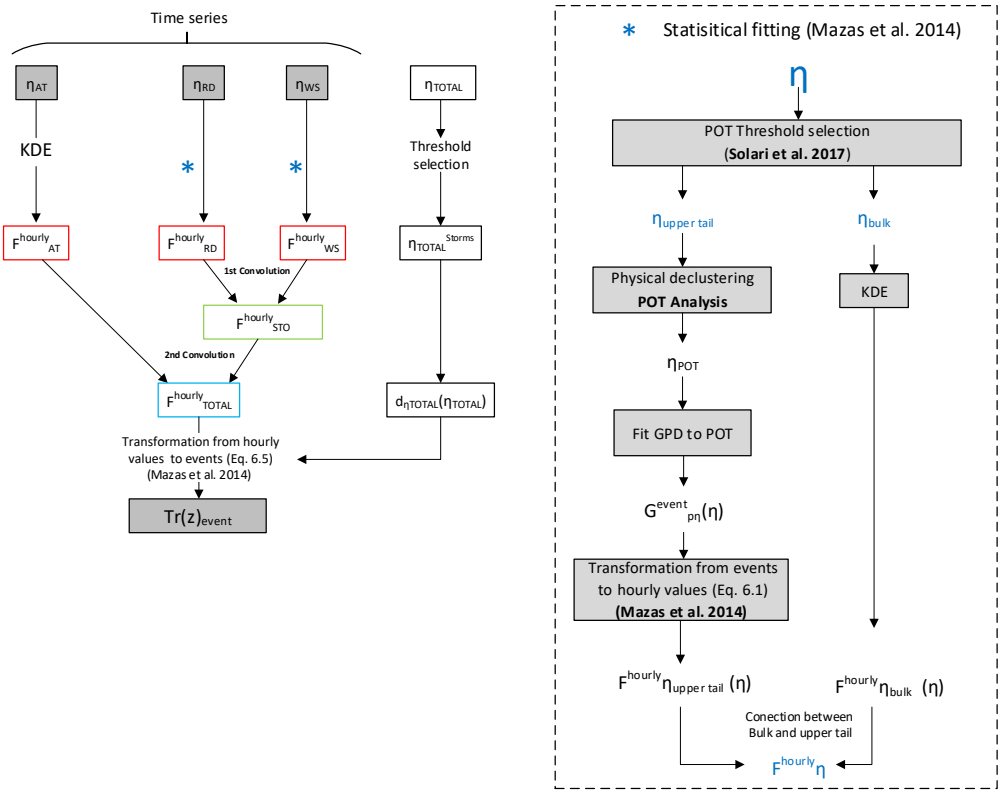

Figure 6.2.1: Diagram of the JPM methodology to characterize the probability of the extreme total water level events during the historical period.

First, the different components of the total water level are split into two mutually exclusive classes, i.e., values above and below a certain threshold (u), which separates the bulk from the upper tail. The selection of a proper threshold is necessary for a confident fitting of the extreme domain. There is several possibilities for this purpose (see, e.g., Coles (2001), Beguería (2005), and Thompson et al. (2009)). Here, as mentioned before we propose using the automatic methodology from Solari et al. (2017) because it quantifies the uncertainty of threshold estimation and its impact on the uncertainty of long return period quantiles.

For the statistical fitting, the work by Mazas et al. (2014) is followed. The lower part of the distribution (bulk values), where the data are dense enough, is modeled by an empirical density function via a nonparametric kernel density estimator (KDE). For the statistical extrapolation of the upper tail (extremes), a POT approach for declustering extreme events is first performed. Then, a GPD (Coles, 2001) is fitted to all independent and identically distributed peak exceedances over the threshold $G_{p\eta}^{events}(\eta)$. Each one of these peaks is associated with an extreme independent event. Finally, the distribution of extreme events is transformed into the distribution of the extreme hourly values ($F(\eta)$) via Eq. 6.1.

$$F(\eta) = 1 + \frac{n_p}{\nu K} d(\eta) \left[G_{p\eta}(\eta) - 1 \right], \quad \text{for } \eta > u \tag{6.1}$$

where η represents each component of total water level, n_p is the number of independent peak exceedances over u, K is the duration of the time series of observations, in years, ν is the number of observations (hours) per year and $d(\eta)$ is a parametric function fitted to the duration of the independent extreme events of the water level components over a threshold u. Then, the central region and the upper tail of the distribution are connected at the threshold value. As a result, the hourly distribution function of the components of the water level $F_{AT}(\eta_{AT})$, $F_{RD}(\eta_{RD})$ and $F_{WS}(\eta_{WS})$ are obtained.

As stated, the method is based on the double convolution of the marginal distributions of the three components of the water level. According to the definition of the convolution, if X and Y are two independent random variables with probability density functions f and g, respectively, then the probability density of the sum X + Y will be given by the convolution $f * g$, which is defined as the integral of the product of both functions after moving one of them a distance t (Eq. 6.2).

$$(f * g)(t) = \int_{-\infty}^{+\infty} f(\eta) g(t - \eta) d\eta. \tag{6.2}$$

Once the mixture distribution function is fitted to the components of the water level, the probability density function of the hourly tide-surge water level (F_{AT-WS}) is computed by convolving the density functions of the deterministic (η_{AT}) and the weather surge (η_{WS}) water levels by the expression:

$$P[\eta_{AT-WS} \leq y] = \int_{-\infty}^{y} \left(\int_{-\infty}^{+\infty} P(\eta_{AT} = x) \cdot P(\eta_{WS} = y - x) \cdot dx \right) \cdot dt \tag{6.3}$$

Then, the second convolution is performed to obtain the probability density function of the sum of the three water level components (F_{Joint}).

$$\begin{aligned} P[\eta_{Joint} \leq z] &= \int_{-\infty}^{z} \left(\int_{-\infty}^{+\infty} P(\eta_{AT} + \eta_{WS} = y) \cdot P(\eta_{RD} = z - y) \cdot dy \right) \cdot dt = \\ &= \int_{-\infty}^{z} \left(\int_{-\infty}^{+\infty} \left(\int_{-\infty}^{+\infty} P(\eta_{AT} = x) \cdot P(\eta_{WS} = y - x) \cdot dx \right) P(\eta_{RD} = z - y) \cdot dy \right) \cdot dt \end{aligned} \tag{6.4}$$

Finally, the corresponding total water level event (z) of return period $T_r(z)$ is obtained by Eq. 6.5 (Mazas et al., 2014),

$$T_r(z)_{events} = \frac{1}{\frac{\nu}{d_z(z)} [1 - F_{Joint}(z)]} \tag{6.5}$$

where ν is the number of observations (hours) per year, $d_z(z)$ is a parametric function fitted to the duration of the independent extreme events of total water level over a threshold z and F_{Joint} is the joint cumulative distribution function of total water level obtained by the double convolution. Since the model proposed in Mazas et al. (2014) for the duration curves $d_z(z)$ does not lead to a good fit for our data, piecewise functions with three subdomains are proposed to define these curves in this Thesis. To assess the uncertainty associated with the estimation of extreme total water level peak distributions, the 5% and 95% confidence intervals for the quantiles are computed by parametric bootstrapping.

In this Thesis, Joint Extreme Total Water Levels (JETWLs) represent the extreme total water level events for the return periods obtained in this way. The use of the JPM allows considering all the possible combinations between the extreme and non-extreme values of the water level components and not only those that took place in the historical period. As will be seen in the results, this is relevant in highly regulated transitional

coastal areas where the dam releases leading to extreme river discharge events usually occur during low tides to reduce the risk of flooding.

On the other hand, in assessing the JETWLs, no physical limitation is imposed regarding the crest height of the flood defenses (overtopping). Thus, this method allows for an accurate assessment of the agents' capacity to increase water levels. JETWLs obtained in this way are then compared with the return levels estimated from the annual maxima of the reconstructed total water level (dependent approach) with and without overtopping, denominated from now on as observed return levels with and without overflowing respectively.

6.2.2 Future period: 2020 - 2100

In the previous section, a double convolution technique of the marginal distribution of the historical water level components (F_{AT},F_{WS},F_{RD}) for a single nodal cycle between 1995 and 2015 was used to obtain the probability density function of the sum of the water level components (F_{Joint}). In this section, seven nodal cycles from 2020 to 2100 with a time step of ten years are considered. Fig. 6.2.2 illustrates the conceptual framework used to obtain the JETWLs along the 21st-century.

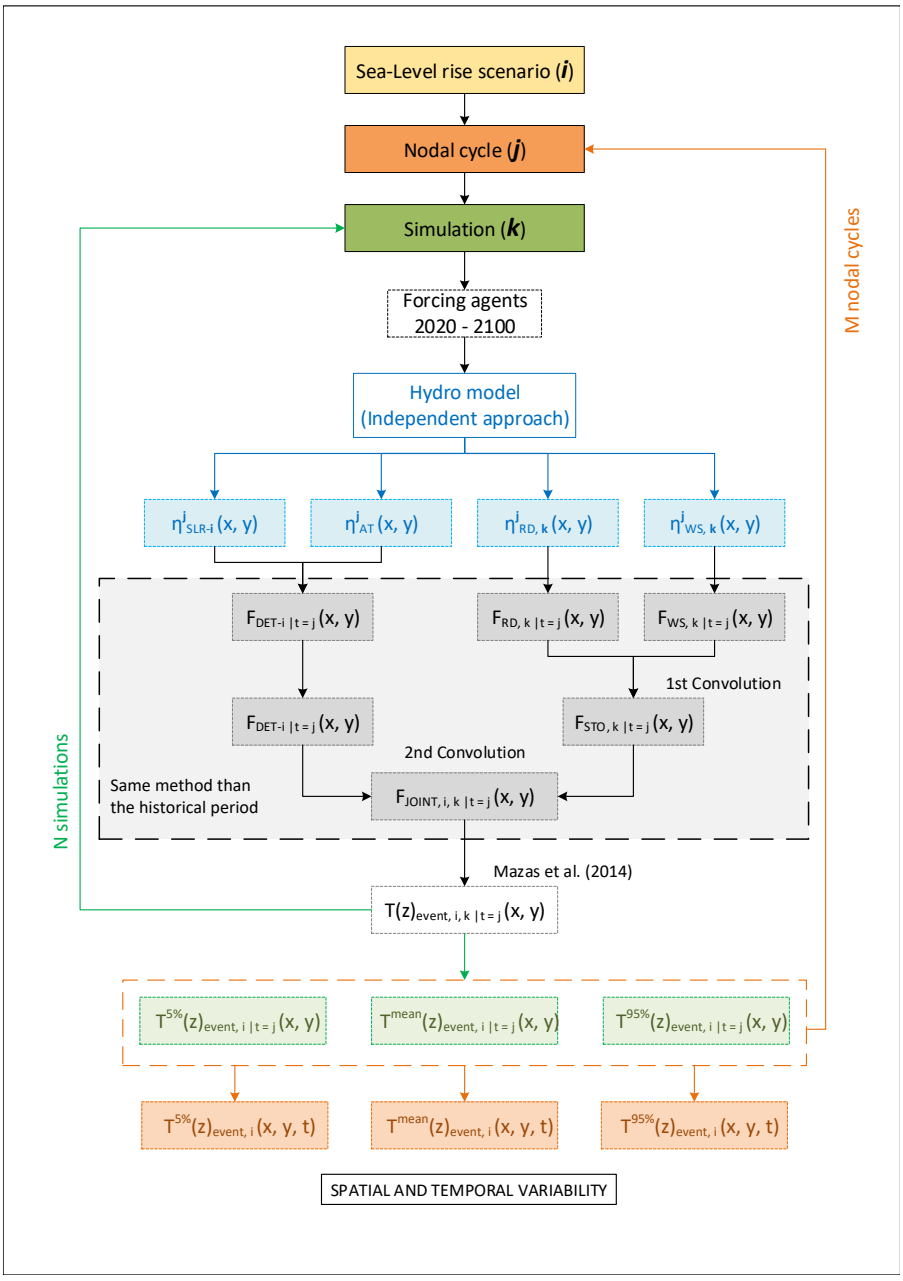

Figure 6.2.2: Conceptual methodology to obtain the magnitude of the extreme events of total level associated to the different return values together with their spatial and temporal variation for the 21st-century along the CTS.

First, the water level components associated with the first set of simulated forcing agents for the initial nodal cycle (2020 -2040) and a selected SLR scenario are extracted. The sum of the astronomical tide and SLR time series constitutes the deterministic component of the total water level. The water level components' statistical fitting follows the same procedure, as shown in the historical period. The hourly stochastic water level (F_{STO}) is then calculated by the first convolution between the stochastic components (η_{WS},η_{RD}). Then, the second convolution is performed to obtain the probability density function of the hourly joint total water level (F_{Joint}). After that, the corresponding total water level event (z) of return period $T_r(z)$ is obtained by Eq. 6.5. Due to a large number of simulations of the water level components computed in this section, the automatic algorithm of piecewise functions with three subdomains developed to fit the historical duration curves $d_z(z)$ is used here. To evaluate the uncertainty associated with the estimation of extreme total water level event distributions, the 5% and 95% confidence intervals for the quantiles are computed by parametric bootstrapping. So far, the presented method allows us to obtain the mean and 95% confidence bands of the JETWL in terms of return periods for only one future simulation of the water level components and only one nodal cycle in the period 2020-2100 and SLR scenario.

The overall process is repeated for each simulation of the water level components, in each of the seven nodal cycles and for both SLR scenarios. As a result, a bunch of mean, upper, and lower confidence bands of the JETWL is obtained for each nodal cycle, SLR scenario, and control point of the TCE. The mean of the central bands, the 97.5% percentile of the upper confidence bands, and the 2.5% percentile of the lower bands are extracted. As a result, the mean and 95%confidence bands of the JETWL values associated with each return period and conditioned to each nodal cycle are obtained along the TCE for the different SLR scenarios. The importance of the non-linear effects in the calculation of the extreme total water level events can be assessed through the analysis described in the next chapter (section 7.2). If these terms are not negligible, the procedures proposed by Mazas et al. (2014) and Dixon and Tawn (1995) and Dixon and Tawn (1999) can be implemented.

6.3 Results

6.3.1 Statistical fitting to the water level components

In this section, the bulk (the most common) and extreme values of the historical water level components series in the Guadalete estuary are statistically characterized following the methodology described in section 6.2.1. First, the Solari et al. (2017) method is applied for the threshold selection of the stochastic components of the water level (weather surge and river discharge) to separate the upper tail from the rest of the distribution. For the

astronomical tide, a percentile of 99.5 is used as the threshold value.

For the stochastic components, the lower and central parts of the hourly values distribution are modeled by the KDE functions. Then, a GPD distribution function is fitted to the declustered data (POT). Next, Eq. 6.1 is used to transform the distribution of the POT regimen into the upper tail of the distribution of the hourly values. Both parts are then connected at the threshold value. This process is repeated for each component of the total water level at each point for a complete characterization of the elevation along the estuary. For the astronomical tide component the KDE function is fitted for values between the lowest astronomical tide (LAT) and the highest astronomical tide (HAT) at each point.

Fig. 6.3.1 shows the hourly cumulative distribution function (CDF) of the components of the total water level in blue, orange, and yellow for the astronomical tide, river discharge, and weather surge, respectively for the historical period. Gray dots represent the sample's empirical distribution, and black points represent the threshold values that delimit the upper tail. The GPD parameters of the upper tail distribution (ξ and σ) are presented at each subplot with the threshold value (u) for the stochastic components. The R^2 determination coefficient between the empirical and GPD distribution is calculated for the upper tail values to indicate the goodness of the fit. Extreme values of the astronomical tide decrease upstream from 1.6 - 1.84 m (CP 1) to 0.73 - 0.9 m (CP 8) above LMSL. The elevation due to the river discharge is almost negligible in the outer part of the estuary (CP 1 and 2). In the middle part from CP 4 to CP 6, threshold values of the water level due to river discharge are approximately 0.2 m, and the maximum empirical values are between 1 and 2 m above LMSL. In the inner part, the river discharge's empirical extremes vary from 0.5 m to 3 m (CP 8). The water level values caused by weather surge are one order of magnitude lower than the rest at each point.

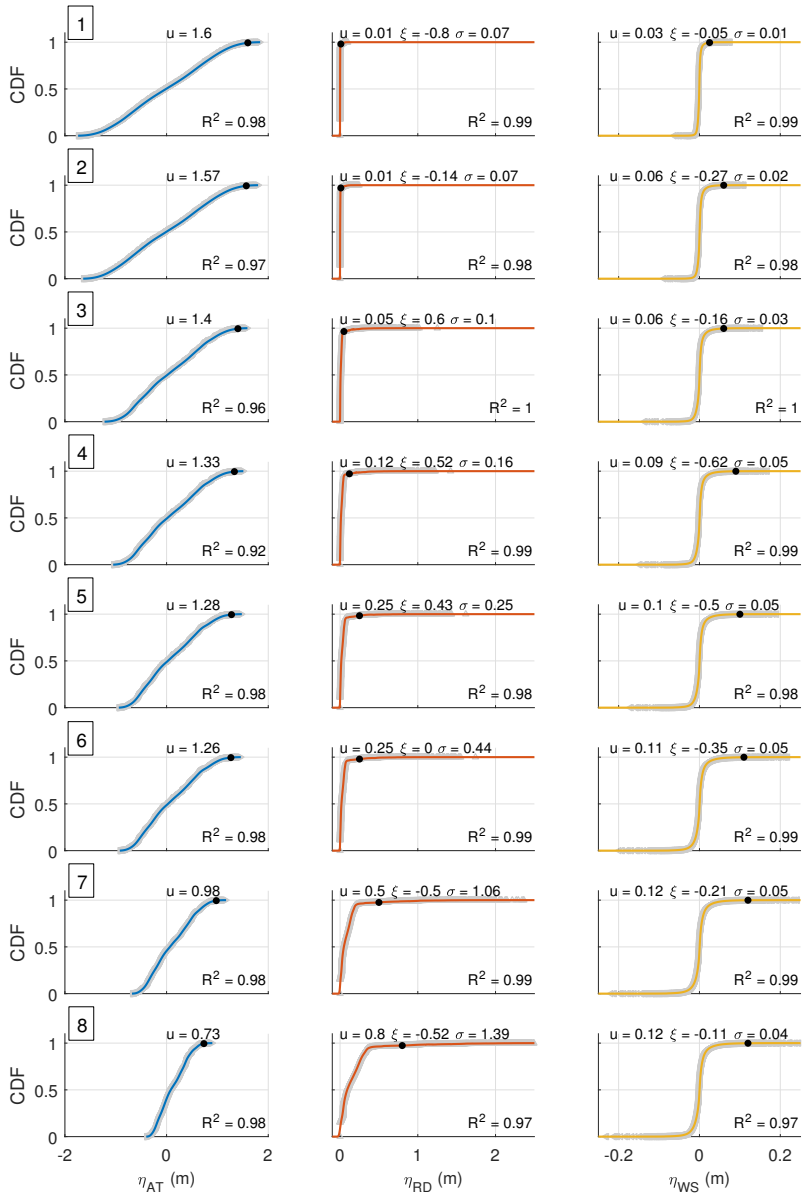

Figure 6.3.1: Statistical fitting of the hourly series of water level due to the astronomical tide (blue), river discharge (orange) and weather surge (yellow) at different points in the Guadalete estuary. Threshold value (u) and shape and scale (ξ and σ) parameters of the GPD distribution are shown. R^2 determination coefficients between empirical and GPD distribution values for the upper tail for each component at each point are also depicted.

6.3.2 Joint extreme total water level for the historical period

The methodology described in section 6.2.1 is used to assess the probability of extreme total water level events along the Guadalete estuary for the historical period of 1995 - 2015. The dashed blue line in Fig. 6.3.2 shows the Joint Extreme Total Water Levels (JETWLs) associated with each return period obtained in this way along the estuary. The continuous and dashed black line represents the crest height of flood defenses and the maximum height of the astronomical tide (HAT) at each point, respectively.

In the outer part of the estuary (CP 1 and 2), the JETWLs are equal to the HAT and always under the crest height. In the middle part (CP 4, 5, and 6), the 10 and 100 years return JETWLs are, on average, 20 cm and 70 cm higher than the crest height, respectively, thus leading to flooding hazards over the surrounding areas. In this part, the maximum values of the astronomical tide reached during high tides in spring tidal cycle are a few centimeters below the crest height of the flood defenses, which implies that any rise of water level induced by the other agents such as river discharge will increase the total level above the edge. In the inner part of the estuary at CP 7 and 8, the return JETWLs indicate that agents at these points can increase the water level over 1 m above the crest height for long return periods.

Gray areas represent the 95% confidence intervals of the JETWL for each return period, obtained via bootstrapping techniques. For this purpose, the original sample of sequences of exceedances over a threshold of η_{WS} was resampled with replacement, and the same was performed for η_{RD}. The size of the resampling remained fixed at each control point. Next, the return values of the JETWL were computed from the resamples via 10000 repetitions to obtain a precise estimate of the Bootstrap distribution of the statistic. Despite the computational effort, the result is 10000^2 different quantiles of the JETWL, whose 2.5% and 97.5% percentiles provide the 95% confidence interval represented in gray in Fig. 6.3.2. As will be seen in the next chapter, at the initial points of the estuary (CP 1 and 2), the water levels associated with the surge and the river flow peaks are nearly negligible, which reduces the width of the bands to almost zero. The opposite is found in the inner part of the estuary. At these points (CP 7 and 8), the JETWLs are very sensitive to the number of very high POT measurements of η_{RD}. The higher the number of these specific discharges during the bootstrapping, the higher the return levels and vice versa. However, the results show that for long return periods close to 50 years, the confidence bands of the extreme total water level events become asymptotic.

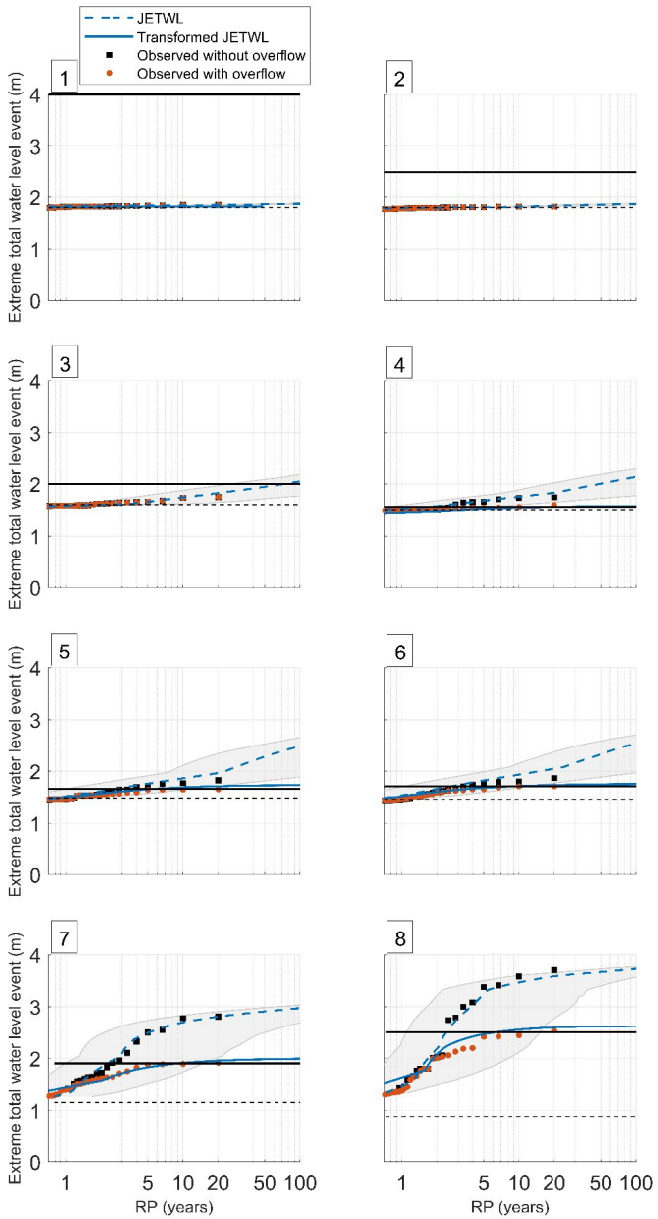

Figure 6.3.2: JETWLs (dashed blue line) with the 95% confidence intervals (gray), Observed levels with overflow (orange dots) and without overflow (black squares) and transformed JETWL (continuous blue line) along the Guadalete estuary. The continuous and dotted black lines represent the height of the edge of the river and the maximum height of the astronomical tide at each point for the 1995-2015 period, respectively.

JETWLs are compared with the observed return levels calculated without allowing the overflowing (black squares), represented by black dots in Fig. 6.3.2. As seen, the values are similar for both sides of the estuary, although differences are observed in the middle part (from CP 4 to 6) for long return periods where the observed return levels are 30% lower than the JETWL on average for the higher return periods. These differences are caused by interactions between the peaks and nonpeaks of the astronomical tide and river discharge described in the next chapter. According to the dam regulation policy, river discharge is spilled in neap tidal cycles to reduce the risk of flooding downstream (Fig. 6.3.3). Thus, the observed return levels without overflow are biased by this regulation, whereas those obtained via the double convolution (JETWL) takes into consideration all the possible combinations between the agents.

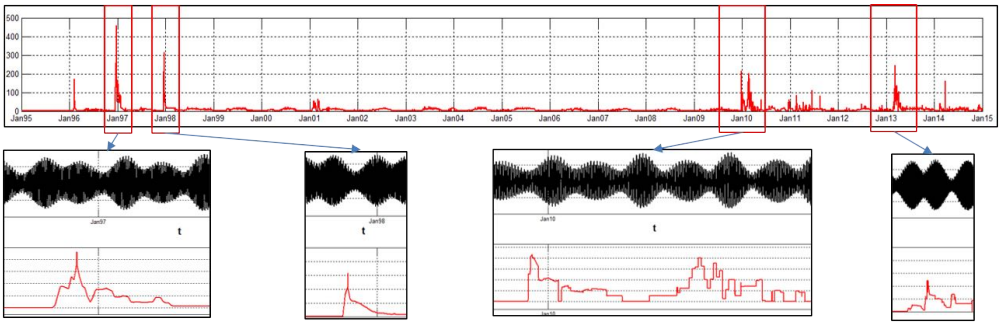

Figure 6.3.3: Historical time series of astronomical tide and river discharge. Simultaneity between river discharge events and neap tides.

Orange dots in Fig. 6.3.2 represent the observed return levels calculated allowing overflowing (orange dots). To compare these values, the JETWLs are modified via a simple physical model that considers the overflow. For this purpose, the Manning formula was used to calculate the relation between the levels with and without overflow for a given range of discharges. In the first case (with overflow), the river channel was supposed to be rectangular, and the floodplains trapezoidal. In the second case (without overflow), an unlimited rectangular river channel was used. These geometries were specifically accommodated to the geometry of the transversal section at each control point. This relation was used to transform the PDF of the JETWL. The transformed JETWLs are depicted in Fig. 6.3.2 with a continuous blue line. The results show a good agreement with the observed data. In the first 4-km of the estuary (CP 1 and 2), both return levels are equal to the HAT. At these points, the astronomical tide dominates the extreme conditions of the estuary. In the middle part of the estuary (from CP 4 to 6), the observed and transformed JETWLs are asymptotic to the edge of the river at the return period

between 5 and 10 years. However, in the inner part (CP 8 onwards), the edge is reached at a return period of 5 years. These results are consistent with historical observations in which three flooding events occurred between 1995 and 2015 since all the dams were active (1996, 2009 and 2010). Hence, the probability of extreme total water level events shows that a flooding event is expected along the middle and inner part of the estuary every seven years.

As seen, the observed and transformed JETWLs allow for the quantification of the frequency of the overflowing. However, they are upper limited because of overflowing over the channel edge, limiting our understanding of each event's magnitude. Without additional 2D analysis, these JETWL do not provide clear information about the "flooding potential" of the agents and their combination. Thus, the JETWLs without transformation provides an accurate assessment of the agents' capacity to increase the water level above the edge of the river and, hence, the magnitude of the flooding event. The differences in the magnitude of the extreme total water level peaks between the different levels are summarized in Tab.6.3.1 for five selected return periods (5, 10, 20, 50, and 100 years).

Points	1	2	3	4	5	6	7	8
River edge (m LMSL)	4.0	2.5	2.0	1.6	1.7	1.7	1.9	2.5
JETWL (m LMSL)	1.8	1.8	1.7	**1.7**	**1.8**	**1.8**	**2.5**	**3.2**
	1.8	1.8	1.7	**1.8**	**1.9**	**1.9**	**2.7**	**3.5**
	1.9	1.9	1.8	**1.8**	**2.0**	**2.1**	**2.9**	**3.6**
	1.9	1.9	**2.1**	**2.1**	**2.3**	**2.3**	**3.0**	**3.7**
	1.9	1.9	**2.1**	**2.2**	**2.5**	**2.6**	**3.0**	**3.8**
Transformed JETWL (m LMSL)	-	-	-	1.5	1.6	1.6	1.8	**2.5**
	-	-	-	**1.6**	**1.7**	**1.7**	**1.9**	**2.5**
	-	-	-	**1.6**	**1.7**	**1.7**	**2.0**	**2.6**
	-	-	-	**1.6**	**1.7**	**1.8**	**2.0**	**2.6**
	-	-	-	**1.6**	**1.7**	**1.8**	**2.0**	**2.6**
Observed level without overflow (m LMSL)	1.8	1.8	1.6	**1.7**	**1.8**	**1.7**	**2.5**	**3.4**
	1.8	1.8	1.7	**1.7**	**1.8**	**1.8**	**2.7**	**3.6**
	1.8	1.8	1.7	**1.7**	**1.8**	**1.9**	**2.8**	**3.7**
Observed level with overflow (m LMSL)	1.8	1.8	1.6	1.5	1.6	1.6	1.8	**2.5**
	1.8	1.8	1.7	**1.6**	**1.7**	**1.7**	**1.9**	**2.5**
	1.8	1.8	1.7	**1.6**	**1.7**	**1.7**	**1.9**	**2.5**

Table 6.3.1: River edge (first row), JETWL (second row), transformed JETWL (third row), observed return levels without overflow (fourth row) and observed return levels with overflow (fifth row) at the different control points along the Guadalete estuary referenced to the LMSL. Each subrow corresponds to return periods of 5, 10, 20, 50 and 100 years. Numbers in bold represent values higher than or equal to the river edge at each point.

6.3.3 Joint extreme total water level for the future period

In this section, the methodology described in section 6.2.2 was used to assess the magnitude of the extreme total water level events (JETWL) in terms of the return period and conditioned to each nodal cycle (temporal evolution) along the estuary (spatial variability)

for the different SLR scenarios. The results for the RCP8.5_95 and RCP4.5_05 SLR scenario are shown in Fig. 6.3.4 and 6.3.6. The different rows in Fig. 6.3.4 depict the spatial variation along the control points of the estuary. The x-axis of each subplot shows the temporal evolution along the nodal cycles. To assess the variability of the 100 simulations of the forcing agents, results are presented for the mean (middle column), and the lower (left column) and upper (right column) band of the 95 % confidence intervals of the JETWL. The lower band corresponds to "low-frequency discharge simulations". In contrast, the upper band is associated with "high-frequency discharge simulations" (see section 3.3.3.2).

Within each subplot, the magnitude of the JETWLs for the different return periods conditioned to each nodal cycle is represented by contour lines. To identify the influence of the river discharge, JETWL values higher than the highest astronomical tide plus the maximum SLR in the nodal cycle (HAT-SLR) are represented by a scale colormap from 0 to 5 referred to LMSL, while values equal or under the HAT-SLR are depicted with white color. To identify the failures, a red grid is superimposed to the JETWL higher than the flood defenses' crest height, which is depicted with a red contour line for each control point.

According to the results, three different areas can be distinguished. In the mouth region, which corresponds to the first 4 km of the estuary (CP 1 and CP 2), no significant differences are observed between the mean and the confidence band values of the JETWLs. As seen, for the RCP8.5_95 SLR scenario (first and second rows of Fig. 6.3.4), JETWL contour lines are vertical. Therefore, the maximum variations of the JETWL are observed from one nodal cycle to another, whereas no differences are observed between return periods for a selected nodal cycle. At these points, JETWLs are lower than the HAT-SLR (white color). The dominance of the deterministic tidal component results in the extreme values in this region not varying between the different return periods, always reaching the same value (same behavior than in the historical period). However, the increase of the SLR throughout the 21st-century leads to the growth of the JETWL along the x-axis.

The second significant area is found in the last 4 km of the estuary (CP 7 and CP 8), where the opposite situation occurs. Maximum differences are found between the mean and the lower and upper confidence band values. As illustrated in the bottom-right subplots of Fig.6.3.4, JETWL values are higher than the HAT-SLR and contour lines are horizontal for the high-frequency discharge simulations (upper band). The former indicates that in this area, the temporal evolution of the JETWL along the nodal cycles of the century is negligible. However, a significant variability, more than 2 m, is observed between the JETWL events of 1 year and 100 year return period.

A transitional area is found in the middle estuary (CP 3 to CP 6). Different behavior is observed in this region between the high and low-frequency discharge simulations and between the RCP4.5_05 and RCP8.5_95 SLR scenarios. In the case of low-frequency discharge simulations (left column of Fig. 6.3.4), the behavior is similar to that of the mouth region (CP 1 and CP 2). JETWL values are under HAT-SLR because of the limited influence of the river discharge. Besides, the influence of the SLR is lower than in the mouth region.

Consequently, the JETWL contour lines tend to be horizontal as we move upstream, reducing the temporal evolution of the JETWL. Besides, the dominance of the astronomical tide also limits the variabilities in the magnitude associated with the different return values. In the case of high-frequency discharge simulations (right column of Fig. 6.3.4), the behavior of the JETWL is more similar to the head of the estuary (CP 7 and CP 8). Contour lines quickly transform from vertical in CP 2 to horizontal in CP 3, making the temporal evolution insignificant from CP 3 inwards. As seen, the space between the contour lines reduces as we move upstream due to the increased effect of the discharge events.

The worst overflowing conditions are found in the middle part of the estuary. In this area, the levees' height is located at 2.0, 1.6, 1.7, and 1.7 m for CP 3, CP 4, CP 5, and CP 6, respectively. As seen, JETWL exceeds the height of the levees independently of the frequency of the river discharge events (left and right columns). However, the biggest vulnerability problem in this area is associated with the fact that the sum of extreme astronomical tidal events in combination with the SLR (HAT-SLR) is already above the levee height, as shown in the white areas with the red grid superimposed in the left column subplots of CP3, CP4, CP5, and CP6. These results are linked with the observations made in Fig. 5.3.2 regarding the number of flood defenses failures in this area and with those made in Fig. 6.3.2 related with the historical period.

The magnitude of the JETWL obtained in the previous figure allows the design of the crest height of the flood defenses needed to mitigate the probability of flooding in the estuary as a function of time, space, and for the different return periods. For example, if the estuary's central region is intended to be protected against events with a 50-year return period in 2100, a crest elevation of 2.5 m or 4 m will be necessary to prevent flooding with a 50 % and 95 % confidence, respectively. In some cases, this type of protective measure, known as "hard structures," will be unfeasible for environmental reasons. In these cases, it will be necessary to act on the agents responsible for producing these extreme events, as shown in the following chapeter.

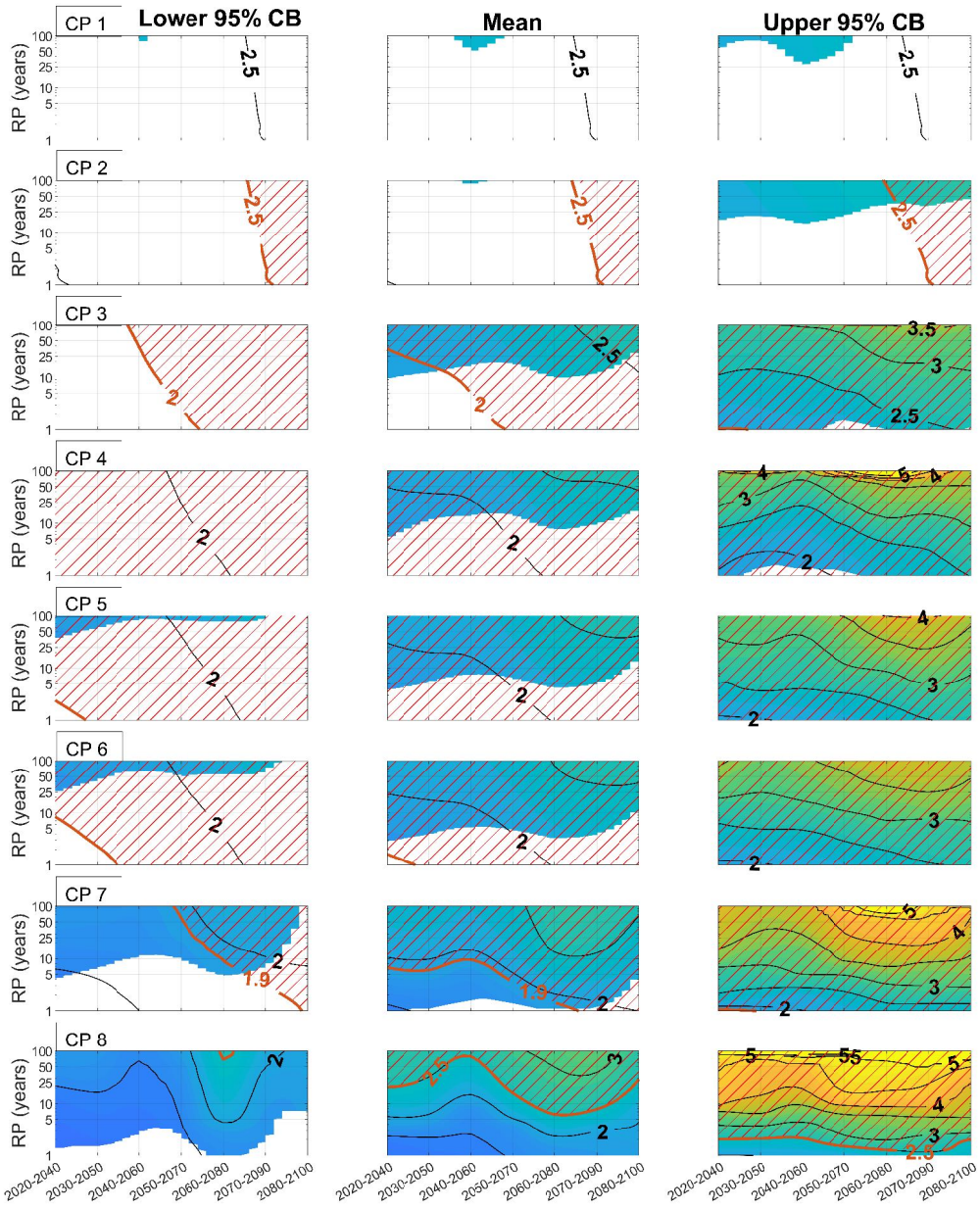

Figure 6.3.4: Contour plots of JETWL events with the spatial (rows) and temporal (x-axis) evolution of the mean (central column), lower (left column) and upper (right column) band of the 95 % confidence intervals for the different return periods between 1 to 100 (y-axis) for the RCP8.5_95 SLR scenario. JETWL events are represented with a scale colormap between 0 to 5 m (LMSL). Values lower than the HAT-SLR are represented in white and those higher than the flood defense height (in red contour line) are represented with red stripes.

The increase of the JETWL in percent with respect to the historical period from 1995 to 2015 is shown in Fig. 6.3.5 for the RCP8.5_95 SLR scenario. A color scale between -50% (yellow) and +50% (green) is used for the representation. Greenish and yellowish tones depicted positive and negative values, respectively. As seen, the higher the SLR and the frequency of the discharges, the higher the increase of the magnitude of the JETWL events, with maximum positive differences between 40 and 50 % observed by the end-century. However, negative differences can be observed in low-frequency discharge simulations compared to the historical period in the upper part of the estuary. This suggests that the high-frequency discharge simulations (right columns of Fig. 6.3.4 and 6.3.5) are more similar to the real river discharge time series observed during the historical period. The results for the RCP4.5_05 SLR scenarios are presented in Fig. 6.3.6 and 6.3.7.

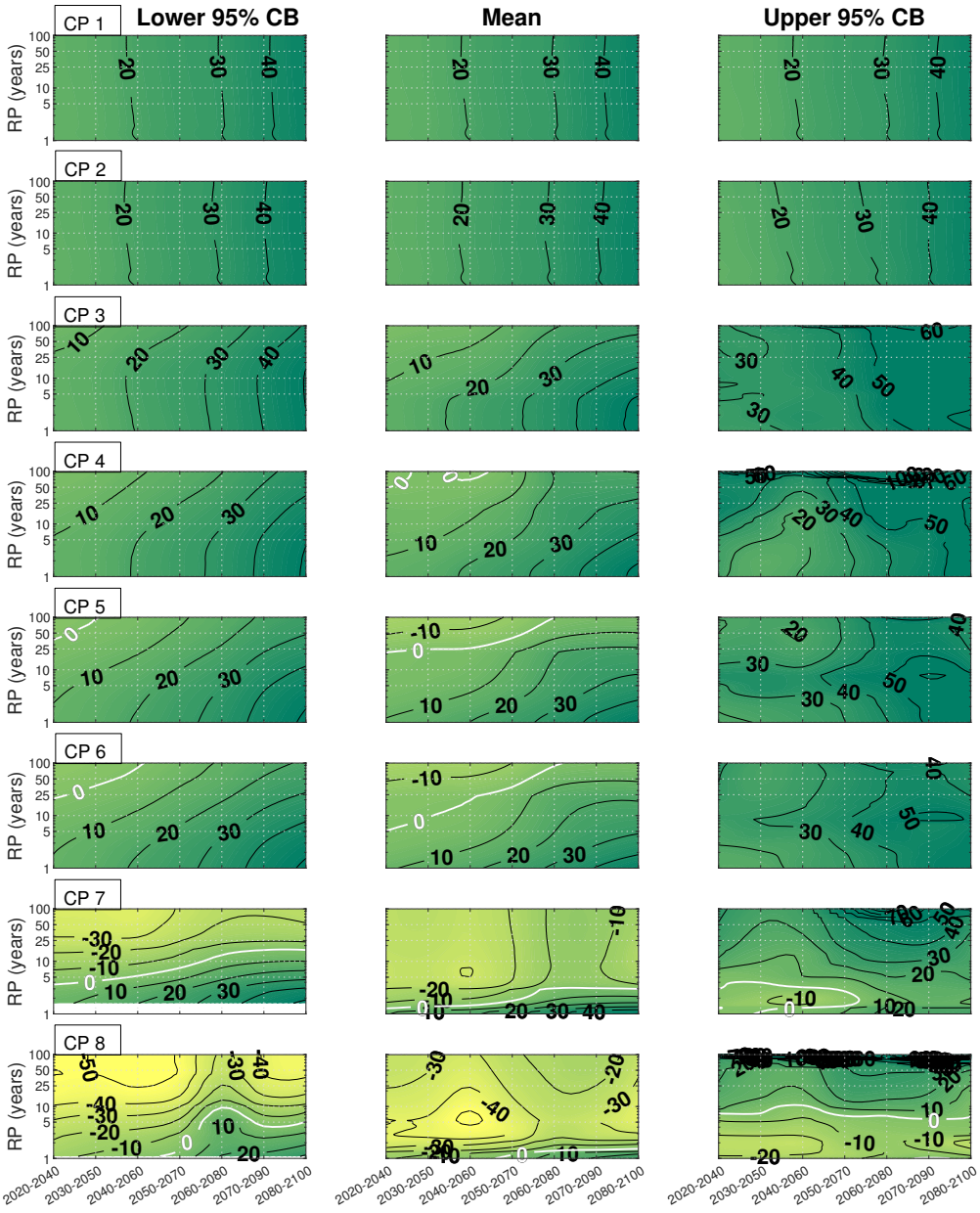

Figure 6.3.5: Contour plots with the differences in percent between the JETWL along the 21st-century and the JETWL calculated during the historical period from 1995 to 2015 for the RCP8.5_95 SLR scenario. Values are represented with a scale colormap between -50% (yellowish) to +50% (greenish).

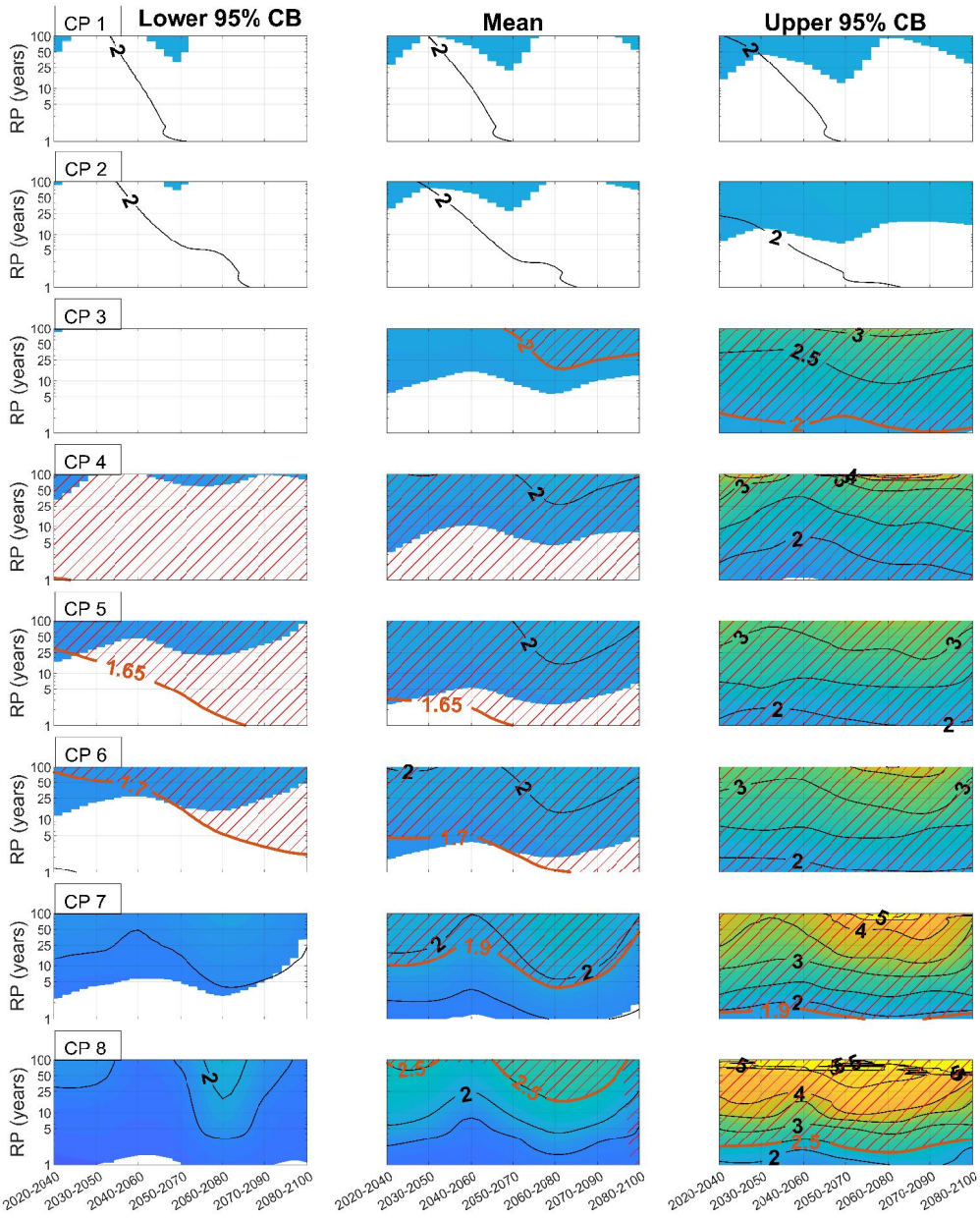

Figure 6.3.6: Contour plots of JETWL events with the spatial (rows) and temporal (x-axis) evolution of the mean (central column), lower (left column) and upper (right column) band of the 95 % confidence intervals for the different return periods between 1 to 100 (y-axis) for the RCP4.5_05 SLR scenario. JETWL events are represented with a scale colormap between 0 to 5 m (LMSL). Values lower than the HAT-SLR are represented in white and those higher than the flood defense height (in red contour line) are represented with red stripes.

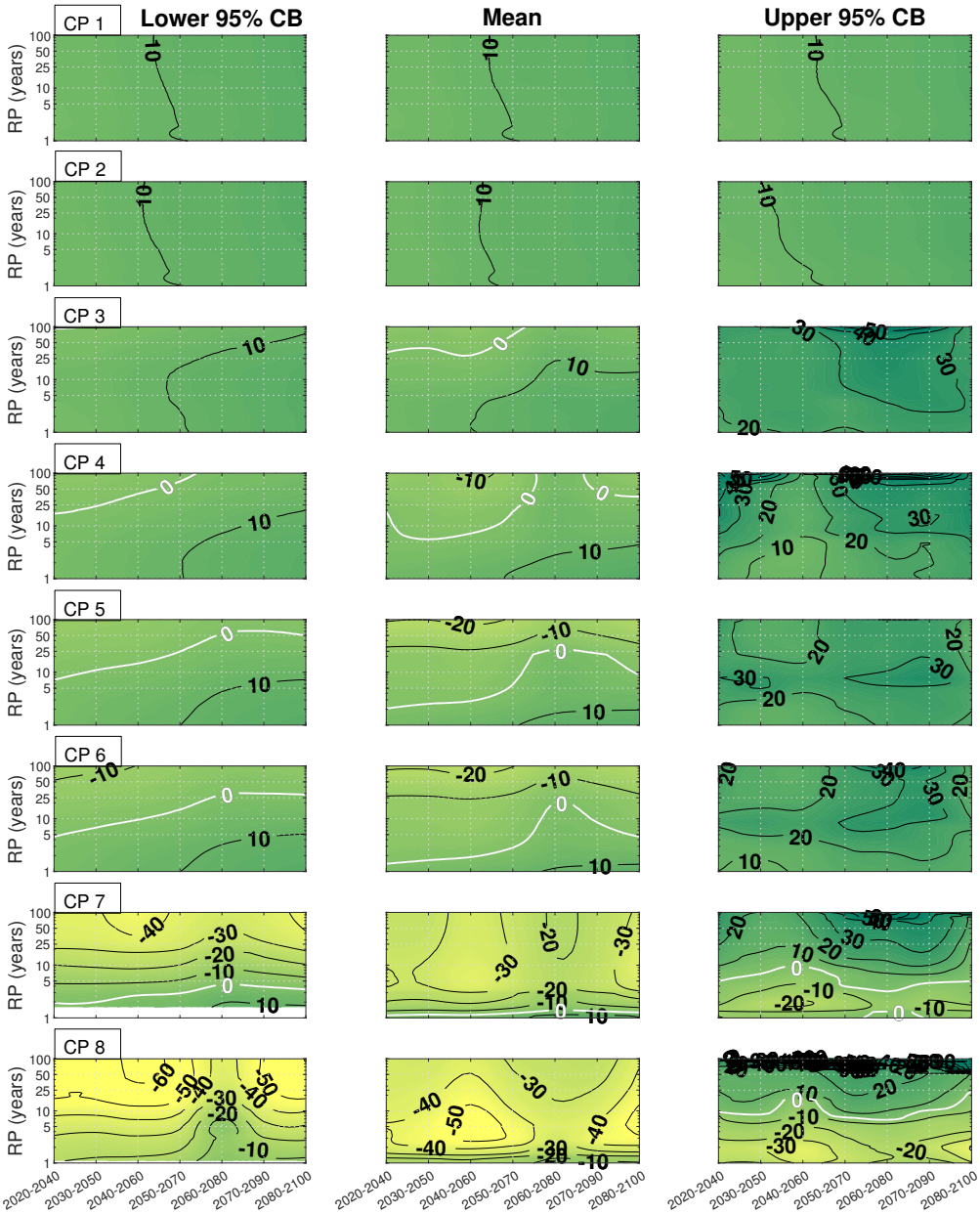

Figure 6.3.7: Contour plots with the differences in percent between the JETWL along the 21st-century and the JETWL calculated during the historical period from 1995 to 2015 for the RCP4.5_05 SLR scenario. Values are represented with a scale colormap between -50% (yellowish) to +50% (greenish).

6.4 Summary and conclusions

The individual water level components obtained through the independent approach are used in this chapter to assess the probability of the extreme total water level events in terms of return period along the estuary and the 21st-century. The presented methodology allows coastal engineers and managers to characterize the expected magnitude of the extreme flood events in probabilistic terms and the associated uncertainty assessment. To this end, this chapter successfully adapts the well-known Joint Probability Method to transitional coastal environments with simultaneous agents and a progressive sea-level rise induce by global warming. The main advantage of the method is that it easily allows switching between probability distribution functions with hourly frequency to event frequency and vice versa. To perform this, a mixture model (central body and upper tail) is fitted to the hourly water level components to obtain the total water level events' probability distribution function. The methodology is first applied to the historical water level time series and then to the 21st-century period. The following conclusions can be drawn from the analysis during the historical period:

- In the outer estuary (CP 1 and 2), the Joint Extreme Total Water Levels (JETWL) events obtained by applying the proposed method, are equal to the highest astronomical tide, and always under the height of the flood defenses. In the middle estuary, the 10 and 100 years return period JETWLs are, on average, 20 cm and 70 cm higher than the flood defense height, respectively. However, in the inner estuary (CP 7 and 8), these values are 1 m higher than the defenses' crest.
- When JETWLs are compared with observed return levels, obtained via the annual maxima method, similar values are found at both sides of the estuary. However, differences are observed in the middle part (CP 4 to CP 6) for long return periods, where the observed return levels are 30 % lower than the JETWL on average. These differences are caused by the interactions between the peaks and non-peaks of the astronomical tide and river discharge. According to the dam regulation policy, river discharge is spilled in neap tidal cycles to reduce the risk of flooding downstream. Thus, the observed return levels are biased by this regulation, whereas the JETWL takes into consideration all the possible combinations between the agents.
- No physical limitation is imposed (overtopping) to the JETWLs calculated by the proposed methodology. Thus, the method allows for an accurate assessment of the agents' capacity to increase the water levels. To model the effect of the overflowing on the return period curves of JETWL, a simplified physical model is developed.
- The analysis of the probability of extreme total water level events shows that a flooding event is expected along the middle and inner parts of the estuary every

seven years on average. These results are consistent with the historical observation in which three flooding events occurred in the period between 1995 - 2015 since all the dams were active (1996, 2009, and 2010)

In the historical period, a single series of historical water level components for a single nodal cycle between (from 1995 to 2015) was used to obtain the sum of the water level components' probability distribution function. However, for the future period, seven nodal cycles from 2020 to 2100 with a ten-year time step are considered for two sea-level rise scenarios and 100 simulations of the water level components. Therefore, the former method is repeated 1400 ($100 \times 7 \times 2$) times to obtain the temporal and spatial evolution of the mean and the 95 % confidence bands of the JETWL values associated with each return period along the 21st-century and the transitional coastal environments. In the case that the current coastal flood defenses are not sufficient to protect the territory against global warming throughout the 21st-century, this method allows managers and stakeholders to know the expected magnitude of future flood events in probabilistic terms. This makes it possible to design the coastal defenses' necessary height at any point of the estuary or period of time, thus optimizing the costs of protection. The following conclusions can be drawn from the analysis during the future period:

- The worst overflowing conditions for the 21st-century are found in the middle part of the estuary (from CP 3 to CP 6). JETWL exceeds the height of the levees independently of the frequency of the river discharge events. However, the biggest vulnerability problem in this area is the fact that the sum of extreme astronomical tidal events combined with the sea-level rise is already above the height of the levees. These results are linked with the observations made in the last chapter regarding the number of flood defenses failures in this area.
- The magnitude of the JETWL obtained after applying the presented method allows designing the crest height of the flood defenses needed to mitigate the probability of flooding in the estuary as a function of time, space, and for the different return periods. For example, if the estuary's central region is intended to be protected against events with a 50-year return period in 2100, a crest elevation of 2.5 m or 4 m will be necessary to prevent flooding with a 50 % and 95 % confidence, respectively. In some cases, this type of protective measure, known as "hard structures," will be unfeasible for environmental reasons. In these cases, it will be necessary to act on the agents responsible for producing these extreme events, as shown in the following chapter.
- The increase of the JETWL in percent with respect to the historical period from 1995 to 2015 is also calculated. The higher the sea-level rise and the frequency of

the discharges, the higher the increase of the magnitude of the JETWL events, with maximum positive differences between 40 and 50 % observed by the end-century.

CHAPTER 7

MECHANISM OF GENERATION OF EXTREME FLOOD EVENTS

7.1 Introduction

In this chapter, all the disaggregated information of the water level components is used to study (i) the contribution of the non-extreme and extreme values of each water level component to the magnitude (mean) and variability (variance) of the extreme events of the total elevation, (ii) the concomitance between extreme values of each component and their relations of dependence with the bulk and the extremes of the other variables, (iii) the importance of the non-linear interaction term in the formation of the extreme events, and (iv) the degree of dependence or independence between the different components of the total water level. Once the magnitude of the flooding events has been characterized, it is necessary to disaggregate and understand the mechanisms of the formation of such extreme events to know on which agents it is necessary to act to optimize the costs of the mitigation measurements. The methodology presented in this chapter is built upon the work developed by Folgueras (2016). In this work, the statistical relations established between a random variable that is a linear combination of a set of others acting simultaneously and the variables obtained from classifying each component in a set of mutually exclusive classes are analyzed. This chapter adapts these relations developed by Folgueras (2016) to the particular case of water levels in transitional coastal environments to address the mechanisms of the formation of extreme total water level events. The sections of this chapter organize as follows. In §7.2, the relations of simultaneity, and compatibility between the water level components are addressed. The

results, presenting the mechanisms of formation of flood events in the Guadalete estuary, are shown in §7.3.1 for the historical period and §7.3.2 for the 21st-century.

7.2 Analysis of the simultaneity and compatibility relationship between the water level components.

7.2.1 Formulation

7.2.1.1 Definitions

Given a random vector η_T^e, defined as the exceedances over the threshold of the total water level, formed by D components, defined as the concomitant values of the water level components ($\eta_{AT}|\eta_T^e$, $\eta_{RD}|\eta_T^e$, $\eta_{WS}|\eta_T^e$ and $\eta_{NL}|\eta_T^e$) that have the common characteristic of acting simultaneously and whose values can be classified into C mutually exclusive classes (extremes and non-extremes), the following random variables are defined:

- η_d is the d component of the total water level (i.e., $\eta_{AT}|\eta_T^e$, $\eta_{RD}|\eta_T^e$, $\eta_{WS}|\eta_T^e$ and $\eta_{NL}|\eta_T^e$)
- η_T^e is the sum of the η_d components and represent the random vector of the extreme total water level events.
- $\eta_{d,c}$ is the random variable that characterizes the values of η_d belonging to class c (e.g., $\eta_{RD,1}$ is a random vector containing only the extreme values of the component $\eta_{RD}|\eta_T^e$).
- η_C is the sum of the values of the random vector $\eta_{d,c}$, i.e, the sum of the values of the water level components belonging to the class c.
- N is the size of the extreme total water level event sample
- $n_{d,c}$ is the size of the subsample $\eta_{d,c}$. It is verified that $n_{d,c} \leq N$.

Fig.7.2.1 shows an outline with the defined variables. In the left panel, the values of the components η_d of a sample of size N are presented vertically. The sum of the components of each sampled vector results in an observation of the random vector η_T^e. Assuming that the values of each η_d component are classified in C mutually exclusive classes, the variables corresponding to each class are shown in the right panel. As in the left panel, the values of the variables $\eta_{d,c}$ are shown vertically, indicating with a $\ominus$ sign those observations of the component η_d that does not have a value in class c, that is to say, $\ominus \Rightarrow \nexists \eta_{d,c_n}$. Under each variable $\eta_{d,c}$ the number of elements $n_{d,c}$, present in a

sample of $\eta_{d,c}$, is indicated. This value is, in general, another random variable. Finally, the sum of the components of η_{d,c_n} gives the value of the variable η_{c_n}

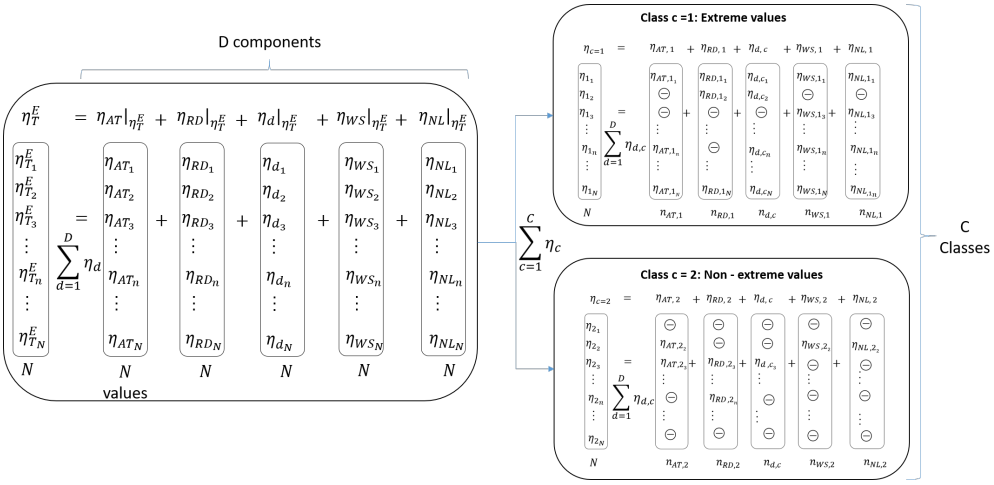

Figure 7.2.1: Diagram of relationships between the defined variables

7.2.1.2 Relationships between the statistical descriptors of the variables

The following hierarchical structure between components, classes and resultant is established and described in Fig.7.2.2:

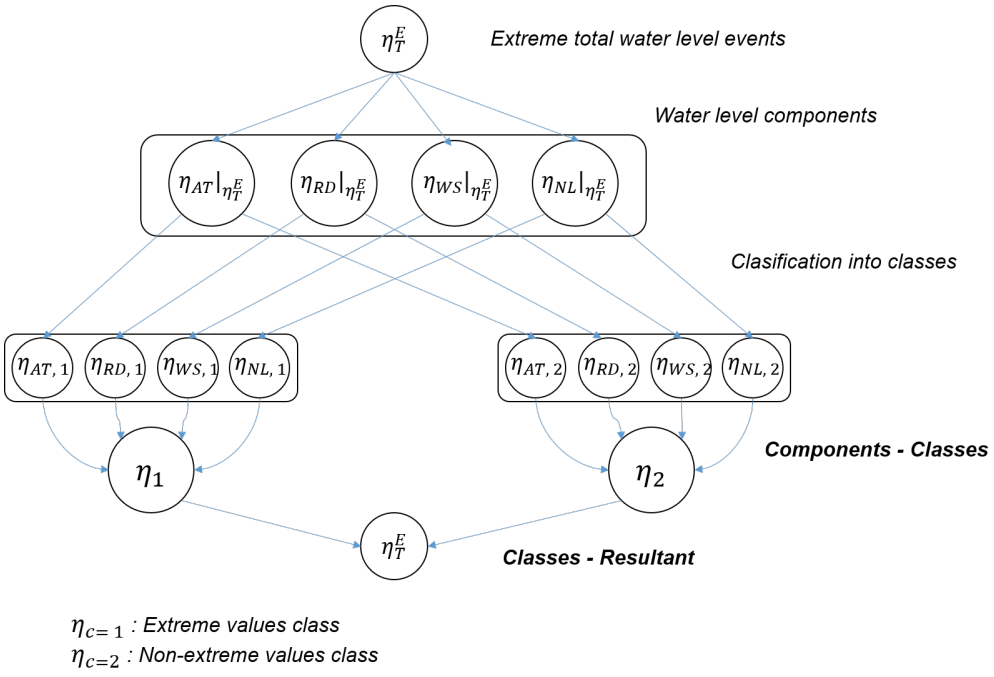

Figure 7.2.2: Hierarchical relationship between components, classes and resultant

Relationships between Classes - Resultant

In this group are the relationships that link the characteristics of the contributions of each class η_C with the resulting η_T^e. These relations depend on: (1) the statistical properties of each class and (2) the conditions of compatibility between them. The Eq. 7.1 and 7.2 show these relations in terms of the mean ($E[X]$) and variance ($Var(X)$) statistics.

$$E[\eta_T^e] = \sum_{c=1}^{C} E[\eta_c] \tag{7.1}$$

$$Var(\eta_T^e) = \sum_{c=1}^{C} Var(\eta_c) + 2\sum_{i \neq j}^{C} Cov(\eta_i, \eta_j)] \tag{7.2}$$

where $Cov(\eta_i, \eta_j)$ is the covariance operator between the different classes. Therefore, this operator represents the correlations between classes called from now on “inter-class correlations.”

Relationships between Components - Classes

In this group are the relationships that link the characteristics of the variables $\eta_{d,c}$ with the contribution of each class η_c. These are conditioned by (1) the statistical properties of the components that belong to class c, (2) the simultaneity between them, and (3) the compatibility of the simultaneous values. The Eq. 7.3 and 7.4 describe these relationships in terms of the mean ($E[X]$) and variance ($Var(X)$) statistics.

$$E[\eta_c] = \sum_{d=1}^{D} \frac{n_{d,c}}{N} E[\eta_{d,c}] \tag{7.3}$$

$$Var[\eta_c] = \sum_{d=1}^{D} Var[\eta_{d,c}] \left[1 + \frac{N - n_{d,c}}{N} \left[\frac{n_{d,c}}{N} \frac{1}{CV^2(\eta_{d,c})} - 1\right]\right] + 2 \sum_{i \neq j}^{D} Cov(\eta_{i,c}, \eta_{j,c}) \tag{7.4}$$

where CV^2 is the coefficient of variation squared $CV^2(\eta_{d,c}) = \frac{Var(\eta_{d,c})}{E^2[\eta_{d,c}]}$, $Cov(\eta_{i,c}, \eta_{j,c})$ is the covariance operator between the components belonging to the same class c, $\frac{n_{d,c}}{N}$ is an estimator of the probability that an element of component d belongs to class c.

The development for obtaining the expression of the first term of the variance is shown below. First, the expression of the variance of η_c and $\eta_{d,c}$ in terms of the mean is assumed.

$$Var(\eta_c) = E[\eta_c^2] - E^2[\eta_c] = \sum_{d=1}^{D} \left[\frac{n_{d,c}}{N} E[\eta_{d,c}^2] - \frac{n_{d,c}^2}{N^2} E^2[\eta_{d,c}]\right]$$

$$\sum_{d=1}^{D} Var(\eta_{d,c}) = \sum_{d=1}^{D} E[\eta_{d,c}^2] - \sum_{d=1}^{D} E^2[\eta_{d,c}]$$

Making the difference between both expressions and reordering:

$$Var(\eta_c) = \sum_{d=1}^{D} Var(\eta_{d,c}) + \sum_{d=1}^{D} \left[\frac{n_{d,c-N}}{N} E[\eta_{d,c}^2] - \frac{n_{d,c}^2 - N^2}{N^2} E^2[\eta_{d,c}]\right]$$

Operating:

$$
\begin{aligned}
Var(\eta_c) &= \sum_{d=1}^{D} Var(\eta_{d,c}) \left[1 + \frac{n_{d,c-N}}{N} \frac{E[\eta_{d,c}^2]}{Var(\eta_{d,c})} - \frac{n_{d,c}^2 - N^2}{N^2} \frac{E^2[\eta_{d,c}]}{Var(\eta_{d,c})} \right] \\
&= \sum_{d=1}^{D} Var(\eta_{d,c}) \left[1 + \frac{n_{d,c-N}}{N} \frac{Var(\eta_{d,c}) + E^2[\eta_{d,c}]}{Var(\eta_{d,c})} - \frac{n_{d,c}^2 - N^2}{N^2} \frac{E^2[\eta_{d,c}]}{Var(\eta_{d,c})} \right] \\
&= \sum_{d=1}^{D} Var(\eta_{d,c}) \left[1 + \frac{n_{d,c-N}}{N} \left[1 + \frac{E[\eta_{d,c}^2]}{Var(\eta_{d,c})} \right] - \frac{n_{d,c}^2 - N^2}{N^2} \frac{E^2[\eta_{d,c}]}{Var(\eta_{d,c})} \right]
\end{aligned}
$$

Considering the definition of coefficient of variation CV as $CV = \frac{\sigma}{\mu}$ and squaring it, we can say that $CV^2(\eta_{d,c}) = \dfrac{Var(\eta_{d,c})}{E^2[\eta_{d,c}]}$. Substituting this expression into the above equation gives the following expression:

$$
\begin{aligned}
Var(\eta_c) &= \sum_{d=1}^{D} Var(\eta_{d,c}) \left[1 + \frac{n_{d,c-N}}{N} + \frac{n_{d,c-N}}{N} \frac{1}{CV^2(\eta_{d,c})} - \frac{n_{d,c}^2 - N^2}{N^2} \frac{1}{CV^2 \eta_{d,c}} \right] \\
&= \sum_{d=1}^{D} Var[\eta_{d,c}] \left[1 + \frac{N - n_{d,c}}{N} \left[\frac{n_{d,c}}{N} \frac{1}{CV^2(\eta_{d,c})} - 1 \right] \right]
\end{aligned}
$$

Regarding the covariance operator between the components belonging to the same class c, $Cov(\eta_{i,c}, \eta_{j,c})$, it is necessary to make the following distinction. If only the covariance between the simultaneous values of the different components were considered, this covariance would respond to the following expression (Folgueras, 2016):

$$
Cov(\eta_{i,c}, \eta_{j,c}) = \frac{n_{i_s j,c}}{N} E[\eta_{i_s j,c} \eta_{j_s i,c}] - \frac{n_{i_s j,c} n_{j_s i,c}}{N^2} E[\eta_{i_s j,c}] E[\eta_{j_s i,c}] \tag{7.5}
$$

However, in the case analyze in this Thesis, the combination of water level components that combine to give an extreme value of total water level, forces to consider not only situations where an extreme value of a component acts simultaneously with another extreme of another component, but also situations where a non-extreme value is combined with other extremes and non-extremes. By making this distinction, the expression of Eq. 7.6 it is obtained.

$$
\begin{aligned}
Cov(\eta_{i,c},\eta_{j,c}) = & \underbrace{\frac{n_{i_s j,c}}{N} E[\eta_{i_s j,c}\eta_{j_s i,c}] - \frac{n_{i_s j,c} n_{j_s i,c}}{N^2} E[\eta_{i_s j,c}]E[\eta_{j_s i,c}]}_{A} - \\
& \underbrace{- \frac{N - n_{i_s j,c}}{N} E[\eta_{i_s j,c}\eta_{j_s i,c}] + \frac{N^2 - n_{i_s j,c}^2}{N^2} E[\eta_{i_s j,c}]E[\eta_{j_s i,c}]}_{A} - \\
& \underbrace{- \frac{n_{i_{ns} j,c}}{N} E[\eta_{i_{ns} j,c}] - \frac{n_{j_{ns} i,c}}{N} E[\eta_{j_{ns} i,c}]}_{B} - \\
& \underbrace{- \frac{n_{i_s j,c}}{N} E[\eta_{i_s j,c}] - \frac{n_{j_{ns} i,c}}{N} E[\eta_{j_{ns} i,c}]}_{C} - \\
& \underbrace{- \frac{n_{j_s i,c}}{N} E[\eta_{j_s i,c}] - \frac{n_{i_{ns} j,c}}{N} E[\eta_{i_{ns} j,c}]}_{C}
\end{aligned}
\tag{7.6}
$$

where $\eta_{i_s j,c}$ are the values of the water level component $\eta_{i,c}$ that occur simultaneously with the values of the water level component $\eta_{j,c}$ both belonging to class c, likewise $\eta_{j_s i,c}$ are the values of the water level component $\eta_{j,c}$ that occur simultaneously with the values of the water level component $\eta_{i,c}$ both belonging to class c, $\eta_{i_{ns} j,c}$ are the values that do not meet this condition, in other words, they are the values of the water level component $\eta_{i,c=m}$ belonging to class $c = m$ that occur simultaneously with the values of the water level component $\eta_{j,c=n}$ belonging to another class $c = n$. In the same way, $n_{i_s j,c}$ and $n_{i_{ns} j,c}$ are the number of simultaneous and non-simultaneous values of the pairs $i - j$ in a sample size of N, respectively. Fig. 7.3.3 shows a theoretical example of the meaning of each of the variables.

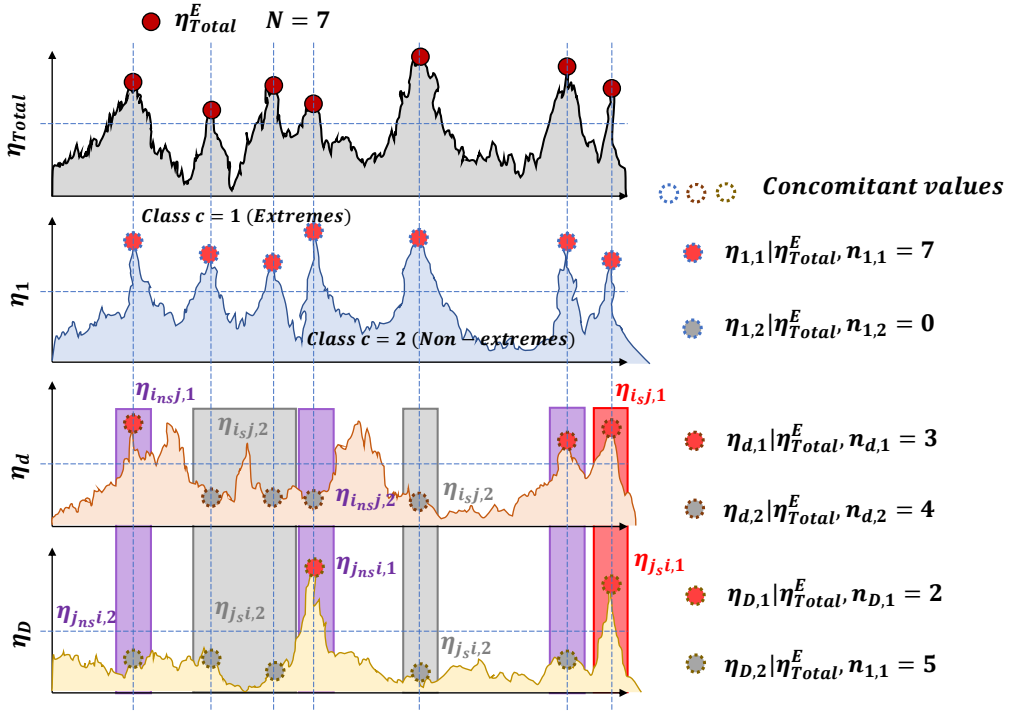

Figure 7.2.3: Theoretical example of the relations of simultaneity and compatibility between the water level components.

The interpretation of the covariance of Eq. 7.6 is complicated because of the large number of terms involved. To facilitate their interpretation it is possible to isolate three blocks: (A) the isolated effect of the correlation between simultaneous components belonging to the same class and therefore included in the “intra-class” correlation; (B) the isolated effect of the correlation between non-simultaneous components or, in other words, the correlation between components belonging to different classes and therefore included in the “inter-class correlation”; and (C) a combination of both whose contribution is equally distributed between the inter-class and intra-class correlation.

Relationships between Components - Resultant

Previous expressions can be combined to obtain the relationships between the statistics of the resultant and the components belonging to a specific class.

$$E[\eta_T^e] = \sum_{c=1}^{C} \underbrace{\left\{ \underbrace{\sum_{d=1}^{D} \underbrace{\frac{n_{d,c}}{N} E[\eta_{d,c}]}_{E_A}}_{E_B} \right\}}_{} + \underbrace{E[\eta_{NL} | \eta_T^e]}_{E_C} \tag{7.7}$$

where E_A is the contribution of each component to the class mean; E_B is the contribution of each class to the mean of the extreme total water level events; E_C is the contribution of the non-linear term to the mean of the extreme total water level events.

$$
\begin{aligned}
Var(\eta_T^e) = \sum_{c=1}^{C} \Bigg\{ \underbrace{\sum_{d=1}^{D} \underbrace{Var[\eta_{d,c}] \left[1 + \frac{N - n_{d,c}}{N} \left[\frac{n_{d,c}}{N} \frac{1}{CV^2(\eta_{d,c})} - 1 \right] \right]}_{Var_A}}_{Var_B} \Bigg\} + \\
+ \underbrace{Var(\eta_{NL}|\eta_T^e) + 2Cov(\eta_{NL}|\eta_T^e, \eta_T^e)}_{Var_C} + \\
+ \underbrace{2 \sum_{i \neq j}^{C} Cov(\eta_i, \eta_j)]}_{Var_{D_1}} + \sum_{c=1}^{C} \Bigg\{ \underbrace{2 \sum_{i \neq j}^{D} \frac{n_{i_{ns}j,c}}{N} E[\eta_{i_{ns}j,c}] - \frac{n_{j_{ns}i,c}}{N} E[\eta_{j_{ns}i,c}] -}_{Var_{D_2}} \\
\underbrace{- \frac{1}{2} \frac{n_{i_sj,c}}{N} E[\eta_{i_sj,c}] - \frac{n_{j_{ns}i,c}}{N} E[\eta_{j_{ns}i,c}] - \frac{1}{2} \frac{n_{j_si,c}}{N} E[\eta_{j_si,c}] - \frac{n_{i_{ns}j,c}}{N} E[\eta_{i_{ns}j,c}]}_{Var_{D_3}} \Bigg\} + \\
+ \sum_{c=1}^{C} \Bigg\{ \underbrace{2 \sum_{i \neq j}^{D} \frac{n_{i_sj,c}}{N} E[\eta_{i_sj,c} \eta_{j_si,c}] - \frac{n_{i_sj,c} n_{j_si,c}}{N^2} E[\eta_{i_sj,c}] E[\eta_{j_si,c}] -}_{Var_{E_1}} \\
\underbrace{- \frac{1}{2} \frac{n_{i_sj,c}}{N} E[\eta_{i_sj,c}] - \frac{n_{j_{ns}i,c}}{N} E[\eta_{j_{ns}i,c}] - \frac{1}{2} \frac{n_{j_si,c}}{N} E[\eta_{j_si,c}] - \frac{n_{i_{ns}j,c}}{N} E[\eta_{i_{ns}j,c}]}_{Var_{E_2}} \Bigg\}
\end{aligned}
\tag{7.8}
$$

where Var_A is the contribution of each component to the class variance; Var_B is the contribution of each class to the variance of the extreme total water level events; Var_C is the contribution of the non-linear term to the variance of the extreme total water level events; Var_D is the inter-class correlation which is composed of Var_{D_1}: the covariance between classes; Var_{D_2}: the covariance between non-simultaneous components belonging to different classes; and Var_{D_3}: the 50 % of covariance between simultaneous and non-simultaneous components; Var_E is the intra-class correlation, which is composed of Var_{E_1}: the covariance between simultaneous components belonging to the same class; Var_{E_2}: the other 50 % of covariance between simultaneous and non-simultaneous

components.

7.3 Results

7.3.1 Historical

The theoretical expressions presented in the last sections can now be applied to the historical water level series of the Guadalete estuary. For each exceedance over the threshold of the total water level (η_T^e), the concomitant values of the components, including the non-linear term ($\eta_{AT}|_{\eta_T^e}$, $\eta_{RD}|_{\eta_T^e}$, $\eta_{WS}|_{\eta_T^e}$, $\eta_{NL}|_{\eta_T^e}$), are classified according to whether they belong to the normal regime (Class 1) or extreme regime (Class 2). The thresholds for distinguishing between these classes are obtained as indicated in section 6.3.1. Then, the equations in section 7.2 are used to analyze the contribution of each component and class to the mean (magnitude) and variance (variability) of η_T^e at each control point of the estuary.

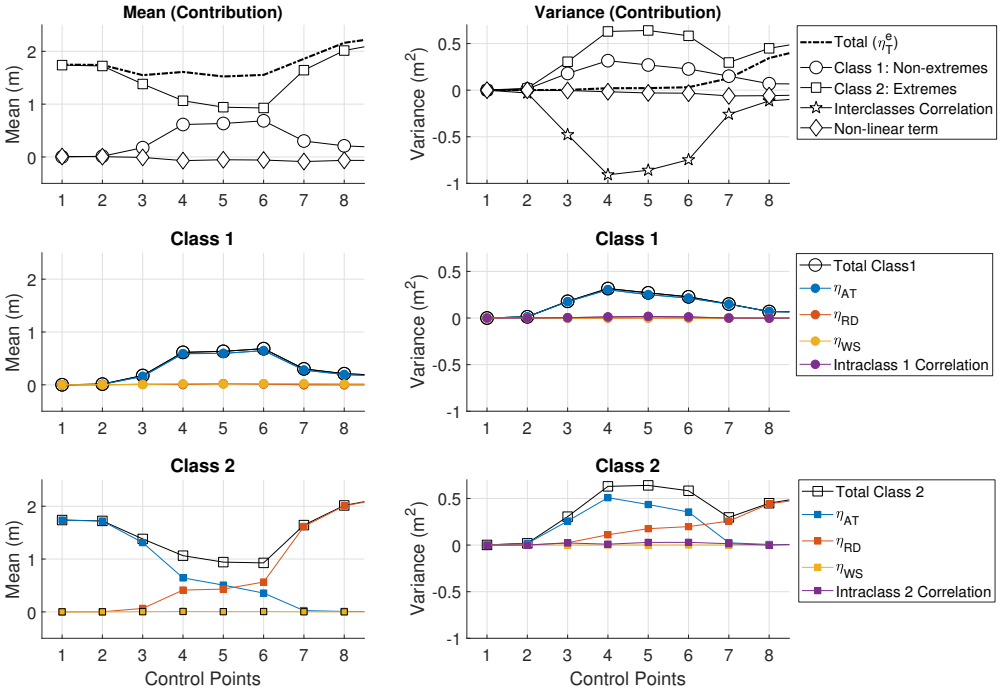

Figure 7.3.1: Contribution of the water level components to the mean (left panels) and variance (right panels) of the extreme values of the total water level. The first row shows the class contributions, whereas the second and third rows show the component contributions to each class.

The upper-left panel of Fig.7.3.1 shows the mean of the extreme values of the total water level (η_T^e) at each point in black line, and it remains constant from CP 1 to 6 and progressively increases in the inner part of the estuary (from CP 7 onwards). This mean is decomposed into the non-extremes (Class 1) contribution, represented by circles and extremes (Class 2), represented by squares, and non-linear term, represented by diamonds. The main contribution comes from Class 2 (extremes) in the outer and inner part of the estuary. However, in the middle estuary, the mean is explained by a combination of Class 1 and Class 2. The non-linear term's contribution is nearly zero, indicating that its effects on the extreme events of total water level are negligible for their magnitude.

The middle-left and lower-left panels show each component's contribution to Class 1 and Class 2, respectively. The elevation due to astronomical tide dominates Class 1 (non-extremes) at all points. In contrast, Class 2 (extremes) is dominated by the astronomical tide in the outer estuary and by the river discharge in the inner estuary. Both contributions decrease out of these areas, being the crossing point (equal contribution) in the middle estuary (CP 5). In summary, the extreme values of the total water level are explained by (1) the extreme values of the astronomical tide in the outer estuary; (2) the extreme values of the river discharge in the inner estuary; and (3) an equal contribution between the extreme values of river discharge and the extreme and non-extreme values of the astronomical tide in the middle estuary.

The right panels repeat the previous study for the variance of the extreme values of the total water level (black line). The upper-right panel decomposes this variance into the contribution of the simultaneous values of Class 1 (circles), Class 2 (squares), the non-linear term (diamonds), and the effect of the correlations between values from different classes (inter-classes correlation). Near-zero variance from CP 1 to 6 and a progressive increase in the inner estuary (CP 7 onwards) are observed, and the contribution of the non-linear term to the total variance is found to be nearly zero.

Three different behaviors can be found along the estuary. In the outer estuary, the variance is almost negligible. In the inner estuary, the total variance is explained by the variability of the extremes of the river discharge (lower-right panel) and a lesser contribution of the variability of the non-extremes of the astronomical tide (middle-right panel). In the middle estuary, the variance is caused by non-extremes of the astronomical tide and the extremes of river discharge and the astronomical tide. However, these contributions are almost compensated with a negative correlation between the contribution from different classes (upper-right panel), which can be partly explained by the dam regulation policy in which the most substantial discharges usually coincide with neap tides to reduce the risk of flooding downstream (Fig. 6.3.3). Finally, the lack of

correlations among the simultaneous values, intraclass correlation lines in the middle, and lower-left panels indicate that they can be considered independent.

The simultaneity between concomitant values from the extreme or the normal regime of the components is analyzed in Fig.7.3.2. The left panel shows the probability of an extreme value of a component to be involved in the arising of an extreme value of the total water level. These probabilities are high for the astronomical tide (AT) and the river discharge (RD) at the outer and the inner estuary, respectively, with intermediate transitions. The weather surge (WS) almost always contributes values of the normal regime.

The right panel shows the probability that combinations of extreme or non-extreme values of the AT and RD will be involved in generating extreme values of the total water level. These extremes at the outer estuary can be explained by the combination of extreme values of AT ($EV\eta_{AT}$) with mean values of RD ($MV\eta_{RD}$). The opposite is true in the inner estuary. The probabilities are more distributed in the middle estuary. The highest corresponds to extreme values of RD ($EV\eta_{RD}$) combined with mean values of AT ($MV\eta_{AT}$) (diamonds), although the combination of two extreme values (circles) must also be considered.

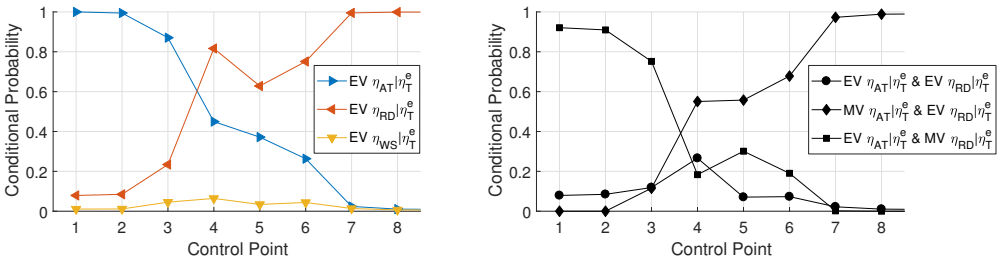

Figure 7.3.2: Left panel shows the probability of occurrence of an extreme value of a water level component conditioned to extreme values of the total water level. Right panel shows the probability of the combination of extreme (EV) and mean (MV) values of the AT and RD conditioned to extreme values of the total water level.

7.3.2 Future

The compatibility and simultaneity analysis is now applied to the forecasted water level components along the 21st-century. Therefore, the spatial variability and temporal evolution of the results across the estuary are analyzed for the different SLR scenarios. To address the temporal evolution, three nodal cycles are represented. The first corresponds to the historical period (1995-2015) analyzed in the previous section, and the others are from 2020 to 2040 and from 2080 to 2100.

In Fig. 7.3.3 the temporal evolution through three different nodal cycles is shown in columns. The left column corresponds to the historical nodal cycle between 1995 and 2015, and the middle and right columns correspond to the periods of 2020-2040 and 2080-2100, respectively. Results for the future periods are represented in boxplots to assess the variability of the 100 simulations of the forcing agents. Inside each panel, the spatial variability along the estuary is shown by the x-axis, where the estuary's control points are represented. In the first row, panels show the mean of the extreme values of the total water level (η_T^e) at each point in the black line. Following the same criteria than in the historical period, this mean is decomposed into the contribution of the non-extremes (Class 1), extremes (Class 2), and the non-linear term, which are represented by circles, squares and diamonds, respectively.

In the 1995-2015 period, the mean of the extreme total water level events remains almost constant from CP 1 to CP 6, increasing in the last two control points. However, these mean values in the lower and middle part of the estuary increase as a consequence of the SLR throughout the 21st-century, leading to a horizontal line by the end-century (upper left panel). No significant variations are found in the temporal evolution of the extremes (squares). They are maximum at the mouth and at the head of the estuary, and minimum in the middle part around CP 5 and CP 6. Regarding the non-extremes (circles), the opposite behavior is observed. In the period 1995-2015, they are maximum in the middle estuary and almost zero in the mouth and the head, whereas these non-extremes increase, leading to a horizontal line as a consequence of the SLR in the period 2080-2100. As a consequence, both classes are asymptotic from CP 5 onward by the end-century. The non-linear term's contribution remains nearly zero, indicating that its effects on the extreme events of total water level are negligible in this estuary during the historical period as well as the 21st-century.

The second and third rows in Fig. 7.3.3 show the contribution of each water level component to Class 1 and Class 2, respectively. Class 1 (non-extremes) is only explained by the astronomical tide in the 1995-2015 period. As we move towards the end of the 21st-century, the SLR contribution, which is uniform along the estuary, is larger than the astronomical tide at all the control points.

Although the contribution of the extremes (Class 2) does not change in time, there is a significant variation in the contribution of its components. In the historical period, Class 2 is dominated by the astronomical tide in the estuary's mouth and by the river discharge in the upper part of the estuary. Both contributions decrease outside these areas, being the crossing point (equal contribution) in CP 5. However, as observed in the lower-middle and lower-left Panels of Fig.7.3.3, in the future periods the crossing point moves 4 km towards the inner estuary, from CP 5 in 1995-2015 to CP 7 in 2080-2100, limiting the

effects of the river discharge to the upper part of the estuary. As seen, the effects of the weather surges (waves and wind) remain insignificant compared to the rest of the components. Although not represented in this Thesis for brevity, similar results have been obtained for the RCP4.5_05 SLR scenario, except for a smaller SLR contribution for the non-extremes (Class 1).

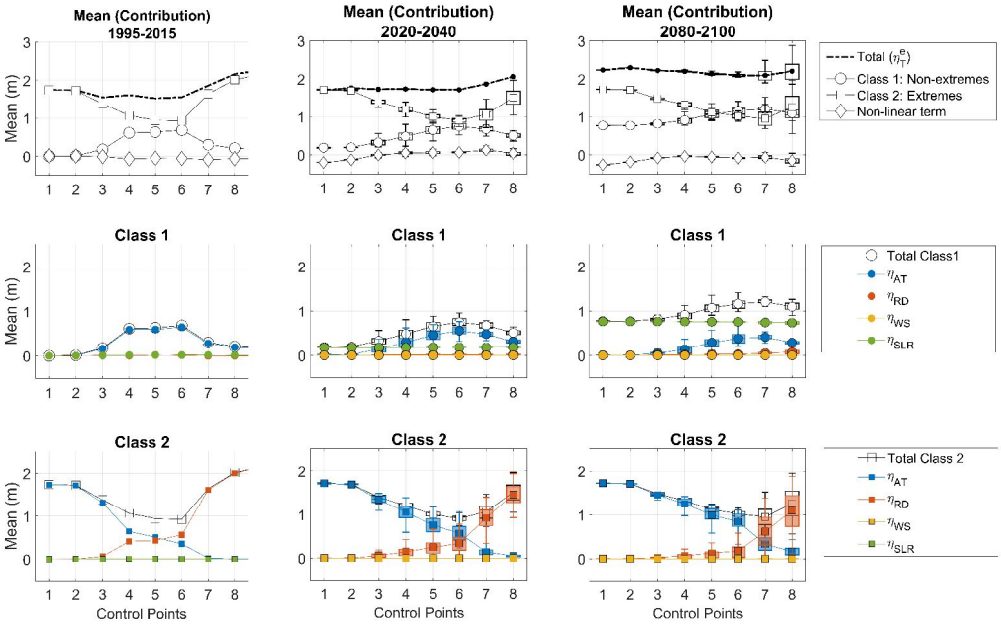

Figure 7.3.3: Contribution of the water level components to the mean of the extreme values of the total water level for the periods: 1995-2015 (left column), 2020-2040 (middle column) and 2080-2100 (right column) for the RCP8.5_95 SLR scenario. The first row shows the class contributions, whereas the second and third rows show the component contributions to each class.

Fig. 7.3.4 repeats the above analysis for the variance of the extreme values of the total water level. The left panel represents the results for the historical period (1995 - 2015), while the right panel represents the results for the end of the century (2080 - 2100). No significant differences are observed in the temporal variation for the variance. The first row decomposes this variance into the contribution of the simultaneous values of Class 1 (circles), Class 2 (squares), the non-linear term (diamonds), and the effect of the correlations between values from different classes (interclass correlation). Near-zero variance from CP 1 to CP 6 and a progressive increase in the upper estuary (CP 7 onwards) are observed. Again, the contribution of the non-linear term to the total variance is found to be nearly zero. In the mouth region, the variance is almost negligible

because of the tidal domain.

In the inner estuary, the total variance is explained by the variability of the extremes of the river discharge (lower-right panel) and a lesser contribution of the variability of the non-extremes of the astronomical tide (middle-right panel). In the middle estuary, the variance is caused by the non-extremes of the astronomical tide and the extremes of river discharge and the astronomical tide. Finally, the lack of correlations among the simultaneous extreme values of the different water level components, (intraclass correlation lines in the middle and lower-left Panels), indicates that they can be considered independent.

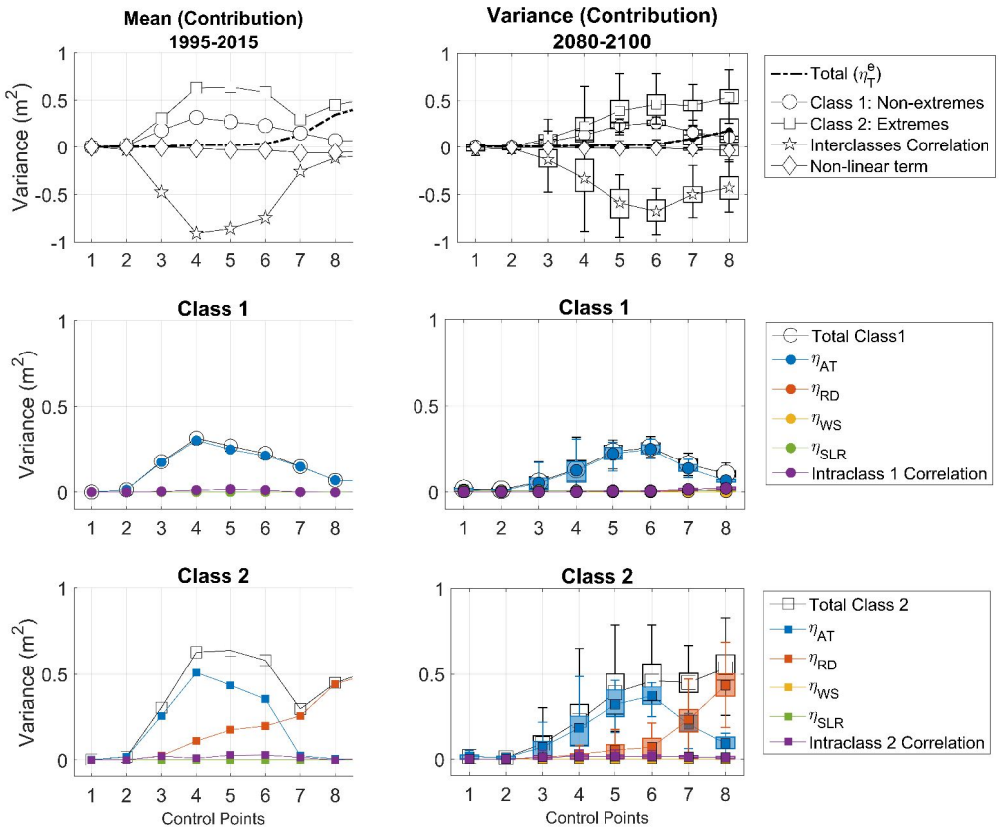

Figure 7.3.4: Contribution of the water level components to the variance of the extreme values of the total water level for the periods: 1995-2015 (left column) and 2080-2100 (right column) for the RCP8.5_95 SLR scenario.

7.4 Summary and conclusions

In this chapter, all the disaggregated information of the water level components is used to study the mechanisms of the formation of extreme flood events. The development of a method that allows the identification of the agents responsible for the flooding processes and the combinations of extreme and non-extreme values that cause flooding is a great advance in the field of Coastal Engineering aimed at protecting coastal urban fronts against global warming. The information provided by the methodology presented in this chapter allows the optimization of costs derived from protection measures since it is known on which agents and regime (extreme or normal) it is necessary to act for flooding risk mitigation. To this end, the statistical relationships that are established between the total water level, that is a linear combination of a set of water level components that act simultaneously, and the variables that are obtained from classifying each water level component in a set of mutually exclusive classes (extreme and non-extreme) are analyzed. These relationships depend on (i) the statistical properties of each component that belong to the class c, (ii) the statistical properties of each class, (iii) the simultaneity between the water level components that belong to the class c, and (iv) the compatibility of the simultaneous values. The methodology is first applied to the nodal cycle of the historical period and then repeated for each nodal cycle along the 21st-century. The following conclusions can be drawn from the analysis during the historical period:

- The analysis of the Guadalete estuary indicates that the extreme values of the total water level are explained only by the extremes of the astronomical tide in the outer estuary and only by the extremes of the river discharge in the inner estuary. However, a similar contribution between extreme values of the river discharge and extreme and mean values of the astronomical tide is found in the middle part of the estuary.

- Regarding the variability of the extremes, three different behaviors are found along the Guadalete estuary. In the outer estuary, the variance is negligible, whereas, in the inner estuary, the total variance is explained by the variability of the extremes of the river discharge. Additionally, a more complex hydrodynamic pattern is found in the middle estuary. Finally, the lack of correlation between simultaneous extreme values of the water level components indicates that they can be considered as independent. Furthermore, these analyses indicate that in the Guadalete estuary case, the non-linear term's contribution to the magnitude and variability of the extreme events of total water level is nearly negligible.

- According to the obtained results, waves do not substantially impact on the water levels along the Guadalete estuary. The reason is found in the two breakwaters

that protect the inlet from waves and the lack of waves breaking along the estuary. Therefore, checking the impact of waves on the water levels is recommended before applying the presented method at another location to avoid unnecessary computational costs. If waves affect the results, special attention must be paid to the calibration of both the significant wave heights and wave directions before applying the proposed method.

For the 21st-century period, the 100 simulated water level components were analyzed for each of the seven nodal cycles between 2020 and 2100 for the two sea-level rise scenarios. The following conclusions can be drawn from the analysis during the 21st-century period for the RCP8.5_95 SLR scenario:

- The contribution of the non-extremes equals the contribution of the extremes in the formation of flood events by the end-century from CP 4 onwards as a consequence of sea-level rise.
- By the end of the 21st-century, the sea-level rise contribution, which is uniform along the estuary, is larger than the astronomical tide at all the control points.
- In the historical period, Class 2 was dominated by the astronomical tide in the estuary's mouth and by the river discharge in the upper part of the estuary. However, in the 21st-century, the crossing point between tidal and river discharge dominance moves 4 km towards the inner estuary, from CP 5 in 1995-2015 to CP 7 in 2080-2100, limiting the effects of the river discharge to the upper part of the estuary. As seen, the effects of the weather surges (waves and wind) remain insignificant compared to the rest of the components.
- No significant differences are observed in the temporal variation for the variance, and the contribution of the non-linear term to the formation of extreme flood events remains nearly zero along the 21st-century.

Part IV

Total cost calculations of maritime structures and guidelines for flood management

CHAPTER 8

TOTAL COST QUANTIFICATION OF COASTAL FLOOD DEFENSES OVER ITS LIFE-TIME FOLLOWING THE ROM 1.1 GUIDELINES.

8.1 Introduction

International maritime transport accounts for about 90% of global trade in commodities, resulting in the most efficient and cost-effective international transport system. In the future to come, maritime ports will increasingly grow to allow the entry of deeper-draught ships. Therefore, they will need larger protective maritime structure of O(1000 m long, 100 m wide and around 20-30 m depth). On the other hand, the Spanish coastline is about 7.905 km length, a third of which coexists with a broad range of human activities. Therefore, throughout the 21st-century, approximately 3000 km of coastline will need to be protected either with marine protection structures or with beach regeneration as a consequence of SLR induced by GW. If it is decided to protect with maritime structures, breakwaters of O(10.000 m long, 10 m wide and around 1-5 m depth) will be necessary. However, if the decision is made to regenerate beaches, it will be necessary to provide between 500 and 1000 m^3 of sand per linear meter of beach every one or two years.

Protective breakwaters are often the single most expensive infrastructure of a harbor and coastal protection. According to ROM-0.0 (2001), their design can be performed from two complementary and mutually-enriching perspectives: the project requirements related to safety and operationality in each project phase, and the economic optimization (minimum cost) of the project during its life cycle. Hence, the design of a breakwater is

considered to be optimum when it meets the requirements at minimum total cost (Kreeke and Paape, 1964; Losada, 1990). Due to this fact, the accurate assessment of the total cost of protective maritime structures along the life cycle constitutes a unique challenge because of the vast number of variables involved and the stochastic nature of the driving forces.

In the past, different procedures to assess the total cost of a maritime protective breakwater configuration were proposed. Already in the early 50s, Gesler (1951) defined the basis of the economic analysis of coastal structures. This author was a pioneer in emphasizing the importance of the economic aspect compared to the rest of the functional factors of breakwaters such as location, type, and materials. Kreeke and Paape (1964) made a step forward defining the concept of optimum design of a breakwater. They proposed the discretization of the total cost in the costs of (1) construction, (2) associated to the storm damages, and (3) the economic loss due to failure of the structure. In this sense, they were able to obtain the first simple and analytical expressions for the total cost as a function of the design wave, its probability of exceedance in any given year, and the cost of repairing for monolith and rubble-mound structures.

A complete and detailed guide for the breakwater design, including numerical examples, was presented by Massie (1976). In this volume, chapters 11 and 19 focus on minimizing the sum of the construction and repair costs during the breakwater lifetime. The cost of construction is obtained multiplying the unit price of the materials by the dimensions obtained using both the wave height and the water level. A breakthrough was made in the calculation of the repair cost by (i) the inclusion of three simple strategies of damages reparation and (ii) the relations between the wave height and the expected damage using laboratory experiments. Finally, the annual repair cost is obtained multiplying the probability of exceedance of the design wave height by the damage percentage and the unit cost of repair. To calculate the breakwater structure's optimum total cost, the procedure is repeated for all the different sections of the structure and for different design wave heights. However, this work assumes that the repair is made immediately regardless of its extent. Hence, partial damage is not considered. Such an approach is conservative because unrepair damage can lead to more severe damage in the next storm.

During last decades improvements in computational capabilities and advances in coastal process, modeling opened the door to time-dependent life-cycle modeling of protective breakwaters (Minguez et al., 2006; Males and Melby, 2011; Diaz-Hernandez, Losada, and Mendez, 2017). In this respect, a systematic model for automatically optimize the design of a protective breakwater was presented by Minguez et al. (2006). This work considers the division of the structure into multiple failure modes and allows us to obtain

the optimal yearly failure rates for the identified modes of failure. The former minimizes the expected total cost of the structure, including maintenance and construction costs during its lifetime. Furthermore, this work provides a sensitivity analysis of the input parameters that can be used to assess each variable's influence into the total expected cost. However, this model also presents limitations, such as the minimum time step being one year (seasonal, monthly, or daily events can not be considered). Failure accumulation is not considered, and repair costs are estimated as a fraction of the construction costs without including any repair strategy.

Males and Melby (2011) presented a Monte Carlo simulation model for the economic evaluation of rubble mound breakwater. This model permits the risk-based life cycle analysis of breakwater projects by simulating the structure life-time several times. The former leads to a complete set of results that can be analyzed statistically, including assessing the uncertainties. It also accounts for repair strategies and damage progression on the different modes of the rubble mound breakwater, and repairs are not instantaneous processes. However, the model has two significant limitations. Firstly, it only simulates storm events and does not consider the wave climate during the calm periods between storms; this limitation can lead to non-realistic durations of the repair maneuvers because of the repair machinery's operative conditions. Secondly, the model is only designed for rubble mound breakwater.

To be competitive, the Coastal Engineering of the 21st-century must be performed with the highest level of efficiency. This is accomplished by optimizing the total costs and limiting the investment risk. Therefore, methods and instruments to optimize the total costs of a breakwater project from the technical-economic and financial-economic perspective are needed. These methods must also be capable of limiting the uncertainty introduced by the stochastic character that governs the climatic, forcing agents and the processes involved. In recent years, ROM-1.1 (2018) in combination with MEIPORT (2016) have developed the most innovative and complete conceptual framework for optimizing the total costs of a maritime structure up to date. These works gather the latest theoretical and numerical advances in the field of maritime structure design and financial and coastal modeling to state how the technical-economic and financial-economic optimization must be carried out. However, a global and step-by-step method to calculate the total costs of a protective breakwater has not been performed yet. To tackle this challenge, the main objective of this chapter is to provide a detailed method and an associated open-access numerical tool for the calculation of the probability distribution function of the total costs for any type of protective maritime structure at any location during its life-time cycle following the guidelines of ROM-1.1 (2018) as a function of the forcing agents, the design and project factors and the work planning and strategies

for construction and repair during the life-time of the structure. The latest version of the developed tool is available in the following public repository: https://github.com/gdfa-ugr/total_costs. The method must be able to: (1) consider the randomness of the agents and their interaction with the breakwater, (2) adapt to the spatio-temporal characteristics of the project, (3) consider the failure not as a binary phenomenon but as an evolving process that is susceptible to intervention and (4) present flexibility in the design of action strategies.

This chapter is organized as follows. The background definition necessary to understand the chapter are described in §8.2. In §8.3 the total costs definitions are formulated, together with the formulation of its multiple components. Then, §8.4 shows the steps for calculating the distribution function of the total costs with practical and gradual application examples. Finally, results are shown in §8.5.

8.2 Background definitions

The presented method is based on the following general definitions and concepts defined in ROM-1.1 (2018):

- *Construction project*: The document defines the project objectives, factors, geometry, structural attributes, and materials of the breakwater (and its parts), as well as the procedures necessary for construction, maintenance and repair, and the costs within its life cycle. The design should be supported by the calculations of the probability of failure within its project phases and an estimate of the harbor area's operationality.
- *Project objectives*. They include the fulfillment of the functional and structural requirements, as well as the financial-economic profitability and the financial sustainability of the harbor area. They are defined by the developer and by the regulations.
- *Project factors*: The parameters, agents, and actions used to define, design, verify, and optimize the total costs of the construction project in a useful life.
- *Useful life*: The time during which the structure or one of its subsets fulfills the main function for which it was conceived.
- *Life Cycle*: Is the time period from the beginning of its construction until its transformation, change of use, or dismantling. The investment project of the breakwater extends throughout this cycle.

- *Subset*. A continuous set of sections (or breakwater alignments) that fulfills a specific function in line with the objectives and exploitation requirements of the structure.
- *Failure mode*. Geometric, physical, mechanical, chemical, or biological form or mechanism that causes the structure or one of its components to go out of service because of structural reasons.

8.3 Problem Statement, definitions and formulations

8.3.1 Definition of the total costs

The main variable of this chapter is the total cost of any protective marine structure, which is composed, on the one hand, from the execution of the construction/dismantling and repair works and, on the other hand, from costs of exploitation during the operating phase as shown in Fig. 8.3.1.

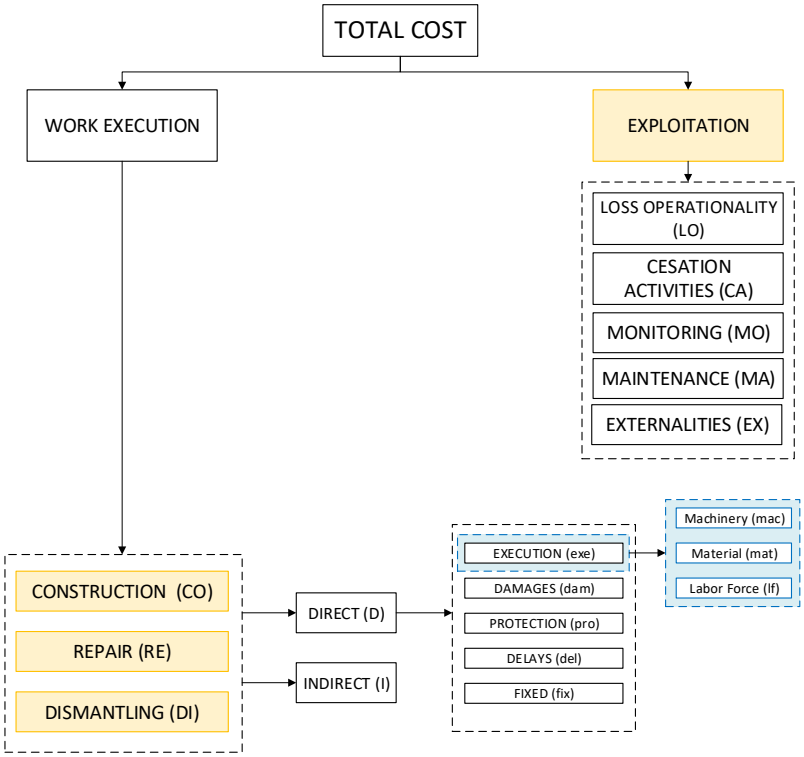

Figure 8.3.1: Disaggragation of the total costs of a maritime structure

According to this definition, the total costs, C_T can be expressed by the terms in the following equation:

$$C_T(t) = \sum_{\tau=1}^{T}\left(\sum_{\sigma=1}^{S}\left(\sum_{\epsilon=1}^{E}\left(C_{CO_{\tau,\sigma,\epsilon}} + C_{RE_{\tau,\sigma,\epsilon}} + C_{DI_{\tau,\sigma,\epsilon}}\right)\right)\right) + C_{EX} = f(H,\lambda,\overline{x},\Psi,i,t) \quad (8.1)$$

where the subindexes τ,σ,ϵ represent the hierarchy of spatial scales: subset, subsystem, and element, respectively. The subindexes CO,RE,DI,EX, represent the hierarchy of temporal scales associated to each project phase of construction, repair, dismantling, and exploitation, respectively. As shown in Fig. 8.3.2, the main variables that modify this total costs C_T, most of them of stochastic nature, are: the forcing agents (H), the design of the structure (λ), the project factors ($\overline{x}$), the organization and work planning definition including the decision and actions (strategies) taking during the life cycle (Ψ), the interactions between the former elements (i) and the useful life-time (t).

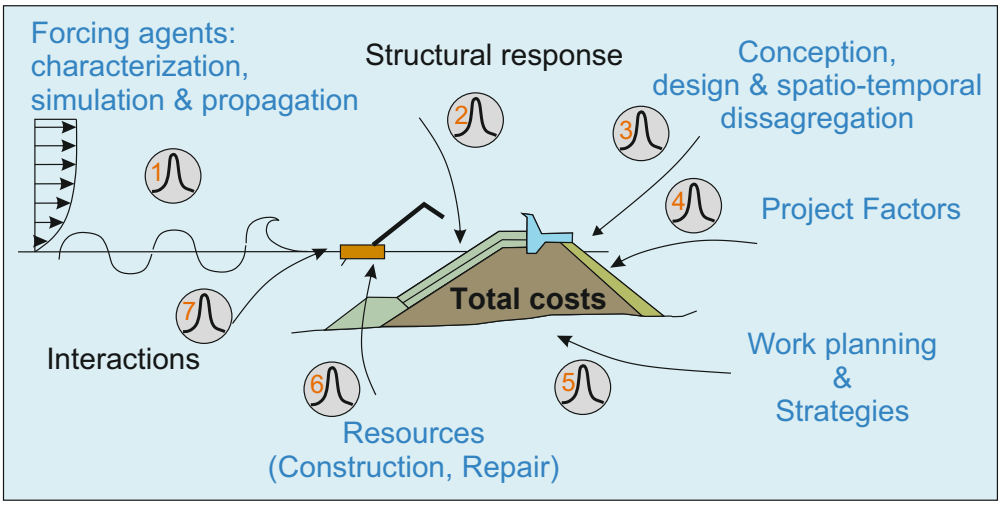

Figure 8.3.2: Sources of variability and uncertainty in the calculation of the total cost of a protective maritime structure.

8.3.1.1 Components of the total costs

The construction and dismantling costs include the initial and final investment corresponding to the execution of the works detailed in the construction project. Costs during the repair phase are associated with the execution works to reestablish the damaged

sections of the structure. Both types of costs present a stochastic behavior because of the interaction between the structural processes and the natural agents. The exploitation costs attributable to the breakwater include (1) the costs due to partial loss of operationality of the port area, (2) the costs for total stoppage of activities, (3) the periodic costs of monitoring and maintenance, and (4) other externalities attributable to the project, such as the social and environmental impact on the community. Among them, the first two show a random nature, while the costs of monitoring and maintenance tasks can be treated as a fixed amount. The calculation of externalities requires additional considerations and will, therefore, not be covered in this Thesis.

The costs derived from the execution works such as construction, repair-maintenance and dismantling (Eq. 8.2, 8.3.1.1 and 8.8), are disaggregated as direct costs (C_D) and indirect costs (C_I). Direct costs include the expenses directly related to the working unit, and its magnitude depends on the volume of the executed work. They are subsumed in the direct costs to the structure, the execution costs, damages and losses, protection, delays, and other fixed costs. On the other hand, indirect costs include all expenses not directly attributable to specific units of the structure, but rather to the entire structure or part of it. The cost equations must be adapted to the characteristics of each specific problem. Although specific equations are proposed in this chapter, in Tab. 8.3.1, a summary of the different types of costs attributable to each phase is shown in order to facilitate the formulation of different ones.

Construction and dismantling costs. $C_{CO_{\tau,s}}$ represents the construction/ dismantling cost descriptor for each subsystem s of any given subset, τ. These costs can be subdivided in execution, damages and losses, protection and fixed costs (subindexes exe, dam, pro, and fix, respectively), as well as indirect costs (C_I). All of them are accumulated for all the sub-phases, p, and, additionally, for each work unit w in the case of execution costs.

$$C_{CO_{\tau,s}} = \sum_{p=1}^{P} \left(\sum_{w=1}^{W} \left(C_{exe_{\tau,s,p,w}} \right) + C_{dam_{\tau,s,p}} + C_{pro_{\tau,s,p}} + C_{fix_{\tau,s,p}} + C_{I_{\tau,s,p}} \right) \tag{8.2}$$

The term related to the execution costs term (C_{exe}) includes the expenses of the execution of the total volume of the working unit. These costs are calculated using: the number N of each type of machinery; the unit costs c of machinery and material and the total execution time and volume of each work unit and sub-phase. Besides, the cost overrun of concluding an activity after the deadline is also considered in the unit cost due to delays.

$$C_{exe_{\tau,s,p,w}} = \left[\sum_{mac=1}^{M} \left(c_{mac_{\tau,s,p,w}} N_{mac_{\tau,s,p,w}} \right) + c_{lf_{\tau,s,p,w}} \right] t_{exe_{\tau,s,p,w}} + c_{del_{\tau,s,p}} t^{del}_{exe_{\tau,s,p}} + c_{mat_{\tau,s,p}} V_{exe_{\tau,s,p}} \tag{8.3}$$

where subindex mac, mat, lf correspond respectively to machinery, materials and labor force; t_{exe} is the duration of the execution of each work; t^{del}_{exe} is the duration of the execution of each work after the deadline and V_{exe} is the execution volume by each sub-phase.

The damage costs term (C_{dam}) includes the expenses associated with the damages and losses due to storm events plus the expenses of the execution works to restore the damaged part of the structure during the construction or dismantling phase. These costs are a function of the executed volume, which is a stochastic variable because it depends on both the maritime climate and the adopted strategy and the unit costs of the execution.

$$C_{dam_{\tau,s,p}} = c_{dam_{\tau,s,p}}(agents) V_{dam_{\tau,s,p}} \tag{8.4}$$

The protection costs term (C_{pro}) are the results of protecting the advance of each sub-phase when there is a prevision of a storm event during the construction phase. This cost depends on the adopted strategy, the length or volume of the sub-phase that needs to be protected, and the unit cost of the working units involved in the protection process. These costs are more frequent in the construction phase, where the inner parts of the structure can be more exposed to the forcing agents.

$$C_{pro_{\tau,s,p}} = c_{pro_{\tau,s,p}}\, t_{pro_{\tau,s,p}} \tag{8.5}$$

where t_{pro} is the duration of the protection process and c_pro its unitary cost.

The fixed costs term (C_{fix}) gathers all the fixed and invariable costs for each working activity during the construction phase.

$$C_{fix_{\tau,s,p}} = c_{fix_{\tau,s,p}}\, t_{exe_{\tau,s,p}} \tag{8.6}$$

where t_{exe} is the duration of the execution of each work and c_fix the fixed cost per unit of time.

Repair costs. $C_{RE_{\tau,s}}$ represents the repair cost descriptor for each subsystem s of any given subset, τ. In this case, the costs are organized by failure modes mf to facilitate the analysis of the maritime structure's performance. These costs can be subdivided in execution (C_{exe}) and indirect costs (C_I).

$$C_{RE_{\tau,s}} = \sum_{mf=1}^{M} \left(C_{exe_{\tau,s,mf}} + C_{I_{\tau,s,mf}} \right) \tag{8.7}$$

The execution costs term (C_{exe}) adds an additional cost to those included in 8.3, corresponding to he machinery and labor force that is permanently in the harbor waiting for being used in the repair works.

$$C_{RE_{\tau,s,mf}} = \left[\sum_{mac=1}^{M} \left[c_{mac_{\tau,s,mf}} N_{mac_{\tau,s,mf}} \right] + c_{lf_{\tau,s,mf}} \right] t_{rep_{\tau,s,mf}} + c_{mat_{\tau,s,mf}} V_{rep_{\tau,s,mf}} + \left[\sum_{mac=1}^{M} \left[c_{mac_{\tau,s,mf}} N_{mac_{\tau,s,mf}} \right] + c_{lf_{\tau,s,mf}} \right] t_{life} \tag{8.8}$$

where t_{life} is the duration of the useful life and V_{rep} is the volume to repair during the repair phase.

All these costs present a stochastic behavior as they are affected by the uncertainty of the maritime climate. Although the shorter duration and magnitude of the repair works reduce their variability, the damage progression can trigger the failure in other modes, increasing the costs. As previously indicated, the indirect costs include all expenses not directly attributable to specific working units, but rather to a number of them (e.g., stockpiles, machinery, workshops, and labor force that are permanently in the harbor waiting for being used, as well as taxes or security). Tab 8.3.1 summarizes the different types of costs attributable to each phase.

Phase	Cost	Type	Nature	Dependency	Brekdown	Independent variable
Construction & Dismatling	Execution	Direct	Deterministic	Design	Machinery, material and labor force	Time, Volumen
	Damages & losses	Direct	Random	Strategy, natural agents		Volume
	Protection	Direct	Random	Strategy, natural agents	Machinery, material and labor force	Volumen
	Delays	Direct	Random	Strategy, natural agents		Time over threshold
	Fixed	Direct	Deterministic	Design, strategy	-	
	Others	Indirect	Deterministic	-	Administrative staff, consumibles, security, services, etc.	Direct costs
Exploitation	Repair	Direct	Random	Strategy, natural agents	Machinery, materials and labor force	Time, volume
	Monitoring, maintenance	Direct	Deterministic	Strategy	Machinery, materials and labor force	
	Loss of operationality	Indirect	Random	Strategy, natural agents	Stoppage duration	
	Cesation of activities	Indirect				
	Externalities					
	Others	Indirect	Random			Direct costs

Table 8.3.1: List and characteristics of each type of cost associated to each project phase.

8.3.1.2 Aggregation of the total costs

The preceding cost equations reflect the spatial-temporal organization of the protective maritime structure. This organization facilitates the calculation of costs derived from the execution of the works in each phase and the losses associated with the (total or partial) non-fulfillment of the project's objectives. The spatial hierarchy organizes the protective maritime structure into elements, subsystems, and systems, fulfilling a specific function within the higher-order level. Each one is defined by its layout dimensions and typology characterized by a specific geometry and a structural and formal configuration. The temporal hierarchy is determined by the variation scales of the dominant agents (states, the sequence of states, seasonal cycles, and meteorological years), which are also integrated into the project phases and, for convenience, grouped into annual cycles. Fig. 8.3.3 shows the spatio-temporal hierarchy of the maritime structure together with the associated processes.

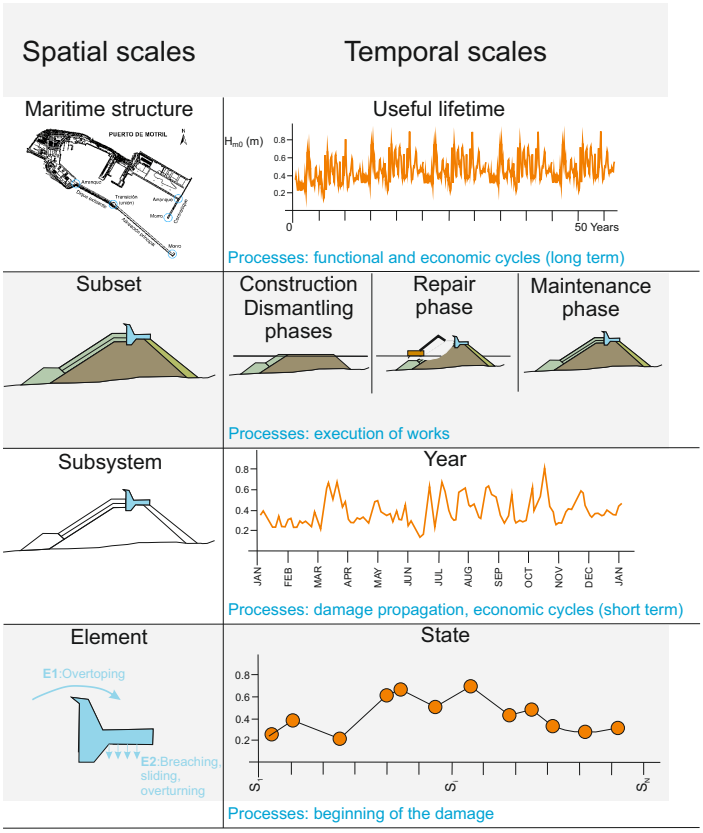

Figure 8.3.3: Spatio-temporal hierarchy of the maritime structure and associated processes.

Hence, the total cost C_T is decomposed into one component per element of the spatio-temporal hierarchy of the structure shown in Fig. 8.3.3 and Eq. 8.1. The total cost of the protective maritime structure can be divided into one component per subset. These components are again divided into a component for each subsystem and structural element. The former constitutes the spatial disaggregation of the total costs. Now, each element's cost is temporarily disaggregated between the different phases of the useful lifetime: construction, repair, maintenance, and operation. Therefore, the aggregated sum of each component's costs over the different phases of the maritime structure constitutes the total costs (Fig. 8.3.4).

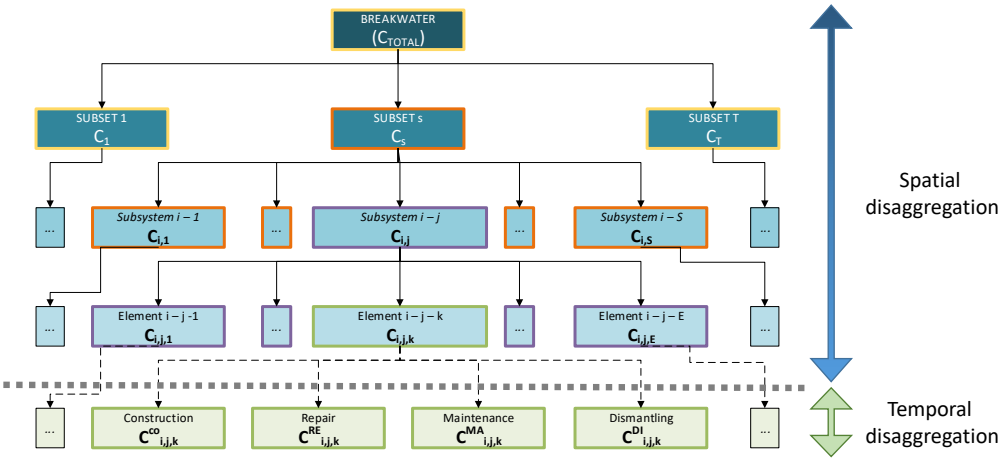

Figure 8.3.4: Spatio-temporal dissagregation of the total costs.

8.4 Methodology for the calculation of the total costs

The methodology for calculating the distribution function of the total costs is structured in the following sequence:

I. *Conception, spatial and temporal disaggregation of the protective maritime structure*. Definition and design of the shape, layout, and elements of the protective maritime structure, their functions, relations, and their time scales of response to the external agents and evolution.

II. *Work planning and strategies definition*. Definition of the project phases and the processes, resources, and strategies, and decisions to execute the works in each of them and the planning of the operational stoppages.

III. *Characterization, simulation, and propagation of maritime climate*. Obtaining the descriptors of the natural agents next to the protective maritime structure and after their interaction with it. For climate simulation, the approach proposed by Solari and Losada (2011), Solari and Losada (2012), and Solari and Gelder (2011) is used. Then the forcing agents are propagated next to the protective maritime structure through downscaling techniques.

IV. *Project phases and damage accumulation modelling*. Sequential characterization of the state and functionality of the protective maritime structure and its elements, as well as the progression of the work to be executed in each phase of the project state by state. As a result, a set of different stochastic durations and executed

volumes are obtained for each spatio-temporal unit of the hierarchical structure of the protective maritime structure.

V. *Cost allocation*. Spatial-temporal characterization of costs in each phase of the project, both partial and aggregated

VI. *Analysis and uncertainty assessment through Monte Carlo technique*. Obtaining the cost distribution function and the statistical characteristics of the results. This allows to: (1) evaluate the uncertainty of the total and individual costs of the different alternatives of the project, (2) compare the cost of the different construction and repair strategies, and (3) identify the influence of each variable over the total costs.

The outline of the proposed methodology is summarized in Fig. 8.4.1, with the six different modules represented in gray. Blue box (panels A and B) represents the input data, while the purple box (panel C) represents the third-party modules used in this approach for climate characterization, propagation, and simulation. Yellow, orange, and green panels indicate the outputs of the model.

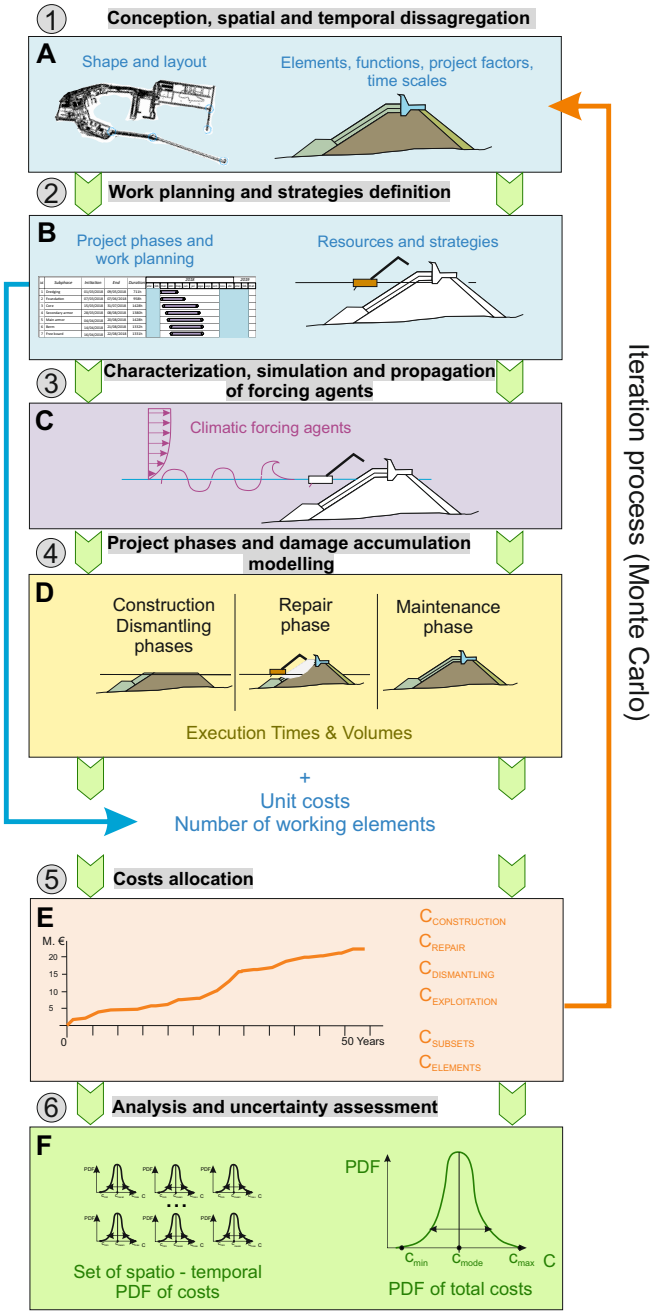

Figure 8.4.1: Diagram with the methodology for the total cost calculation of a marine structure over its lifetime. Data inputs and sources of uncertainty (blue); the modules of the methodology (gray); and outputs of the model (yellow, orange and green) are also represented in the figure.

8.4.1 Examples of application

This section shows a case study application of the methodology described in this chapter to calculate the total costs of a protective maritime structure. First, in section 8.4.1.1, the conception, work planning, and strategies are defined. Section 8.4.1.2 shows the flow charts used for the numerical model for the modeling of the total cost calculations along the useful life. Finally, the outputs of the model are shown in section 8.5 through a series of gradual examples, including the calculation of: (i) the total construction costs; (ii) a single repair costs of a damaged breakwater and (iii) the total cost over the useful life-time of the breakwater. This chapter does not consider either the costs from ceasing the exploitation of the port area due to the failure of the breakwater nor those from conservation and maintenance. Additionally, the verification of project requirements is considered in a simplified manner to focus on the estimation of the distribution function of the costs.

8.4.1.1 Conception, work planning, and strategies definition

Conception

In this case study, a single subset of a rubble mound breakwater of 516 m length, N120E orientation, and located at a water depth of 15 m is considered. The cross-sectional dimensions are shown in Fig. 8.4.2. The considered breakwater is built using seven construction sub-phases whose theoretical execution volumes are shown in Tab. 8.4.1.

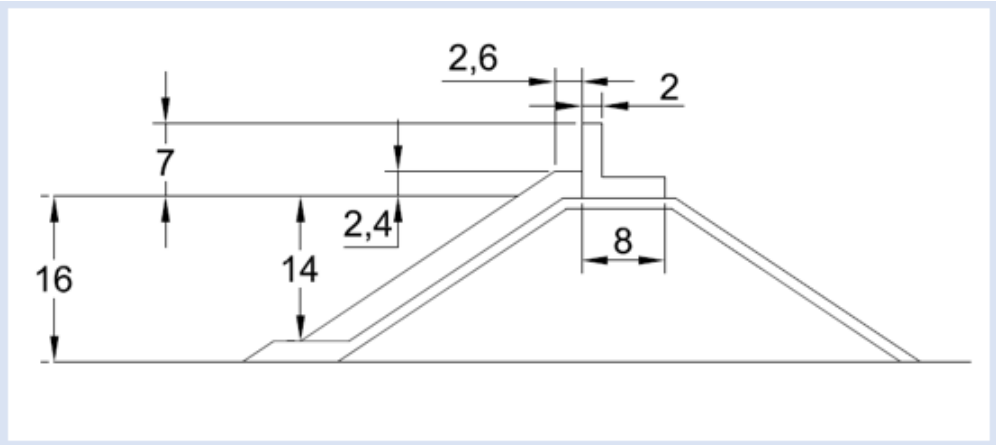

Figure 8.4.2: Cross-sectional geometry of the breakwater subset.

Sub-phase	Theoretical volume
Dredging	189.000 m3
Foundation	200.000 t
Core	288.000 m3
Secondary armor	42.500 m3 (Rockfill 230 kg)
Main armor	47.500 m3 (Concrete block 43 t)
Berm	8.500 m3
Free board	12.500 m3

Table 8.4.1: Construction sub-phases and theoretical volumes

Regarding the project factors, the project's useful life-time of the considered breakwater is 25 years. The breakwater is divided into five subsystems and three failure modes, as shown in Fig. 8.4.3. A spatial and temporal damage evolution model is also considered, as shown in the right panel of Fig. 8.4.3, where the failure progress in one mode triggers the failure initiation in the rest of the modes. The breakwater is considered to fail when a single failure mode reaches the 100 % of damage.

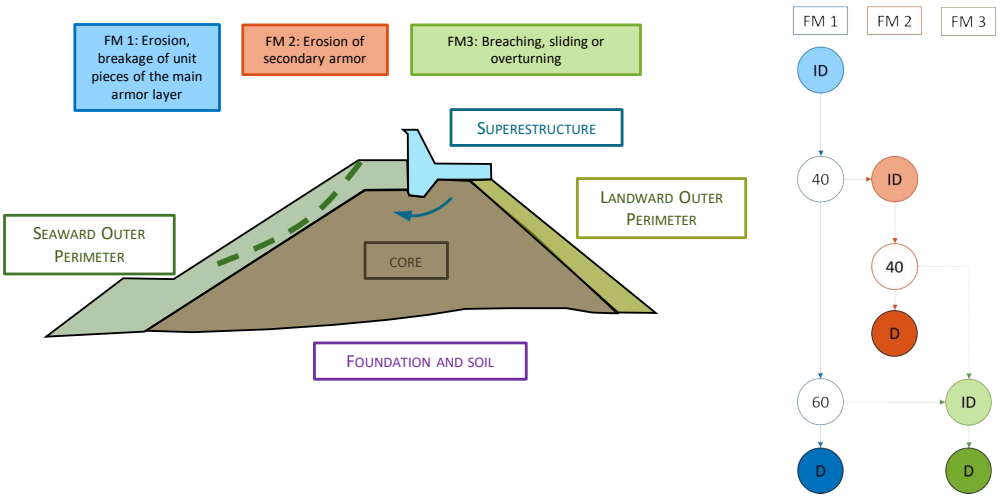

Figure 8.4.3: Left: subsystems and considered failures modes of a rubble mound breakwater subset. Right: failure propagation tree beetween failures modes.

Work planning

Fig. 8.4.4 represents the Gantt diagrams with the theoretical beginning and end of the different constructive sub-phases. Two opposite strategies ("risky" and "conservative")

are considered in this work. The difference between both strategies lies in the restriction of progress between the sub-phases. In the risky strategy, the distance between the sub-phases working fronts is allowed to be higher or equal to 250 m, but never less. Therefore, in this strategy, the construction of the breakwater is developed in "series" mode, where the sub-phases are executed nearly one by one. However, in the conservative strategy, the distance between the working fronts is limited to 50 m, leading to a developedment in "parallel".

Conservative strategy

Id.	Subphase	Initiation	End	Duration
1	Dredging	01/03/2018	09/05/2018	711h
2	Foundation	07/03/2018	07/06/2018	958h
3	Core	15/03/2018	31/07/2018	1428h
4	Secondary armor	28/03/2018	08/08/2018	1380h
5	Main armor	04/04/2018	20/08/2018	1428h
6	Berm	14/04/2018	21/08/2018	1332h
7	Free board	16/04/2018	22/08/2018	1331h

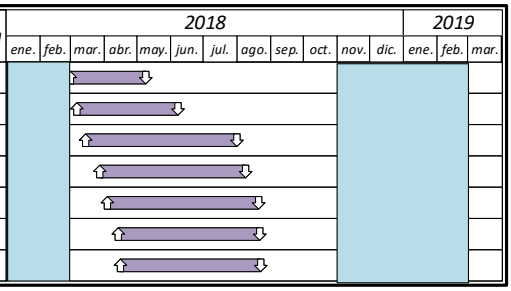

Risky strategy

Id.	Subphase	Initiation	End	Duration
1	Dredging	01/01/2018	10/03/2018	711h
2	Foundation	05/02/2018	08/05/2018	958h
3	Core	22/03/2018	07/08/2018	1428h
4	Secondary armor	28/05/2018	11/08/2018	788h
5	Main armor	05/07/2018	27/10/2018	1188h
6	Berm	30/08/2018	30/10/2018	636h
7	Free board	01/10/2018	06/11/2018	383h

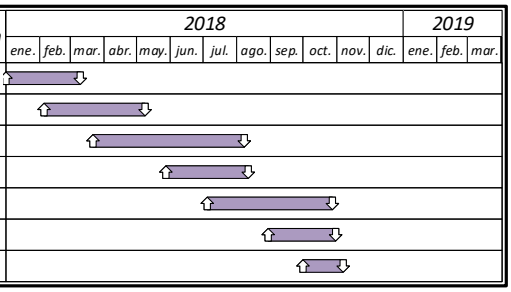

Figure 8.4.4: Gantt diagram with theoretical start and finish times for each construction sub-phase and strategy.

Definition of the construction strategies

Fig. 8.4.5 illustrates the input data needed to define a construction strategy according to the method proposed in this Thesis. This data is organized into three blocks: resources, protection before eventualities, and work planning.

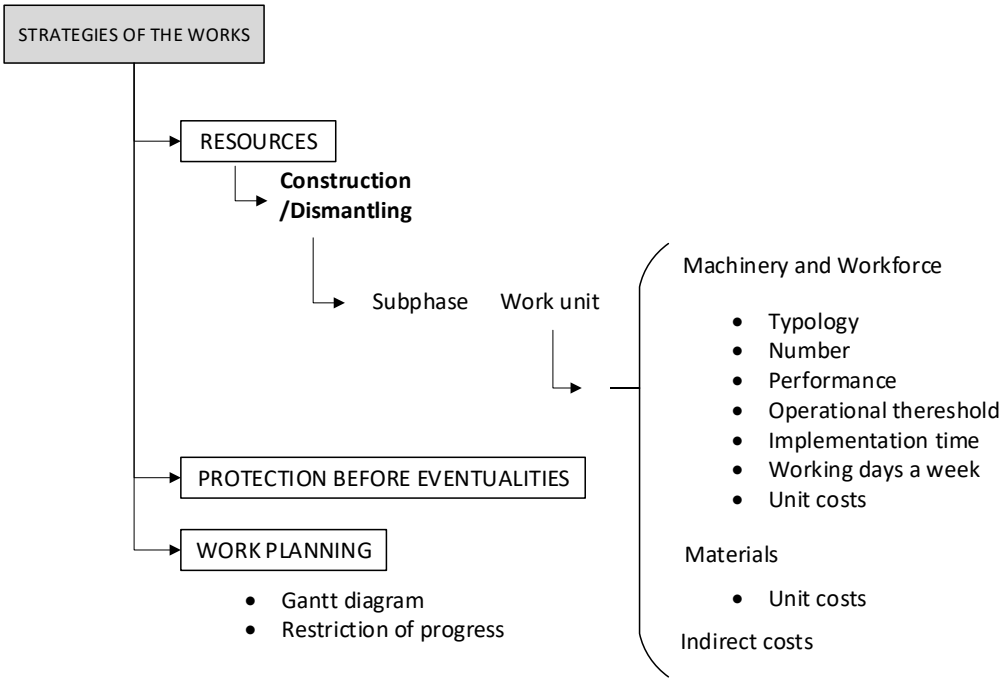

Figure 8.4.5: Flow chart of the input data needed for the definition of the construction strategy

Resources are defined for each work unit inside each sub-phase. Each type of machinery is defined by: the number machines, the performance executed (volume per hour), the time needed to start the work, the number of working hours a day and working days a week, the unit cost (euros per hour), and the operational threshold. Then, the unit cost of the material and the indirect costs are also defined. Finally, the sub-phase performance is calculated as the minimum performance of the different working units that integrate the sub-phase. Tab. 8.4.3 shows an example of the resources defined for the construction of the main armor sub-phase. In order to compare the performance of the series and parallel strategies, the same resources are considered for both construction strategies in these examples.

Sub-phase:		Main armor				
Working unit:		Terrestrial resources				
Machinery Type 1:		Dumper Truck				
Number of machinery	Unit performance	Initiation time	Working hours a day	Working days a week	Unit cost	Operational threshold
8	20 $m^3 h^{-1}$	0	12 h	6 d	55 € h^{-1}	-
Machinery Type 2:		Crane 110 t				
Number of machinery	Unit performance	Initiation time	Working hours a day	Working days a week	Unit cost	Operational threshold
3	54 $m^3 h^{-1}$	0	12 h	6 d	195 €h^{-1}	-
sub-phase performance:		160 $m^3 h^{-1}$				
Material costs:		90.91 € m^3				
Indirect cost:		10 % of direct costs				

Table 8.4.2: Parameters of the resources for the construction of the main armor sub-phase.

Two different alternatives are considered in this example to protect the sub-phases from climatic externalities during the construction. The first option is stopping the work during the winter months (from November to February). During these months, the subset is considered to be protected, and the works are stopped. This is only considered in the conservative strategy. The second option is to use the advance of the one sub-phase to protect the former sub-phase (i.e., the advance of the second armor protect the core of the subset). Therefore, as sub-phase progress, it is considered to protect the former sub-phase from the storm cycles. In this sense, the risky strategy supposes a series advance of the constructive sub-phases and no stop during the winter months while the advance of the conservative strategy is carried out in parallel, protecting much more each one of the sub-phases with the advance of the next ones. Besides, in this strategy, the construction of the breakwater is stopped and protected during the winter months. Regarding the work planning, the Gantt diagrams shown in Fig. 8.4.4 illustrates the theoretical beginning and ending of each sub-phase in both strategies.

Definition of the repair strategies

Fig. 8.4.6 illustrates the input data needed to define a repair strategy. This data is organized in four blocks: resources, the threshold for initiate the repair works, the priority of repair, and the permanent resources at the port. Same two different strategies (conservative and risky) are also considered in the repair phase.

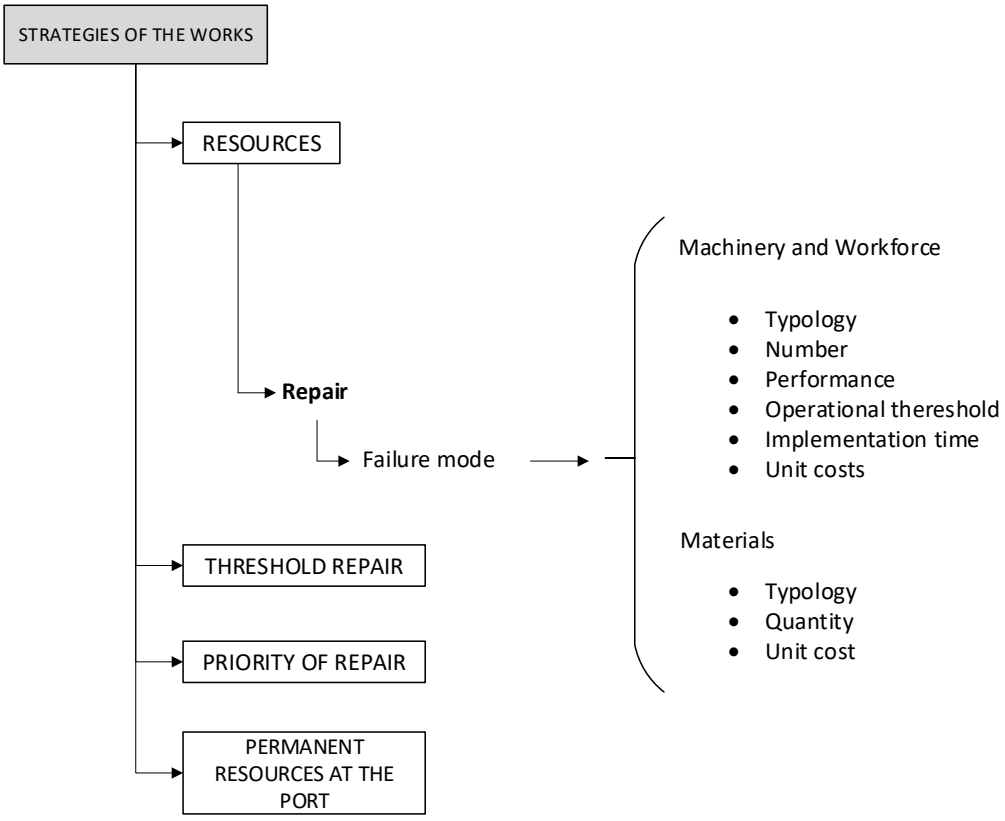

Figure 8.4.6: Flow chart of the input data needed for the definition of the repair strategy.

The resources needed to repair each failure mode must be defined. Each type of machinery and workforce is defined by: the typology, the quantity, the performance of repair, the operational threshold, the necessary implementation time from the time the order to repair is given until the repair work starts, and the unit costs. The materials are defined by: the typology, the quantity, and the unit costs. The damage thresholds to start the repair works and priority of repair between the failure modes also need to be defined for each strategy from 0 to 100 %. Finally, if permanent resources are going to be considered at the port for the repair works, they must also be included in the strategy definition. In these examples, both strategies have the same resources for repairing each failure mode, and no permanent resources are considered. In the conservative strategy, the damage threshold for repair is set up to 20%, indicating that the failure mode needs to be repaired when the damage reaches the 20 %; therefore, only soft damage is allowed in this strategy. However, in the risky strategy, the damage thresholds for repair are set to

45%, 50%, and 60% for failure mode 1 (FM 1), FM 2, and FM 3, respectively, allowing hard damage in the breakwater. Tab. 8.4.3 shows the parameters of the resources considered for the repair works of the FM 1. The priority of repair and the considered thresholds for initiate the repair works are also shown in Tab. 8.4.4.

Failure mode:	1: Erosion breakage of unit pieces of the main armor layer		
Machinery type 1:	Dumper Truck		
Number of machinery 2	Implementation time 24 h	Operational threshold -	Unit cost 55 € h^{-1}
Machinery type 2:	Hopper barge		
Number of machinery 1	Implementation time 24 h	Operational threshold $hs < 2$ m	Unit cost 170 € h^{-1}
Machinery type 3:	Crane 110 t		
Number of machinery 1	Implementation time 24 h	Operational threshold -	Unit cost 195 € h^{-1}
Work force type 1:	Machinist		
Number of work force 5	Implementation time 24 h		Unit cost 15 € h^{-1}
Materials type 1:	Concrete blocks 30 - 60 t		
Quantity 14250 m^3	Implementation time 24 h		Unit cost 1.3 M € per repair work
Performance of repair:	0.05 %;h^{-1}		

Table 8.4.3: Parameters of the resources for the repair works of the FM1.

Priority of repair	Repair threshold
FM 1	0.2 - 0.45
FM 2	0.2 - 0.50
FM 3	0.2 - 0.60

Table 8.4.4: Priority of repair and conservative (left) and risky (right) theresholds for initiate the repair works.

8.4.1.2 Project phases modeling

Modelling of construction phase

The diagram in Fig. 8.4.7 shows the flow chart followed by the proposed tool for the modeling of the construction phase. During the modeling, the scheme shown is applied state by state for each of the construction sub-phases of each of the sections of the dam in an iterative way. Upper blue and red boxes indicate the start and the end of the modeling process, respectively. As seen, all flows in the diagram converge in the red box. The yellow boxes show all the checks on the model throughout the modeling of the construction

process. As shown, after each check, the subphase adopts a different status shown by the green boxes. Finally, when the check reaches the lower blue box, the subphase has been executed completely.

As can be seen, the tool checks if the sub-phase suffers damages as a result of the propagated climate, then checks if the sub-phase has to work according to the strategy and planning of the previously defined works. After making all the checks, a situation is finally assigned to the sub-phase: protected, in losses, working, working delayed, or finished. Each situation is associated with a different action, and therefore the work is executed until all the volumes projected for the different sub-phases have been executed.

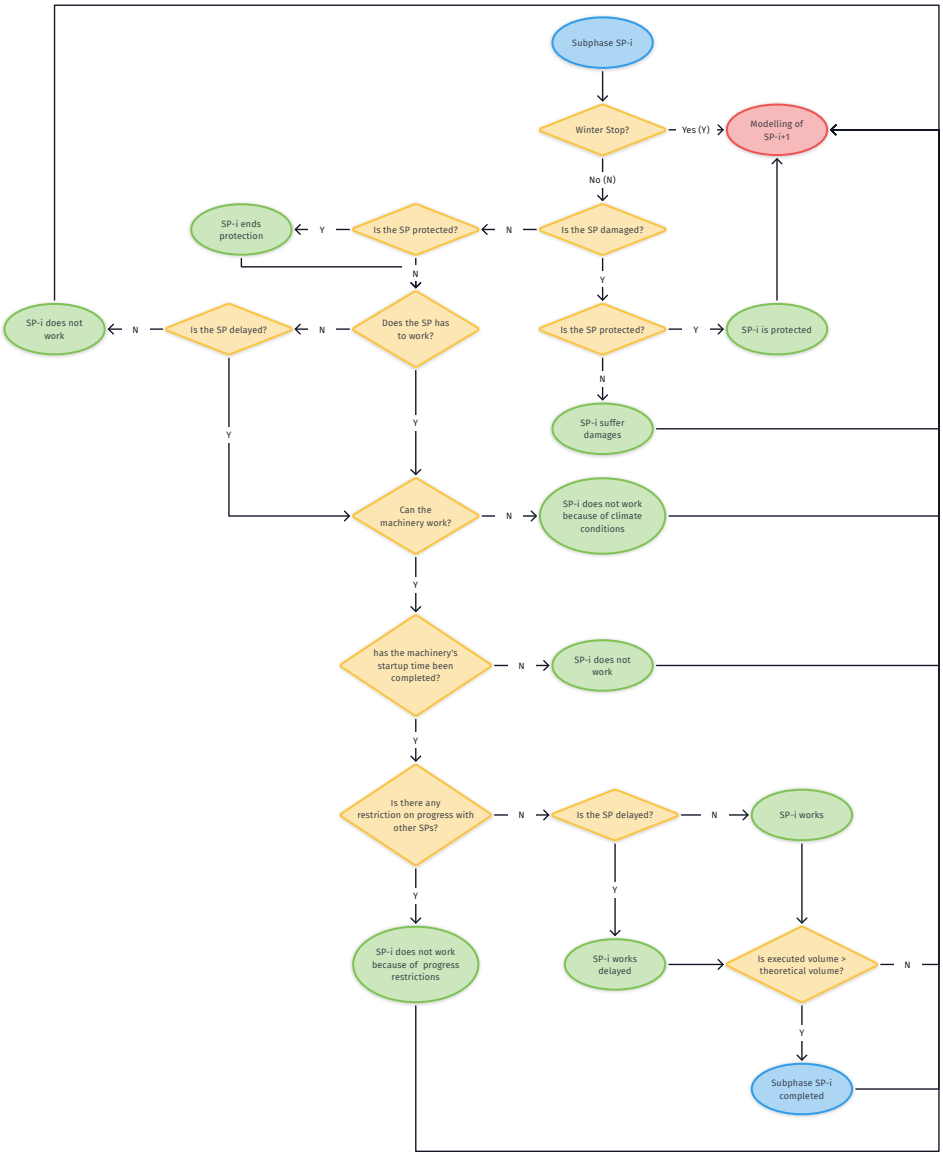

Figure 8.4.7: Flow chart for the modeling of the construction process for the sub-phase i (SP_i) during the state h.

Modelling of the useful life-time

Following the same criteria, diagrams in figures 8.4.8 and 8.4.9 show the flow chart followed by the proposed tool for modeling the life-time cycle once the maritime structure has been built and has become operational. The tool checks through each of the protective maritime structure's failure modes state by state, and together with the climate data, it checks if there is an initiation of damage, if there is damage propagation or if repair work has to be started.

During the life-time cycle, the developed tool for the cost calculation first analyze whether the state belogs to a calm or a storm period. During storm periods (Fig. 8.4.8), the tool analyze if failure is started in the failure mode and calculated the accumulated damage using the previously defined damage accumulation model. Assessed the damage in the state, the tool checks if the progression of damage initiates the failure in the others failure modes using the failure propagation tree. Finally, at the end of a state belonging to a storm period, the tool must analyze if the total destruction of the protective maritime structure occurs as a consequence of the propagation of the damage.

However, if the state belongs to a calm period (Fig. 8.4.9) the tool focuses on repair works. To determine if repair works can be initiated or continued, the tool checks if damage exceeds the repair threshold and the operation thereshold of the machinery. If they are positive, the tool repairs the failure mode.

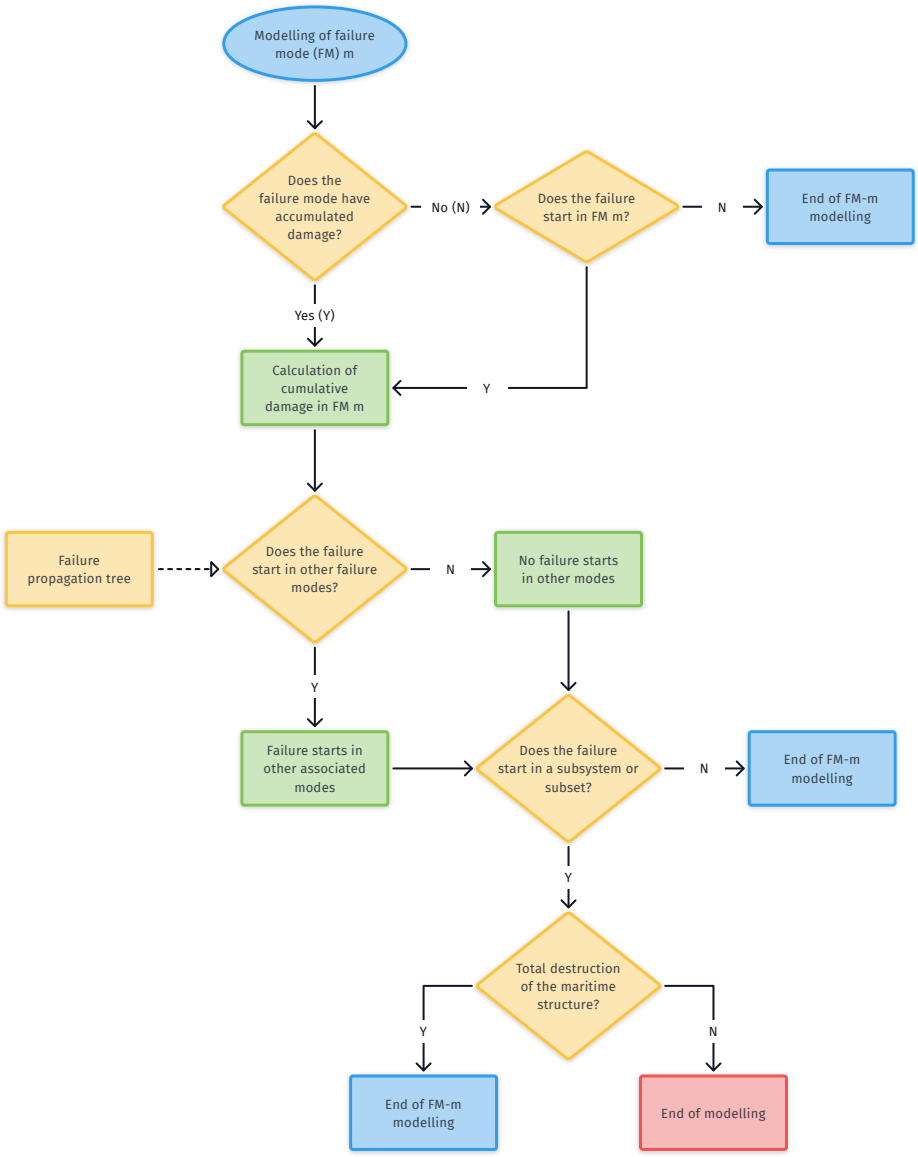

Figure 8.4.8: Flow chart for the modeling of the useful life-time during storm cycle.

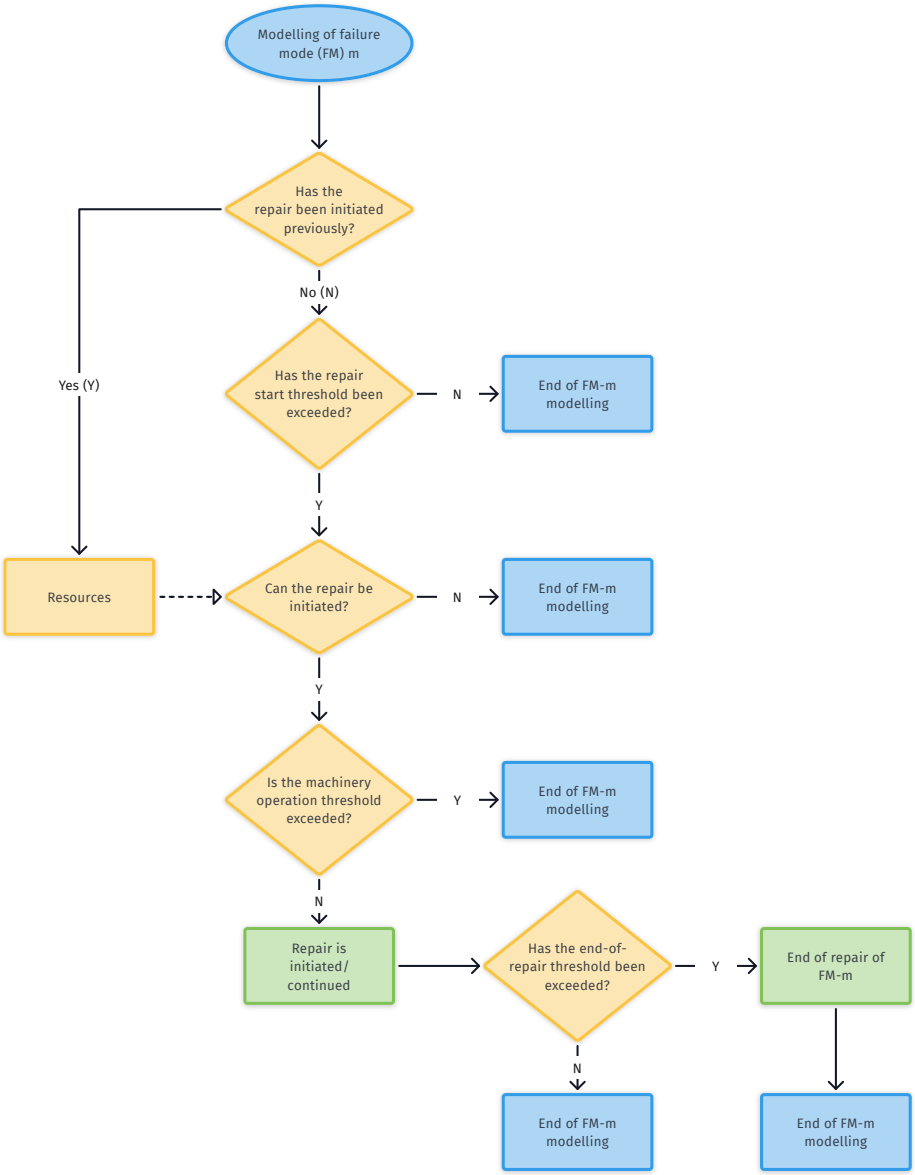

Figure 8.4.9: Flow chart for the modeling of the useful life-time during calm period.

8.5 Results

8.5.1 Example 1: Construction costs

This section analyses the results obtained after submitting the two construction strategies to 100 maritime climate simulations. Firstly, the results relating to the time and volume of execution of each construction sub-phase are analyzed. Then, the disaggregated costs of each sub-phases are analyzed, as well as the total construction costs.

8.5.1.1 Times and volumes

The start and end dates of each sub-phase obtained after the modeling of the construction process are shown in the boxplots of Fig. 8.5.1 for both strategies. Triangles indicate the theoretical start and end dates defined in the Gantt chart. Within each Boxplot, the horizontal line represents the median of the data, while the circular point represents the mean value. As can be seen, in the conservative strategy (left), the end dates are always met except in sub-phases 1 and 2 due to delays caused by wave storms. This causes these sub-phases to end between 1 and 2 months later than planned, as shown in the figure's left panel. However, in the risky strategy, the obtained start and end dates of the sub-phases after the simulation do not coincide with the theoretical values, and it is necessary to reformulate the organization of the construction process for this specific strategy. The reason for this observed mismatch between modeling and theoretical endings is mainly due to two reasons. Firstly, "series" execution makes the sub-phases more unprotected against storms, causing greater damage and delays in execution. At the same time, this advance in series, although it allows a smaller number of machinery in work at the same time, causes that delays in a sub-phase cause delays in the beginnings of the rest of sub-phases causing a mismatch in the times of all the work.

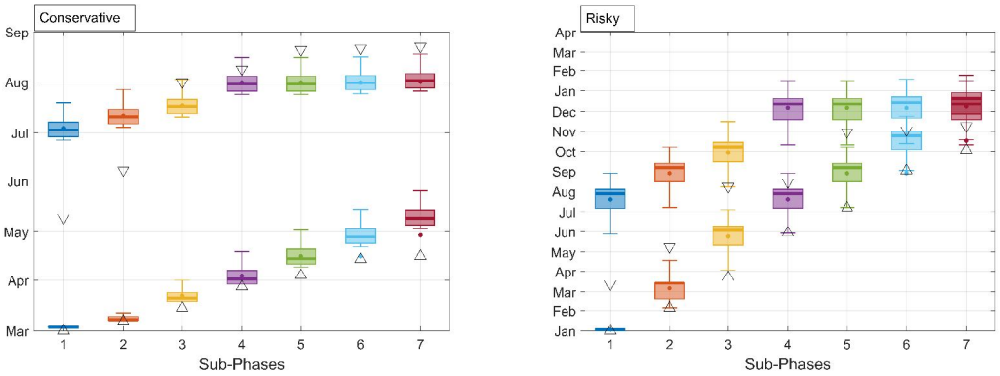

Figure 8.5.1: Boxplot with the start and end dates obtained for each sub-phase after the modeling of the construction process. The triangles indicate the theoretical start and end dates defined in the Gantt chart. Left (right) panel shows the results for the conservative (risky) strategy.

Figure 8.5.2 compares the different states of each of the construction sub-phases throughout the entire construction process between the two strategies. The states in which a sub-phase can be found are: (1) working, when the sub-phase is working within the established deadlines, (2) working delayed, when the sub-phase is working after the theoretical end date defined in the Gantt diagram, (3) not working by restriction, when the sub-phase cannot advance so as not to exceed the distance from the advance front of the next sub-phase established in the strategy, (4) damage, when the sub-phase suffers damage as a result of wave storm cycles and (5) others such as stops for operation.

It is observed that in the risky strategy, all sub-phases show a higher number of working hours delayed as a consequence of having to finish the construction of the sub-phase behind the theoretical completion date. It is also interesting to highlight how, according to the chosen work planning, the number of hours in which the sub-phase cannot work due to restriction with the advance of the next sub-phase is as high or more than the working hours of the sub-phase itself. This happens when the performance of a sub-phase is higher than that of the sub-phase ahead. As a solution, either the performance of these sub-phases (SP3, SP5, and SP7) should be reduced, or the start of these sub-phases should be delayed in time.

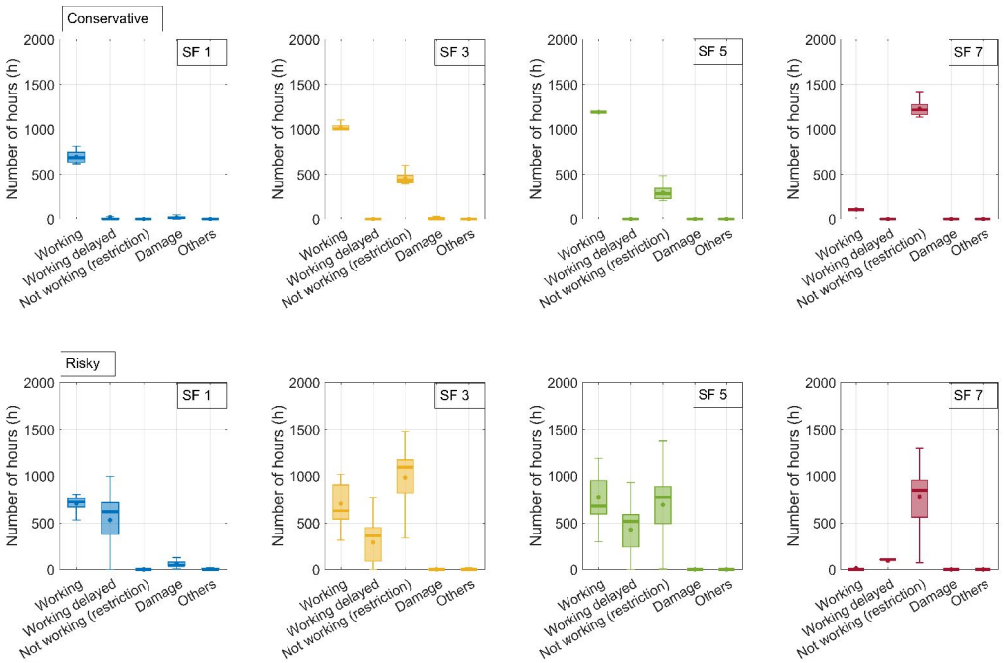

Figure 8.5.2: Boxplot with the comparison between the states of each sub-phase throughout the construction process for each strategy.

Figure 8.5.3 shows the comparison between projected theoretical volumes (triangular point) and executed real volumes (boxplot) for each construction sub-phase and strategy. It can be seen that the most significant differences occur in SF 1 (dredging) and mainly in the risky strategy as a consequence of the lack of protection against storms during the months of the winter.

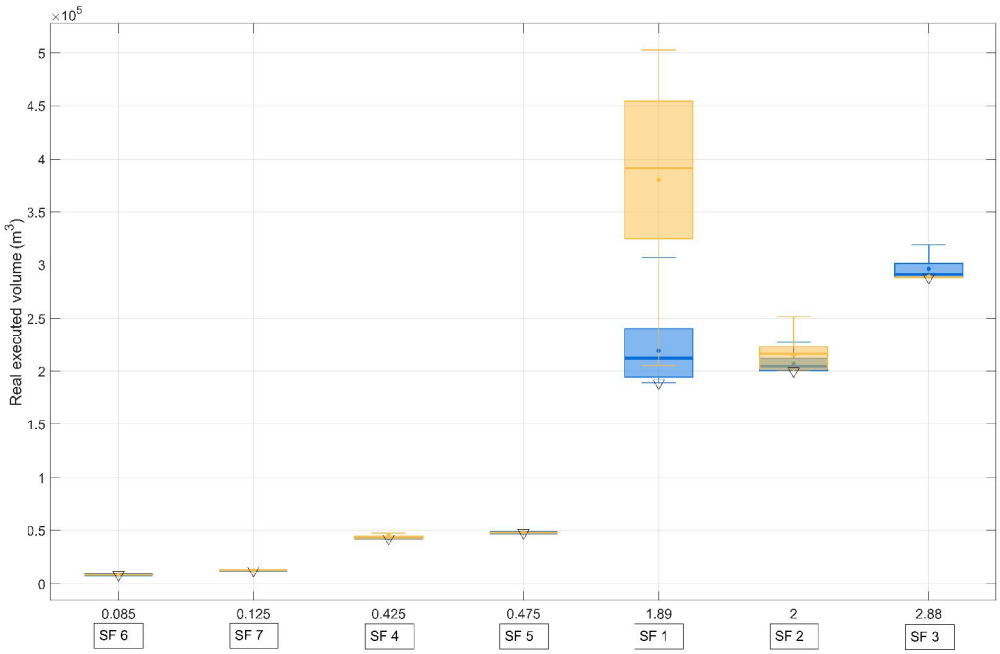

Figure 8.5.3: Comparison between the real, projected and lost volumes for each sub-phase throughout the construction process between the two strategies.

8.5.1.2 Construction costs

After the analysis of times and volumes, Fig. 8.5.4 displays the disaggregation of the total construction costs by sub-phase by component (direct costs, indirect costs, and losses due to damage) and by strategy. This allows managers and public administrations responsible for the construction of coastal protection works to quickly identify at a glance, those elements that most influence the total cost. As shown, SF 2, SF 3, and SF 5 are the three sub-phases that significantly impact the total cost. However, SF 1 and SF 2 are the ones that experience the highest costs due to storm damage during the construction process and, therefore, the ones that should be protected the most in order to avoid such costs. When comparing the cost between strategies, it can be seen that the most significant differences occur in SF 1, followed by SF 4.

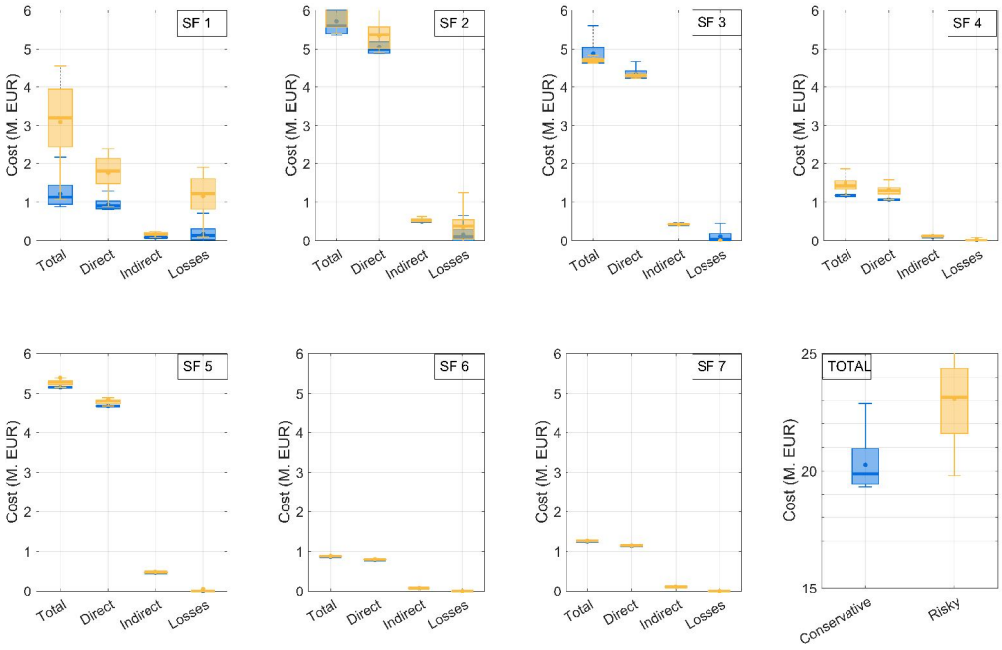

Figure 8.5.4: Comparison betwwen total, direct, indirect and losses cost between sub-phases and strategies. Blue (yellow) colors corresponds to the conservative (risky) strategy.

Finally, Fig. 8.5.5 shows a comparison between the PDF and the CDF of total construction costs between the conservative (blue) and the risky strategies (yellow). It can be seen that the range of total construction costs for the conservative strategy (19 - 23 M. EUR) is narrower than for the risky strategy (19 - 28 M. EUR). In the conservative strategy, the most likely value is around EUR 20 million, while in the risky strategy, it is around EUR 23.5 million. In probabilistic values, the value of the total construction cost in EUR millions corresponding to the 50th, 90th 95th, and 99th percentiles are shown in Tab. 8.5.1. Therefore, these results constitute a useful tool for managers and decision-makers in the task of analyze the construction costs of protective maritime structures from flood.

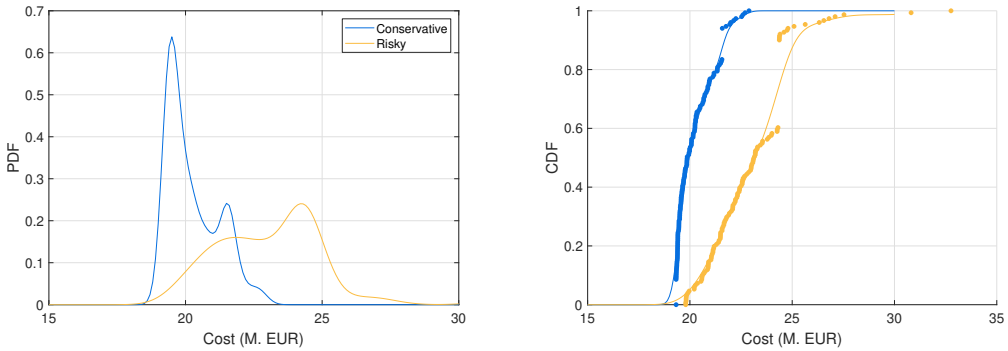

Figure 8.5.5: PDF and CDF of the total cost of construction of the subset for booth strategies.

Percentile	Conservative (M. EUR)	Risky (M.EUR)	Diference (M. EUR)
50th	20	23	3
90th	21	25	4
95th	22	26	4
98th	22	27	5
99th	23	28	5

Table 8.5.1: Total cost of construccion associated to the 50th, 90th 95th and 99th percentiles for the conservative and risky strategies.

8.5.2 Example 2: Cost of repair of a failure mode

This section analyses the progression of damage in and between different failure modes throughout the damage propagation tree and damage evolution model once the failure has started. This example then compares the evolution of the repair works and the associated cost between the conservative and the risky strategy.

As seen in Fig. 8.5.6 failure starts in FM 1 (blue) as a consequence of a storm event in both the conservative and the risky strategy. In the conservative strategy, when the damage surpasses the 20 % repair works start (blue triangle) and finish (inverse blue triangle) without any problem. However, in the risky strategy, the damage progresses until a 40 % and 60 % of damage when, according to the failure propagation tree, this level of damage triggers the failure in FM 2 (vertical orange line) and FM 3 (vertical green line) respectively. Although the threshold for repair works in FM 1 is set at a 45 % of damage, the repair does not start until a 65 % of damage because in the storm that took place at the end of 2024 in the simulation used in this example (see Fig. 8.5.6).

Once the failure has started in FM 2 and FM 3, the damage progresses until the repair threshold (50 % and 60 % of damage). It is also interesting to see that the repair works in FM 2 also suffer damages due to the storm events occurring during the repair.

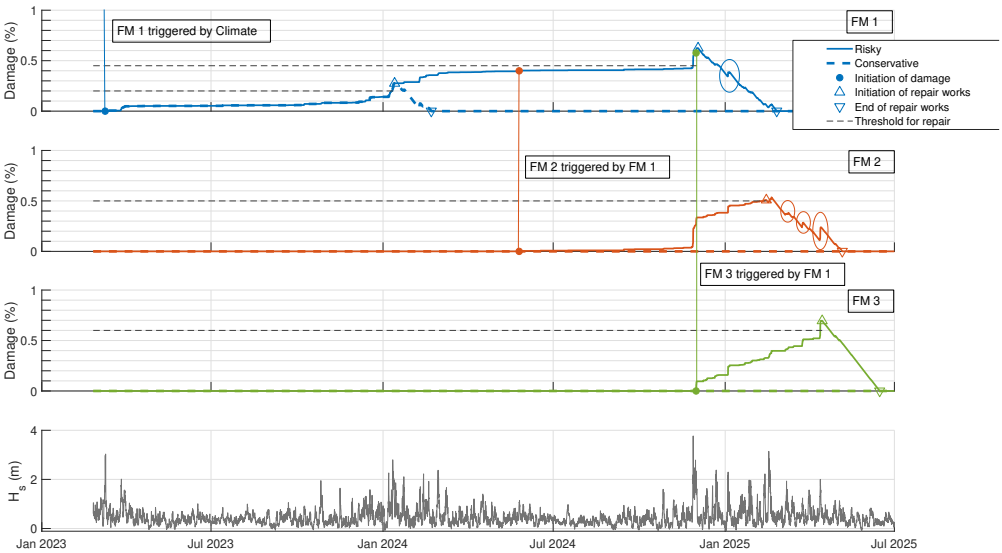

Figure 8.5.6: Temporal evolution of damage for each failure mode and strategy. The vertical lines highlight the start of damage in one failure mode due to damage propagation in another mode throughtout the damage propagation tree. Ellipses indicates the moments of the repair works when the damage increases as a consequence of a storm cycle.

Figure 8.5.7 shows the disaggregation of the total cost of this repair works by the failure modes and the components of the cost for the risky strategy. As seen, according to this modelization of the repair, a single repair of the FM 1, FM 2, and FM 3 cost around 6, 3, and 3 M. EUR, respectively, leading to a total cost around 12 M. EUR. This value represents approximately 50% of the total construction cost obtained in the previous section. However, it is essential to highlight that this cost corresponds to hard damage, where the damage in the three failure modes exceeds the 50 % before the repair works start.

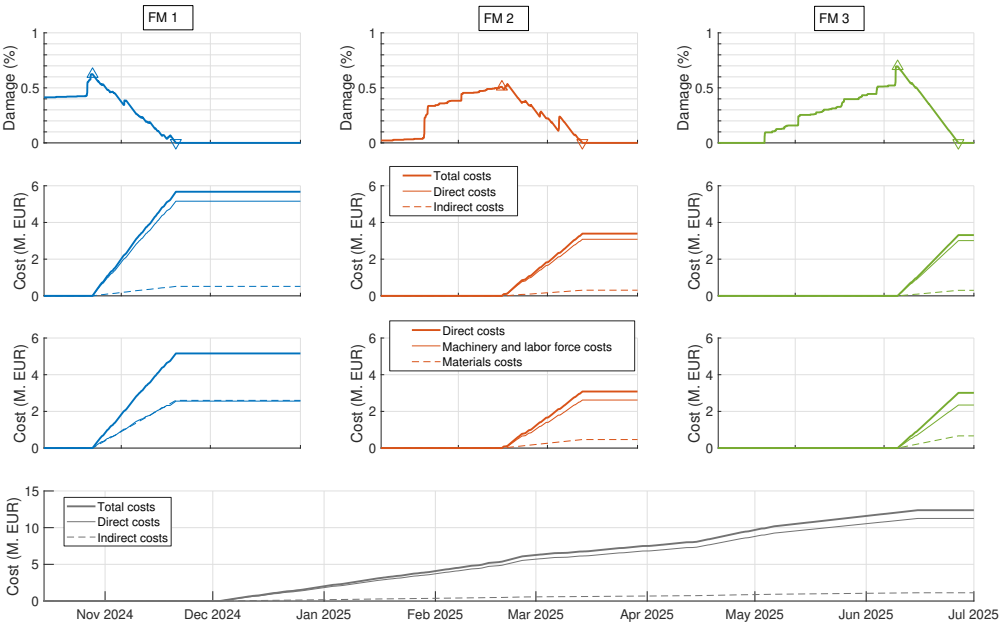

Figure 8.5.7: Temporal evolution of the costs for each failure mode during the repair works for the risky strategy.

8.5.3 Example 3: Total costs during useful life time

Fig. 8.5.8 shows a comparison between both strategies for the temporal evolution of the damage and the repair cost along the useful life of the breakwater. As seen, in the risky strategy, failure is propagated through the three failures modes more often than in the conservative one. Therefore the final repair cost obtained in this simulation at the end of the useful life is much higher in the risky strategy, around 90 M EUR vs. 25 M. EUR.

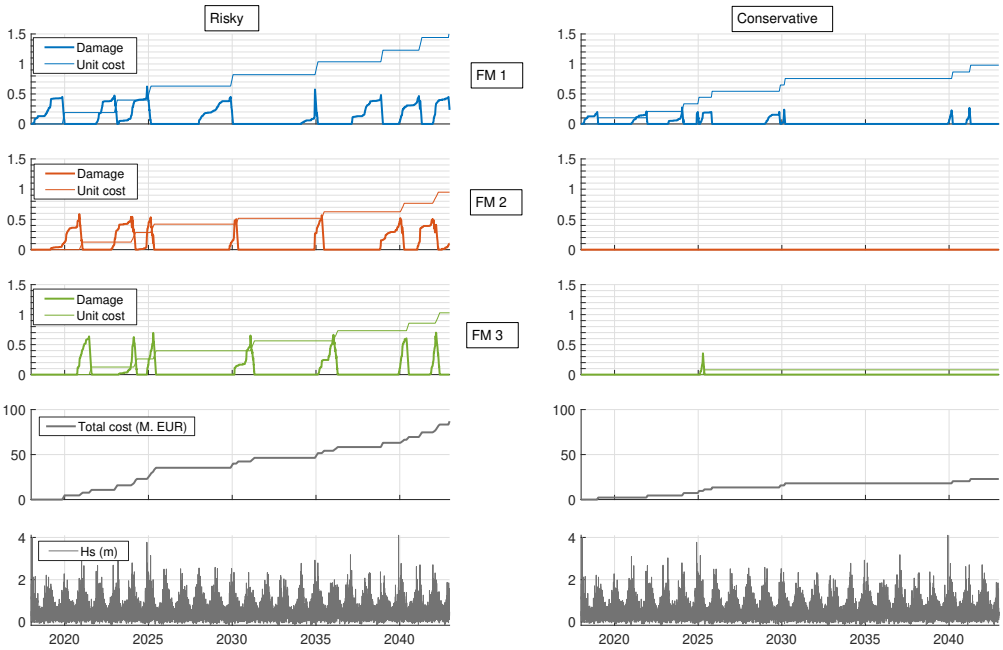

Figure 8.5.8: Temporal evolution of the damage and the unit cost along the useful lifetime of the breakwater for a single simulation in booth strategies. Unit cost is obtained by dividing the repair cost of the failure mode by the construction cost of the associated subphse.

To determine whether the failures are caused by the natural agents' storm event or by the progress of the damage in the other modes along the useful life, Fig. 8.5.9 is created. Each row represents the number of initiation of damage in each failure mode as a result of damage propagation in FM 1 (first column), FM 2 (second column), and FM 3 (third column) or as a result of a storm cycle (fourth column). The fifth column corresponds to the sum of the total number of failures for each of the failure modes. Each panel shows the comparison between the two strategies through a boxplot. As seen, failure in FM 1 is always initiated by the climate. Moreover, as shown in the figure, the conservative strategy experiments a higher number of initiation of damage than the risky strategy. This is due to the fact that in the conservative strategy, the damage is not allowed to progress more than 20 % so that when repairing earlier, more initiation of damage to occur instead of the damage progressing. The opposite is found in FM 2, where the failure is always initiated by the progression of damage in FM 1. A mixed behavior is found in FM 3, where failures are due to storm events (climate) and progression of damage in FM 1 and FM 3 in the risky strategy.

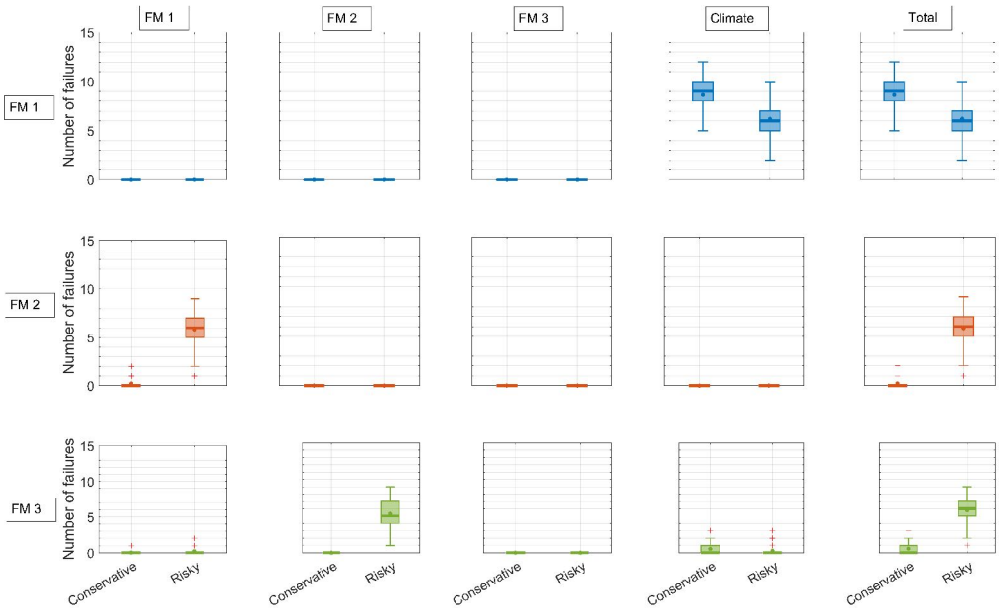

Figure 8.5.9: Each row represents the number of initiation of damage in each failure mode as a result of damage propagation in FM 1 (first column), FM 2 (second column), and FM 3 (third column) or as a result of a storm cycle (fourth column). The fifth column corresponds to the sum of the total number of failures for each of the failure modes. Each panel shows the comparison between the two strategies through a boxplot.

Figures 8.5.10 show the variability in the annual repair cost accumulated over the life-time for each of the three failure modes and strategies. These figures allow a total breakdown of the costs, which allows the rapid identification of which failure modes and periods of time have the greatest influence on the total cost. Fig. 8.5.11 shows the total cost of repair accumulated year by year. As shown, there is a large difference between the two strategies, being the conservative strategy the one with the lowest cost.

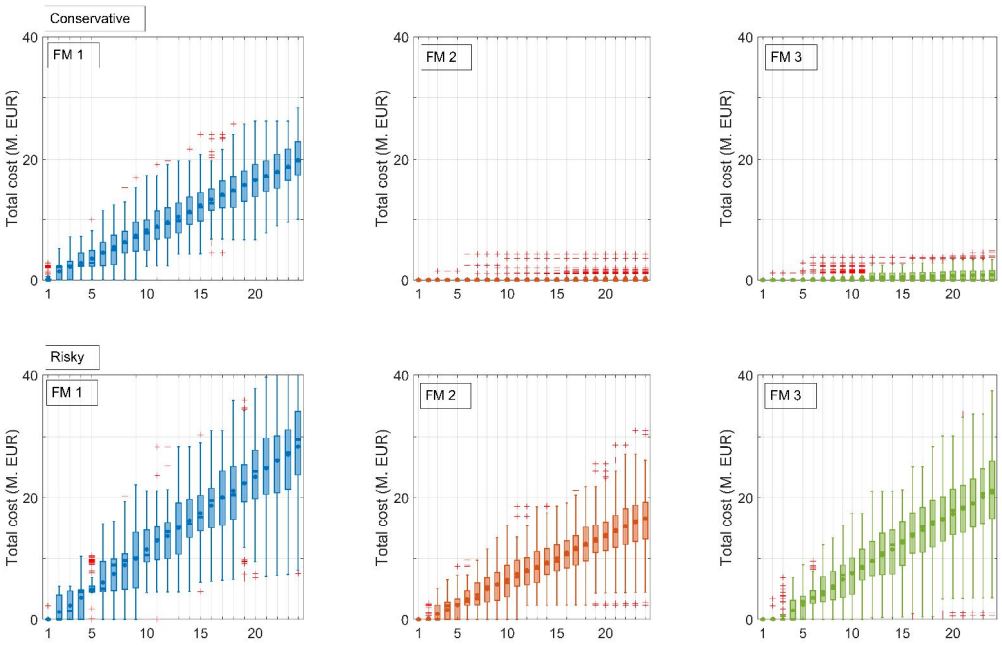

Figure 8.5.10: Boxplot with the cost of repair accumulated year by year (y-axis) over the useful life-time (x-axis) disaggregated by failure modes.

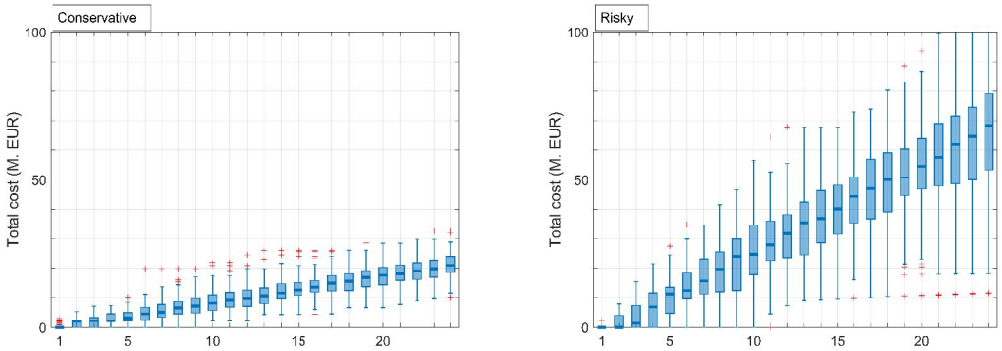

Figure 8.5.11: Boxplot with the total cost of repair accumulated year by year over the useful lifetime.

Finally, the total cost distribution function for repair over the life-time is shown in Fig. 8.5.12 for the conservative (blue) and risky (yellow) strategy.

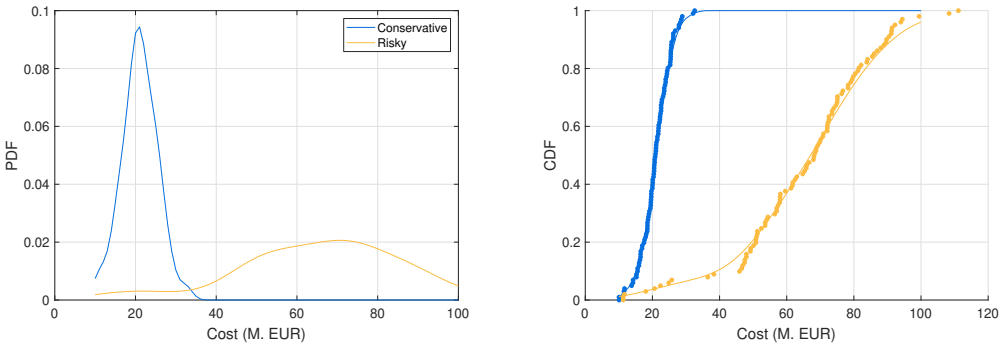

Figure 8.5.12: PDF and CDF of the total cost of repair of the subset for booth strategies.

8.6 Summary and conclusions

Once the impact of the sea-level rise on flood failure along transitional coastal environments has been assessed, methods, and instruments to optimize the total cost of the protective maritime structures are needed. Thus, in this chapter, a detailed method and an associated open-access numerical tool for calculating the probability distribution function of the total costs for any type of protective maritime structure at any location during its life-time cycle follow the guidelines of the latest version of the ROM program (ROM-1.1, 2018) is presented. The latest version of the developed tool is available in the following public repository: `https://github.com/gdfa-ugr/total_costs`. The definition of the total costs is defined at first as the sum of the execution costs of construction, dismantling, and repair works as well as the costs of exploitation during the operating phase. The main variables that modify these costs, most of them of stochastic nature are: (i) the forcing agents, (ii) the design of the structure, (iii) the project factors, (iv) the organization and work planning definition including the decision and actions (strategies) taking during the life cycle, (v) the interactions between the former elements, and (vi) the useful life-time. Then, the methodology for the calculation of the total costs following the ROM-1.1 (2018) is presented in six steps: conception, spatial and temporal disaggregation of the maritime structure; work planning and strategies definition; characterization, simulation and propagation of maritime climate; project phases and damage accumulation modeling; cost allocation; and analysis and uncertainty assessment through Monte Carlo techniques.

As a case study example of application, this chapter presents a series of gradual examples using the associated open-access numerical tool, including the calculation of: the total construction costs, a single repair costs of a damaged breakwater, and the total cost over the useful life-time of the breakwater. The following conclusions can be drawn

from the analysis presented in the previous sections:

- The presented tool allows a detailed definition of construction and repair strategies. The tool allows going in-depth to specify the characteristics of each type of machinery (typology, performance, working days a week, and unit costs among others), material and labor force, and the thresholds and priorities for the works executions. This tool also allows the precise definition of the theoretical beginnings and endings of the execution of each work, as well as the stopping times during the winter.

- During the simulation, the maritime structure's useful-life structure is modeled step-by-step following the flow charts presented in this chapter. At the beginning of each step, the tool checks the status of each element of the structure to analyze if: the structure suffers damages as a result of the propagated climate; it has to work according to the defined strategy and planning; it is delay; or if it has to repair according to the accumulated damage and repair thresholds. Once verifies the status during the state, different actions are taking during the modeling process until the construction of the protective maritime structure is finished or the useful life-time is completed.

- In the examples presented in this chapter, two opposite strategies "risky" and "conservative" are defined. The difference between both strategies lies in the restriction of progress between the breakwater elements and the repair threshold. In the risky strategy, the breakwater is developed in series, where each element is executed nearly one-by-one, and the repair threshold is higher than in the conservative. In contrast, in the "conservative" strategy, all the elements are developed simultaneously, and the repair threshold is lower, meaning that repair works are executed before without allowing the damage progression.

- The results during the construction phase indicates that the conservative strategy execution times fit much be the theoretical end times defined in the work planning. Furthermore, the variability in the execution times is also shown by the tool through boxplots graphics. Results indicate that the executed volume by the first sub-phase (dredging) of the risky strategy doubled the projected theoretical volume. The reason is due to the fact that the risky strategy also works during the winter months without protection were the climate is severe, while conservative strategy does not. Therefore, differences between 3 to 5 million euros are found between the 50th and 99th percentiles of the cumulative distribution functions of the construction costs between booth strategies, being the risky strategy the most expensive. However, these differences increases during the repair phase, where

differences around 60 million euros are obtained between both strategies for the higher percentiles.

- Although the examples represented in this chapter are theoretical, the proposed tool, which follows the ROM-1.1 (2018) recommendations, allows the estimation of the costs associated with the different design strategies, work planning, and decisions. This type of tool represents a before and after for public administrations since they no longer depend solely on the budgets given by construction companies. Now it is possible to model each of the alternatives, strategies, decisions, and planning to obtain the associated costs and the limited uncertainty. This makes it possible to discard unprofitable alternatives quickly and economically, such as the risky strategy presented in this chapter as an example.

CHAPTER 9

GUIDELINES FOR ASSESSING THE IMPACT OF GLOBAL WARMING ON TRANSITIONAL COASTAL ENVIRONMENTS

9.1 Introduction

This chapter integrates the methodology developed throughout this Thesis to present comprehensive guidelines for the assessment of the SLR impact on coastal urban fronts at local scale. These guidelines are built upon the knowledge developed throughout: (i) this thesis, (ii) the PROTOCOL project, and (iii) the latest edition of the recommendations for maritime works (ROM-1.1, 2018). These guidelines are not intended to replace any of the previous documents, as these guidelines do not go into as much detail. However, they do integrate these documents to offer a step-by-step method from the problem's definition to the calculation of the solution's total costs. However, at each point of these guidelines, it will be necessary to check the former sources and the different chapters of this Thesis on which these guidelines are based to be able to go deeper and apply the different proposed methods. As a result, this chapter is designed to provide managers, coastal engineers, and decision-makers guidelines together with a set of practical tools to assess whether coastal defenses will be sufficient to withstand the impact that SLR will have on coastal urban fronts. Furthermore, if they are not, to address the questions of where and when flood defenses will fail, and by how much.

The key and differentiating element of these guidelines is that they apply the principle of preventive medicine to Coastal Engineering in what we have called "preventive

engineering," that is, not waiting until there is a problem to solve, but anticipating it. Therefore, these guidelines are structured in three main blocks: identification of the problem -preferably a future problem (symptoms)-, identification of the causes (diagnosis) and identification of the possible solutions (treatment) as shown in Fig. 9.1.1.

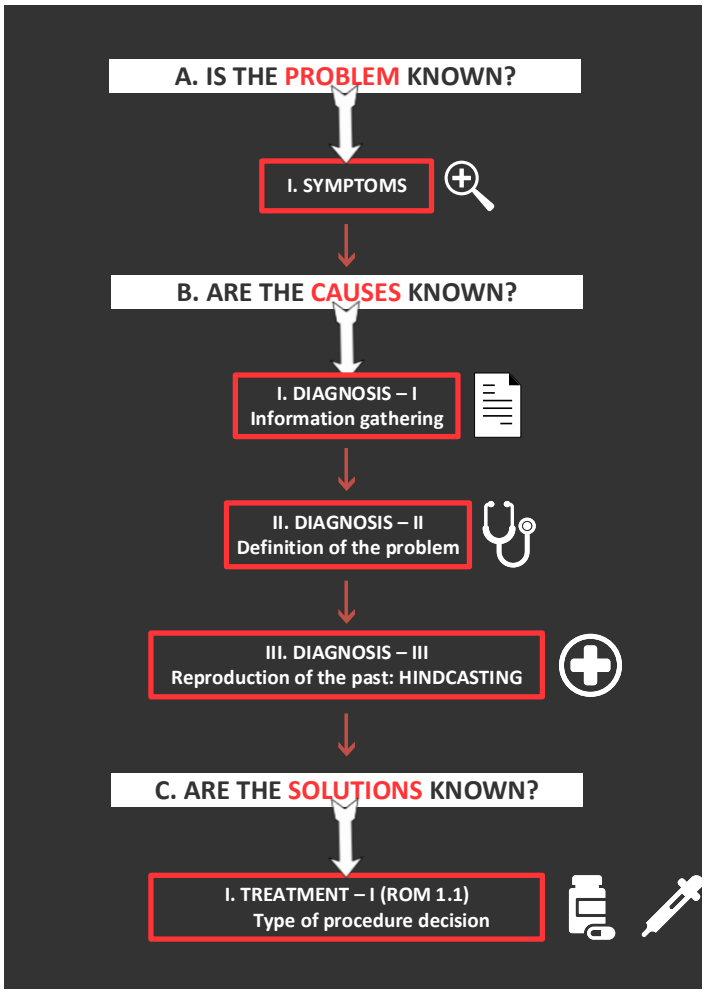

Figure 9.1.1: General organigram with the main blocks of the preventive engineering guidelines.

9.2 A. Is the problem known? Symptoms

The first module (A.I.1) in the first block of symptoms (Fig. 9.2.1) is to identify the problem that is either already occurring or is expected to occur in our coastal system in

the coming years, which in medical terminology is known as “defining the symptoms”. Once the problem has been identified (flooding, erosion, overtopping, among others), defining what is at risk (A.I.2) is necessary. The urgency, the methods to be used, and the risk and uncertainty to be assumed in the solution to be proposed will highly depend on the elements that are at risk, among which we can differentiate the following: human life, infrastructure, economic activities, or ecosystems. Finally, and only if there are historical records, it is necessary to define the frequency and intensity of the damage caused by the failure (A.I.3) qualitatively. With all this information, the definition of the symptoms can be considered complete.

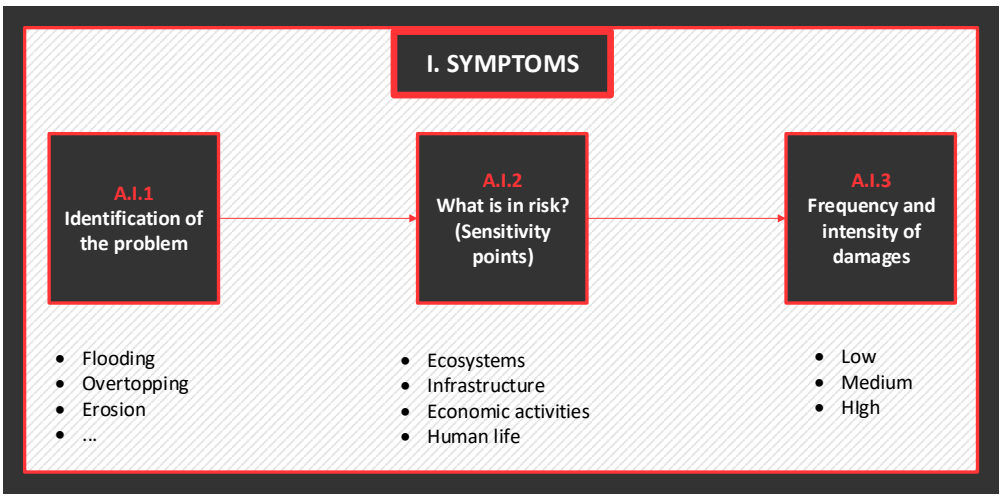

Figure 9.2.1: Modules of the first block: symptoms

9.3 B. Are the causes known? Diagnosis

The second block, to address the causes that are generating the previously identified problem, is structured into three main modules (Fig. 9.1.1): information gathering, the definition of the problem and reproduction of the past, which are in turn divided into different submodules as seen in next sections.

9.3.1 Diagnosis-I: Information gathering

In this section, the first module of the diagnosis block is discussed. Fig. 9.3.1 shows the organization of the different submodules of the information gathering module. In these guidelines, the type of procedure to be applied is highly dependent on the quantity and quality of the information available (B.I.1). The table is shown in Fig. 9.3.2 shows the

different categories of information that need to be collects and their classification into: minimum information required, acceptable, and ideal extracted from Silva (2019).

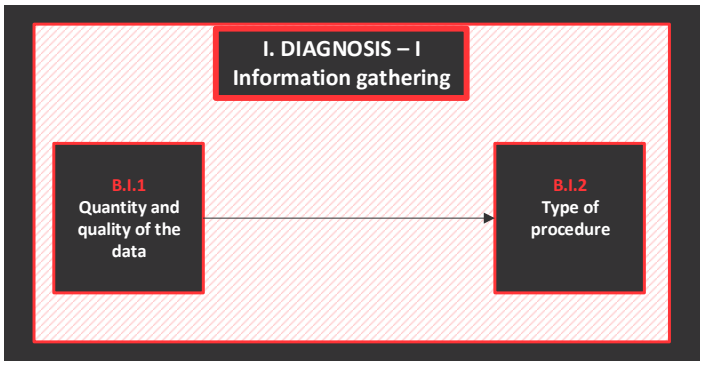

Figure 9.3.1: Submodules of the information gathering module.

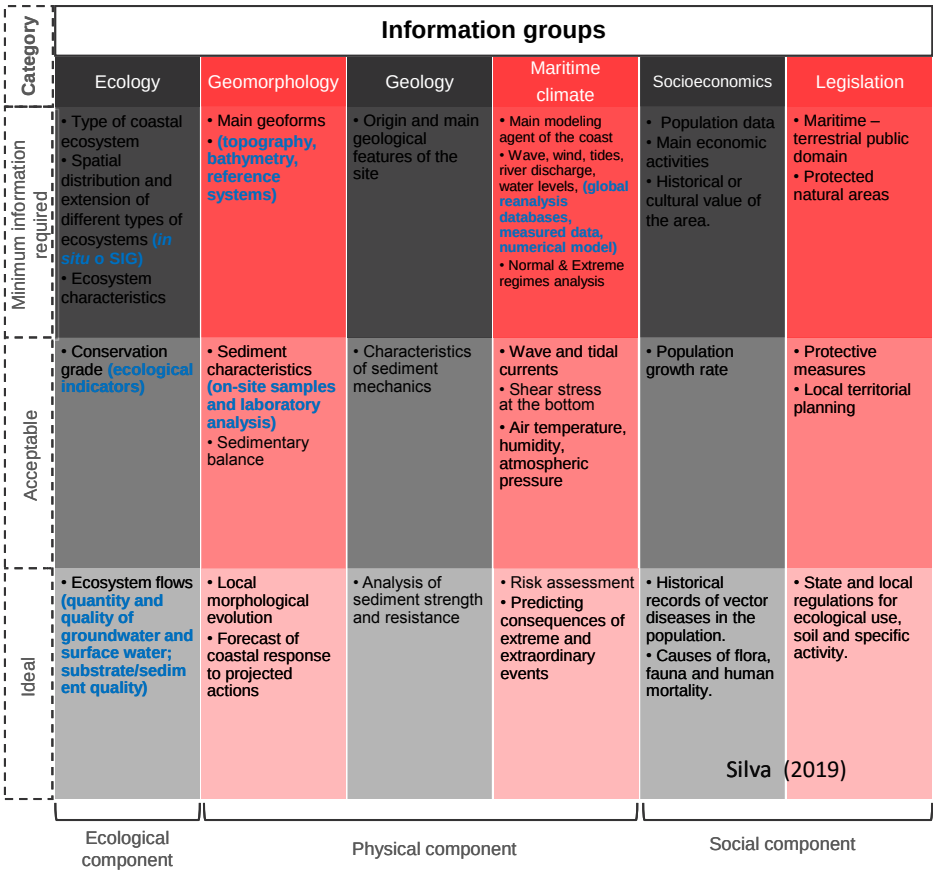

Figure 9.3.2: Categories of information to be collected classified by their importance.

As in medicine, the type of treatment applied to the patient depends on the information and tests performed. In the case that the available information is not sufficient, the guidelines propose not to take any action and instead to place monitoring teams and continue research to gather information (Fig. 9.3.3). If the available information reaches the minimum required category, it is advisable to act on the most critical problems. However, at the same time, it is necessary to continue investigating to have more information that will allow us to design a solution that either stabilizes the problem in the medium term or designs a long-term solution. However, as in medicine, there will be patients and problems that require treatment on a continuous basis for life because the problem has become chronic. When studying possible solutions, it will be necessary to consider all these aspects to evaluate whether to offer a transitory solution versus a definitive

long-term solution. Once the type of treatment (solution to the problem) has been chosen, ROM-1.1 (2018) proposes to design the solution by means of successive iterations through various levels of development from the preliminary studies to the maximum level of development, the investment project as shown in Fig. 9.3.3.

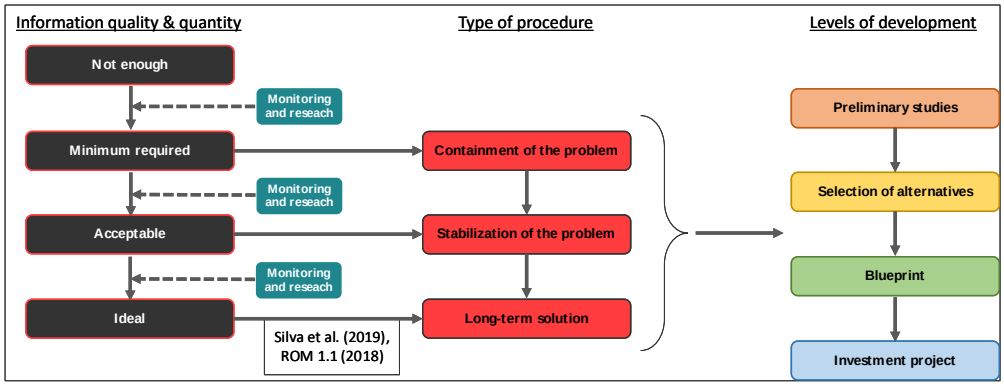

Figure 9.3.3: Type of procedure and level of development as a function of the information quality and quantity.

9.3.2 Diagnosis-II: Definition of the problem

The second module of the diagnosis block focuses on defining the problem to be globally solved (i.e., defining each of the variables and aspects that affect the system). As described in Fig. 9.3.4, first, it is necessary to define the general objective along with the specific objectives we want to achieve in solving the problem (B.II.1). It is then necessary to define the temporal and spatial scales of our study area (B.II.2) as well as the spatial and temporal resolution we are going to work with (B.III.3): kilometers, meters, days, or hours. Once the scales have been defined, it is necessary to characterize and analyze the forcing climatic agents, whether they are maritime, fluvial, or atmospheric (B.II.4). The definition of the problem must also highlight all the human actions that alter the system in an unnatural way, such as dredging, maritime structures, and urbanized areas. Finally, the considered hypotheses of the study must also be defined. Chapters 2 and 3 of this Thesis present a practical case study for problem definition together with the tool for climate characterization.

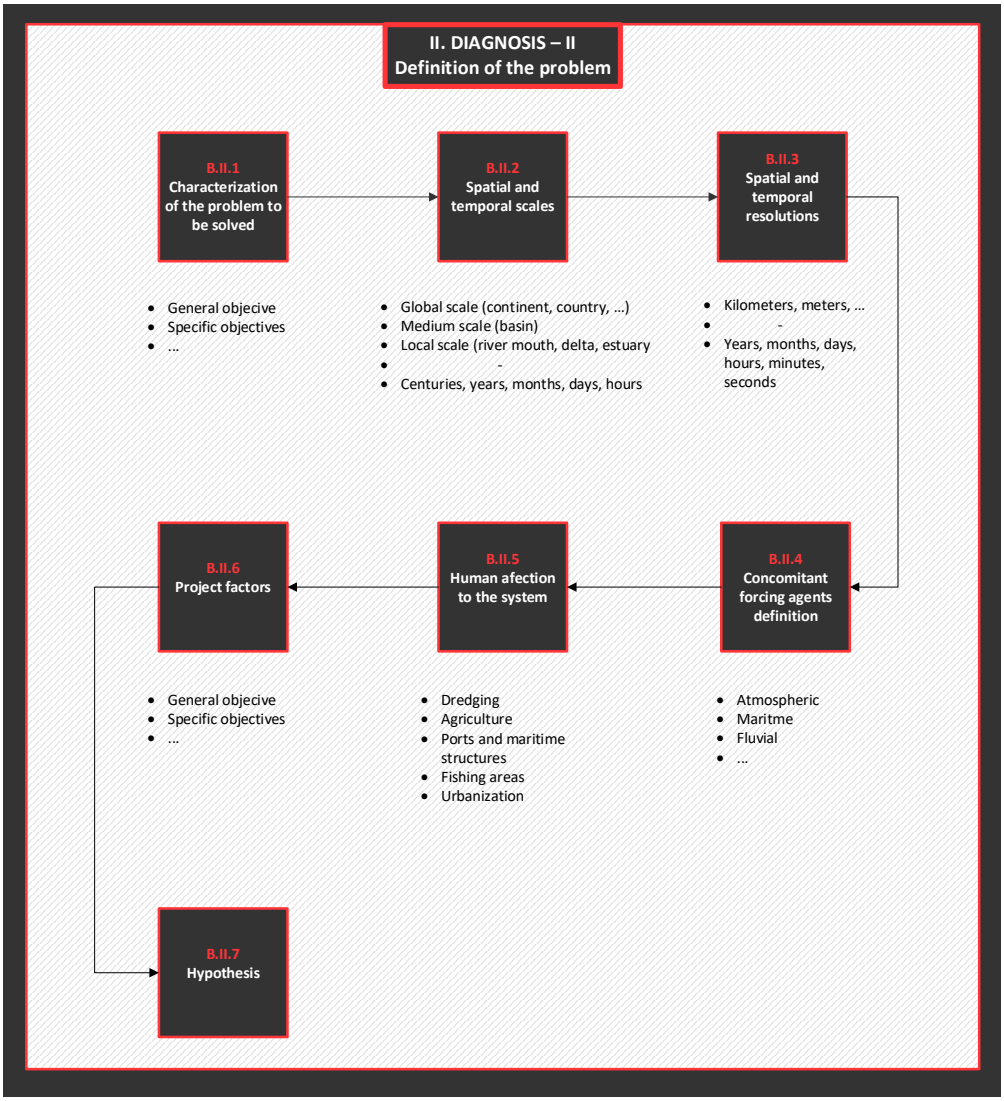

Figure 9.3.4: Submodules of the definition of the problem module.

9.3.3 Diagnosis-III: Reproducing the past - Hindcasting

The block of identifying the causes that are generating the problem culminates with the module of reproduction of the historical conditions of the past in order to (i) verify that the set-up of our models is correct and (ii) characterize both the frequency and magnitude of the failure, as well as identify the mechanisms that caused the failure in the past. The diagram in Fig. 9.3.5 shows the steps to follow according to the methodology

proposed in this Thesis. The first submodule begins with the characterization of the offshore climatic agents (B.III.1). The process follows with the implementation of the hydrodynamic propagation model to transfer the dynamics of the offshore forcing agents to our transitional coastal environment (TCE) (B.III.2 and B.III.3) applying downscaling techniques (selection of representative cases, hydrodynamic propagation, and continuous time series reconstruction). Once the hydrodynamic variables are propagated along the TCE, the statistical analysis can be performed (B.III.4) to quantify the historical number of failures, their frequency, magnitude in terms of the return period, and finally, identify the mechanisms that originate them applying the methodologies developed in this Thesis. Results obtained through this analysis can be specified in zonation maps (B.III.5) specially designed for management, where all the information is integrated. These management maps can be used by stakeholders to support decision-making based on risk analysis, identify vulnerable areas, quantify the frequency of flooding, and identify the agents responsible for flooding at each area.

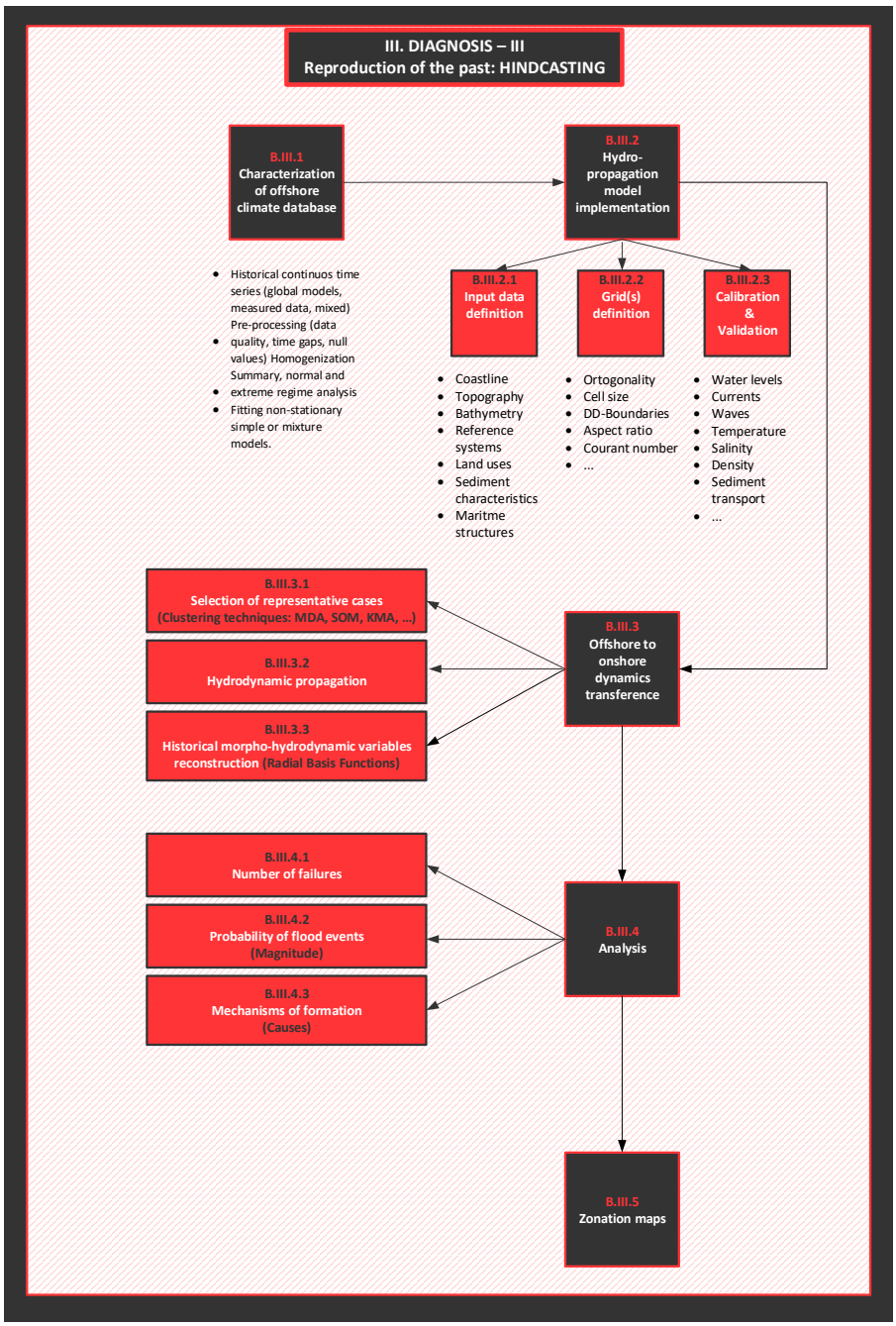

Figure 9.3.5: Submodules of the reproduction of the past module.

The diagram in Fig. 9.3.6 shows the proposed flow chart for the implementation of the proposed guidelines. The black boxes indicate the inputs of the method, and the grey boxes indicate the outputs of each module, separated by colors. Each module of the diagram shown in Fig. 9.3.6 shows the chapter of this Thesis in which the methodology of that module is explained in-depth, as well as its example of application.

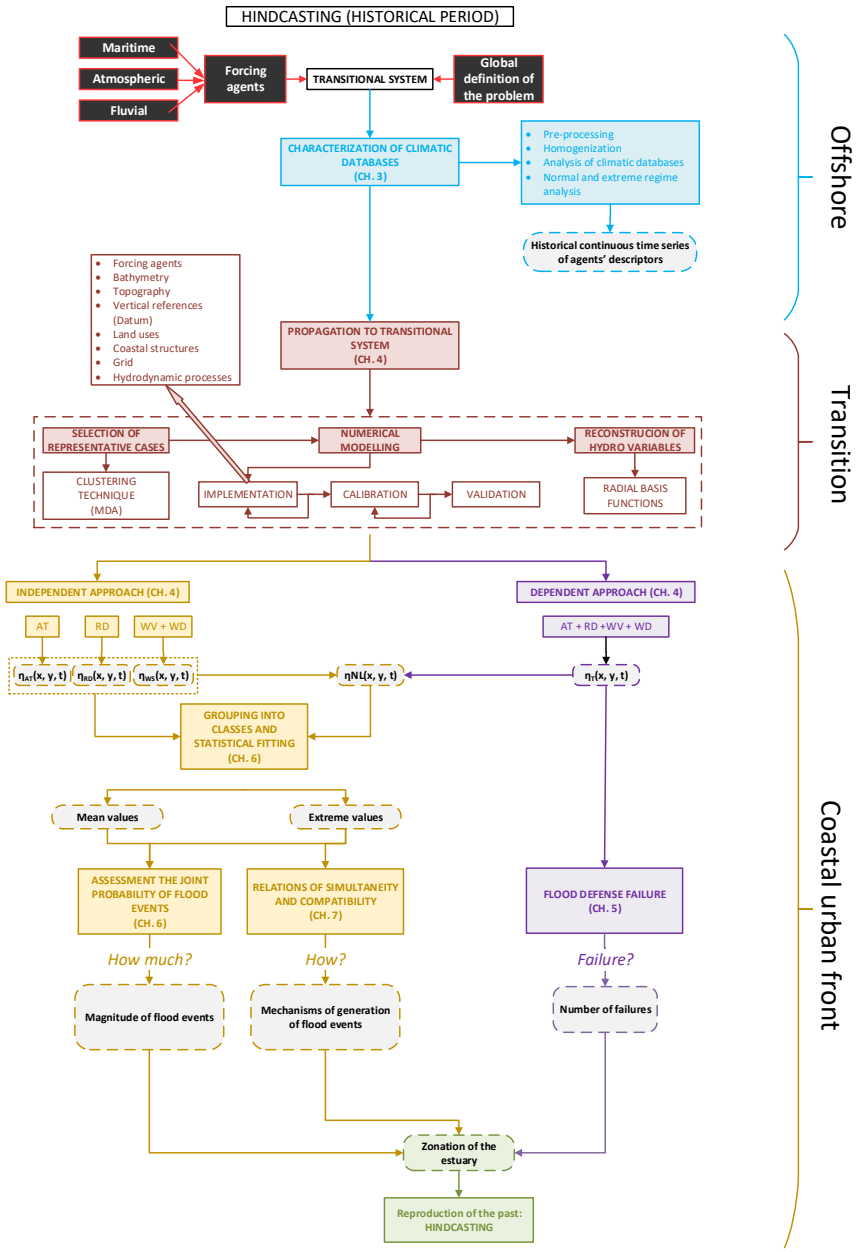

Figure 9.3.6: Flow chart for the implementation of the guidelines for the reconstruction of the past. Black boxes indicate the inputs of the method, and the grey boxes indicate the outputs of each module, separated by colors. Each module of the diagram shows the chapter of this Thesis in which the methodology of that module is explained in depth.

As an example, Fig. 9.3.7 illustrates the zonation of the Guadalete Estuary based on the results obtained throughout the Thesis after the analysis of historical data (1995-2015) following the flow chart explained in Fig. 9.3.6. This zonation is assessed via three criteria: (i) the probability of flooding, (ii) the dominance of the agents, and (iii) the combinations between simultaneous extremes and/or non-extreme values of the concomitant agents resulting in extreme events of total water level. Regarding the first criterion, three zones are identified in the Guadalete estuary. The outer part corresponds to the first 4 km (from CP 1 to 3) of the estuary, where the probability of flooding is null. Then, from CP 3-4 to CP 7-8 (intermediate 8 km), the overflow is produced once every 5 - 10 years. In this part, the 5- and 10-year return levels can exceed the river's edge by 10 and 20 cm, respectively. Finally, areas, where the overflow is produced once every five years or less, are also identified in the inner part of the estuary (from CP 7-8 onwards). Due to the dams' proximity, agents at these points can increase the water level over 1 m above the edge for long return periods. A transitional behavior is found at approximately CP 3 and 7.

Once the frequency of flooding is characterized at each area, the second and third criteria of zonation are applied to classify the estuary into areas with one dominant agent, two dominant agents, and three dominant agents. Besides, areas where more than one agent controls the hydrodynamics in extreme conditions, the combination of agents needs to be assessed.

According to the results, in the first 3 km (CP 1 and 2-3) of the estuary, tides dominate. As seen in chapter 4, the maximum values of the astronomical tide are obtained at the mouth (1.6 - 1.8 m), whereas the elevation due to the rest of the agents is almost negligible. Results in chapter 7 indicate that in this area, extreme values of the total water level are explained only by the extreme values of the astronomical tide ($EV\eta_{AT}$), and variability and interactions among the rest of the agents are not observed. Hence, the first homogeneous area is identified in the first 3 km and called *tidal section*, and it is characterized by the dominance of the astronomical tide and a lack of interactions with the rest of the water level components and presents no risk of flooding.

A more complex section is identified between CP 3-4 and 6-7. Results of chapter 6 and 7 shows that in this section, both astronomical tide and river discharge exert strong control on the hydrodynamics. The relative dominance between them depends on the agents that are at normal and extreme conditions. In this part of the estuary, special attention needs to be paid to the combination between normal and extreme conditions of both agents. According to the analysis shown in chapter 7, extreme values of the total water level are mainly produced by the combination of mean values of the astronomical tide ($MV\eta_{AT}$) with extreme events of river discharge ($EV\eta_{RD}$) as

well as the combination between extreme events of the astronomical tide ($EV\eta_{AT}$) and mean values of river discharge ($MV\eta_{RD}$). Also, a lesser contribution between extreme values of the astronomical tide and river discharge must be considered. Hence, a second homogeneous area is identified in the middle estuary between 5 and 11 km from the mouth, which is denominated as *tidal-fresh section* (Figure 9.3.7).

The inner part of the estuary, from 13 to 17 km, is dominated by the fluvial discharges with a minor contribution of the astronomical tide. Peaks of water level due to river discharge are 2-3 m, whereas amplitudes due to the astronomical tide are limited to 0.9 m. Again, results in chapter 6 and 7 show that this area exhibits the highest variability among extreme values of the total water level. The magnitude and variability of the extreme events are driven by river discharge's extremes and a lesser contribution of the mean values of the astronomical tide. Therefore, a *fluvial section* is found in the inner part of the estuary from CP 7-8 onward. Finally, two transitional areas are identified around CP 3 and 7.

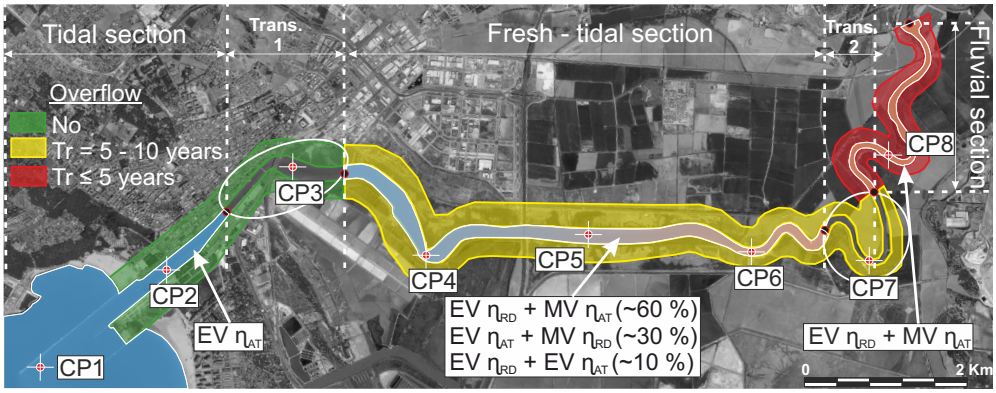

Figure 9.3.7: Zonation of the Guadalete estuary based on the probability of overflowing (margin colors), the dominance of the agents (river sections) and the combinations between simultaneous agents (text boxes).

Zonation based on these criteria helps managers to map the estuary into zones where special attention must be focused on the risk of overflowing and to identify the responsible agents and its combinations. This type of analysis constitutes a useful tool for understanding what is occurring in the past and even it is the beginning of the definition of strategies related to risk mitigation measures, such as river regulations to avoid peaks of river discharge with the astronomical tide in the *tidal-fresh section*, natural marshes or evacuation alerts among others. However, more work needs to be done to assess the solution accurately. Therefore, it necessary to continue to the next section, the definition

of the solutions.

9.4 C. Are the solutions known? Treatment

The third and last block of these guidelines (Fig. 9.3.6) focuses on defining the appropriate solution for the mitigation of the consequences caused by the defined problem once the past is understood and reproducible.

9.4.1 Treatment-I: Type of procedure and development level

As explained in the previous section and shown in Fig. 9.3.3, the type of solution proposed directly depends on the quality and quantity of the available data. Before continuing, it is important to define the type of procedure to be carried out based on the information available. Once the type of procedure is selected, the implementation of the solutions follows a set of three different development levels that progressively increase in complexity and accuracy simultaneously as it delimits its uncertainty. Following the ROM-1.1 (2018) recommendations, these guidelines propose the following development levels:

I. Preliminary studies

II. Study of alternatives

III. Blueprint and investment project

The following sections summarize the main aspects to be highlighted in each of the three levels of development. For further information on the technical and economical implementation of the protection measures, readers are referred to the ROM-0.0 (2001), ROM-1.0 (2009), and ROM-1.1 (2018).

9.4.2 Treatment-II: Preliminary studies

Fig. 9.4.1 shows the required information for the elaboration of the preliminary studies, the specific objectives, and the most relevant activities (task) to be performed extracted from the ROM-1.1 (2018).

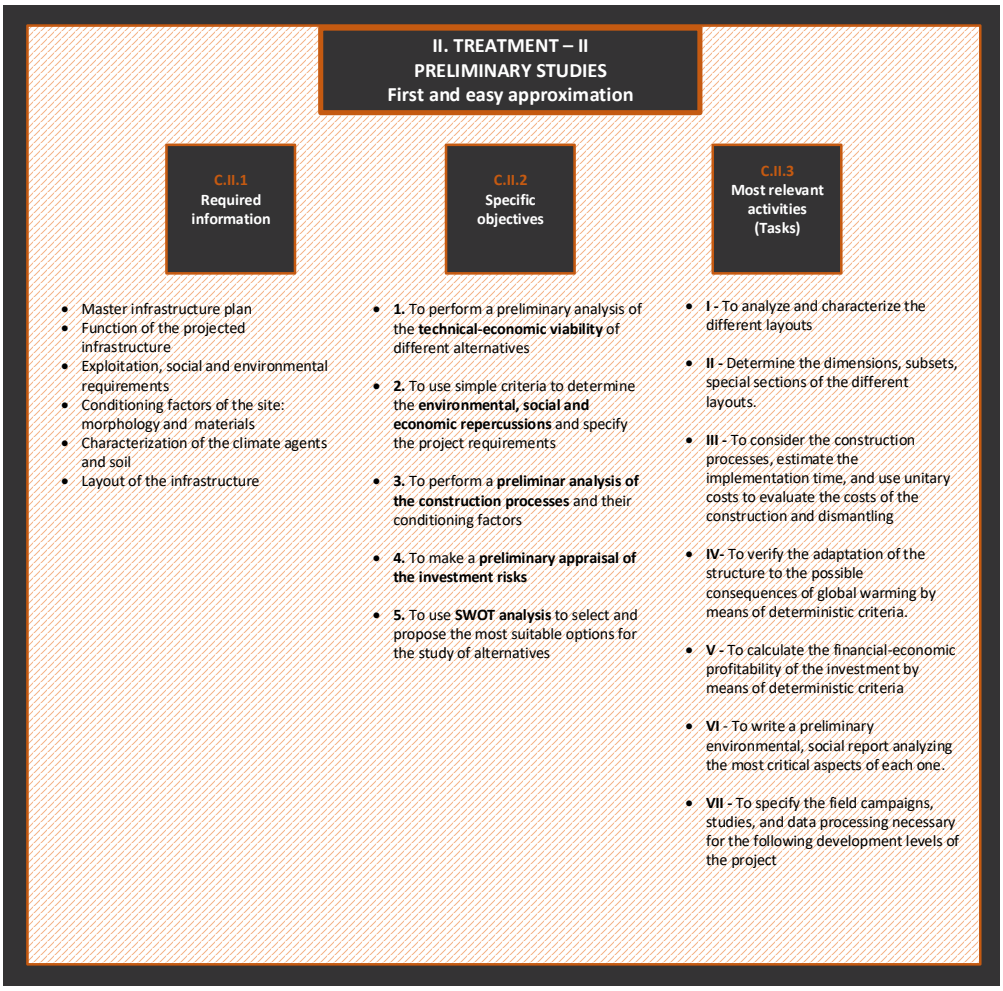

Figure 9.4.1: Required information for the elaboration of the preliminary studies, the specific objectives, and the most relevant activities (task) to be performed. Data extracted from the ROM-1.1 (2018)

9.4.2.1 Contents of the preliminary studies

The preliminary studies will be defined in a document containing a justified and hierarchical catalog of the most suitable options to begin the study of alternatives and solutions. Tab. 9.4.1 summarizes the contents of the preliminary studies' development level.

	Development	Tools
Conception of the structure		
Hierarchy of the structure	Preliminary	Diagrams of components
Characterization of modes and relations	Preliminary	-
Temporal evolution of the breakage	NO	
Spatial evolution of the breakage	NO	
Probability distribution	Preliminary	Distribution techniques
Decision-making		
Timing strategies	Preliminary	Descriptive Tools
Repair strategies	NO	-
Verification of requirements		
Reliability evaluation	Preliminary	Standard statistics, Diagrams of components, Level I
Operationality evaluation	Preliminary	Standard statistics, Level I
Calculation of costs		
Construction costs	Preliminary	General tables
Repair costs	Preliminary	Coefficients
Loss of operationality and externalities	Preliminary	Coefficients
Dismantling costs	Preliminary	Coefficients
Selection criteria	YES	SWOT or similar
Sensitivity and optimization	preliminary	Critical variables, Discrete analyses

Table 9.4.1: Summary table of preliminary studies. Source: ROM-1.1 (2018).

9.4.3 Treatment-III: Study of alternative

The next development level for the definition of the solution is the study of alternatives, where the different alternatives must be defined, tested, and selected. Fig. 9.4.2 shows the required information for the elaboration of the study of alternatives, the specific objectives, and the most relevant activities (task) to be performed obtained from the ROM-1.1 (2018)

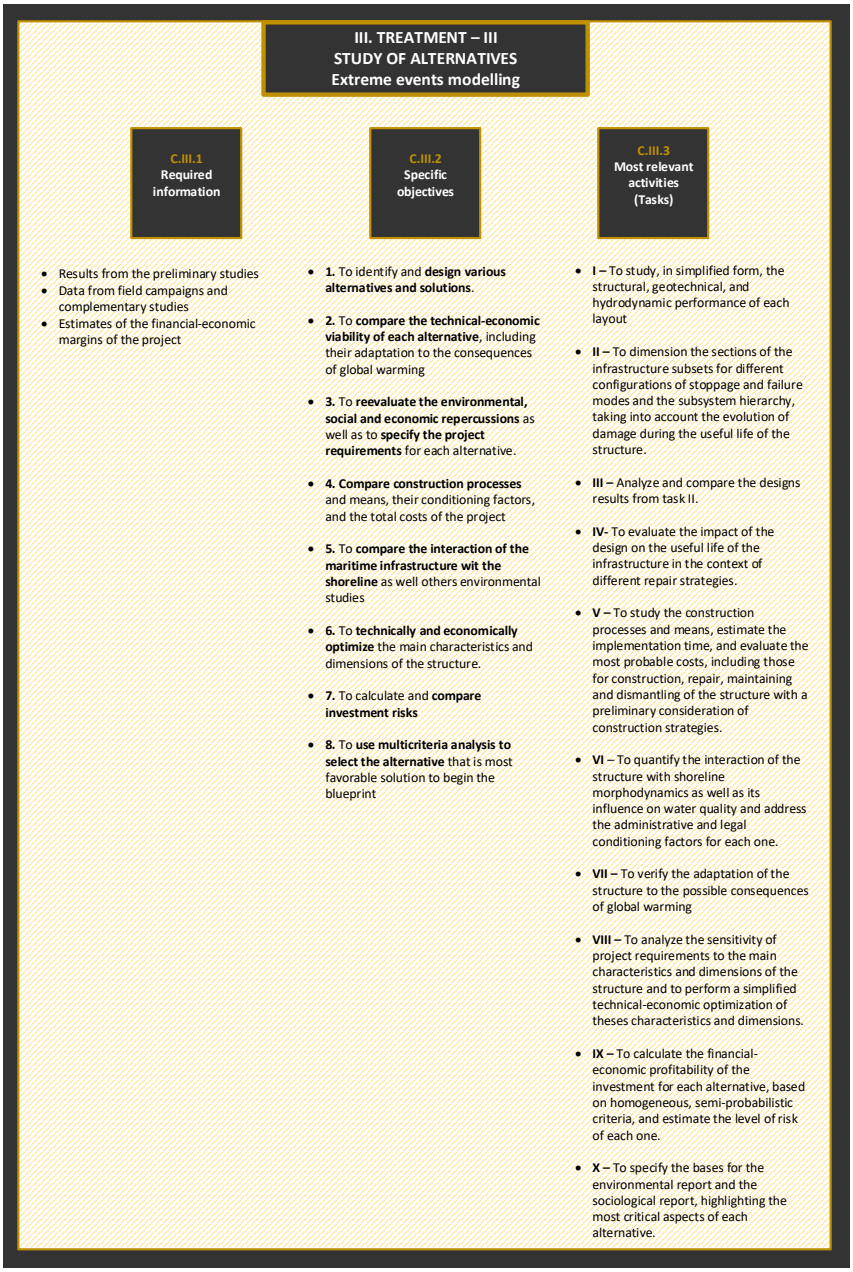

Figure 9.4.2: Required information for the elaboration of the study of alternatives, the specific objectives, and the most relevant activities (task) to be performed. Data extracted from the ROM-1.1 (2018)

To facilitate the application of these guidelines, Fig. 9.4.4 includes a flow chart with the sequence of steps (modules) to be taken to select the best alternatives for coast protection. The first module (C.III.1) consists of identifying the different alternatives. In this step, it is important to differentiate between soft or green measures, such as the well-known nature-based solutions versus hard or grey measures such as the construction of coastal protection structures such as a breakwater. It is also recommendable to analyze the alternative of "do nothing", the relocation of existing infrastructure, or the relocation of the population.

The next module (C.III.2) focuses on the definition and design of the alternatives. In this step, all the considered alternatives must be properly defined from the layout and the shape to the definition of the failure modes and evolution and propagation of damage models (ROM-1.1, 2018). For the design, conception, and definition of coastal protection alternatives, readers are referred to the following references, such as ROM-0.0 (2001), ROM-1.0 (2009), ROM-1.1 (2018), MEIPORT (2016), Schoonees et al. (2019), and Sutton-Grier, Wowk, and Bamford (2015). Fig. 9.4.3 shows a table with a summary of selected design guidelines for coastal structures extracted from Schoonees et al. (2019). Just as an ilustration of the different possibilities, Fig 9.4.5, 9.4.6 and 9.4.7 show a different gradual example for the definition of the different alternatives from green softer to gray harder techniques. It is important to highlight that guidelines proposed in this chapter are intended to help about which steps should be taken and which aspects should be considered, but ultimately it is the job of the designer and coastal engineer to decide and design which alternatives to implement for each particular study area.

Guideline (Reference)	Structure type	Country	Content
Shore Protection Manual (CERC 1984)	Seawalls, revetments. Groynes, breakwaters and jetties	International	Structure types, functions and limitations Design conditions and practices Construction materials
Recommendations for marine works [in Spanish] (ROM 2009)	Seawalls, revetments. Groynes, breakwaters and jetties	Spain	Structure types, functions and failure mechanisms Design guidance (planning, site conditions and data collection, geometry, building materials, construction, environmental considerations)
The Rock Manual (CIRIA 2007)	Rock structures including breakwaters, groynes, detached breakwaters, revetments and seawall toe	International	Structure types, functions and failure mechanisms Design guidance (planning, site conditions and data collection, geometry, building materials, construction, environmental considerations) Maintenance and monitoring
Coastal Engineering Manual (USACE 2002)	Sea dikes, seawalls, revetments. Groynes, breakwaters (various types) and jetties	International	Structure types, functions and failure mechanisms Design guidance (planning, site conditions, data collection, geometry, building materials, construction, environmental considerations) Maintenance and monitoring
Manual on wave overtopping of sea defences and related structures (EurOtop 2018)	Coastal dikes, revetments, seawalls and breakwaters	International	Wave overtopping limits Wave run-up and overtopping prediction including influence factors
The International Levee Handbook (CIRIA 2013)	Coastal, estuarine and river dikes	International	General information (functions, forms and failure mechanisms) Design guidance (from site characterisation and data collection to design and construction) Maintenance and monitoring
Design Guidance for Coastal Structures [in German] (EAK 2002)	Coastal and estuarine dikes	Germany	Loads on coastal structures Geotechnical investigations and processes Building materials Design and construction

Figure 9.4.3: Summary of selected design guidelines for coastal structures extracted from Schoonees et al. (2019)

Once the alternatives have been defined, the next step is the characterization of the climatic forcing to extract a selection of representative storm events characteristic of the climate next to the structure (C.III.3 and C.III.4). In order to study the alternatives and choose the best ones, four different types of analysis must be carried out: hydrodynamic analysis (C.III.5) using numerical modeling; structural and geotechnical analysis (C.III.6) by means of lab tests; economic and financial analysis (C.III.7) employing total costs calculation; and environmental and social analysis (C.III.8). In the hydrodynamic analysis, the structure is tested for just the selected extreme events in the previous step to verify their effectiveness in terms of risk reduction. The structural and geotechnical analysis allows, using laboratory tests, to verify the behavior and structural resistance of the protection work at preliminary levels of study of alternatives. Based on the reports obtained through each of the four analyses for each of the alternatives analyzed, those alternatives that go on to the next level of development will be chosen using multi-criteria analysis techniques (C.III.9).

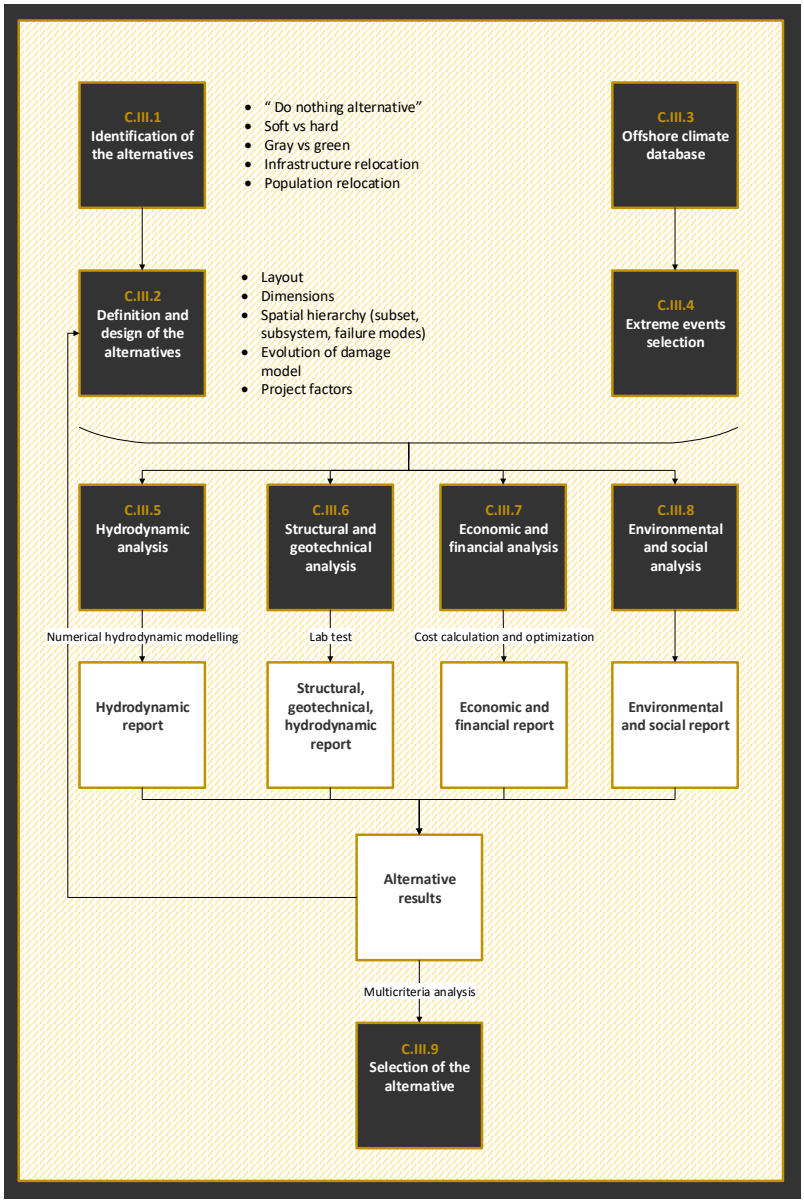

Figure 9.4.4: Sequence of modules with the steps to be taken to select the alternatives for the coastal protection at the study of alternatives development level.

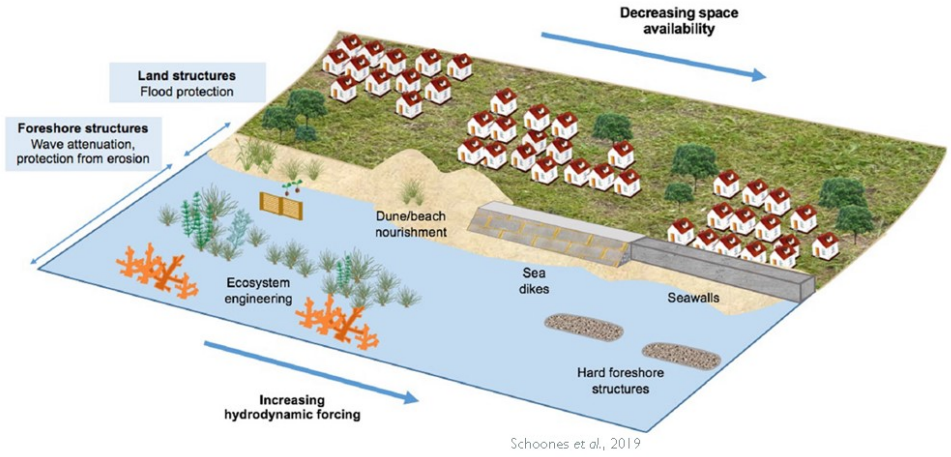

Figure 9.4.5: Implementation of hard solutions related to land use and hydrodynamic forcing. Source: Schoonees et al. (2019).

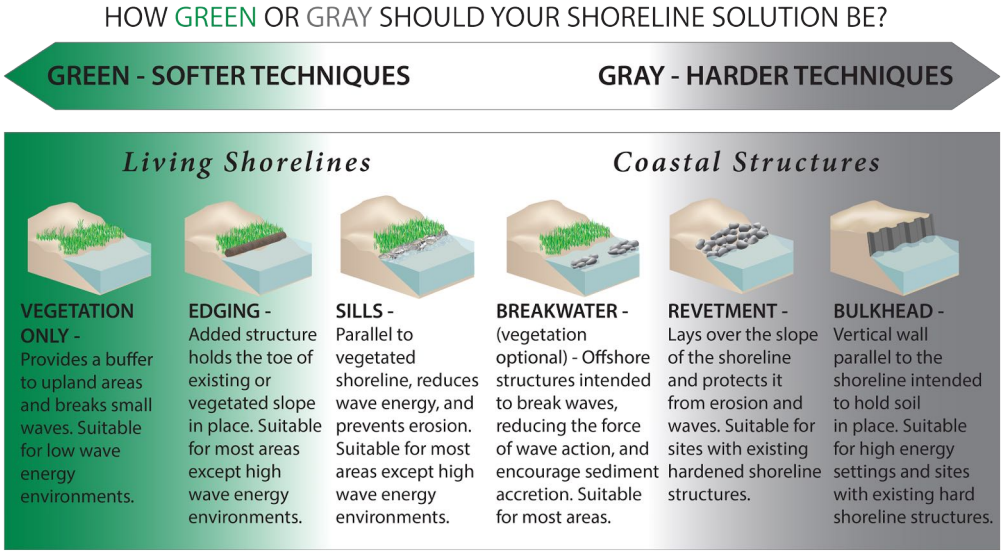

Figure 9.4.6: How green or gray should your shoreline solution be? Source: NOAA (2015)

Minimal Defense
Many communities have developed right along the ocean with only minimal natural defenses from a small strip of beach between them and the ocean.

Natural
Natural habitats that can provide storm and coastal flooding protection include salt marsh, oyster and coral reefs, mangroves, seagrasses, dunes, and barrier islands. A combination of natural habitats can be used to provide more protection, as seen in this figure. Communities could restore or create a barrier island, followed by oyster reefs and salt marsh. Temporary infrastructure (such as a removable sea wall) can protect natural infrastructure as it gets established.

Managed Realignment
Natural infrastructure can be used to protect built infrastructure in order to help the built infrastructure have a longer lifetime and to provide more storm protection benefits. In managed realignment, communities are moving sea walls farther away from the ocean edge, closer to the community and allowing natural infrastructure to recruit between the ocean edge and the sea wall.

Hybrid
In the hybrid approach, specific built infrastructure, such as removable sea walls or openable flood gates (as shown here) are installed simultaneously with restored or created natural infrastructure, such as salt marsh and oyster reefs. Other options include moving houses away from the water and/or raising them on stilts. The natural infrastructure provides key storm protection benefits for small to medium storms and then when a large storm is expected, the built infrastructure is used for additional protection.

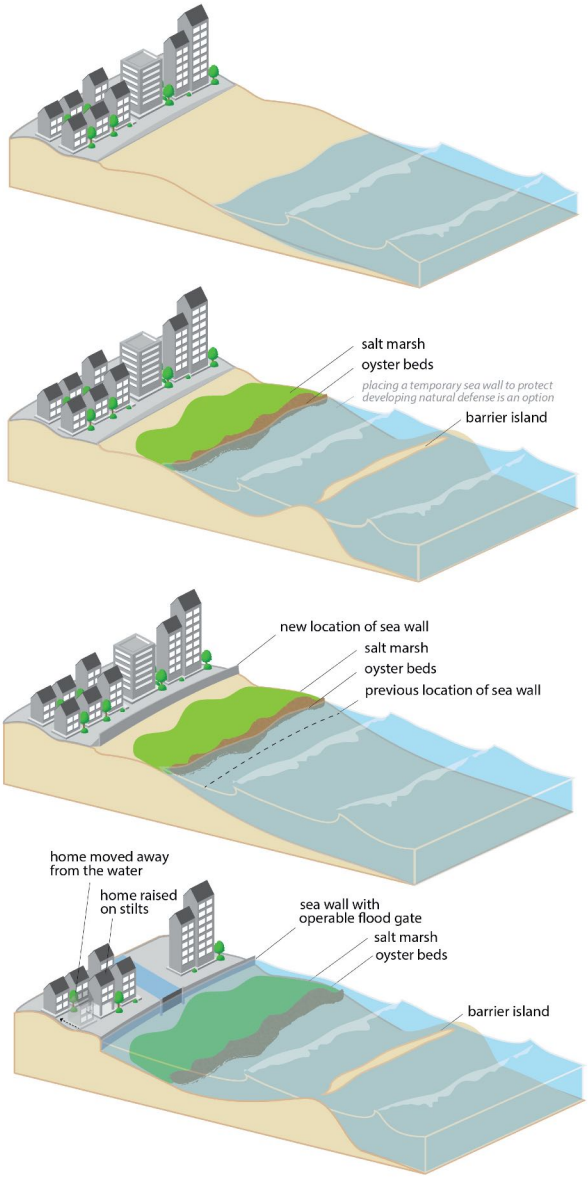

Figure 9.4.7: Examples of coastal defenses including natural infrastructure, managed realignment, and hybrid approaches. Source: Sutton-Grier, Wowk, and Bamford (2015)

	Development	Tools
Conception of the structure		
Hierarchy of the structure	Simplified	Diagram of components
Characterization of modes and relations	Simplified	Upper and lower bounds
Temporal evolution of breakage	Simplified	Standard models
Spatial evolution of the breakage	NO	
Distribution probabilities	YES	Distribution techniques
Decision-making		
Timing strategies	Simplified	Chronogram
Repair strategies	Simplified	Upper and lower bounds
Verification of project requirements		
Evaluation of reliability	Simplified	Standard statistics, Diagrams of components Synthetic cycles
Evaluation of operationality	Simplified	Standard statistics Numerical modelling studies Field campaign data
Cost calculation		
Construction costs	Simplified	Chronogram Tables of costs
Repair costs	Simplified	Standard statistics
Loss of operationality and externality	Simplified	Scenarios
Dismantling costs	Simplified	Chronogram Tables of costs
Selection criteria	YES	Multi-criteria or similar Decision theory
Sensitivity and optimization	Simplified	'Critical' variables Continuous analyses Scenarios Classification algorithms

Table 9.4.2: Summary of the study of alternatives and solutions

9.4.3.1 Contents of the study of alternatives and solutions

Alternatives and solutions will be analyzed in a report that contains a hierarchical and justified catalog of the alternatives and solutions selected to begin the blueprint and the investment project. An environmental report and sociological report should be included. Tab. 9.4.2 summarizes the contents of the study of alternatives development levels.

9.4.4 Treatment-IV: Blueprint and Investment project

The blueprint and investment project constitutes the maximum development level of the solution. In these levels, the selected alternative after the study of alternatives must be defined and analyzed in depth. Fig. 9.4.8 shows the required information for the elaboration of the blueprint, the specific objectives, and the most relevant activities (task) to be performed obtained from the ROM-1.1 (2018). An organizational chart has been included in Fig. 9.4.9 to facilitate the implementation of the guidelines at this level of development.

Figure 9.4.8: Required information for the elaboration of the blueprint, the specific objectives, and the most relevant activities (task) to be performed. Data extracted from the ROM-1.1 (2018)

In the blueprint, the considered solution after the selection in former levels of development must be defined entirely in-depth (C.IV.1). The offshore climatic forcing agents need to be forecasted, including the GW effects (C.IV.2) and propagated next to the

protective maritime structure using the hybrid downscaling technique (C.IV.3). As a result, a continuous time series of every hydrodynamic variable along the 21st-century must be obtained next to the structure before proceeding with the different analysis. According to this guidelines, the hydrodynamic report at the blueprint level must assess the spatial and temporal evolution of: (i) the number of flood defenses failures; (ii) the magnitude of the flood event; and (iii) the mechanism of generation of the flood events along the 21st-century with and without the proposed maritime structure in order to evaluate the effectiveness of the solution in terms of risk mitigation. In this regard, Fig. 9.4.10 includes a step-by-step flowchart with references to the chapter of this Thesis in order to elaborate the hydrodynamic report at the blueprint level.

The major difference in the hydrodynamic report between the blueprint and the investment project is in the evaluation of uncertainty. At the level of development of the blueprint, it is sufficient to apply the methodology of Fig 9.4.10 for a single future time series of the forcing agents. However, the investment project requires the application of Monte Carlo methods to limit the uncertainty associated with the obtained results. Therefore, this methodology must be repeated for a sufficient number of simulations of climate forcing agents.

The results obtained through the application of these guidelines can be converted into management maps to facilitate knowledge-based decision making. The management maps presented in this section take a step forward in environmental management and flood risk analysis by characterizing the three main variations of the magnitude of extreme total water level events in transitional environments, i.e., the variations over space, time, and over the different return periods. The maps depict the spatial variability controlled by the dominance and interactions between the forcing agents, the temporal evolution driven by the SLR along the 21st-century, and the variability of the magnitude between the different return periods, explained by the intensity and frequency of the main stochastic component events.

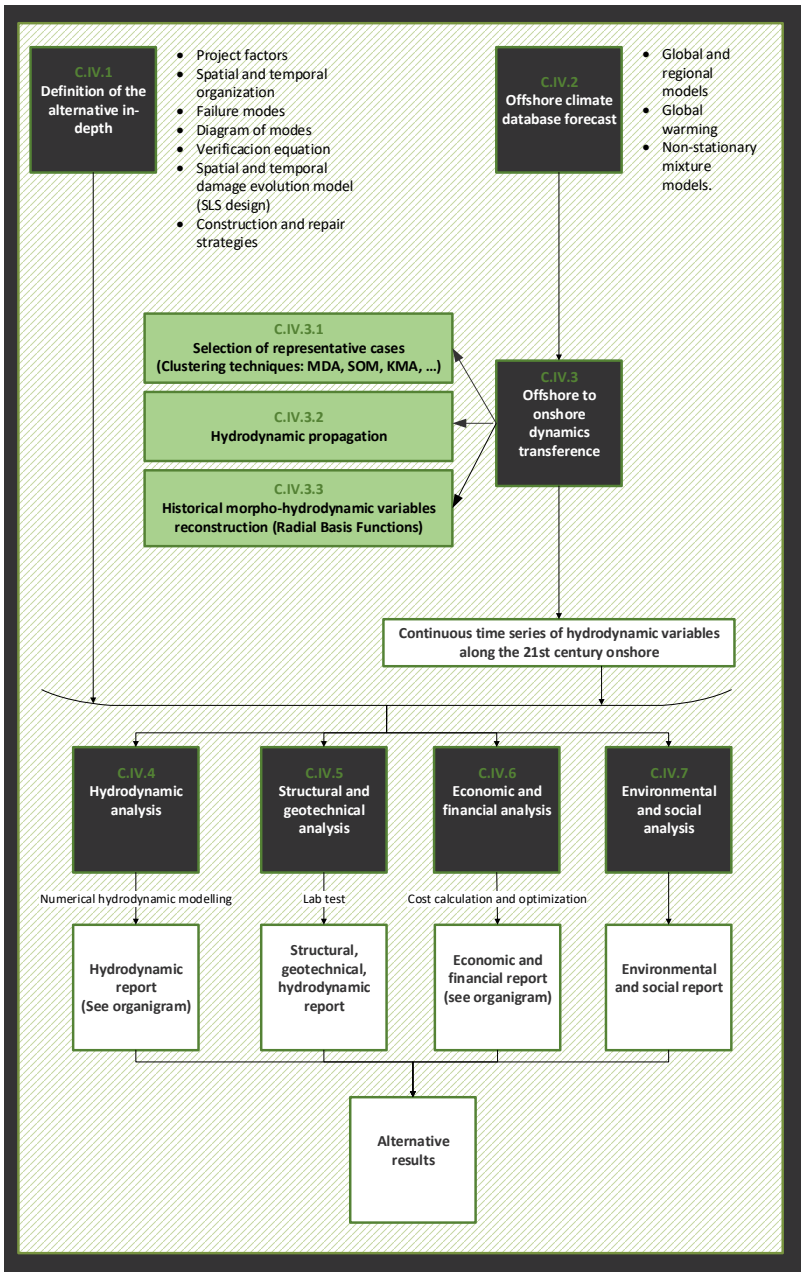

Figure 9.4.9: Sequence of modules with the steps to be taken at the blueprint development level.

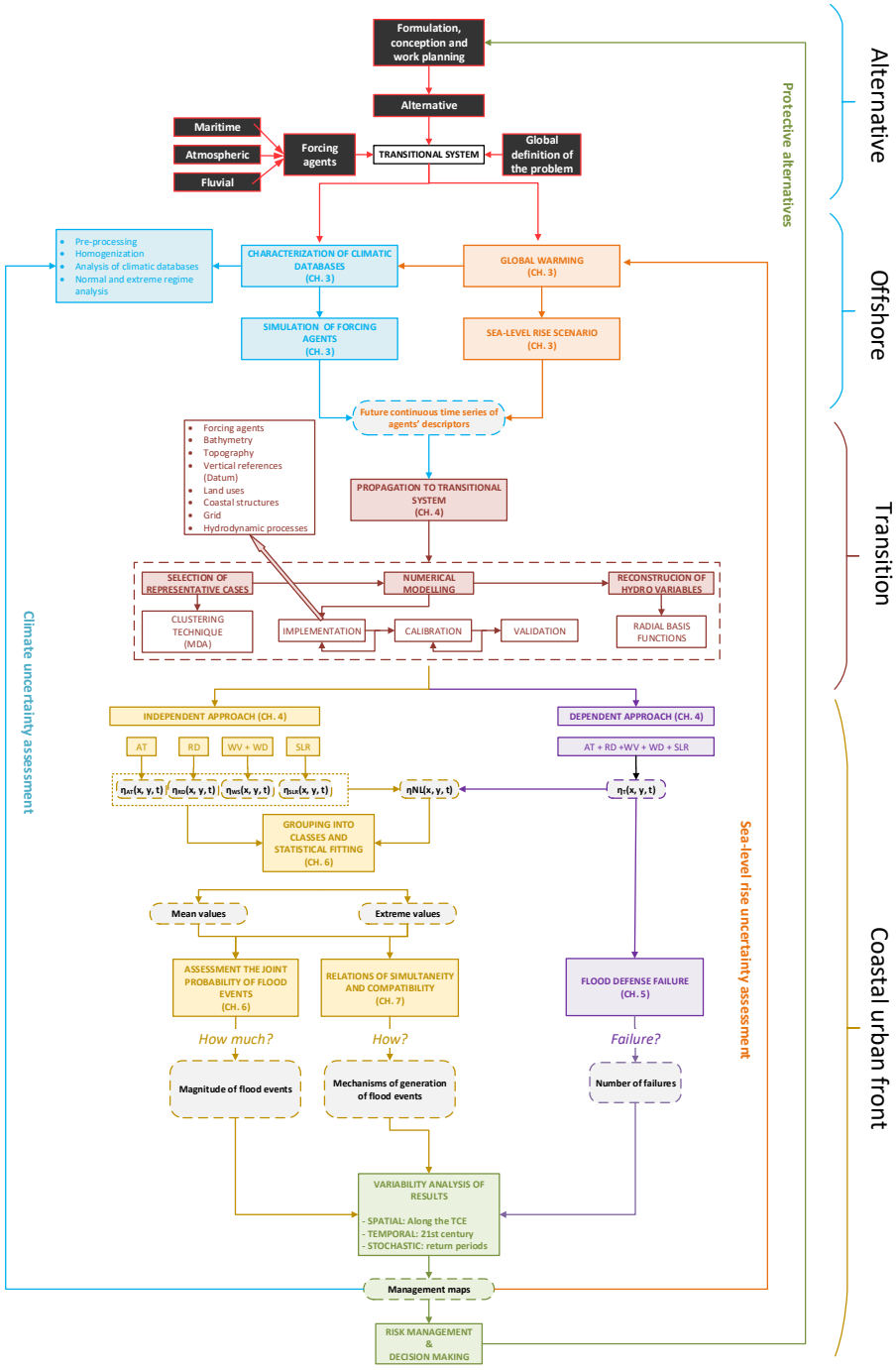

Figure 9.4.10: Flowchart with references to the chapters of this Thesis to elaborate the hydrodynamic report at the blueprint level.

These management maps also allow the identification of hotspots of vulnerability along the estuary by quantifying the number of failures per year of the flood defenses. In addition, to assess the uncertainty related to the SLR scenarios and the stochastic forecasting of the forcing agents, especially for river discharge, four different maps are created (Fig. 9.4.11). The upper Panels (A and C) correspond to nodal cycles with "high-frequency discharge simulations" (3.3.3.2), while the lower Panels (B and D) correspond to nodal cycles with "low-frequency discharge simulations". The right (A and B) and left (C and D) Panels correspond to the RCP4.5_05 and RCP8.5_95 SLR scenarios, respectively.

Inside each Panel, the forcing agents' dominance is represented along the main channel of the river. Blue identifies tidal domain areas while orange is used for river domain areas. A color gradient and stripes represent the transition zone between them. Areas, where the magnitude of extreme level events varies over time, are represented by the continuous line on the left of the main channel. The dotted line shows the variation in the magnitude of the extreme events between the different return periods. Cold colors (blue and green) indicate low variation, whereas warm colors (orange and red) indicate high variation. The hotspots of vulnerability along the estuary are also represented by the number of flood defense failures per year in the current situation (the inner circle), in the middle of the century (middle circle), and by the end of the century (outer circle). Again, cold colors (blue and green) indicate a null or low number of failures, whereas warm colors (orange and red) indicate a high number.

As seen, the minimum variability is found when the intensity of river discharge is low (A and C Panels), and in particular, when this situation is combined with the RCP4.5_05 SLR scenario (Panel A). In these cases, a tidal estuary is observed, and the river effects are limited to only the last kilometers near the dam. A transition region between the tidal and fluvial domain is limited in this case to the area around CP 7 (10 km from the mouth). The temporal evolution of the magnitude of the extreme water level throughout the 21st-century is more significant in the first 2 km of the estuary (CP 1 and CP 2) than in the rest of the estuary, where the effects of the SLR are higher compared with the rest of the forcing agents. However, in the case of low-frequency discharge simulations and RCP8.5_95 SLR scenario (Panel C), this temporal evolution is remarkable until CP 7.

Maximum variability is found when the high-frequency discharge simulations are combined with the RCP4.5_05 and RCP8.5_95 SLR scenarios (B and D Panels). In these cases, the influence of the astronomical tide and SLR is limited to the mouth (CP 1 and CP 2), while a long transition region is developed from CP 2 to CP 7, where the fluvial domain begins. The maximum variability in the magnitude of the extreme water levels across the different return periods is also shown in these Panels. In terms of vulnerability, the most sensitive area is in the middle estuary, where the effects of the tide and the

river discharge converge, aggravated by the SLR. The upper part constitutes the second region in terms of sensitivity to flooding. In contrast, no risk of flooding is predicted at the mouth over the 21st-century for the SLR scenarios considered.

This type of map constitutes a useful tool for managers and stakeholders to quickly identify the most vulnerable areas of the estuary, as well as the sources and mechanisms leading to flooding. All the information is represented in a joint and orderly manner, facilitating the visualization of the results and helping in the analysis of flood risk and the decision-making process. As an example of application, these maps reveal that a self-closing flood barrier could be installed at the mouth of the estuary to prevent water levels from reaching the crest of the flood defenses during spring tides in the middle and lower estuary. Another solution could be to allow controlled flooding in some areas such as the marshes on the river's left bank. These marshes are connected to the San Pedro River and could drain all the excess water directly into the bay.

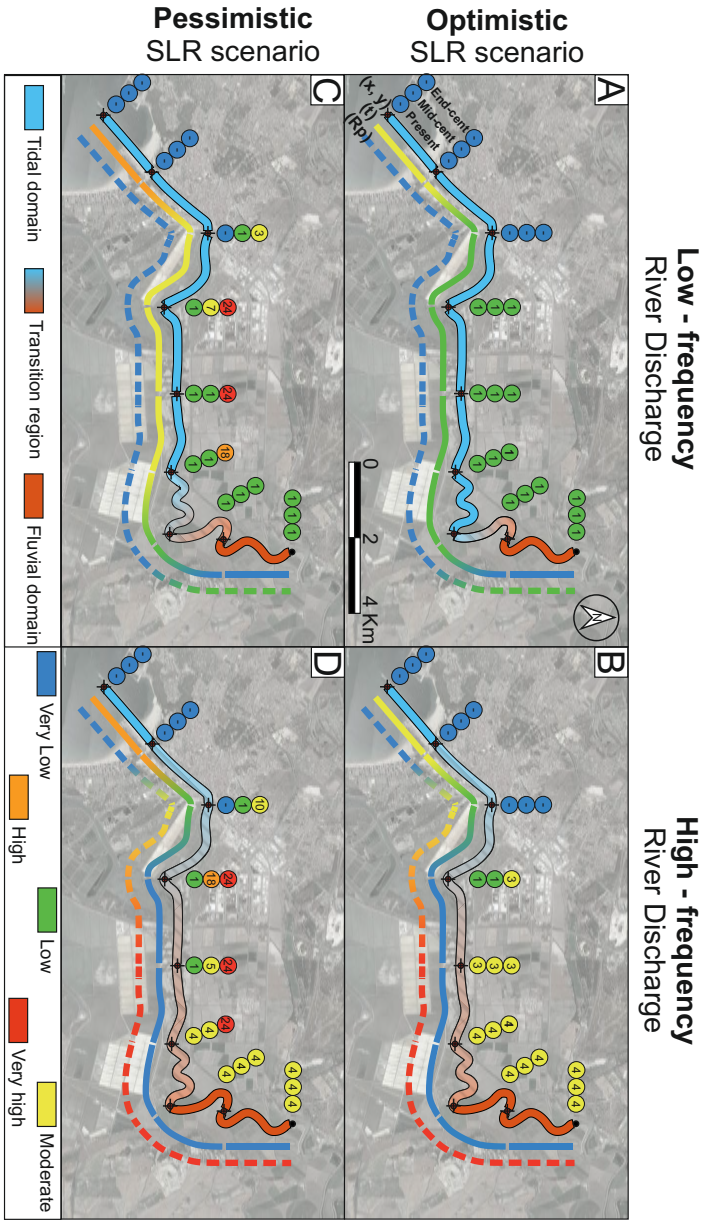

Figure 9.4.11: Management maps of the Guadalete estuary based on the dominance of the forcing agents (x, y) (color line along the main channel), the temporal evolution (t) along the 21st-century (continuous line on the left of the main channel), the variability of the magnitude (Rp) over the different return periods (discontinuous line), and the vulnerability of the estuary represented by the mean number of failures per year in the current situation (the inner circle), mid-century (middle circle) and end-century (outer circle).

	Development	Tools
Conception of the structure		
Hierarchy of the structure	Complete with details	Diagram of components
Characterization of modes and relations	Complete with details	Dependency models
Temporal evolution of the breakage	Complete with details	Specific models
Spatial evolution of the breakage	Complete with details	Spreading activation networks
Probability distribution	NO	-
Decision-making		
Timing strategies	Complete with details	-
Repair strategies	Complete with details	Bounds, Decision trees
Verification of requirements		
Reliability evaluation	Complete with details	Diagrams of components Spreading activation networks, Decision trees, Physical model tests
Evaluation of operationality	Complete with details	Physical model tests
Calculation of costs		
Construction costs	Complete with details	Timing strategy
Repair costs	Complete with details	Repair strategy
Loss of operationality and externalities	Complete with details	
Dismantling costs	Complete	Dismantling strategies
Selection criteria	NO	-
Sensitivity and optimization	YES	Specific techniques

Table 9.4.3: Summary table of the blueprint

9.4.4.1 Contents of the blueprint

The blueprint consists of a report that explains the purpose and nature of the infrastructure and its formal and structural conceptualization. It also specifies the results of the financial-economic profitability study as well as the investment risk level. Furthermore, it contains annexes with the information, basic premises, conditioning factors, requirements, and crucial indicators for elaborating the investment project. Tab. 9.4.2 summarizes the contents of the blueprint development level.

9.5 Conclusions

Managers of transitional coastal environments (TCE) are currently facing decisions that may condition these environments' future. The increasing risk of flooding resulting from the SLR highlights the need to tackle the problems that lie ahead before they become disasters. In this regard, coastal managers must address whether current coastal defenses are prepared to resist the SLR expected in this century. Furthermore, if they are not, they need to know when and where the failure will occur and what crest height is required to reduce the probability of flooding. Therefore this chapter integrates the methodology developed throughout this Thesis to present comprehensive guidelines for the assessment of the SLR impact on coastal urban fronts at a local scale. These guidelines are built upon the knowledge developed throughout: (i) this thesis, (ii) the PROTOCOL project, and (iii) the latest edition of the recommendations for maritime works (ROM-1.1, 2018).

Following the principles of "preventive medicine," these guidelines are structured in three main blocks: identification of the problem -preferably a future problem (symptoms)-, identification of the causes (diagnosis) and identification of the possible solutions (treatment). During the symptoms block, it is necessary to define what is at risk. The urgency, the methods to be used, and the risk and uncertainty to be assumed in the solution to be proposed will highly depend on the elements that are at risk, among which we can differentiate the following: human life, infrastructure, economic activities, or ecosystems. In the diagnosis block, these guidelines address the causes that are generating the previously identified problem. To achieve it, this block is, in turn, divided into three steps: information gathering, the definition of the problem and reproduction of the historical conditions of the past in order to (i) verify that the set-up of our models is correct and (ii) characterize both the frequency and magnitude of the failure, as well as identify the mechanisms that caused the failure in the past. This second block ends with the generation of zonation maps, where all the results obtained during the reproduction of the past are gathered in one schematic map to divide the estuary into homogeneous areas. These maps can be used by managers and stakeholders to support decision-making based on risk analysis, identify vulnerable areas, quantify the frequency of flooding, and identify the agents responsible for flooding at each area. Particularly, three sections can be identified in the Guadalete estuary. The *tidal section* is identified in the first 3 km of the estuary; the *fluvial section*, in the last 4 km of and a *tidal-fresh section* is identified in the intermediate 6 km of the estuary.

The third and last block of these guidelines focuses on defining the appropriate solution for the mitigation of the consequences caused by the defined problem once the past is understood and reproducible following the ROM-1.1 (2018) recommendations for maritime works. Three different development levels are defined: preliminary studies, study of alternatives, and blueprint and investment project. Each one of these development levels must culminate with an: hydrodynamic report; structural and geotechnical report; economic and financial report; and an environmental and social report. These reports help decide the best alternatives for flooding risk mitigation in a specific area of transitional coastal environments. To facilitate knowledge-based decision making, the results obtained through the application of these guidelines can be converted into management maps. These maps illustrate the impact of SLR on flooding along the TCE by quantifying the number of flood defense failures in each area. In addition, they represent the spatial and temporal variation of the extreme total water levels along the TCE and the 21st-century for the different scenarios of SLR, and assess the uncertainty related to the stochastic forecasting of the forcing agents. The former facilitates the understanding of the mechanisms of the formation of extreme events and their evolution along the 21st-century, which can be useful for managers interested in developing cost-effective

coastal protection measures to mitigate the risks associated with GW.

Part V

Conclusions

CHAPTER 10

CONCLUSIONS AND FUTURE RESEARCH LINES

10.1 Conclusions

Global warming is driving a progressive sea-level rise, which is expected to continue and accelerate in the next decades, leading to more frequent flooding events on the coast, damage to material assets, and increased risk of loss of human life. Since more than 60% of the world's population lives in low-elevation coastal areas, and mitigation trends indicate that this number is expected to increase along the 21st-century, the general objective of this Thesis is "to develop a comprehensive methodology with practical application tools for the characterization of the impact of global warming on flooding at a local scale in transitional coastal environments". Although progress has been made in this area, comprehensive methods focusing not only on the probabilistic study of flooding events at the local scale, but also on the analysis of the mechanisms underlying the formation of these extreme events caused by multiple concomitant forcing agents, and even more so concerning the effects of sea-level rise, are currently lacking. To meet this objective, this Thesis combines a set of very innovative techniques available separately in the field of Coastal Engineering while inheriting the advance in knowledge through the work of the Environmental Fluid Dynamics Group, e.g., (Solari and Losada, 2011; Egüen, 2016; Folgueras et al., 2016; ROM-1.1, 2018). Therefore, this Thesis allows both managers and stakeholders to address one of the main challenges in the coming decades, particularly in transitional environments, to anticipate whether current food defenses will be sufficient against global warming. Moreover, if they are not, this Thesis addresses

the question of where and when flood defense will fail and by how much from a global, local, multivariate, and probabilistic approach.

The main conclusions of the Thesis are organized according to the specific objectives presented in section 1.2:

I. **To develop an open-access numerical tool for the gathering, homogenization, characterization, and simulation of climate agents databases following software engineering guidelines.**

   An open-access high-quality scientific software for climate analysis to characterize different climatic agents world-wide is developed using the software engineer skills as a primary and necessary step for sea-level rise impact assessment. Six modules have been implemented for reading, pre-processing, standardized, and analyzing climate data. The developed tool allows generating multiple products, from climate databases to automatic climate analysis reports, addressing different users from single source code. This information is used to simulate the forecasted series of climatic agents along the 21st-century, which, together with the sea-level rise scenarios, constitutes the inputs of the methodology presented in this Thesis. For this purpose, the lower limit of the IPCC-AR 5 (Church et al., 2013) RCP4.5 scenario and the upper limit for the RCP8.5 scenario have been considered as the sea-level rise projections.

II. **To reconstruct the time series of historical (hindcasted) and future (forecasted) continuous water levels along transitional coastal environments through advanced hydrodynamic numerical models and downscaling techniques.**

   Systematic measurements of water levels along estuaries are rarely available and expensive, and even less information can be found on the contribution of the different agents to these levels. The downscaling technique, initially used in the field of Coastal Engineering to downscale wavefields has been successfully adapted to being able to reconstruct not only large continuous time series of total water level series but also the water level components due to each individual forcing agents and the non-linear component due to the interaction between them along transitional coastal systems. The implementation of this methodology in the Guadalete estuary, used in this Thesis as the case study area, has shown that these elevations present significant variabilities along the estuary. In particular, maximum elevations due to astronomical tide decrease upstream from the mouth (1.8 m) to the inner part of the estuary (0.9 m) above local mean sea level, whereas river discharge increases

upstream from 0 (mouth) to 3 m (head). Weather surge elevations are found to be significantly lower than the rest of the components.

III. **To quantify the number of flood defense failures to determine the sensitivity of transitional coastal environments to extreme flood events resulting from global warming.**

The reconstructed historical and forecasted total water level series along the estuary is compared to the geometry of different transversal sections of the estuary to assess the number and duration of flood failures per year. Although there are several failure modes related to flood events, in this Thesis failure is defined as water levels higher than the crest height of the flood defenses for a period exceeding 3 hours. To classify two failures as independent, a minimum 14-hour gap is considered to account for the astronomical tide-induced oscillations. This method, quite simple from a conceptual point of view, allows to quickly and inexpensively identify which areas will be the most sensitive to flooding in the coming years. In the case of the Guadalete estuary, an overflowing failure every 15 days coinciding with every spring tidal cycle per year is expected in the middle estuary in the most pessimistic considered sea-level rise scenario if no mitigation actions are taken.

IV. **To assess the probability of extreme total water level events in terms of return period in transitional coastal environments considering the concomitance between the marine, river, and atmospheric forcing agents to characterize the magnitude of the flood events.**

The extra information provided by the individual water level components allows applying the well-known Joint Probability Methods to transitional coastal environments. The method is based on the double convolution of the marginal distributions of the three components of the water level. This allows summing the probability density functions of each component by considering all the possible combinations between them instead of only the ones that occurred in the past. This is especially interesting in highly regulated rivers, where river discharges usually coincide with neap tides. However, the precise statistical fitting of the water level components is required.

Joint extreme total water level (JETWL) events obtained in this way are compared with the observed return levels. Similar values for both sides of the estuary are obtained. However, differences are observed in the middle part (from CP 4 to 6) for long return periods where the observed return levels are 30% lower than the JETWL on average for the higher return periods. These differences are caused by interactions between the peaks and non-peaks of the astronomical tide and river discharge. Thus, we conclude that the observed return levels are biased by this

regulation, leading to lower probabilities than the obtained using the presented methodology, which may be risky in decision-making or urban planning.

On the other hand, the worst overflowing conditions are also found in the middle part of the estuary. The biggest vulnerability problem in this area is the fact that the sum of extreme astronomical tidal events combined with the sea-level rise is already above the levee height. Thus, JETWL in this area will exceed the height of the levees independently of the frequency of the river discharge events.

The application of this method allows managers and coastal engineers to know the expected magnitude of flood events in probabilistic terms and the associated uncertainty, which constitutes the starting point for the design of protective measures. For example, if the estuary's central region is intended to be protected against events with a 50-year return period in 2100, a crest elevation of 2.5 m or 4 m will be necessary to prevent flooding with a 50 % and 95 % confidence, respectively.

V. **To analyze the simultaneity and compatibility relationships between the water level components to characterize the mechanisms underlying the occurrence of extreme total water level events leading to flooding.**

The statistical relationships that are established between the total water level that is a linear combination of a set of water level components that act simultaneously and the variables that are obtained from classifying each water level component in a set of mutually exclusive classes (extreme and non-extreme) are successfully adapted upon the work developed by Folgueras (2016) in transitional coastal environments. Therefore, all the disaggregated information of the water level components is used to study the mechanisms of the formation of extreme flood events. The development of a method that allows the identification of not only the agents responsible for the flooding processes but also of the combinations of extreme and non-extreme values that cause flooding is a significant advance in Coastal Engineering aimed at protecting coastal urban fronts against global warming. The obtained information allows the optimization of costs derived from protection measures since it is known on which agents and regime (extreme or normal) it is necessary to act for flooding risk mitigation.

The Guadalete estuary analysis during the historical period indicates that the extreme values of the total water level are explained only by the extremes of the astronomical tide in the outer estuary and only by the extremes of the river discharge in the inner estuary. However, a similar contribution between extreme values of the river discharge and extreme and mean values of the astronomical tide is found in the middle part of the estuary. The lack of correlation between simultaneous extreme values of the water level components indicates that they can

be considered as independent. Furthermore, these analyses indicate that in the Guadalete estuary case, the non-linear term's contribution to the magnitude and variability of the extreme events of the total water level is nearly negligible. Waves do not substantially impact on the water levels along the Guadalete estuary. The reason is found in the two breakwaters that protect the inlet from waves and the lack of waves breaking along the estuary. Therefore, checking the impact of waves on the water levels is recommended before applying the presented method at other locations to avoid unnecessary computational costs.

For the 21st-century period, the contribution of the non-extremes equals the contribution of the extremes in the formation of flood events by the end-century in the middle and upper estuary as a consequence of sea-level rise. It is also observed that the high interaction between atmospheric and river discharge in the middle estuary is reduced. Therefore, fluvial discharge is limited only to the upper estuary, while the astronomical tide plus the sea-level rise dominated the formation of the flood events in the lower and middle estuary. No significant changes are observed in the formation of extreme flood events between the historical period and 21st-century for the most optimistic sea-level rise scenario.

VI. **To determine the spatio-temporal variability of extreme water level events to characterize where and when flooding will occur.**

Despite the computational effort, all the presented methods along this Thesis has been fruitfully applied at multiple equidistant control points along the estuary and repeated for the eight nodal cycles between 1995 to 2100 for the two sea-level rise scenarios in the Guadalete estuary. As a result, the spatial and temporal evolution of the results has been addressed, providing much more valuable information on the impact of the sea-level rise in the flood events. This information is used to divide the estuary into homogeneous zones via three criteria: (i) the probability of extreme total water level events, (ii) the dominance of the agents, and (iii) the relationships between the components of the water level. These management maps constitute a valuable tool to support decision-making based on risk analysis, identify vulnerable areas, quantify the frequency of flooding, and identify the agents responsible for flooding at each area.

Particularly, three sections can be identified in the Guadalete estuary. The *tidal section* is identified in the first 3 km of the estuary; the *fluvial section*, in the last 4 km of and a *tidal-fresh section* is identified in the intermediate 6 km of the estuary. These maps can be used by managers and stakeholders to support decision-making based on risk analysis, identify vulnerable areas, quantify the frequency of flooding and identify the agents responsible for flooding at each area.

VII. **To develop a detailed method and an associated open-access numerical tool for calculating the probability distribution function of the total costs for any protective maritime structure at any location during its useful life cycle following the guidelines of ROM-1.1 (2018).** Once the impact of the sea-level rise on flood failure along transitional coastal environments has been assessed, methods, and instruments to optimize the total cost of the protective maritime structures are needed. Thus, in this specific objective, a detailed method and an associated open-access numerical tool for the calculation of the probability distribution function of the total costs for any type of protective maritime structure at any location during its life-time cycle following the guidelines of the latest version of the ROM program (ROM-1.1, 2018) is presented. The definition of the total costs is defined at first as the sum of the execution costs of construction, dismantling, and repair works as well as the costs of exploitation during the operating phase. The main variables that modify these costs, most of them of stochastic nature are: (i) the forcing agents, (ii) the design of the structure, (iii) the project factors, (iv) the organization and work planning definition including the decision and actions (strategies) taking during the life cycle, (v) the interactions between the former elements, and (vi) the useful life-time. The developed methodology for the calculation of the total costs following the ROM-1.1 (2018) is presented in six steps: conception, spatial and temporal disaggregation of the maritime structure; work planning and strategies definition; characterization, simulation and propagation of maritime climate; project phases and damage accumulation modeling; cost allocation; and analysis and uncertainty assessment through Monte Carlo techniques.

As a case study example of application, a series of gradual examples using the associated open-access numerical tool are analyzed, including the calculation of: the total construction costs, a single repair costs of a damaged breakwater, and the total cost over the useful life-time of the breakwater. In the analyzed examples, two opposite strategies, “risky” and “conservative”, are defined. The difference between both strategies lies in the restriction of progress between the breakwater elements and in the repair threshold. In the risky strategy, the breakwater is developed in series, and the repair threshold is higher than in the conservative, where each element is executed nearly one-by-one. In contrast, in the “conservative” strategy, all the elements are developed at the same time, and the repair threshold is lower what means that repair works are executed before without allowing the damage progression. The analysis of the results during the construction phase indicates that the conservative strategy execution times fit much be the theoretical end times defined in the work planning. Furthermore, the variability in the execution times is also shown by the tool through boxplots graphics. Results also indicate that the executed volume by the first subphase (dredging) of the risky strategy

double the projected theoretical volume. The reason is due to the fact that the risky strategy also works during the winter months without protection were the climate is severe, while conservative strategy does not. Therefore, differences between 3 to 5 million euros are found between the 50th and 99th percentiles of the cumulative distribution functions of the construction costs between booth strategies, being the risky strategy the most expensive. However, these differences increases during the repair phase, where differences around 60 million euros are obtained between both strategies for the higher percentiles. This type of tool represents a before and after for public administrations since they no longer depend solely on the budgets given by construction companies. Now it is possible to model each of the alternatives, strategies, decisions, and planning to obtain not only the associated costs but also the limited uncertainty. This makes it possible to quickly and economically discard unprofitable alternatives such as the analyzed risky strategy.

VIII. **To integrate the methodology developed throughout this Thesis to present comprehensive guidelines for assessing the sea-level rise impact on coastal urban fronts at a local scale.**

The methodology developed along this Thesis has been integrated into practical and comprehensive guidelines to provide managers, coastal engineers, and decision-makers recommendations together with a set of practical tools to assess the impact that sea-level rise will have on coastal urban fronts at a local scale in transitional environments. These guidelines have been designed following the principles of preventive medicine, where the focus is not the finding of the solution, but the anticipation of the problem. Therefore, the so-called "preventive engineering" guidelines are based on three main blocks: symptoms, diagnosis, and treatment.

In the symptoms stage, guidelines focus on identifying the problem that sea-level rise could originate shortly or during the next decades. During the diagnosis stage, users must be focused on three critical points: the gathering of all the available information and pay attention to monitoring and research if the available information is not sufficient; the in-depth definition of the problem; and the reproduction of the past in order to test and validate the models and methods. Following the ROM-1.1 (2018), the treatment stage is divided into a set of three different development levels progressively increasing in complexity and accuracy: preliminary studies, the study of alternatives, and blueprint-investment project.

10.2 Future research lines

This Thesis provides a comprehensive methodology and practical application tools that increase our understanding of the impact that sea-level rise will have on coastal urban

fronts along transitional coastal environments. However, there are some points of the developed methodology that can be extended in further studies. After the realization of this work, these studies should focus on three main lines:

I. The first line should focus on including the latest advances in the effects of global warming on the forcing agents' descriptors instead of only using the sea-level rise scenarios. Therefore, the considered distribution functions of the maritime, atmospheric, and fluvial agents used for the climatic simulations of the natural agents should include these effects. Resulting water levels affected by global warming should be compared to those obtained in this Thesis to address the magnitude of these effects compared to the sea-level rise. Furthermore, the latest developments of the IPCC AR6 in the sea-level rise scenarios should also be included to update the methodology.

II. The second line should focus on the second part of the risk definition proposed by Losada et al. (2009). Risk is defined as the product of probabilities by the consequences. As shown in this Thesis, the probabilities of the failure of flooding have been widely characterized. However, no comment has been made regarding the consequences of flood failures. The assessment of the consequences of flood failures, in economic terms, would allow comparing the effectiveness of the different protective measurements as well as to complete the definition of the risk assessment along the transitional coastal environments. This line should also focus on defining and designing the different alternatives of coastal flood defenses, which have also been set aside in the guidelines chapter of this Thesis.

III. The main variable of this Thesis is the water level. Thus, failure is only defined in the presented method as water levels exceeding the height of the flood defenses along the transitional coastal system. This is the reason why the third line should focus on including other hydrodynamic variables to the methodology. First, longitudinal and transversal instant currents should be included to complement the analysis of water levels. However, other variables, such as salinity, temperature, water quality indexes, and density, among others, could also be reconstructed using the proposed methodology without adding much difficulty. The inclusion of former variables would increasingly complement the analysis of the impact of the sea-level rise transitional environments.

IV. Finally, although the analysis has also been tested on other estuaries such as the Mondego River in Figueira da Foz (Portugal), the proposed methodology will be enriched as it is applied in new study areas, which will make it possible to add new features that are not already covered by the existing methodology.

Bibliography

Anderson, D., Rueda, A., Cagigal, L., Antolinez, J. A. A., Mendez, F. J., and Ruggiero, P. (2019). "Time-Varying Emulator for Short and Long-Term Analysis of Coastal Flood Hazard Potential". In: *Journal of Geophysical Research: Oceans* 124.12, pp. 9209–9234. URL: https://doi.org/10.1029/2019JC015312.

Baker, M. (2017). "Scientific computing: Code alert". In: *Nature* 541, pp. 563–565. URL: https://doi.org/10.1038/nj7638-563a.

Baquerizo, A. and Losada, M. A. (2008). "Human interaction with large scale coastal morphological evolution. An assessment of the uncertainty". In: *Coastal Engineering* 55.7, pp. 569 –580. ISSN: 0378-3839. URL: https://doi.org/10.1016/j.coastaleng.2007.10.004.

Barredo, J. I. (2007). "Major flood disasters in Europe: 1950–2005". In: *Natural Hazards* 42.1, pp. 125–148. ISSN: 0921-030X. URL: https://doi.org/10.1007/s11069-006-9065-2.

Bars, D. L., Drijfhout, S., and Vries, H. de (2017). "A high-end sea level rise probabilistic projection including rapid Antarctic ice sheet mass loss". In: *Environmental Research Letters* 12.4. URL: https://doi.org/10.1088/1748-9326/aa6512.

Beguería, S. (2005). "Uncertainties in partial duration series modelling of extremes related to the choice of the threshold value". In: *Journal of Hydrology* 303.1, pp. 215–230. ISSN: 0022-1694. URL: https://10.1016/j.jhydrol.2004.07.015.

Bermúdez, M., Cea, L., and Sopelana, J. (2019). "Quantifying the role of individual flood drivers and their correlations in flooding of coastal river reaches". In: *Stochastic Environmental Research and Risk Assessment* 33.10, pp. 1851–1861. ISSN: 1436-3259. URL: https://doi.org/10.1007/s00477-019-01733-8.

Booij, N., Ris, R. C., and Holthuijsen, L. H. (1999). “A third-generation wave model for coastal regions: 1. Model description and validation”. In: *Journal of Geophysical Research: Oceans* 104.C4, pp. 7649–7666. URL: https://doi.org/10.1029/98JC02622.

Brett, A., Croucher, M., Haines, R., Hettrick, S., Hetherington, J., Stillwell, M., and Wyatt, C. (2017). “Research Software Engineers: State of the Nation Report 2017”. In: URL: https://zenodo.org/record/495360#.Xryi4MCWrIW.

Bryant, R. E. (2011). “Data-Intensive Scalable Computing for Scientific Applications”. In: *Computing in Science & Engineering* 13.6, pp. 25–33.

Callaghan, D. P., Nielsen, P., Short, A., and Ranasinghe, R. (2008). “Statistical simulation of wave climate and extreme beach erosion”. In: *Coastal Engineering* 55.5, pp. 375 –390. ISSN: 0378-3839. URL: https://doi.org/10.1016/j.coastaleng.2007.12.003.

Cameron, W. M. and Pritchard, D. W. (1963). *Estuaries. In The Sea, vol. 2. pp. 306–324*. Ed. by M. N. Hill. John Wiley and Sons: New York.

Camus, P., Mendez, F. J., and Medina, R. (2011). “A hybrid efficient method to downscale wave climate to coastal areas”. In: *Coastal Engineering* 58.9, pp. 851–862. ISSN: 0378-3839. URL: https://doi.org/10.1016/j.coastaleng.2011.05.007.

Camus, P., Mendez, F. J., Medina, R., and Cofiño, A. S. (2011). “Analysis of clustering and selection algorithms for the study of multivariate wave climate”. In: *Coastal Engineering* 58.6, pp. 453–462. ISSN: 0378-3839. URL: https://doi.org/10.1016/j.coastaleng.2011.02.003.

Chen, W. and Swart, H. E. de (2018). “Estuarine residual flow induced by eddy viscosity-shear covariance: Dependence on axial bottom slope, tidal intensity and constituents”. In: *Continental Shelf Research* 167, pp. 1 –13. ISSN: 0278-4343. URL: https://doi.org/10.1016/j.csr.2018.07.011.

Chen, W.-B. and Liu, W.-C. (2014). “Modeling Flood Inundation Induced by River Flow and Storm Surges over a River Basin”. In: *Water* 6.10, pp. 3182–3199. ISSN: 2073-4441. URL: https://doi.org/10.3390/w6103182.

Church, J. A. et al. (2013). “Sea Level Change In T. F. Stocker et al. (Eds.), Climate change 2013: The physical science basis, contribution of working group I to the fifth assessment report of the intergovernmental panel on climate change”. In: Cambridge,

United Kingdom and New York, NY, USA: Cambridge University Press. Chap. 13, 1137–1216. ISBN: ISBN 978-1-107-66182-0. URL: https://doi.org/10.1017/CBO9781107415324.026.

Coles, S. (2001). *An Introduction to Statistical Modeling of Extreme Values*. I. Springer-Verlag London. ISBN: 978-1-84996-874-4. URL: https://doi.org/10.1007/978-1-4471-3675-0.

DeConto, R. M. and Pollard, D. (Mar. 2016). "Contribution of Antarctica to past and future sea-level rise". In: *Nature* 531.7596, pp. 591–597. ISSN: 1476-4687. URL: https://doi.org/10.1038/nature17145.

Dee, D. P. et al. (2011). "The ERA-Interim reanalysis: configuration and performance of the data assimilation system". In: *Quarterly Journal of the Royal Meteorological Society* 137.656, pp. 553–597. URL: https://doi.org/10.1002/qj.828.

Del-Rosal-Salido, J., Magaña, P., and Ortega-Sánchez, M. (2019). "Bridging the gap between software and hydraulic engineering: the development of a climatic open-access tool". In: *Proceedings of 38th IAHR World Congress (IAHR 2019)*. Panamá city, Panamá.

Del-Rosal-Salido, J. et al. (2018a). "Protection of coastal urban fronts against global warming". In: *Proceedings of EGU General Assembly 2018*. Vienna, Austria.

— (2019a). "Addressing the challenge of flooding risk induced by global warming: PROTOCOL Project". In: *Proceedings of 38th IAHR World Congress (IAHR 2019)*. Panamá city, Panamá.

Del-Rosal-Salido, J., Folgueras, P., Ortega-Sánchez, M., and Losada, M. A. (2017a). "Metodología para la tramificación de zonas de transición basada en la interacción entre agentes". In: *Proceedings of XIV Jornadas Españolas de Ingeniería de Costas y Puertos*. Alicante, Spain.

— (2017b). "Probabilities of extreme water levels on estuarine urban fronts". In: *Proceedings of International Short Course and Conference on Applied Coastal Research (SCACR 2017)*. Santander, Spain.

— (2019b). "Beyond flood probability assessment: An integrated approach for characterizing extreme water levels along transitional environments". In: *Coastal Engineering*

152, p. 103512. ISSN: 0378-3839. URL: https://doi.org/10.1016/j.coastaleng.2019.103512.

Del-Rosal-Salido, J., Folgueras, P., Ortega-Sánchez, M., and Losada, M. A. (2019c). "Método integrado para la gestión del efecto combinado de agentes climáticos en sistemas costeros de transición". In: *Proceedings of XV Jornadas Españolas de Ingeniería de Costas y Puertos*. Torremolinos, Spain.

— (2020). "Flood management challenges in transitional environments: assessing the effects of sea-level rise on compound flooding in the 21st century". In: *Coastal Engineering (Under review)*.

Del-Rosal-Salido, J., Magaña, P., Bergillos RJ. Díaz-Carrasco, P., and Ortega-Sánchez, M. (2018b). "Easing entry barriers into coastal flooding risk analysis for both end users and researchers: the development of a climatic open-access tool". In: *Proceedings of EGU General Assembly 2018*. Vienna, Austria.

Del-Rosal-Salido, J., Zarzuelo-Romero, C., Díez-Minguito, M., Ortega-Sánchez, M., and Losada, M. A. (2015a). " Circulación residual en la Bahía de Cádiz: análisis de datos de campo y modelado numérico". In: *Proceedings of XIII Jornadas Españolas de Ingeniería de Costas y Puertos*. Avilés, Spain.

— (2015b). "Residual circulation in the Bay of Cádiz (SW Spain): field analysis and numerical modeling". In: *Proceedings of 2015 Aquatic Sciences Meeting*. Granada, Spain.

Delft, T. U. (2020). *Delft3D-WAVE. Simulation of short-crested waves with SWAN. User manuals (V. 3.05)*. Tech. rep. Delft University of Technology. URL: https://oss.deltares.nl/web/delft3d/manuals.

Diakakis, M. and Deligiannakis, G. (2017). "Flood fatalities in Greece: 1970-2010". In: *Journal of Flood Risk Management* 10.1, pp. 115–123. ISSN: 1753318X. URL: http://doi.wiley.com/10.1111/jfr3.12166.

Dias, J. M. and Lopes, J. F. (2006). "Implementation and assessment of hydrodynamic, salt and heat transport models: The case of Ria de Aveiro Lagoon (Portugal)". In: *Environmental Modelling & Software* 21.1, pp. 1 –15. ISSN: 1364-8152. URL: https://doi.org/10.1016/j.envsoft.2004.09.002.

Diaz-Hernandez, G., Losada, I. J., and Mendez, F. J. (2017). "Improving construction management of port infrastructures using an advanced computer-based system". In: *Automation in Construction* 81, pp. 122 –133. URL: https://doi.org/10.1016/j.autcon.2017.06.020.

Dixon, M. J. and Tawn, J. A. (1999). "The effect of non-stationarity on extreme sea-level estimation". In: *Journal of the Royal Statistical Society. Series C: Applied Statistics* 48.2, pp. 135–151. URL: https://doi.org/10.1111/1467-9876.00145.

Dixon, M. J. and Tawn, J. A. (1995). *Extreme sea-levels at the UK A-class sites: optimal site-by-site analyses and spatial analyses for the east coast*. Tech. rep. Lancaster University and the Proudman Oceanographic Laboratory. URL: https://www.ntslf.org/products/reports-other.

Dodet, G., Bertin, X., and Taborda, R. (2010). "Wave climate variability in the North-East Atlantic Ocean over the last six decades". In: *Ocean Modelling* 31.3, pp. 120 –131. ISSN: 1463-5003. URL: https://doi.org/10.1016/j.ocemod.2009.10.010.

Díez-Minguito, M., Contreras, E., Polo, M. J., and Losada, M. A. (2013). "Spatio-temporal distribution, along-channel transport, and post-riverflood recovery of salinity in the Guadalquivir estuary (SW Spain)". In: *Journal of Geophysical Research: Oceans* 118.5, pp. 2267–2278. URL: https://doi.org/10.1002/jgrc.20172.

Egbert, G. D. and Erofeeva, S. Y. (2002). "Efficient Inverse Modeling of Barotropic Ocean Tides". In: *Journal of Atmospheric and Oceanic Technology* 19.2, pp. 183–204. URL: https://doi.org/10.1175/1520-0426(2002)019<0183:EIMOBO>2.0.CO;2.

Egüen, M., Aguilar, C., Solari, S., and Losada, M. A. (2016). "Non-stationary rainfall and natural flows modeling at the watershed scale". In: *Journal of Hydrology* 538, pp. 767 –782. ISSN: 0022-1694. URL: https://doi.org/10.1016/j.jhydrol.2016.04.061.

Egüen, M. (2016). "Fuentes de variabilidad en los agentes forzadores de la dinámica de los estuarios atlánticos en Andalucía". PhD thesis. University of Granada (in Spanish). URL: https://digibug.ugr.es/handle/10481/39634?locale-attribute=en.

Elias, E. P. L., Gelfenbaum, G., and Westhuysen, A. J. Van der (2012). "Validation of a coupled wave-flow model in a high-energy setting: The mouth of the Columbia River". In: *Journal of Geophysical Research: Oceans* 117.C9. URL: https://agupubs.onlinelibrary.wiley.com/doi/abs/10.1029/2012JC008105.

Elias, E. P. L. and Hansen, J. E. (2013). “Understanding processes controlling sediment transports at the mouth of a highly energetic inlet system (San Francisco Bay, CA)”. In: *Marine Geology* 345. A multi-discipline approach for understanding sediment transport and geomorphic evolution in an estuarine-coastal system: San Francisco Bay, pp. 207 –220. ISSN: 0025-3227. URL: https://doi.org/10.1016/j.margeo.2012.07.003.

Enríquez, A. R., Marcos, M., Falqués, A., and Roelvink, D. (2019). “Assessing Beach and Dune Erosion and Vulnerability Under Sea Level Rise: A Case Study in the Mediterranean Sea”. In: *Frontiers in Marine Science* 6, p. 4. ISSN: 2296-7745. URL: https://doi.org/10.3389/fmars.2019.00004.

Fernandez-Fernandez, S., Ferreira, C. C., Silva, P. A., Baptista, P., Romao, S., Fontan-Bouzas, A., Abreu, T., and Bertin, X. (2019). “Assessment of Dredging Scenarios for a Tidal Inlet in a High-Energy Coast”. In: *Journal of Marine Science and Engineering* 7.11. ISSN: 2077-1312. URL: https://doi.org/10.3390/jmse7110395.

Folgueras, P. (2016). “Studio sobre la combinación de variables geofísicas extremas en la definición de criterios de diseño”. PhD thesis. University of Granada (in Spanish). URL: https://digibug.ugr.es/handle/10481/46331?locale-attribute=fr.

Folgueras, P., Del-Rosal-Salido, J., Moragues, M. V., Lopez, J. D., and Losada, M. A. (2018). “Accumulated damage evolution and investment costs of breakwaters”. In: *Proceedings of 36th International Conference on Coastal Engineering (ICCE)*. Baltimore, Maryland, USA.

Folgueras, P., Solari, S., Mier-Torrecilla, M., Doblaré, M., and Losada, M. A. (2016). “The extended Davenport peak factor as an extreme-value estimation method for linear combinations of correlated non-Gaussian random variables”. In: *Journal of Wind Engineering and Industrial Aerodynamics* 157, pp. 125–139. ISSN: 0167-6105. URL: https://doi.org/10.1016/j.jweia.2016.07.014.

Fortunato, A. B., Freire, P., Bertin, X., Rodrigues, M., Ferreira, J., and Liberato, M. L. R. (2017). “A numerical study of the February 15, 1941 storm in the Tagus estuary”. In: *Continental Shelf Research* 144, pp. 50 –64. ISSN: 0278-4343. URL: https://doi.org/10.1016/j.csr.2017.06.023.

Franke, R. (1982). “Scattered Data Interpolation: Tests of Some Method”. In: *Mathematics of Computation* 38.157, pp. 181–200. ISSN: 00255718, 10886842. URL: https://doi.org/10.2307/2007474.

Gesler, E. (1951). “ECONOMICS OF COASTAL STRUCTURES”. In: *Coastal Engineering Proceedings* 1.2, p. 21. ISSN: 2156-1028. URL: https://doi.org/10.9753/icce.v2.21.

Gil-Guirado, S., Pérez-Morales, A., and Lopez-Martinez, F. (2019). “SMC-Flood database: a high-resolution press database on flood cases for the Spanish Mediterranean coast (1960–2015)”. In: *Natural Hazards and Earth System Sciences* 19.9, pp. 1955–1971. ISSN: 1684-9981. URL: https://doi.org/10.5194/nhess-19-1955-2019.

Goble, C. (2014). “Better Software, Better Research”. In: *IEEE Internet Computing* 18, pp. 4–8.

Gouldby, B., Méndez, F. J., Guanche, Y., Rueda, A., and Mínguez, R. (2014). “A methodology for deriving extreme nearshore sea conditions for structural design and flood risk analysis”. In: *Coastal Engineering* 88, pp. 15–26. ISSN: 0378-3839. URL: https://doi.org/10.1016/j.coastaleng.2014.01.012.

Guanche, Y., Camus, P., Guanche, R., Mendez, F. J., and Medina, R. (2013). “A simplified method to downscale wave dynamics on vertical breakwaters”. In: *Coastal Engineering* 71, pp. 68–77. ISSN: 0378-3839. URL: https://doi.org/10.1016/j.coastaleng.2012.08.001.

Guedes-Soares, C. and Ferreira, A. M. (1996). “Representation of non-stationary time series of significant wave height with autoregressive models”. In: *Probabilistic Engineering Mechanics* 11.3, pp. 139 –148. ISSN: 0266-8920. URL: https://doi.org/10.1016/0266-8920(96)00004-5.

How do scientists develop and use scientific software? (2009). IEEE, pp. 1–8.

Hans, H. et al. (2019). *Global reanalysis: goodbye ERA-Interim, hello ERA5*. Vol. Meteorology, pp. 17–24.

Hardy, R. L. (1990). “Theory and applications of the multiquadric-biharmonic method 20 years of discovery 1968–1988”. In: *Computers & Mathematics with Applications* 19.8, pp. 163–208. ISSN: 0898-1221. URL: https://doi.org/10.1016/0898-1221(90)90272-L.

Hawkes, P. J. (2008). “Joint probability analysis for estimation of extremes”. In: *Journal of Hydraulic Research* 46.sup2, pp. 246–256. URL: https://doi.org/10.1080/00221686.2008.9521958.

Hawkes, P. J., Gouldby, B. P., Tawn, J. A., and Owen, M. W. (2002). "The joint probability of waves and water levels in coastal engineering design". In: *Journal of Hydraulic Research* 40.3, pp. 241–251. URL: https://doi.org/10.1080/00221680209499940.

Hinkel, J. et al. (2014). "Coastal flood damage and adaptation costs under 21st century sea-level rise". In: *Proceedings of the National Academy of Sciences* 111.9, pp. 3292–3297. ISSN: 0027-8424. URL: https://doi.org/10.1073/pnas.1222469111.

Hogarth, P. (2014). "Preliminary analysis of acceleration of sea level rise through the twentieth century using extended tide gauge data sets (August 2014)". In: *Journal of Geophysical Research: Oceans* 119.11, pp. 7645–7659. URL: https://doi.org/10.1002/2014JC009976.

Iglesias, G. and Carballo, R. (2010). "Effects of high winds on the circulation of the using a mixed open boundary condition: the Ría de Muros, Spain". In: *Environmental Modelling & Software* 25.4, pp. 455 –466. ISSN: 1364-8152. URL: https://doi.org/10.1016/j.envsoft.2009.10.013.

Iglesias, G., Sánchez, M., Carballo, R., and Fernández, H. (2012). "The TSE index – A new tool for selecting tidal stream sites in depth-limited regions". In: *Renewable Energy* 48, pp. 350 –357. ISSN: 0960-1481. URL: https://doi.org/10.1016/j.renene.2012.05.012.

Ince, D. C., Hatton, L., and Graham-Cumming, J. (2012). "The case for open computer programs". In: *Nature* 482.7386, pp. 485–488. URL: https://doi.org/10.1038/nature10836.

Jevrejeva, S., Frederikse, T., Kopp, R. E., Le Cozannet, G., Jackson, L. P., and Wal, R. S. W. van de (2019). "Probabilistic Sea Level Projections at the Coast by 2100". In: *Surveys in Geophysics* 40.6, pp. 1673–1696. ISSN: 1573-0956. URL: https://doi.org/10.1007/s10712-019-09550-y.

Jevrejeva, S., Jackson, L. P., Grinsted, A., Lincke, D., and Marzeion, B. (2018). "Flood damage costs under the sea level rise with warming of 1.5 ºC and 2 ºC". In: *Environmental Research Letters* 13.7, p. 074014. URL: https://doi.org/10.1088%2F1748-9326%2Faacc76.

Kreeke, J. van de and Paape, A. (1964). "ON OPTIMUM BREAKWATER DESIGN". In: *Coastal Engineering Proceedings* 1.9, p. 34. URL: https://doi.org/10.9753/icce.v9.34.

Kumbier, K., Carvalho, R. C., Vafeidis, A. T., and Woodroffe, C. D. (2018). "Investigating compound flooding in an estuary using hydrodynamic modelling: a case study from the Shoalhaven River, Australia". In: *Natural Hazards and Earth System Sciences* 18.2, pp. 463–477. URL: https://doi.org/10.5194/nhess-18-463-2018.

Landau, S., Legro, S., and Vlašić, S. (2008). *A Climate for Change: Climate change and its impacts on society and economy in Croatia*. Tech. rep. United Nations Development Programme (UNDP) in Croatia. URL: http://hdr.undp.org/en/content/climate-change.

Lesser, G. R. (2009). "An approach to medium-term coastal morphological modelling". PhD thesis. Department of Hydraulic Engineering, Delft University of Technology, p. 255. URL: https://repository.tudelft.nl/assets/uuid:62caa573-4fc0-428e-8768-0aa47ab612a9/PHD_THESIS_LESSER.pdf.

Lesser, G. R., Roelvink, J. A., Kester, J. A. T. M. van, and Stelling, G. S. (2004). "Development and validation of a three-dimensional morphological model". In: *Coastal Engineering* 51.8. Coastal Morphodynamic Modeling, pp. 883–915. ISSN: 0378-3839. URL: https://doi.org/10.1016/j.coastaleng.2004.07.014.

Lian, J. J., Xu, K., and Ma, C. (2013). "Joint impact of rainfall and tidal level on flood risk in a coastal city with a complex river network: a case study of Fuzhou City, China". In: *Hydrology and Earth System Sciences* 17.2, pp. 679–689. URL: https://doi.org/10.5194/hess-17-679-2013.

Lichter, M., Vafeidis, A. T., Nicholls, R. J., and Kaiser, G. (2011). "Exploring Data-Related Uncertainties in Analyses of Land Area and Population in the "Low-Elevation Coastal Zone" (LECZ)". In: *Journal of Coastal Research* 27.4, pp. 757–768. ISSN: 07490208,15515036. URL: https://doi.org/10.2112/JCOASTRES-D-10-00072.1.

Lincke, D. and Hinkel, J. (2018). "Economically robust protection against 21st century sea-level rise". In: *Global Environmental Change* 51, pp. 67–73. ISSN: 0959-3780. URL: https://doi.org/10.1016/j.gloenvcha.2018.05.003.

Lira-Loarca, A., Cobos, M., Losada, M. A., and Baquerizo, A. (2020). "Storm characterization and simulation for damage evolution models of maritime structures". In: *Coastal Engineering* 156, p. 103620. ISSN: 0378-3839. URL: https://doi.org/10.1016/j.coastaleng.2019.103620.

López-Ruiz, A., Bergillos, R. J., Lira-Loarca, A., and Ortega-Sánchez, M. (2018). "A methodology for the long-term simulation and uncertainty analysis of the operational lifetime performance of wave energy converter arrays". In: *Energy* 153, pp. 126 –135. ISSN: 0360-5442. URL: https://doi.org/10.1016/j.energy.2018.04.018.

Losada, M. A., Díez-Minguito, M., and Reyes-Merlo, M. A. (2017). "Tidal-fluvial interaction in the Guadalquivir River Estuary: Spatial and frequency-dependent response of currents and water levels". In: *Journal of Geophysical Research: Oceans* 122.2, pp. 847–865. URL: https://doi.org/10.1002/2016JC011984.

Losada, M. A. (1990). "Recent developments in the design of mound breakwaters". In: *Handbook of Coastal and Ocean Engineering*. Ed. by J. B. Herbich. Vol. I. Gulf Publishing Co. Chap. 21, p. 105.

Losada, M. A., Baquerizo, A., Ortega-Sánchez, M., Santiago, J. M., and Sánchez-Badorrey, E. (2009). "Socioeconomic and Environmental Risk in Coastal and Ocean Engineering". In: *Handbook of Coastal and Ocean Engineering*. Ed. by Y. C. Kim. (California State University, Los Angeles, USA). Chap. Chapter 47, 1355–1384. URL: https://www.worldscientific.com/doi/abs/10.1142/9789813204027_0047.

MEIPORT (2016). *Revisión y Actualización del Método de Evaluación de Inversiones Portuarias (MEIPOR)*. Puertos del Estado, Madrid. ISBN: 978-84-88975-73-7. URL: http://www.puertos.es/es-es/BibliotecaV2/MEIPOR_mayo_2016.pdf.

Magaña, P., Del-Rosal-Salido, J., Cobos, M., Lira-Loarca, A., Ortega-Sánchez, M., and Losada, M. A. (2019). "Desarrollo de software científico en el ámbito de la ingeniería de costas". In: *Proceedings of XV Jornadas Españolas de Ingeniería de Costas y Puertos*. Torremolinos, Spain.

Magaña, P., Bergillos, R. J., Rosal-Salido, J. D., Reyes-Merlo, M. A., Díaz-Carrasco, P., and Ortega-Sánchez, M. (2018a). "Integrating complex numerical approaches into a user-friendly application for the management of coastal environments". In: *Science of The Total Environment* 624, pp. 979 –990. ISSN: 0048-9697. URL: https://doi.org/10.1016/j.scitotenv.2017.12.154.

— (2018b). "Integrating complex numerical approaches into a user-friendly application for the management of coastal environments". In: *Science of The Total Environment* 624, pp. 979 –990. ISSN: 0048-9697. URL: https://doi.org/10.1016/j.scitotenv.2017.12.154.

Magaña, P., Del-Rosal-Salido, J., Cobos, M., Lira-Loarca, A., and Ortega-Sánchez, M. (2020). "Approaching Software Engineering for Marine Sciences: A Single Development Process for Multiple End-User Applications". In: *Journal of Marine Science and Engineering* 8.5. ISSN: 2077-1312. URL: https://doi.org/10.3390/jmse8050350.

Magaña, P., López-Ruiz, A., Lira, A., Ortega-Sánchez, M., and Losada, M. A. (2014). "A public, open Western Europe database of shoreline undulations based on imagery". In: *Applied Geography* 55, pp. 278–291. URL: https://doi.org/10.1016/j.apgeog.2014.09.018.

Males, R. M. and Melby, J. A. (2011). "Monte Carlo simulation model for economic evaluation of rubble mound breakwater protection in Harbors". In: *Frontiers of Earth Science* 5.4, pp. 432–441. URL: https://doi.org/10.1007/s11707-011-0200-3.

Marcos, M., Rohmer, J., Vousdoukas, M. I., Mentaschi, L., Le Cozannet, G., and Amores, A. (2019). "Increased Extreme Coastal Water Levels Due to the Combined Action of Storm Surges and Wind Waves". In: *Geophysical Research Letters* 46.8, pp. 4356–4364. URL: https://doi.org/10.1029/2019GL082599.

Marcos, M. and Woodworth, P. L. (2017). "Spatiotemporal changes in extreme sea levels along the coasts of the North Atlantic and the Gulf of Mexico". In: *Journal of Geophysical Research: Oceans* 122.9, pp. 7031–7048. URL: https://doi.org/10.1002/2017JC013065.

Masina, M., Lamberti, A., and Archetti, R. (2015). "Coastal flooding: A copula based approach for estimating the joint probability of water levels and waves". In: *Coastal Engineering* 97, pp. 37–52. ISSN: 0378-3839. URL: https://doi.org/10.1016/j.coastaleng.2014.12.010.

Massie, W. (1976). *Coastal engineering. Volume III: Breakwater design*. January. TU Delft, Section Hydraulic Engineering.

Mazas, F. and Hamm, L. (2017). "An event-based approach for extreme joint probabilities of waves and sea levels". In: *Coastal Engineering* 122, pp. 44–59. ISSN: 0378-3839. URL: https://doi.org/10.1016/j.coastaleng.2017.02.003.

Mazas, F., Kergadallan, X., Garat, P., and Hamm, L. (2014). "Applying POT methods to the Revised Joint Probability Method for determining extreme sea levels". In: *Coastal Engineering* 91, pp. 140–150. ISSN: 0378-3839. URL: https://doi.org/10.1016/j.coastaleng.2014.05.006.

McGranahan, G., Balk, D., and Anderson, B. (2007). "The rising tide: assessing the risks of climate change and human settlements in low elevation coastal zones". In: *Environment and Urbanization* 19.1, pp. 17–37. URL: https://doi.org/10.1177/0956247807076960.

Mentaschi, L., Vousdoukas, M. I., Voukouvalas, E., Dosio, A., and Feyen, L. (2017). "Global changes of extreme coastal wave energy fluxes triggered by intensified teleconnection patterns". In: *Geophysical Research Letters* 44.5, pp. 2416–2426. URL: https://doi.org/10.1002/2016GL072488.

Merali, Z. (2010). "Computational science.Error". In: *Nature* 467, pp. 775–777. URL: https://doi.org/10.1038/467775a.

Merkens, J.-L., Reimann, L., Hinkel, J., and Vafeidis, A. T. (2016). "Gridded population projections for the coastal zone under the Shared Socioeconomic Pathways". In: *Global and Planetary Change* 145, pp. 57–66. ISSN: 09218181. URL: https://doi.org/10.1016/j.gloplacha.2016.08.009.

Michele, C. D., Salvadori, G., Passoni, G., and Vezzoli, R. (2007). "A multivariate model of sea storms using copulas". In: *Coastal Engineering* 54.10, pp. 734–751. ISSN: 0378-3839. URL: https://doi.org/10.1016/j.coastaleng.2007.05.007.

Miller, G. (2006). "Scientific publishing. A scientist's nightmare: software problem leads to five retractions." In: *Science (New York, N.Y.)* 314, pp. 1856–1857. URL: https://doi.org/10.1126/science.314.5807.1856.

Minguez, R., Castillo, E., Castillo, C., and Losada, M. A. (2006). "Optimal cost design with sensitivity analysis using decomposition techniques. Application to composite breakwaters". In: *Structural Safety* 28.4, pp. 321 –340. ISSN: 0167-4730. URL: https://doi.org/10.1016/j.strusafe.2005.08.005.

NOAA (2015). "Living shorelines". In: URL: https://www.habitatblueprint.noaa.gov/living-shorelines/.

Olabarrieta, M., Warner, J. C., and Kumar, N. (2011). "Wave-current interaction in Willapa Bay". In: *Journal of Geophysical Research: Oceans* 116.C12. URL: https://doi.org/10.1029/2011JC007387.

Olbert, A. I., Comer, J., Nash, S., and Hartnett, M. (2017). "High-resolution multi-scale modelling of coastal flooding due to tides, storm surges and rivers inflows. A Cork

City example". In: *Coastal Engineering* 121, pp. 278–296. ISSN: 0378-3839. URL: https://doi.org/10.1016/j.coastaleng.2016.12.006.

Orejarena-Rondón, A. F., Sayol, J. M., Marcos, M., Otero, L., Restrepo, J. C., Hernández-Carrasco, I., and Orfila, A. (2019). "Coastal Impacts Driven by Sea-Level Rise in Cartagena de Indias". In: *Frontiers in Marine Science* 6, p. 614. ISSN: 2296-7745. URL: https://doi.org/10.3389/fmars.2019.00614.

Ortega-Sánchez, M., Moñino, A., Bergillos, R. J., Magaña, P., Clavero, M., Díez-Minguito, M., and Baquerizo, A. (2018). "Confronting learning challenges in the field of maritime and coastal engineering: Towards an educational methodology for sustainable development". In: *Journal of Cleaner Production* 171, pp. 733–742. URL: https://doi.org/10.1016/j.jclepro.2017.10.049.

Payo, A., Baquerizo, A., and Losada, M. A. (2004). "Uncertainty assesment of long term shoreline prediction". In: chap. Vol. 4, pp. 2087–2096. URL: https://doi.org/10.1142/9789812701916_0167.

Payo, A., Baquerizo, A., and Losada, M. (2008). "Uncertainty assessment: Application to the shoreline". In: *Journal of Hydraulic Research* 46.sup1, pp. 96–104. URL: https://doi.org/10.1080/00221686.2008.9521944.

Peng, R. D. (2011). "Reproducible research in computational science". In: *Science* 334.6060, pp. 1226–1227. URL: https://doi.org/10.1126/science.1213847.

Perkel, J. M. (2015). "Programming: Pick up Python". In: *Nature* 518, pp. 125–126. URL: https://doi.org/10.1038/518125a.

— (2018). "Why Jupyter is data scientists' computational notebook of choice". In: *Nature* 563, pp. 145–146. URL: https://doi.org/10.1038/d41586-018-07196-1.

Plomaritis, T. A., Ferreira, Óscar, and Costas, S. (2018). "Regional assessment of storm related overwash and breaching hazards on coastal barriers". In: *Coastal Engineering* 134. RISC-KIT: Resilience-increasing Strategies for Coasts – Toolkit, pp. 124 –133. ISSN: 0378-3839. URL: https://doi.org/10.1016/j.coastaleng.2017.09.003.

ROM-0.0 (2001). *General procedure and requirements in the design ofharbor and maritime structures. Part I.* Puertos del Estado, Madrid (Keynote: Losada, M.A.) ISBN: 978-84-88975-73-7. URL: http://www.puertos.es/es-es/ROM.

ROM-1.0 (2009). *Recommendations for the Project Design and Construction of Breakwaters (Part I: Calculation and Project Factors. Climate Agents)*. Puertos del Estado, Madrid (Keynote: Losada, M.A.) ISBN: 978-84-88975-73-7. URL: http://www.puertos.es/es-es/ROM.

ROM-1.1 (2018). *Recommendations for Maritime Works ROM 1.1-18 (Articles)*. Puertos del Estado, Madrid (Keynote: Losada, M.A.) ISBN: 978-84-88975-73-7. URL: http://www.puertos.es/es-es/ROM.

Rijn, L. C. van, Walstra, D. J. R., Grasmeijer, B., Sutherland, J., Pan, S., and Sierra, J. P. (2003). "The predictability of cross-shore bed evolution of sandy beaches at the time scale of storms and seasons using process-based Profile models". In: *Coastal Engineering* 47.3, pp. 295 –327. ISSN: 0378-3839. URL: https://doi.org/10.1016/S0378-3839(02)00120-5.

Rippa, S. (1999). "An algorithm for selecting a good value for the parameter c in radial basis function interpolation". In: *Advances in Computational Mathematics* 11.2, pp. 193–210. ISSN: 1572-9044. URL: https://doi.org/10.1023/A:1018975909870.

Robert, B., Chue Hong, N., Dirk, G., James, H., and Ilian, T. (2012). "The Research Software Engineer". In: *The Research Software Engineer*. Playmoth, United Kingdom.

Rueda, A., Gouldby, B., Méndez, F. J., Tomás, A., Losada, I. J., Lara, J. L., and Díaz-Simal, P. (2015). "The use of wave propagation and reduced complexity inundation models and metamodels for coastal flood risk assessment". In: *Journal of Flood Risk Management* 9.4, pp. 390–401. URL: https://doi.org/10.1111/jfr3.12204.

Santamaria-Aguilar, S., Arns, A., and Vafeidis, A. T. (2017). "Sea-level rise impacts on the temporal and spatial variability of extreme water levels: A case study for St. Peter-Ording, Germany". In: *Journal of Geophysical Research: Oceans* 122.4, pp. 2742–2759. URL: https://doi.org/10.1002/2016JC012579.

Sayol, J. M. and Marcos, M. (2018). "Assessing Flood Risk Under Sea Level Rise and Extreme Sea Levels Scenarios: Application to the Ebro Delta (Spain)". In: *Journal of Geophysical Research: Oceans* 123.2, pp. 794–811. URL: https://doi.org/10.1002/2017JC013355.

Schinko, T. et al. (2020). "Economy-wide effects of coastal flooding due to sea level rise: a multi-model simultaneous treatment of mitigation, adaptation, and residual

impacts". In: *Environmental Research Communications* 2.1, p. 015002. URL: https://doi.org/10.1088/2515-7620/ab6368.

Schoonees, T., Gijón Mancheño, A., Scheres, B., Bouma, T. J., Silva, R., Schlurmann, T., and Schüttrumpf, H. (2019). "Hard Structures for Coastal Protection, Towards Greener Designs". English. In: *Estuaries and Coasts* 42.7. Special Issue: Integrating Ecosystems and Coastal Engineering Practice, pp. 1709–1729. ISSN: 1559-2723. URL: https://doi.org/10.1007/s12237-019-00551-z.

Serafin, K. A., Ruggiero, P., Parker, K., and Hill, D. F. (2019). "What's streamflow got to do with it? A probabilistic simulation of the competing oceanographic and fluvial processes driving extreme along-river water levels". In: *Natural Hazards and Earth System Sciences* 19.7, pp. 1415–1431. URL: https://doi.org/10.5194/nhess-19-1415-2019.

Serrano, M. A., Cobos, M., Magaña, P. J., and Díez-Minguito, M. (2020). "Sensitivity of Iberian estuaries to changes in sea water temperature, salinity, river flow, mean sea level, and tidal amplitudes". In: *Estuarine, Coastal and Shelf Science* 236, p. 106624. ISSN: 0272-7714. URL: https://doi.org/10.1016/j.ecss.2020.106624.

Silva, R. (July 2019). "Experiencias en la implementación de infraestructura verde en América Latina y el Caribe". In: *Granada (Spain)*. Andalusian Inter-University Institute for Earth System Research (IISTA-CEAMA). Av. del Mediterráneo, S/N, 18006 Granada.

Solari, S. and Losada, M. A. (2011). "Non-stationary wave height climate modeling and simulation". In: *Journal of Geophysical Research: Oceans* 116.C9. URL: https://doi.org/10.1029/2011JC007101.

— (2012). "Unified distribution models for met-ocean variables: Application to series of significant wave height". In: *Coastal Engineering* 68, pp. 67 –77. ISSN: 0378-3839. URL: https://doi.org/10.1016/j.coastaleng.2012.05.004.

— (2016). "Simulation of non-stationary wind speed and direction time series". In: *Journal of Wind Engineering and Industrial Aerodynamics* 149, pp. 48 –58. ISSN: 0167-6105. URL: https://doi.org/10.1016/j.jweia.2015.11.011.

Solari, S. (2011). "Metodología de simulación de agentes naturales y desarrollo de sistemas. Modelo de verificación y gestión de terminales portuarias. Aplicación al puerto

de la Bahía de Cádiz". PhD thesis. University of Granada (in Spanish). URL: https://digibug.ugr.es/handle/10481/20322.

Solari, S., Egüen, M., Polo, M. J., and Losada, M. A. (2017). "Peaks Over Threshold (POT): A methodology for automatic threshold estimation using goodness of fit p-value". In: *Water Resources Research* 53.4, pp. 2833–2849. URL: https://doi.org/10.1002/2016WR019426.

Solari, S. and Gelder, P. H. A. J. M. van (Jan. 2011). "On the use of vector autoregressive (VAR) and Regime Switching VAR models for the simulation of sea and wind state parameters". In: *Marine Technology and Engineering. Taylor & Francis Group, London* 1, pp. 217–230. URL: https://www.scopus.com/inward/record.uri?eid=2-s2.0-84864065879&partnerID=40&md5=1a3720a592dccdf08e4c9163b0939382.

Sutton-Grier, A. E., Wowk, K., and Bamford, H. (2015). "Future of our coasts: The potential for natural and hybrid infrastructure to enhance the resilience of our coastal communities, economies and ecosystems". In: *Environmental Science and Policy* 51, pp. 137 –148. ISSN: 1462-9011. URL: https://doi.org/10.1016/j.envsci.2015.04.006.

Svensson, C. and Jones, D. A. (2004). "Dependence between sea surge, river flow and precipitation in south and west Britain". In: *Hydrology and Earth System Sciences* 8.5, pp. 973–992. URL: https://doi.org/10.5194/hess-8-973-2004.

Tawn, J. A., Vassie, J. M., and Gumbel, E. J. (1989). "Extreme Sea Levels; The Joint Probabilities Method Revisited and Revised." In: *Proceedings of the Institution of Civil Engineers* 87.3, pp. 429–442. URL: https://doi.org/10.1680/iicep.1989.2975.

Tawn, J. A. (1992). "Estimating Probabilities of Extreme Sea-Levels". In: *Journal of the Royal Statistical Society. Series C (Applied Statistics)* 41.1, pp. 77–93. ISSN: 00359254, 14679876. URL: https://doi.org/10.2307/2347619.

Thompson, P., Cai, Y., Reeve, D., and Stander, J. (2009). "Automated threshold selection methods for extreme wave analysis". In: *Coastal Engineering* 56.10, pp. 1013–1021. ISSN: 0378-3839. URL: https://doi.org/10.1016/j.coastaleng.2009.06.003.

Toimil, A., Losada, I. J., Nicholls, R. J., Dalrymple, R. A., and Stive, M. J. F. (2020). "Addressing the challenges of climate change risks and adaptation in coastal areas: A review". In: *Coastal Engineering* 156, p. 103611. ISSN: 0378-3839. URL: https://doi.org/10.1016/j.coastaleng.2019.103611.

Townend, I. and Pethick, J. (2002). “Estuarine flooding and managed retreat”. In: *Philosophical Transactions of the Royal Society of London. Series A: Mathematical, Physical and Engineering Sciences* 360.1796, pp. 1477–1495. URL: https://doi.org/10.1098/rsta.2002.1011.

Tánago, M. G. del, Bejarano, M. D., Jalón, D. G. de, and Schmidt, J. C. (2015). “Biogeomorphic responses to flow regulation and fine sediment supply in Mediterranean streams (the Guadalete River, southern Spain)”. In: *Journal of Hydrology* 528, pp. 751–762. ISSN: 0022-1694. URL: https://doi.org/10.1016/j.jhydrol.2015.06.065.

Vicente-Serrano, S. M., Beguería, S., and López-Moreno, J. I. (2010). “A Multiscalar Drought Index Sensitive to Global Warming: The Standardized Precipitation Evapotranspiration Index”. In: *Journal of Climate* 23.7, pp. 1696–1718. URL: https://doi.org/10.1175/2009JCLI2909.1.

Vitousek, P. M., Mooney, H. A., Lubchenco, J., and Melillo, J. M. (1997). “Human Domination of Earth’s Ecosystems”. In: *Science* 277.5325, pp. 494–499. ISSN: 0036-8075. URL: https://doi.org/10.1126/science.277.5325.494.

Vitousek, S., Barnard, P. L., Fletcher, C. H., Frazer, N., Erikson, L., and Storlazzi, C. D. (2017). “Doubling of coastal flooding frequency within decades due to sea-level rise”. In: *Scientific Reports* 7.1, p. 1399. ISSN: 2045-2322. URL: https://doi.org/10.1038/s41598-017-01362-7.

Vousdoukas, M. I., Mentaschi, L., Voukouvalas, E., Verlaan, M., and Feyen, L. (2017). “Extreme sea levels on the rise along Europe’s coasts”. In: *Earth’s Future* 5.3, pp. 304–323. URL: https://doi.org/10.1002/2016EF000505.

Vousdoukas, M. I., Mentaschi, L., Voukouvalas, E., Verlaan, M., Jevrejeva, S., Jackson, L. P., and Feyen, L. (June 2018). “Global probabilistic projections of extreme sea levels show intensification of coastal flood hazard”. In: *Nature Communications* 9.1, p. 2360. ISSN: 2041-1723. URL: https://doi.org/10.1038/s41467-018-04692-w.

Vousdoukas, M. I., Ranasinghe, R., Mentaschi, L., Plomaritis, T. A., Athanasiou, P., Luijendijk, A., and Feyen, L. (Mar. 2020). “Sandy coastlines under threat of erosion”. In: *Nature Climate Change* 10.3, pp. 260–263. ISSN: 1758-6798. URL: https://doi.org/10.1038/s41558-020-0697-0.

WW3DG (2019). “User Manual and System Documentation of WAVEWATCH III version 6.07, The WAVEWATCH III Development Group”. In: *Tech. Note 326 pp. + Appendices, NOAA/NWS/NCEP/MMAB*.

Woodworth, P. L., Menéndez, M., and Roland Gehrels, W. (Sept. 2011). “Evidence for Century-Timescale Acceleration in Mean Sea Levels and for Recent Changes in Extreme Sea Levels”. In: *Surveys in Geophysics* 32.4, pp. 603–618. ISSN: 1573-0956. URL: https://doi.org/10.1007/s10712-011-9112-8.

Y. Cai B. Gouldby, P. D. and Hawkes, P. (2007). “A simulation method for flood risk variables”. In: Institute of Mathematics and its Applications (Oxford, United Kingdom).

Ye, F. et al. (2020). “Simulating storm surge and compound flooding events with a creek-to-ocean model: Importance of baroclinic effects”. In: *Ocean Modelling* 145, p. 101526. ISSN: 1463-5003. URL: https://doi.org/10.1016/j.ocemod.2019.101526.

Yin, K., Xu, S., and Huang, W. (2018). “Estimating extreme sea levels in Yangtze Estuary by quadrature Joint Probability Optimal Sampling Method”. In: *Coastal Engineering* 140, pp. 331–341. ISSN: 0378-3839. URL: https://doi.org/10.1016/j.coastaleng.2018.08.007.

Zarzuelo, C., Díez-Minguito, M., D’Alpaos, A. D., Carniello, L., Del-Rosal-Salido, J., and Ortega-Sánchez, M. (2016). “Morphodynamic response to human activities in the Bay of Cádiz (2012-2015)”. In: *35th International Conference on Coastal Engineering (ICCE)*. Istanbul , Turkey.

Zarzuelo, C., Díez-Minguito, M., Ortega-Sánchez, M., López-Ruiz, A., and Losada, M. A. (2015). “Hydrodynamics response to planned human interventions in a highly altered embayment: The example of the Bay of Cádiz (Spain)”. In: *Estuarine, Coastal and Shelf Science* 167. Coastal systems under change: tuning assessment and management tools, pp. 75–85. ISSN: 0272-7714. URL: https://doi.org/10.1016/j.ecss.2015.07.010.

Zellou, B. and Rahali, H. (2019). “Assessment of the joint impact of extreme rainfall and storm surge on the risk of flooding in a coastal area”. In: *Journal of Hydrology* 569, pp. 647–665. ISSN: 0022-1694. URL: https://doi.org/10.1016/j.jhydrol.2018.12.028.